OFFICIAL JOURNAL OF THE SCIENTIFIC SOCIETY OF ANATOMISTS, HISTOLOGISTS, EMBRYOLOGISTS AND TOPOGRAPHIC ANATOMISTS OF UKRAINE

DOI: 10.31393 ISSN 1818-1295 eISSN 2616-6194

BICHИК МОРФОЛОГІЇ REPORTS OF MORPHOLOGY

VOL. 31, №3, 2025

Scientific peer-reviewed journal in the fields of normal and pathological anatomy, histology, cytology and embryology, topographical anatomy and operative surgery, biomedical anthropology, ecology, molecular biology, biology of development

Published since 1993 Periodicity: 4 times a year

ВІСНИК МОРФОЛОГІЇ - REPORTS OF MORPHOLOGY

Founded by the "Scientific Society of Anatomists, Histologists, Embryologists, and Topographic Anatomists of Ukraine" and National Pyrogov Memorial Medical University, Vinnytsya in 1993

Certificate of state registration KB №9310 from 02.11.2004

Professional scientific publication of Ukraine in the field of medical sciences in specialties 221, 222, 228, 229

According to the list of professional scientific publications of Ukraine, approved by the order of the Ministry of Education and Science of Ukraine
No. 1188 of 24.09.2020

Professional scientific publication of Ukraine in the field of biological sciences in specialty 091

According to the list of professional scientific publications of Ukraine, approved by the order of the Ministry of Education and Science of Ukraine No. 1471 of 26.11.2020

Chairman of the Editorial Board - Gunas I.V. (Vinnytsya)

Vice-Chairman of Editorial Board - Berenshtein E.L. (Jerusalem), Kovalchuk O.I. (Kyiv)

Secretary - Kaminska N.A. (Vinnytsya)

Editorial Board Members:

Byard R. (Adelaida), Graeb C. (Hof), Gunas V.I. (Vinnytsya), Juenemann A. (Rostock), Maievskyi O.Ye. (Kyiv), Moskalenko R.A. (Sumy), Nebesna Z.M. (Ternopil), Pivtorak V.I. (Vinnytsya), Rejdak R. (Lublin), Romaniuk A.M. (Sumy), Shinkaruk-Dykovytska M.M. (Vinnytsya), Skibo G.G. (Kyiv), Vlasenko O.V. (Vinnytsya), Voloshchuk N.I. (Vinnytsya)

Editorial Council:

Appelhans O.L. (Odesa), Bulyk R.Ye. (Chernivtsi), Dgebuadze M.A. (Tbilisi), Fedonyuk L.Ya. (Ternopil), Fomina L.V. (Vinnytsya), Furman Yu.M. (Vinnytsya), Gerasymyuk I.Ye. (Ternopil), Golovatskyy A.S. (Uzhgorod), Guminskyi Yu.Y. (Vinnytsya), Herashchenko S.B. (Ivano-Frankivsk), Kostylenko Yu.P. (Poltava), Kryvko Yu.Ya. (Lviv), Lutsyk O.D. (Lviv), Mateshuk-Vatseba L.R. (Lviv), Mishalov V.D. (Kyiv), Ocheredko O.M. (Vinnytsya), Olkhovskyy V.O. (Kharkiv), Piskun R.P. (Vinnytsya), Rudyk S.K. (Kyiv), Sarafyniuk L.A. (Vinnytsya), Shepitko V.I. (Poltava), Sherstyuk O.O. (Poltava), Shevchuk Yu.G. (Vinnytsya), Shkolnikov V.S. (Vinnytsya), Sikora V.Z. (Sumy), Slobodian O.M. (Chernivtsi), Sokurenko L.M. (Kyiv), Stechenko L.O. (Kyiv), Tereshchenko V.P. (Kyiv), Topka E.G. (Dnipro), Tverdokhlib I.V. (Dnipro), Tykholaz V.O. (Kyiv), Yatsenko V.P. (Kyiv), Yeroshenko G.A. (Poltava)

Approved by the Academic Council of National Pyrogov Memorial Medical University, Vinnytsya, protocol №1 from 05.09.2025.

Indexation: Scopus, CrossRef, Index Copernicus, Google Schoolar Metrics, National Library of Ukraine Vernadsky

Address editors and publisher:

Pyrogov Str. 56, Vinnytsya, Ukraine - 21018 Tel.: +38 (0432) 553959 E-mail: nila@vnmu.edu.ua Computer page-proofs - Slobodianiuk L.M. Translator - Gunas V.I. Technical support - Levenchuk S.S. Scientific editing - editorship

The site of the magazine - https://morphology-journal.com

CONTENT

Kobzina-Didukh D. S., Fomina L. V., Tiron O. I., Galunko G. M., Sprut O. V., Vasenko T. B., Hrynchak N. M.
Histological changes in the adrenal glands of rats one hour after exposure to the venom of Leiurus macroctenus scorpions
Poladych I. V., Savosko S. I., Grabovyi O. M., Govsieiev D. O. Morphogenetic changes in the rat placenta under vitamin D ₃ deficiency
Mizyakina K. V., Dzyak L. A., Tverdokhlib I. V. Dynamics of structural rearrangements in the entorhinal cortex in rats with various neurocognitive disorders after traumatic brain injury
Gunas V. I. Morphological changes in the bronchi and lung parenchyma of laboratory rats one hour after administration of Leiurus macroctenus scorpion venom
Khamidova F. M., Abdullayev B. S., Sulaymonova M. J., Zhovlieva M. B.,, Aminova N. A. Structural components and immunohistochemical features of the respiratory organs in children with bronchiectasis
Chebernina I. O., Nebesna Z. M., Ohinska N. V., Hetmaniuk I. B., Kulbitska V. V. Histological changes in the dentate gyrus of the hippocampus in rats with induced colon adenocarcinoma and after correction with nanomaterials
Orlovskyi I. V., Beliaiev E. V., Isakova N. M., Kasianenko D. M., Cherkasova L. A., Dyakova O. V., Gunas I. V. Modeling of the linear dimensions required for constructing the correct dental arch form in young males and females with physiological occlusion, regardless of facial type, based on the characteristics of cephalometric parameters according to the Burstone method and computed tomographic tooth measurements
Haidai O. S., Dzevulska I. V., Samborska I. A., Shvager O. V. Differences in the structural organisation of liver tissue in experimental rats 1 and 3 hours after administration of Leiurus macroctenus scorpion venom
Hryntsova N. B., Romaniuk A. M. Long-term effects of heavy metal salts on morphometric parameters and functional state of the sexually mature rats' pineal gland
Katsenko A. L., Sherstiuk O. O., Hryn V. H, Svintsytska N. L., Bilash V. P., Ustenko R. L., Piliuhin A. V. Morphology and morphometry of the rat lacrimal gland duct system: a comparative analysis of the extraorbital, intraorbital, and Harderian glands

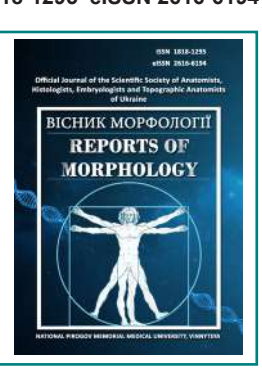
ISSN 1818-1295 eISSN 2616-6194



REPORTS OF MORPHOLOGY

Official Journal of the Scientific Society of Anatomists, Histologists, Embryologists and Topographic Anatomists of Ukraine

journal homepage: https://morphology-journal.com



Histological changes in the adrenal glands of rats one hour after exposure to the venom of Leiurus macroctenus scorpions

Kobzina-Didukh D. S.¹, Fomina L. V.¹, Tiron O. I.², Galunko G. M.¹, Sprut O. V.¹, Vasenko T. B.¹, Hrynchak N. M.¹

National Pirogov Memorial Medical University, Vinnytsya, Ukraine

International Academy of Ecology and Medicine, Odessa, Ukraine

ARTICLE INFO

Received: 19 November 2024 Accepted: 12 June 2025

UDC: 616.514-037:572.087+612-071

CORRESPONDING AUTHOR

e-mail: darakobzina@gmail.com Kobzina-Didukh D. S.

CONFLICT OF INTEREST

The authors have no conflicts of interest to declare.

FUNDING

Not applicable.

DATA SHARING

Data are available upon reasonable request to corresponding author.

The venom of scorpions of the genus Leiurus is considered among the most dangerous of known animal toxins, as its action can lead to severe systemic disorders and a high risk of fatal outcomes. The complex of biologically active substances that make up the venom is capable of affecting multiple target organs, including the cardiovascular, respiratory, and nervous systems. Particular attention is given to the impact of the toxin on endocrine glands, which play a key role in the formation of stress responses in the body. At the same time, morphological changes in such an important organ as the adrenal glands remain insufficiently studied, which highlights the need for further research in this area. The aim of the study was to determine the morphological changes in the adrenal glands of rats one hour after exposure to the venom of Leiurus macroctenus scorpions. Laboratory rats were divided into two groups: a control group (n=5), which received a single intramuscular injection of 0.5 ml of physiological saline, and an experimental group (n=5), which received a single intramuscular injection of 0.5 ml of Leiurus macroctenus venom. One hour after venom administration, the experimental rats were euthanized, and the adrenal glands were removed for subsequent histological analysis. After fixation in neutral formalin solution, standard dehydration was performed followed by paraffin embedding. Histological sections 4-5 µm thick were stained with hematoxylin and eosin and using the Azan Trichrome method. For a more detailed study of cellular structures, semithin sections 1-2 µm thick were prepared and stained with methylene blue. Microscopic analysis was carried out using a light microscope at magnifications of ×100 and ×400. Morphological analysis of the adrenal glands of rats one hour after inoculation with Leiurus macroctenus venom revealed pronounced vascular and cellular disturbances. In the cortical substance, dilation of small vessels, their deformation, and congestion with erythrocyte aggregation were observed. The zona fasciculata appeared the most vulnerable, showing signs of edema, disorganization of cellular structures, and karyopyknosis in the nuclei of endocrinocytes. In the zona glomerulosa, changes in nuclear shape and a chaotic distribution of heterochromatin were noted, suggesting damage to protein components of the karyoskeleton. The cytoplasm of endocrinocytes was filled with lipid inclusions, and cell boundaries became indistinct. In the zona reticularis, vascular disorders predominated, although the cells maintained a relatively preserved architecture. The medulla remained without significant pathological changes. Alterations in the capsule and interstitium confirmed the systemic nature of adrenal gland injury. Thus, Leiurus macroctenus venom induces early microcirculatory and cellular disturbances in the adrenal cortex, most pronounced in the zona fasciculata, while the medulla remains intact. The observed changes indicate a zonal specificity of the toxic effect.

Keywords: anatomy, histology, morphology of the adrenal glands, venom of the scorpion Leiurus macroctenus.

Introduction

Scorpionism is a significant medical and biological problem affecting many countries with warm and dry climates

where venomous scorpions are widespread. According to estimates by the World Health Organization, more than 1.2 million cases of scorpion stings are registered worldwide each year, about 0.27 % of which result in death [22]. In many regions of the Middle East, North Africa, South America, and Asia, scorpion envenomation is one of the leading causes of hospitalization due to toxic injuries. For example, in Luxor, Egypt, among 300 analyzed cases of scorpion stings, Leiurus quinquestriatus and Androctonus crassicauda predominated, with children under 15 years being the most vulnerable age group, accounting for 42.6 % of all victims [1].

In Latin America, the problem is particularly prevalent. In Brazil, up to 90,000 cases of scorpionism are reported annually, with some regions recording incidence rates as high as 52 cases per 100,000 population [26]. In Mexico, where more than 250 scorpion species have been described, about 15 are clinically significant, causing over 300,000 stings each year, of which approximately 0.1-0.2 % are fatal [27]. According to González-Santillán and Possani, cases in the United States have shown mortality rates of up to 25 % in children if antivenom is not administered in time [13]. A similar situation is observed in Iraq, where between 2015 and 2019 the incidence reached 5.6 cases per 1,000 people, with an average fatality rate ranging from 0.5-1 % [16].

In India, around 50,000 people are affected by scorpion stings annually, with members of the genera Mesobuthus and Hottentotta posing the greatest danger. Mortality ranges from 1 to 8 %, particularly among children, who are more sensitive to the toxin [18]. An epidemiological study in Shiraz, Iran, reported over 20,000 cases in 5 years, with most victims under the age of 30, and clinical manifestations ranging from local pain to generalized convulsions and cardiotoxic effects [31]. Similar findings were confirmed by Mousavi et al., who reported more than 100,000 cases over five years in Southwestern Iran, corresponding to 550 cases per 100,000 population [24].

In Latin American and Middle Eastern countries, the intensity of scorpion sting incidence is significantly influenced by urbanization. Studies in Brazil and Mexico have shown that with increasing urbanized areas, the number of scorpion stings has doubled over the last decade [8]. This is explained by the fact that scorpions, as synanthropic species, readily adapt to new living conditions, invading residential zones and household premises. In Ecuador, between 2021-2024, the prevalence of scorpion stings in suburban areas was 37 % higher than in rural ones [32]. Urbanization also alters food sources and ecological niches, promoting scorpion proliferation in human settlements.

In France, despite the relatively low overall incidence, certain regions (Corsica, overseas territories) remain at high risk. Specifically, Buthus pyrenaeus is recognized as a species of potential clinical concern, although fatal cases are rare [33, 34].

Particular danger lies in the venom of scorpions of the genus Leiurus. This genus belongs to the Buthidae family, whose members are the most dangerous to humans.

The most well-known species is Leiurus quinquestriatus, distributed in North Africa and the Middle East. Its venom contains neurotoxins capable of blocking sodium channels, leading to severe disturbances of the nervous and cardiovascular systems [3].

The clinical course of envenomation ranges from local pain to severe systemic manifestations, including cardioand neurotoxic effects. Among the factors determining the severity of intoxication, the most important are the species and age of the scorpion, the amount of venom injected, the site of the sting, as well as the victim's age, body mass, and general health status [7]. In children, the risk of severe complications is 3-5 times higher than in adults, and mortality may reach 30 % without timely medical intervention [26].

Recent studies show that despite pronounced toxic properties, components of scorpion venom also possess potential pharmacological benefits. In particular, some peptides can modulate ion channels, which may hold promise for the development of new drugs [3].

Thus, the epidemiology of scorpionism demonstrates its global spread, with particularly high danger in Africa, Latin America, and Asia. Of special importance are species of the genus Leiurus, whose venom can cause systemic damage to vital organs. In this context, studying morphological changes in organs such as the adrenal glands is crucial for elucidating mechanisms of toxic action and predicting health risks.

The aim of the study was to determine the morphological changes in the adrenal glands of rats one hour after exposure to the venom of Leiurus macroctenus scorpions.

Materials and methods

Scorpions of the species Leiurus macroctenus were identified by typical morphological features [21]; they were provided by a private breeder in Ibbenbüren (Germany), owned by Mark Stockmann. All individuals originated from captivity and were sexually mature (15 males and 15 females). Venom was obtained by single "milking" according to the method of Ozkan and Filazi [25], as modified by Yaqoob et al. [36], performed one month after the animals were transported from the breeding facility. Toxin samples were stored at -20 °C until use [14].

The study involved 10 male white laboratory rats weighing 200±10 g, bred in the vivarium of the Educational and Scientific Center "Institute of Biology and Medicine" of Taras Shevchenko National University of Kyiv. Experiments were carried out on the basis of the cooperation agreement between Taras Shevchenko National University of Kyiv, National Pirogov Memorial Medical University of Vinnytsya and I. Horbachevsky Ternopil National Medical University (2021). The housing conditions of the rats complied with the "Standard rules for the arrangement, equipment, and maintenance of experimental biological clinics (vivariums)." All procedures were performed in accordance with the "European Convention for the Protection of Vertebrate Animals Used for Experimental and Other Scientific Purposes" [20] and the Law of Ukraine "On the Protection

of Animals from Cruelty" (No. 3447-IV of February 21, 2006) (Bioethics of National Pirogov Memorial Medical University, Vinnytsya, protocol № 11 from 12.11.2024).

The animals were divided into two groups: a control group (5 rats that received an intramuscular injection of 0.5 ml of physiological saline; tissue sampling was carried out 1 hour later) and an experimental group (5 rats that received a single intramuscular injection of 0.5 ml of Leiurus macroctenus venom solution at a concentration of 28.8 μ g/ ml; LD₅₀=0.08 mg/kg [15]). Euthanasia was performed by CO₂ inhalation, after which the adrenal glands were immediately harvested at 4 °C.

Organ samples were fixed in 10 % neutral formalin, followed by dehydration in graded alcohols and processing in a Logos ONE histoprocessor (MILESTONE, Italy). The material was embedded in paraffin blocks using an automated embedding station TEC 2800 (HESTION, Australia). Histological sections 4-5 µm thick were prepared with a rotary microtome AMR-400 (Amos Scientific Pty, Australia) and stained with hematoxylin–eosin and by the Azan Trichrome method.

For semithin sections (1-2 μ m), tissues were fixed in 2.5 % glutaraldehyde solution (pH 7.3-7.4) with subsequent postfixation in 1 % osmium tetroxide. After dehydration in graded alcohols, the material was embedded in a mixture of epoxy resins followed by polymerization. Sections were prepared using an Ultrotome LKB 4801 A ultramicrotome (Bromma, Sweden) and stained with methylene blue.

Microscopic analysis of the adrenal glands was performed with an OLIMPUS BX 41 light microscope at magnifications of ×100 and ×400. Digital visualization and morphometric studies were carried out using Quickphoto micro 2.3 software. The description of histological specimens was conducted according to generally accepted pathomorphological criteria.

Results

The first, though subtle, manifestations of cellular response to the venom could already be detected one hour after its inoculation. In particular, examination of the cortical substance at ×100 magnification, which provides a panoramic view of the organ, revealed numerous dilations of small blood vessels located among the cells of all three cortical zones of the adrenal gland (Fig. 1). The most pronounced congestion was observed in the zona fasciculata. In the control group, the cells of this zone formed regular parallel rows, whereas here they appeared displaced by the dilated vessels and arranged in a rather chaotic manner. While in the untreated group the blood vessels were narrow and oriented perpendicularly to the organ capsule, in the experimental group they exhibited irregular, indistinct boundaries, and their lumina were filled with aggregated erythrocytes.

It is noteworthy that the inner cortical zones – the zona fasciculata and zona reticularis – demonstrated vascular pathological processes to a greater extent, as these two zones are primarily responsible for the synthesis and secretion of corticosterone in response to stress. It may be

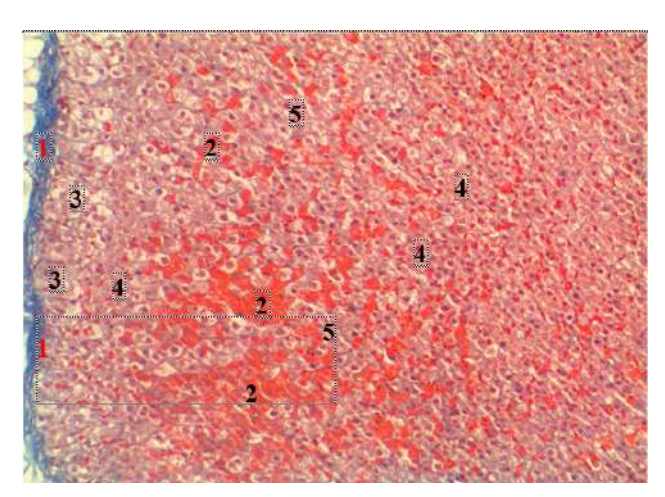


Fig. 1. Morphological structure of the rat adrenal gland one hour after the experiment. 1 – capsule, 2 – dilation of small blood vessels with aggregated erythrocytes in the lumina, 3 – endocrinocytes of the zona glomerulosa with irregular nuclei, 4 – blurred cell boundaries, 5 – disruption of cellular bundle organization. Azan trichrome staining. ×100.

assumed that this functional role contributed to the observed alterations in the vascular component of the organ.

Examination of the cells of the zona glomerulosa demonstrated the early stages of potentially hazardous processes within them. The nuclei of some of these cells exhibited a somewhat irregular, distorted shape, which may be associated with damage to proteins of the submembranous complex (see Fig. 1, Fig. 2). As is well known, karyoskeletal proteins are responsible not only for maintaining the rounded and regular shape of nuclei but also for the structural organization of heterochromatin through its attachment to the nuclear envelope. In many endocrinocytes, such organization was disrupted: heterochromatin was distributed chaotically throughout the nucleus, forming numerous dark clumps.

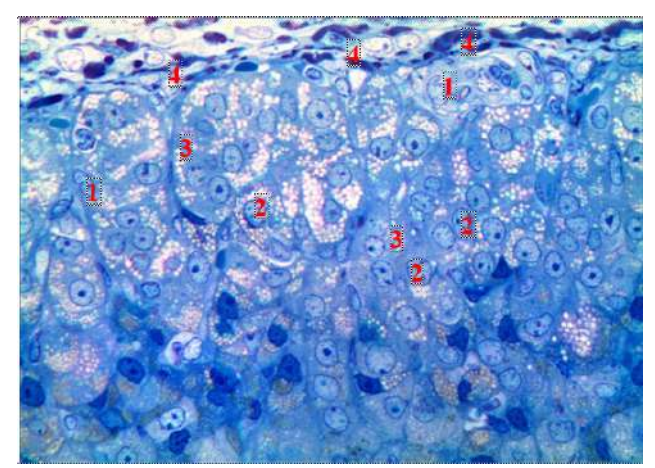


Fig. 2. Morphological structure of the superficial zones of the rat adrenal cortex one hour after the experiment. 1 – irregularly shaped nuclei, 2 – clumps of heterochromatin, 3 – lipid inclusions, 4 – deformed fibroblast nuclei. Semithin section. Stained with methylene blue. ×400.

Vol. 31, №3, Page 5-12

The nuclear component of the cytoskeleton is fragile, and a protein-toxic effect of the venom on its elements cannot be excluded. In addition, disruption and distortion of nuclear contours represent one of the consequences of developing cellular edema.

As for the cytoplasm of the cells of the zona glomerulosa, at such an early stage it did not exhibit pathological features that could be clearly identified by morphological analysis of histological sections. The only aspect worth noting was the blurred, irregular boundaries of the cells and the outlines of lipid vacuoles within them, which were noticeable with Azan trichrome staining (see Fig. 1). Such changes usually indicate the initial stages of intracellular edema.

Similar alterations in both the nuclei and cytoplasm were also characteristic of the zona fasciculata in this group (see Fig. 1, 2). In addition to the early manifestations of edema, the main morphological changes in this zone, as already mentioned, included vascular congestion and deformation of blood vessels. Like any other endocrine organ, the adrenal glands possess a highly developed network of fenestrated and sinusoidal capillaries for the transport of hormones secreted by endocrinocytes. Therefore, alterations in the microcirculatory bed are clearly visible in preparations of this gland. In the control group, the vessels ran parallel to one another, separating closely adjacent cells of the zona fasciculata, which formed elongated trabeculae. Here, due to changes in the vascular component and cellular edema. this clear organization was disrupted (see Fig. 1, Fig. 3). As a result of such structural changes, the cells of this zone no longer formed organized bundles; in some areas they were arranged chaotically and displayed blurred boundaries between them.

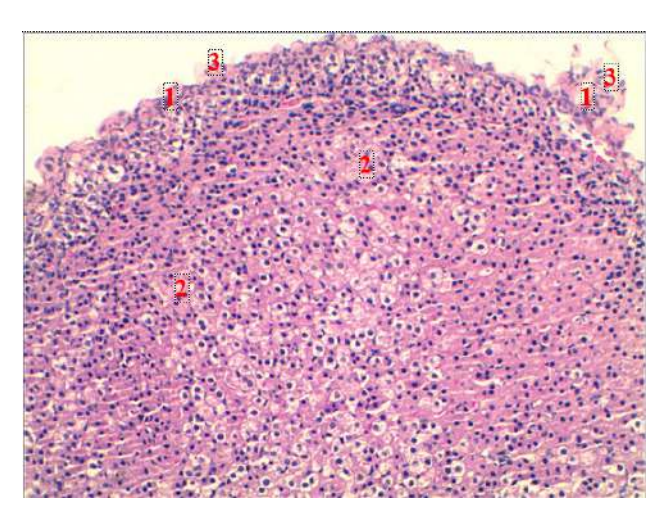


Fig. 3. Morphological structure of the rat adrenal gland one hour after the experiment. 1 – capsule with loosened fibers, 2 – disruption of spatial organization of cells in the zona fasciculata, 3 – fibroblast nuclei. Hematoxylin and eosin staining. ×100.

A very distinctive change compared to the intact group could be observed in the cells of the zona fasciculata on semithin sections. Numerous endocrinocytes displayed dark, slightly shrunken nuclei with irregular contours – features characteristic of karyopyknosis (Fig. 4). Karyopyknosis, as is known, represents the first, although still reversible, step in the pathway leading the cell toward necrosis. Despite the dark appearance of the nuclei, numerous clumps of irregularly distributed heterochromatin were still visible within them. The cytoplasm of the cells was filled with lipid inclusions, which were noticeably more abundant compared to the control group.

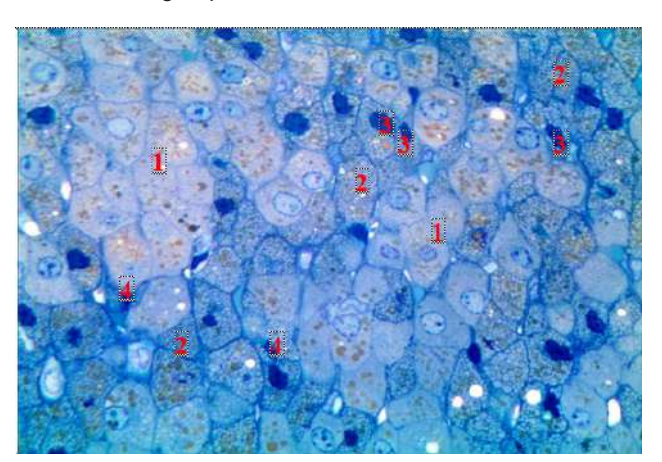


Fig. 4. Morphological structure of the zona fasciculata of the rat adrenal gland one hour after the experiment. 1 – blurred cell boundaries, 2 – lipid inclusions, 3 – karyopyknosis, 4 – indistinct nuclear contours. Semithin section. Stained with methylene blue. ×400.

In addition to the accumulation of lipid inclusions within the cytoplasm, the cells in semithin sections also exhibited blurred boundaries and, in some cases, indistinct nuclear contours.

The cells of the zona reticularis of the adrenal cortex shared with the zona fasciculata the consequences of venom action on the microcirculatory bed (see Fig. 1). Small vessels here were dilated and had indistinct borders, with aggregated erythrocytes visible in their lumina. Nevertheless, the cells in this zone retained their characteristic network-like arrangement, showed no signs of edema, and remained tightly adjacent to one another. Their nuclei were dark and displayed somewhat blurred margins.

Morphological examination of the histological structures of the adrenal medulla in this experimental group revealed no pathological alterations. Large cells maintained clear boundaries and regular nuclear morphology.

Since the condition of the blood vessels has already been described in detail in the characterization of the adrenal parenchyma, within the description of the organ stroma attention is focused on its connective tissue components – the capsule and interstitium.

The integrity of the adrenal capsule was locally compromised: collagen fibers appeared slightly loosened, in some places even protruding outward (see Fig. 3). Among the eosinophilic fibers, flattened dark fibroblast nuclei were observed, some oriented perpendicularly to the organ

surface, which was associated with disorientation of the surrounding connective tissue fibers. In semithin sections, fibroblast nuclei showed slight deformation, resulting in irregular, distorted shapes (see Fig. 2).

Discussion

Thus, one hour after the administration of Leiurus macroctenus scorpion venom to laboratory rats, acute morphological changes were detected in the adrenal glands. These were most evident in the vascular system of the cortex, particularly in the form of capillary dilation, vascular congestion, and erythrocyte aggregation. At the cellular level, the predominant features included signs of edema, nuclear apparatus destruction, and excessive accumulation of lipid inclusions, which were most pronounced in the zona fasciculata. In contrast, the medulla did not exhibit pathological changes, indicating a selective effect of the venom on different structural compartments of the organ. Therefore, the observed alterations display zonal specificity and may be crucial for understanding the mechanisms of scorpion venom toxicity.

Scorpion venom, including that of Leiurus macroctenus, is characterized by its complex action on various organs and tissues, reflected both in systemic toxic effects and in local morphological changes. It is known that venom components interact with immune system cells, inducing the release of proinflammatory mediators and altering the balance between different leukocyte subpopulations, which significantly affects the functional state of target organs [2]. Such immunopathological alterations, caused by activation of cytokines, prostaglandins, and leukotrienes, explain the development of generalized inflammatory responses that underlie adrenal gland damage and injury to other vital organs [19].

A number of studies confirm that venoms of different scorpion species cause widespread morphological alterations in organs. For instance, administration of Buthus lienhardi venom to laboratory animals produced destructive processes at the histological level, including necrotic foci and biochemical changes, combined with impaired motor functions [4]. Similar effects were described with Aegaeobuthus nigrocinctus venom: mice exhibited decreased viability, impaired hematopoiesis, and significant biochemical abnormalities, accompanied by the death of up to 30 % of experimental animals [6]. Other authors have reported complex damage to the CNS, liver, and spleen under the influence of Hottentota gentili, further supporting the multi-organ nature of scorpion venom toxicity [9].

Particular attention has been given to data obtained with Buthus paris, where it was demonstrated that within just a few hours after venom administration, pronounced alterations appeared in the liver and kidneys, as well as disturbances of homeostasis accompanied by intense inflammation [11]. Similar results were reported for Hemiscorpius lepturus, whose venom caused a marked reduction in the total number of leukocytes, particularly lymphocytes, a key mechanism in

the development of immunodeficiency states [12]. Moreover, in cases of Androctonus australis envenomation, a transition was observed from stable hematopoiesis to accelerated granulopoiesis, representing an adaptive response of the organism to massive toxic injury [17].

The adrenal gland injury we observed correlates with these systemic effects described in the literature. Importantly, other studies of Leiurus macroctenus venom have demonstrated significant morphological changes in the kidneys as early as three hours after intoxication, including ischemia, edema, and focal nephron necrosis [23]. This suggests a similar temporal pattern of early lesions that may also apply to the adrenal glands, considering their high sensitivity to circulating toxins.

The spleen is another major target organ where changes under the influence of various animal venoms have been documented. It has been shown that Leiurus quinquestriatus toxins can modify spleen structure in diabetic rats, reducing the severity of pathological changes in tissues and even exerting a partial protective effect [29]. In contrast, Apis mellifera syriaca venom induced pronounced cytokine synthesis in the mouse spleen, reflecting the immunomodulatory potential of venom components [28]. Similar trends were reported for Montivipera bornmuelleri venom, which stimulated proinflammatory cytokine production in the spleen, enhancing immune responses [35]. Collectively, these findings suggest that the spleen plays a central role in the organism's reactions to animal toxins; however, the mechanisms of spleen injury under the influence of Leiurus macroctenus remain poorly studied [30].

Interesting results have also been obtained with venoms of other marine organisms. For example, intoxication with lionfish (Scorpaenidae) venom in rats revealed pronounced biochemical and histological alterations, including parenchymal organ damage and significant changes in blood parameters [5]. Comparable pathological phenomena were recorded in experiments with insect venoms, where structural tissue remodeling and signs of apoptosis were described [10]. These data confirm that animal toxins, regardless of their biological source, are characterized by a universal pathogenic potential.

In summary, our findings are consistent with previous reports indicating the systemic nature of organ damage caused by scorpion venoms. The morphological changes we identified in the adrenal glands reflect a general pathogenic mechanism involving inflammatory activation, immune cell injury, and microcirculatory disturbances. Literature data also highlight the spleen as an organ of particular interest; however, the specific effects of Leiurus macroctenus venom on this organ remain largely unexplored, defining the prospects for future research in this area [30].

Conclusions

In the adrenal glands of rats one hour after the administration of Leiurus macroctenus scorpion venom, complex vascular and cellular responses were observed,

Vol. 31, №3, Page 5-12

reflecting both stress-induced and direct toxic effects. It was established that the zona fasciculata is the most vulnerable, being the first to respond with microcirculatory disturbances, edema, and alterations of the nuclear apparatus, which indicates its key role in the development of the pathological

process. At the same time, the relative preservation of the medulla suggests the selectivity of venom action and the zonal specificity of the organ's response. Thus, the morphological alterations reflect a combination of general toxic and stress-mediated mechanisms of injury.

References

- [1] Abd El, F. E. Z. A., El Shehaby, D. M., Elghazally, S. A., & Hetta, H. F. (2019). Toxicological and epidemiological studies of scorpion sting cases and morphological characterization of scorpions (Leiurusquin questriatus and Androctonus crassicauda) in Luxor, Egypt. *Toxicology reports*, 6, 329-335. doi: 10.1016/j.toxrep.2019.03.004
- [2] Adi-Bessalem, S., Hammoudi-Triki, D., & Laraba-Djebari, F. (2015). Scorpion venom interactions with the immune system. In *Scorpion Venoms* (pp. 87-107). Springer, Dordrecht. doi: 10.1007/978-94-007-6404-0
- [3] Ahmadi, S., Knerr, J. M., Argemi, L., Bordon, K. C., Pucca, M. B., Cerni, F. A., ... & Laustsen, A. H. (2020). Scorpion venom: detriments and benefits. *Biomedicines*, 8(5), 118. doi: 10.3390/biomedicines8050118
- [4] Ait Laaradia, M., El Hidan, M. A., Marhoume, F., Bouimeja, B., Oufquir, S., Sokar, Z., ... & Chait, A. (2018). Buthus lienhardi venom and pathophysiological effects at the histological, hematological, biochemical and motor skills levels. Toxicon, 146, 106-113. doi: 10.1016/j.toxicon.2018.03.001
- [5] Al-Zahrani, M. S., & Wahsheh, H. A. (2022). Leveraging Computational Biology to Assess the Biochemical and Histological Alterations in Rats Following Scorpionfish Envenomation. *Fresenius Environmental Bulletin*, 31(08B), 8711-8718.
- [6] Bakır, F., Ozkan, O., Alcigir, M. E., & Yagmur, E. A. (2021). The lethality, histological, haematological and biochemical alterations in mice envenomated with Aegaeobuthus nigrocinctus venom. *Toxicon*, 200, 118-126. doi: 10.1016/j. toxicon.2021.07.010
- [7] Carmo, É. A., Nery, A. A., Pereira, R., Rios, M. A., & Casotti, C. A. (2019). Factors associated with the severity of scorpio poisoning. *Texto & Contexto-Enfermagem*, 28, e20170561. doi: 10.1590/1980-265X-TCE-2017-0561
- [8] Duarte, L. L., Carvalho, M. A. M., de Araújo, L. M., & de Moura Júnior, N. B. (2024). Urbanization impact on scorpion stings: an epidemiological study. *Toxicon*, 248, 108039. doi: 10.1016/j.toxicon.2024.108039
- [9] El Hidan, M. A., Touloun, O., El Hiba, O., Chait, A., Hafid, J. E., & Boumezzough, A. (2015). Behavioral, histopathological and biochemical impairments observed in mice envenomed by the scorpion: Hottentota gentili (Pallary, 1924). *Toxicon*, 103, 19-29. doi: 10.1016/j.toxicon.2015.06.013
- [10] El-Aziz, A., Dawood, A. F., Refaie, S. M., & Khan, S. (2023). Potentiality Assessment of The Activity of Scorpion Venom as An Insecticide Towards Spodoptera frugiperda: Histological and Electron Microscopy Studies. *Egyptian Academic Journal of Biological Sciences*, D. Histology & Histochemistry, 15(2), 89-100.
- [11] Elmourid, A., Elhidan, M. A., Boussaa, S., Laaradia, M. A., Bouimeja, B., Amahmid, O., ... & Touloun, O. (2024). A comprehensive pathophysiologic, histologic, and biochemical analysis of Buthus paris (CL Koch, 1839) venom. Wilderness & Environmental Medicine, 35(3), 271-277. doi: 10.1177/10806032241249748

- [12] Ghafourian, M., Ganjalikhanhakemi, N., Hemmati, A. A., Dehghani, R., & Kooti, W. (2016). The effect of Hemiscorpius lepturus (Scorpionida: Hemiscorpiidae) venom on leukocytes and the leukocyte subgroups in peripheral blood of rat. *Journal of arthropod-borne diseases*, 10(2), 159-167. PMCID: PMC4906755
- [13] González-Santillán, E., & Possani, L. D. (2018). North American scorpion species of public health importance with a reappraisal of historical epidemiology. *Acta tropica*, 187, 264-274. doi: 10.1016/j.actatropica.2018.08.002
- [14] Gunas, V. I. (2024). Morphological changes in the lung vessels of laboratory rats 1 hour after administration of Leiurus macroctenus scorpion venom. Світ медицини та біології=World of Medicine and Biology, 3(89), 225-229. doi: 10.26724/2079-8334-2024-3-89-225-229
- [15] Gunas, V., Maievskyi, O., Raksha, N., Vovk, T., Savchuk, O., Shchypanskyi, S., & Gunas, I. (2024). Study of the Acute Toxicity of Scorpion Leiurus macroctenus Venom in Rats. *The Scientific World Journal*, 2024(1), 9746092. doi: 10.1155/2024/9746092
- [16] Hussen, F. S., & Ahmed, S. T. (2021). Epidemiological and clinical aspects of scorpion stings in Kurdistan Region of Iraq. Pol J Environ Stud, 30(1), 629-634. doi: 10.15244/ pjoes/122840
- [17] Kaddache, A., Hassan, M., Laraba-Djebari, F., & Hammoudi-Triki, D. (2017). Switch of steady-state to an accelerated granulopoiesis in response to Androctonus australis hector venom. *Inflammation*, 40(3), 871-883. doi: 10.1007/s10753-017-0532-6
- [18] Kumar, R. (2022). An update on epidemiology and management practices of Scorpion envenomation in India. *Journal* of family medicine and primary care, 11(9), 4932-4935. doi: 10.4103/jfmpc.jfmpc_2300_21
- [19] Lamraoui, A., Adi-Bessalem, S., & Laraba-Djebari, F. (2015). Immunopathologic effects of scorpion venom on hepatorenal tissues: Involvement of lipid derived inflammatory mediators. *Experimental and molecular pathology*, 99(2), 286-296. doi: 10.1016/j.yexmp.2015.07.013
- [20] Louhimies, S. (2002). Directive 86/609/EEC on the protection of animals used for experimental and other scientific purposes. Alternatives to Laboratory Animals, 30(2_suppl), 217-219. doi: 10.1177/026119290203002S36
- [21] Lowe, G., Yağmur, E., & Kovařík, F. (2014). A review of the genus Leiurus Ehrenberg, 1828 (Scorpiones: Buthidae) with description of four new species from the Arabian Peninsula. *Euscorpius*, (191), 1-129. doi: 10.18590/euscorpius.2014. vol2014.iss191.1
- [22] Lucas, S. M., & Meier, J. (2017). Biology and distribution of scorpions of medical importance. In *Handbook of clinical* toxicology of animal venoms and poisons (pp. 205-219). CRC Press. ISBN: 9780203719442
- [23] Matkivska, R. M. (2025). Histological changes in the kidneys of experimental rats 3 hours after exposure to the venom of the scorpion Leiurus macroctenus. *Morphologia*, 19(1),

- 31-34. doi: 10.26641/1997-9665.2025.1.31-34
- [24] Mousavi, S. A., Rashidi, H., Faramarzi, A., Feyzi, R., Kaid-khordeh, M., & Fard, P. F. (2023). Epidemiology of scorpion sting in Southwestern Iran over five years. *Trends in Medical Sciences*, 3(1), e133418. doi: 10.5812/tms-133418
- [25] Özkan, Ö., & Fİlazİ, A. (2004). The determination of acute lethal dose-50 (LD50) levels of venom in mice, obtained by different methods from scorpions, Androctonus crassicauda (Oliver 1807). Acta Parasitol Turcica. 28(1), 50-53.
- [26] Queiroz, A. M., Sampaio, V. S., Mendonça, I., Fé, N. F., Sachett, J., Ferreira, L. C. L., ... & Monteiro, W. (2015). Severity of scorpion stings in the Western Brazilian Amazon: a case-control study. *PLoS One*, 10(6), e0128819. doi: 10.1371/journal.pone.0128819
- [27] Riaño-Umbarila, L., Rodríguez-Rodríguez, E. R., Santibañez-López, C. E., Güereca, L., Uribe-Romero, S. J., Gómez-Ramírez, I. V., ... & Becerril, B. (2017). Updating knowledge on new medically important scorpion species in Mexico. *Toxicon*, 138, 130-137. doi: 10.1016/j.toxicon.2017.08.022
- [28] Sahyoun, C., Khoury, M., Mouawad, C., Darazy, D., Roufayel, R., Mattei, C., ... & Karam, M. (2024). Apis mellifera syriaca venom modulates splenic cytokines levels in BALB/c mice. *Infectious Disorders-Drug TargetsDisorders*), 24(1), 41-45. doi: 10.2174/1871526523666230623152045
- [29] Salama, W. M., El-Naggar, S. A., Tabl, G. A. E., El Shefiey, L. M. M., & El-Desouki, N. I. (2023). Treatment with Leiurus quinquestratus scorpion venom ameliorates the histopathological changes of type-2 diabetic rats' splenic tissues. *Journal of Bioscience and Applied Research*, 9(4), 356-365. doi: 10.21608/JBAAR.2023.332608
- [30] Samborska, I., Maievskyi, O., Podzihun, L., & Lavrynenko, V. (2024). Features of immune reactivity of the spleen and mechanisms of organ damage under the influence of animal venom toxins including scorpions. Wiadomosci Lekarskie

- (Warsaw, Poland: 1960), 77(1), 120-125. doi: 10.36740/ WLek202401115
- [31] Sanaei-Zadeh, H., Marashi, S. M., & Dehghani, R. (2017). Epidemiological and clinical characteristics of scorpionism in Shiraz (2012-2016); development of a clinical severity grading for Iranian scorpion envenomation. *Medical journal of the Islamic Republic of Iran, 31*, 27. doi: 10.18869/mjiri.31.27
- [32] Vasconez-Gonzalez, J., Izquierdo-Condoy, J. S., Miño, C., de Lourdes Noboa-Lasso, M., & Ortiz-Prado, E. (2025). Epidemiological and geodemographic patterns of scorpionism in ecuador: a nationwide analysis (2021–2024). *Toxicon: X*, 26, 100218. doi: 10.1016/j.toxcx.2025.100218
- [33] Vaucel, J. A., Gil-Jardine, C., Labadie, M., Larréché, S., Paradis, C., Nardon, A., ... & French PCC Research Group. (2022). Comment on epidemiology of scorpionism in France: Nationwide scorpion exposure. Description of Buthus pyrenaeus envenoming. *Clinical Toxicology*, 60(7), 890-891. doi: 10.1080/15563650.2022.2046776
- [34] Vaucel, J. A., Larréché, S., Paradis, C., Courtois, A., Pujo, J. M., Elenga, N., ... & French Pcc Research Group. (2022). French scorpionism (mainland and oversea territories): narrative review of scorpion species, scorpion venom, and envenoming management. *Toxins*, 14(10), 719. doi: 10.3390/toxins14100719
- [35] Yacoub, T., Rima, M., Sadek, R., Hleihel, W., Fajloun, Z., & Karam, M. (2018). Montivipera bornmuelleri venom has immunomodulatory effects mainly up-regulating pro-inflammatory cytokines in the spleens of mice. *Toxicology reports*, 5, 318-323. doi: 10.1016/j.toxrep.2018.02.011
- [36] Yaqoob, R., Tahir, H. M., Arshad, M., Naseem, S., & Ahsan, M. M. (2016). Optimization of the conditions for maximum recovery of venom from scorpions by electrical stimulation. *Pakistan journal of zoology, 48*(1), 265-269.

ГІСТОЛОГІЧНІ ЗМІНИ В НАДНИРНИКАХ ЩУРІВ ЧЕРЕЗ ОДНУ ГОДИНУ ПІСЛЯ ВПЛИВУ ОТРУТИ СКОРПІОНІВ LEIURUS MACROCTENUS

Кобзіна-Дідух Д. С., Фоміна Л. В., Тірон О. І., Галунко Г. М., Спрут О. В., Васенко Т. Б., Гринчак Н. М.

Отрута скорпіонів роду Leiurus вважається однією з найнебезпечніших серед відомих тваринних токсинів, адже її дія може призводити до тяжких системних порушень і високого ризику летальних наслідків. Комплекс біологічно активних речовин, що входять до складу отрути, здатний уражати різні органи-мішені, включаючи серцево-судинну, дихальну та нервову системи. Особлива увага приділяється впливу токсину на ендокринні залози, які є ключовими у формуванні стрес-реакцій організму. Водночас морфологічні зміни в такому важливому органі, як надниркові залози, залишаються вивченими недостатньо, що зумовлює необхідність подальших досліджень у цьому напрямі. Мета дослідження визначити морфологічні зміни в надниркових залозах щурів через одну годину після впливу отрути скорпіонів Leiurus macroctenus. Лабораторні щури були розділені на дві групи: контрольну (n=5) – введення одноразово внутрішньом'язово 0,5 мл фізіологічного розчину, і експериментальну (п=5) – також одноразово внутрішньом'язово введення 0,5 мл отрути скорпіонів Leiurus macroctenus. Через годину після введення отрути експериментальних щурів евтаназували і вилучали надниркові залози для подальшого гістологічного аналізу. Після фіксації в розчині нейтрального формаліну, за стандартною схемою проводили дегідратацію з подальшою заливкою в парафін. Отримані гістологічні зрізи товщиною 4-5 мкм забарвлювали гематоксиліном еозином та за методом Azan Trichrome. Для детального дослідження клітинних структур виготовляли напівтонкі зрізи товщиною 1-2 мкм, які забарвлювали метиленовим синім. Мікроскопічний аналіз проводили за допомогою світлового мікроскопа зі збільшеннями 100 та 400. Морфологічний аналіз надниркових залоз щурів через одну годину після інокуляції отрути Leiurus macroctenus виявив виражені судинні й клітинні порушення. У кірковій речовині зафіксовано розширення дрібних судин, їх деформацію та повнокрів'я з агрегацією еритроцитів. Найбільш вразливою виявилася пучкова зона, де спостерігалися ознаки набряку, дезорганізація клітинних структур та каріопікноз у ядрах ендокриноцитів. У клубочковій зоні відзначали зміни форми ядер і хаотичний розподіл гетерохроматину, що може свідчити про ушкодження білкових компонентів каріоскелету. Цитоплазма ендокриноцитів була переповнена ліпідними включеннями, а клітинні межі ставали розмитими. У сітчастій зоні домінували судинні розлади, проте клітини зберігали відносно правильну архітектоніку. Мозкова речовина залишалася без помітних патологічних змін. Порушення структури капсули та інтерстицію підтверджували системний характер ураження надниркових залоз. Таким чином, ompyma Leiurus macroctenus спричиняє ранні мікроциркуляторні та клітинні порушення в кірковій речовині надниркових

Vol. 31, №3, Page 5-12

залоз, найбільш виражені в пучковій зоні, тоді як мозкова речовина зберігає інтактність. Виявлені зміни свідчать про зональну специфічність токсичної дії.

Ключові слова: анатомія, еістологія, морфологія надниркових залоз, отрута скорпіона Leiurus macroctenus.

Author's contribution:

Kobzina-Didukh D. S.- research, methodology and writing of the original draft, formal analysis.

Fomina L. V. - conceptualization, review writing and editing.

Tiron O. I. – review writing and editing.

Galunko G. M. - supervision.

Sprut O. V. - data visualization.

Vasenko T. B. - software.

Hrynchak N. M. – validation.

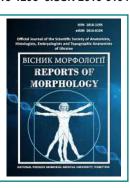
ISSN 1818-1295 eISSN 2616-6194



REPORTS OF MORPHOLOGY

Official Journal of the Scientific Society of Anatomists, Histologists, Embryologists and Topographic Anatomists of Ukraine

journal homepage: https://morphology-journal.com



Morphogenetic changes in the rat placenta under vitamin $\mathbf{D}_{_{\! 3}}$ deficiency

Poladych I. V., Savosko S. I., Grabovyi O. M., Govsieiev D. O.

Bogomolets National Medical University, Kyiv, Ukraine

ARTICLE INFO

Received: 10 December 2024 Accepted: 16 June 2025

UDC: 612.63:591.3:616-056.7

CORRESPONDING AUTHOR

e-mail: iren.poladich@gmail.com Poladych I. V.

CONFLICT OF INTEREST

The authors have no conflicts of interest to declare.

FUNDING

Not applicable.

DATA SHARING

Data are available upon reasonable request to corresponding author.

The placenta is a vital temporary organ that ensures metabolic, respiratory, endocrine, immunological, and barrier functions between the mother and the fetus. Morphofunctional integrity of the placenta is essential for the physiological course of pregnancy, and its structural alterations contribute to the pathogenesis of various gestational complications. Beyond its classical role in calcium-phosphate metabolism, vitamin D, exhibits pleiotropic effects, including immunomodulation, angiogenesis, and regulation of trophoblast invasion. This study aimed to evaluate the morphofunctional status of the placenta in pregnant female rats depending on vitamin D, status, using histological and morphometric analysis. Thirty-six Wistar female rats were divided into three groups: D₂-deficient, D₂-deficient with cholecalciferol correction (1000 IU/ kg), and control. On gestational day 16, placentas were collected for examination. Histological techniques and morphometric analysis were used to detect changes in placental architectonics. Specific areas of fetal capillaries (Fv), maternal blood lacunae (Mv), cytotrophoblasts (Ct) and syncytiotrophoblasts (Syn) were selected for morphometric analysis. In the D₃-deficient group, we observed a significant reduction in the area of syncytiotrophoblast and cytotrophoblast, an increase in maternal lacunae, and a higher Fv/Syn index (fetal capillaries to syncytiotrophoblast ratio), indicating compensatory microvascular remodeling under hypoxic stress. Changes in the placenta architecture, which consist in an increase in the blood supply of maternal lacunae and a decrease in the number of cellular components in the fetal part of the placenta, indicate a compensatory restructuring of the placental architecture under conditions of hypoxia. Correction with vitamin D, partially restored placental architecture, with most morphometric parameters approaching control values. These findings demonstrate the essential role of vitamin $\mathbf{D}_{\scriptscriptstyle 3}$ in labyrinth zone development and suggest that its deficiency may lead to placental dysfunction and fetal growth restriction. As a conclusion, an experimental study proved that vitamin D₃ is necessary for the normal morphogenesis of the placenta, the development of cytotrophobrasts and syncytiotrophoblasts of its labyrinthine zone, which prevents the occurrence of placental dysfunction. The findings could be used to develop approaches for early prevention of gestational complications associated with vitamin D, deficiency.

Keywords: placentation, vitamin D_3 , morphometry, fetoplacental insufficiency, experimental model, rats.

Introduction

The placenta is a unique transient organ that sustains the continuous functionality of the maternal-fetal system throughout the entire course of gestation, performing a wide spectrum of essential functions, including trophic, respiratory, transport, barrier, endocrine, immune, and metabolic roles. Beyond serving as a physical interface, it constitutes an active participant in complex biological processes, such as blastocyst implantation, the establishment of the vascular

system, and the synthesis of hormones and growth factors indispensable for the maintenance of pregnancy [3, 12, 16]. Any structural or morphofunctional alterations of the placenta may lead to profound disturbances of feto-placental circulation, fetal hypoxia, and the development of gestational complications [13, 21, 25].

Over the past decades, scientific attention has increasingly focused on the role of micronutrients, particularly vitamin $D_{\rm q}$,

in ensuring the physiological development of the placenta. Traditionally, vitamin D_3 has been regarded primarily as a regulator of calcium-phosphorus metabolism and bone mineralization [9, 23, 24]. However, emerging evidence indicates that its biological effects are considerably broader. Vitamin D_3 participates in the regulation of more than 3,000 genes, including those involved in immune responses, cellular proliferation and differentiation, angiogenesis, antioxidant defense, as well as the invasive potential of trophoblasts [6, 8, 11, 15].

Currently, it has been demonstrated that vitamin D_3 deficiency in pregnant women is associated with an increased risk of preeclampsia, gestational diabetes, preterm birth, low birth weight, and feto-placental insufficiency [7, 10, 17]. A. Kalok et al. [18] reported that women with hypovitaminosis D_3 have a significantly higher risk of delivering infants with low birth weight and developing complications related to impaired placental function. Similarly, studies by Benachi A. et al. [4] revealed that maternal serum concentrations of $25(OH)D_3$ are lower in pregnancies complicated by preeclampsia compared to healthy controls, thereby reinforcing the association between vitamin D_3 status and gestational pathology.

Vitamin D_3 also regulates the expression of VEGF (vascular endothelial growth factor), HOXA10, CYP27B1, and Toll-like receptors in trophoblasts, which are key determinants of placental vascular bed formation and fetal oxygen supply [5, 19, 22]. Disruption of angiogenesis and trophoblast invasion under vitamin D deficiency creates a pathophysiological basis for abnormal placentation, a defining feature of preeclampsia and feto-placental insufficiency [14, 20].

Given the central role of the placenta in determining pregnancy outcome, and the growing recognition of vitamin D-related gestational disorders, experimental evaluation of placental morphofunctional changes in pregnant Wistar rats with altered vitamin $D_{\scriptscriptstyle 3}$ status provides important translational insights. This not only clarifies the histological correlates of placental dysfunction but also advances our understanding of the molecular mechanisms involved, highlighting novel opportunities for preventive and therapeutic strategies in clinical obstetrics.

The aim of this study was to investigate the morphofunctional characteristics of the placenta in female rats under conditions of experimentally induced vitamin D_3 deficiency and its correction.

Materials and methods

This study was performed in 2024 at the Palladin Institute of Biochemistry, NAS of Ukraine, in the Department of Coenzymes and Vitamins. A total of 36 female Wistar rats, aged 8-10 weeks with a mean body weight of 174.0±12.0 g, were included. Animals were randomly assigned to three groups: control group (n=10) – females receiving standard vivarium chow with unrestricted vitamin D_3 content. Group I (n=14) – females maintained on a rachitogenic diet devoid of vitamin D_3 for 60 days prior to mating to induce vitamin

 D_3 deficiency; Group II (n=12) – females initially maintained on the rachitogenic diet for 60 days, followed by a standard laboratory diet supplemented with oral vitamin D_3 administered via gavage (0.2 ml of an oil-based solution, 1000 IU/kg body weight, cholecalciferol; Sigma, USA) for 2 weeks prior to mating. All animals were housed under standard vivarium conditions at 22±2 °C, 55-60 % relative humidity, with a 12-hour light/dark cycle and ad libitum access to food and water.

All experimental procedures were conducted in accordance with international ethical standards and guidelines for the use of laboratory animals (EU Directive 2010/63/EU). The study was performed under a protocol approved by the Ethics Committee of the O. O. Bogomolets National Medical University (Protocol No. 193, dated 24 March 2023), in compliance with the European Convention for the Protection of Vertebrate Animals used for Experimental and Scientific Purposes (Strasbourg, France; 1986) and national bioethical standards (Kyiv, Ukraine; 2006).

Induction of Vitamin D₃ Deficiency

To induce vitamin D_3 deficiency, females in Group I were maintained on a diet completely devoid of vitamin D_3 for 60 days prior to mating. At the end of the experimental period, blood samples were collected to confirm deficiency. Serum 25-hydroxyvitamin D_3 (25(OH) D_3) levels were measured using a commercial ELISA kit (General 25-Hydroxyvitamin D_3 , HVD3, UNDL00047, AssayGenie), and results were quantified with GainData® software (arigo's ELISA Calculator).

Mating and Determination of Gestational Day

Following confirmation of vitamin D_3 deficiency, females were paired with fertile males at a ratio of 1:2 (female:male). On the following morning, vaginal smears were examined microscopically for the presence of spermatozoa, allowing the designation of gestational day 1 (GD1).

Histological Analysis

To assess morphofunctional alterations of the placenta, tissue samples were collected on gestational day 16 following the termination of the experiment. Placentas were fixed in formalin and processed using standard protocols to prepare histological sections. Hematoxylin-eosin staining was performed to evaluate overall placental architecture, vascularization, and the presence of morphological changes potentially associated with vitamin D_3 deficiency.

Statistical Analysis

Data were analyzed using StatPlus software (version 7.0, AnalystSoft Inc., USA). The Shapiro-Wilk test was applied to assess normality of the data distribution. Differences between group means were evaluated using one-way analysis of variance (ANOVA) followed by Bonferroni post hoc test. Data are presented as mean ± standard deviation (M±SD), and statistical significance was set at p<0.05.

Results

Histological analysis of placentas collected on gestational day 16 revealed heterogeneous architecture, with a clear demarcation between the labyrinthine and spongiotrophoblast zones in the fetal portion, and the decidual layer containing

metrial glands in the maternal portion. A peripheral layer of cytotrophoblasts was also observed (Fig. 1). The labyrinthine zone, which occupied the largest area, consisted of villi containing fetal capillaries (Fv), cytotrophoblasts with large nuclei (Ct), and syncytiotrophoblasts with smaller nuclei (Syn), all surrounded by maternal blood lacunae (Mv) (see Fig. 1). These components were selected for morphometric analysis in both control animals and those with vitamin D₃ deficiency.

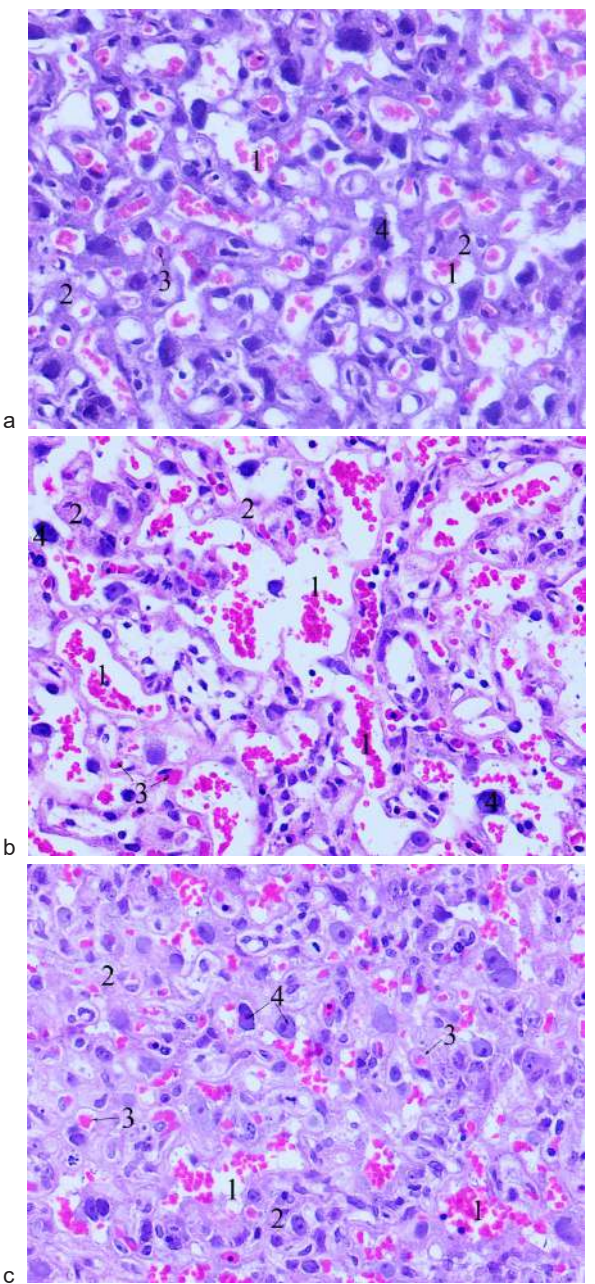


Fig. 1. Placenta of rats under vitamin D_3 deficiency and its correction: a- control group; b- Group I; c- Group II. Significantly dilated, blood-filled maternal placental sinuses and a reduced number of cytotrophoblast nuclei are observed under vitamin D_3 deficiency. Legend: 1- maternal placental sinuses; 2- syncytiotrophoblast; 3- fetal capillaries; 4- trophoblast nuclei. Hematoxylin-eosin staining, ×400.

In intact rats, the proportion of syncytiotrophoblasts averaged 56 %, whereas in rats with vitamin $\rm D_3$ deficiency, this parameter was significantly lower at only 31.8 % (p<0.05) (Fig. 2). The relative nuclear density of cytotrophoblasts also decreased from 4.8 % in the control group to 3.3 % in the deficient group (p<0.05). The proportion of maternal lacunae increased significantly from 23.4 % to 33.4 % (p<0.05). Thus, vitamin $\rm D_3$ deficiency led to morphological alterations characterized by dilation and hyperemia of maternal lacunae and a reduction in the cellular components of the fetal portion of the placenta. Although the absolute density of fetal capillaries did not change significantly, the Fv/Syn index (the ratio of capillary area to syncytiotrophoblast area) increased significantly (p<0.05), indicating compensatory angiogenic remodeling in response to reduced perfusion.

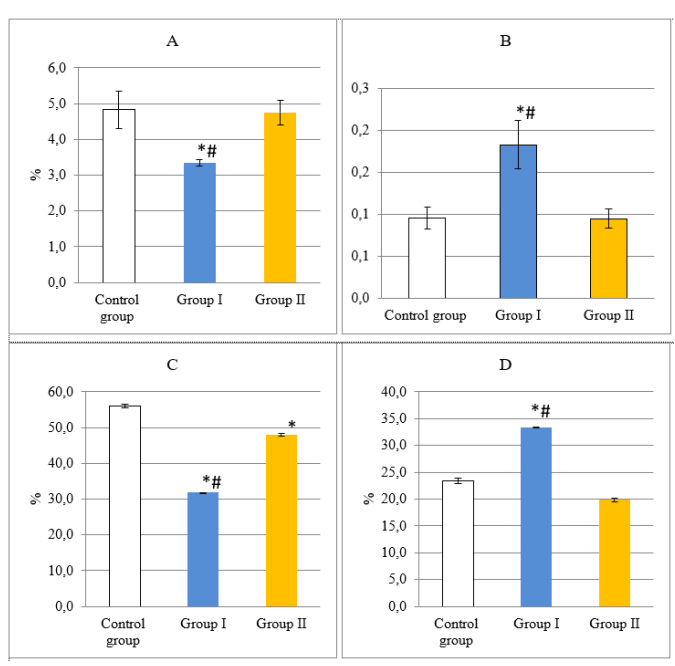


Fig. 2. Morphometric parameters of rat placenta under vitamin D_3 deficiency and its correction. * – significant vs. control group (p<0.05); # – significant vs. Group II (p<0.05). A – relative area of cytotrophoblast nuclei (Ct), %; B – Syn/Fv index; C – relative area of syncytiotrophoblast (Syn), %; D – relative area of maternal lacunae (Mv), %.

In the vitamin $\rm D_3$ -supplemented group, the cytoarchitecture of the labyrinth zone more closely resembled that of controls. The area of cytotrophoblasts approached control values (p>0.05), although the area of syncytiotrophoblasts remained significantly lower (48.1 % vs. 56 %, p<0.05). Both the Fv/Syn index and the area of maternal lacunae normalized (p>0.05), suggesting a beneficial effect of vitamin $\rm D_3$ supplementation on placental structure.

Vitamin D_3 is essential for normal placental morphogenesis and may be effective in restoring structural abnormalities associated with its deficiency. Alterations in the architecture of maternal lacunae could impair oxygenation and nutrient delivery, potentially contributing to abnormal villous

Vol. 31, №3, Page 13-18

development and other placental dysfunctions.

The basal zone of the placenta represents a region of particular scientific interest, as it comprises giant trophoblastic cells (large polyploid cells with prominent nuclei), trophospongial cells, and glycogen-rich cells, the latter two forming distinct cellular aggregates. Nevertheless, the cytoarchitecture of the basal zone is highly heterogeneous, limiting the reliability of morphometric analysis on microsections stained with conventional histological methods and highlighting the need for complementary analytical approaches.

Discussion

This study demonstrates that vitamin D_3 deficiency induces significant morphological alterations in the labyrinth zone of the placenta, which may contribute to impaired placental function and adverse pregnancy outcomes. The most pronounced structural changes in vitamin D_3 -deficient rats included a marked reduction in the relative area of syncytiotrophoblasts and the nuclear density of cytotrophoblasts, accompanied by compensatory enlargement of maternal blood lacunae. These findings suggest that maternal vitamin D_3 status plays a critical role in maintaining the integrity of the feto-maternal interface during placentation.

The syncytiotrophoblast layer is essential for nutrient and oxygen exchange, hormone synthesis, and fetal immune protection. A substantial decrease in the area of syncytiotrophoblasts in vitamin D_3 -deficient rats may reflect impaired trophoblast differentiation or increased apoptosis, as previously reported in experimental and clinical studies [1, 2]. Similarly, the reduction in cytotrophoblast nuclear density indicates decreased proliferative potential, which may further compromise placental development and function.

Another notable observation was the enlargement of maternal blood lacunae in the placenta under vitamin D_3 deficiency. While such expansion may initially appear as a compensatory response to impaired villous perfusion, it may actually reflect hypoxic stress and placental insufficiency. This hypothesis is supported by the increased Fv/Syn index, indicating a relative increase in fetal capillary area in the context of reduced syncytiotrophoblast mass. These structural adaptations likely represent a compensatory angiogenic mechanism aimed at preserving fetal oxygenation under conditions of suboptimal placental exchange.

Pre-mating correction of vitamin D₃ deficiency partially

restored placental architecture. The areas of cytotrophoblasts and maternal lacunae returned to control values, whereas the area of syncytiotrophoblasts, although improved, remained significantly lower than in intact animals. These findings indicate a restorative effect of vitamin $D_{\rm 3}$ on placental morphogenesis; however, complete recovery may require earlier or more prolonged intervention. The normalization of the Fv/Syn index in the supplemented group further supports the influence of vitamin $D_{\rm 3}$ on angiogenic processes within the labyrinth zone.

Although the basal zone of the placenta was not quantitatively assessed in this study due to its highly heterogeneous cytoarchitecture, it may also be affected by vitamin D₂ deficiency. This zone contains giant trophoblastic cells, glycogen-rich cells, and trophospongial elements, all of which play critical roles in implantation and early placental development [16, 26, 27, 28]. Further investigations using immunohistochemistry or in situ hybridization are warranted to elucidate the effects of vitamin D₃ on this morphologically complex and functionally important region. It is most likely that vitamin D₃ primarily influences the development of the labyrinth zone, making it a promising target for future studies, particularly regarding the expression of specific cellular markers to assess the metabolic status of placental tissue under conditions of vitamin D₂ deficiency. Future research should focus on the molecular pathways involved in trophoblast differentiation and angiogenesis regulated by vitamin D₃, as well as the long-term consequences of prenatal vitamin D₃ status on fetal health.

Conclusions

- 1. Vitamin D_3 is essential for placental development, particularly for the formation of the labyrinth zone, which represents a key cytoarchitectural component of the placenta and is crucial for fetal growth and survival.
- 2. In an experimental model of vitamin D_3 deficiency, alterations in the morphogenesis of the placental labyrinth zone were demonstrated, including abnormal maternal blood perfusion, enlargement of maternal lacunae, and a reduction in the relative areas of cytotrophoblasts and syncytiotrophoblasts in the fetal portion of the placenta.
- 3. The placental changes observed in this study provide a basis for considering the role of vitamin D_3 deficiency in the development of fetal hypoxia and intrauterine growth restriction.

References

- [1] Al-Harbi, A. N., Khan, K. M., & Rahman, A. (2017). Developmental vitamin D deficiency affects spatial learning in Wistar rats. *Journal of Nutrition*, 147(9), 1795-1805. doi: 10.3945/jn.117.249953
- [2] Ali, A., Alexander, S., Ko, P., Cuffe, J. S. M., Whitehouse, A. J. O., McGrath, J. J., & Eyles, D. (2021). Developmental vitamin D deficiency in pregnant rats does not induce preeclampsia. *Nutrients*, 13(12), 42-54. doi: 10.3390/ nu13124254
- [3] Azevedo Portilho, N., & Pelajo-Machado, M. (2018).
- Mechanism of hematopoiesis and vasculogenesis in mouse placenta. *Placenta*, 69, 140-145. doi: 10.1016/j. placenta.2018.04.007
- [4] Benachi, A., Baptiste, A., Taieb, J., Tsatsaris, V., Guibourdenche, J., Senat, M. V., ... & Souberbielle, J. C. (2020). Relationship between vitamin D status in pregnancy and the risk for preeclampsia: A nested case-control study. *Clinical Nutrition*, 39(2), 440-446. doi: 10.1016/j.clnu.2019.02.015
- [5] Charoenngam, N., & Holick, M. F. (2020). Immunologic Effects of Vitamin D on Human Health and Disease. *Nutrients*,

- 12(7), 2097. doi: 10.3390/nu12072097
- [6] Chen, Y. H., Liu, Z. B., Ma, L., Zhang, Z. C., Fu, L., Yu, Z., ... & Xu, X. (2020). Gestational vitamin D deficiency causes placental insufficiency and fetal intrauterine growth restriction partially through inducing placental inflammation. *Journal of Steroid Biochemistry and Molecular Biology*, 203, 105733. doi: 10.1016/j.jsbmb.2020.105733
- [7] Chien, M. C., Huang, C. Y., Wang, J. H., Shih, C. L., & Wu, P. (2024). Effects of vitamin D in pregnancy on maternal and offspring health-related outcomes: An umbrella review of systematic review and meta-analyses. *Nutrition & Diabetes*, 14(1), 35. doi: 10.1038/s41387-024-00296-0
- [8] Deepa, R., Schayck, O. C. P. V., & Babu, G. R. (2024). Low levels of vitamin D during pregnancy associated with gestational diabetes mellitus and low birth weight: Results from the MAASTHI birth cohort. Frontiers in Nutrition, 11, 1352617. doi: 10.3389/fnut.2024.1352617
- [9] Fleet, J. C. (2022). Vitamin D-mediated regulation of intestinal calcium absorption. *Nutrients*, 14(16), 3351. doi: 10.3390/ nu14163351
- [10] Freedman, A. A., Silver, R. M., Gibbins, K. J., Hogue, C. J., Goldenberg, R. L., Dudley, D. J., ... & Drews-Botsch, C. (2019). The association of stillbirth with placental abnormalities in growth-restricted and normally grown fetuses. Paediatr Perinat Epidemiol, 33(4), 274-383. doi: 10.1111/ppe.12563
- [11] Ganguly, A., Tamblyn, J. A., Finn-Sell, S., Chan, S. Y., Westwood, M., Gupta, J., ... & Hewison, M. (2018). Vitamin D, the placenta and early pregnancy: Effects on trophoblast function. *Journal of Endocrinology*, 236(2), R93-R103. doi: 10.1530/JOE-17-0491
- [12] Gingrich, J., Ticiani, E., & Veiga-Lopez, A. (2020). Placenta disrupted: Endocrine disrupting chemicals and pregnancy. *Trends in Endocrinology and Metabolism*, 31(7), 508-524. doi: 10.1016/j.tem.2020.03.003
- [13] Giourga, C., Papadopoulou, S. K., Voulgaridou, G., Karastogiannidou, C., Giaginis, C., & Pritsa, A. (2023). Vitamin D Deficiency as a Risk Factor of Preeclampsia during Pregnancy. *Diseases*, 11(4), 158. doi: 10.3390/ diseases11040158
- [14] Hirsch, A., Rotem, R., Ternovsky, N., & Hirsh Raccah, B. (2022). Pravastatin and placental insufficiency associated disorders: A systematic review and metaanalysis. Front Pharmacol, 9(13), 1021548. doi: 10.3389/ fphar.2022.1021548
- [15] Hollis, B. W., & Wagner, C. L. (2017). Vitamin D supplementation during pregnancy: Improvements in birth outcomes and complications through direct genomic alteration. Mol Cell Endocrinol, 15(453), 113-130. doi: 10.1016/j.mce.2017.01.039
- [16] Huang, C. C., Hsueh, Y. W., Chang, C. W., Hsu, H. C., Yang, T. C., Lin, W. C., & Chang, H. M. (2023). Establishment of the fetal-maternal interface: developmental events in human implantation and placentation. *Front Cell Dev Biol*, *17*, (11), 1200330. doi: 10.3389/fcell.2023.1200330
- [17] Ideraabdullah, F. Y., Belenchia, A. M., Rosenfeld, C. S., Kullman, S. W., Knuth, M., Mahapatra, D., ... & Peterson,

- C. A. (2019). Maternal vitamin D deficiency and developmental origins of health and disease (DOHaD). *J Endocrinol*, 241(2), R65-R80. doi: 10.1530/JOE-18-0541
- [18] Kalok, A., Aziz, N. H. A., Malik, D. A., Shah, S. A., Nasuruddin, D. N., Omar, M. H., ... & Shafiee, M. N. (2020). Maternal serum vitamin D and spontaneous preterm birth. *Clin. Exp. Obstet. Gynecol*, 47(1), 16-20. doi: 10.31083/j.ceog.2020.01.4930
- [19] Karras, S. N., Anagnostis, P., Bili, E., Naughton, D. P., Petroczi, A., Papadopoulou, F., & Goulis, D. G. (2014). Maternal vitamin D status in pregnancy and offspring bone development: the unmet needs of vitamin D era. *Osteoporos Int*, 25(3), 795-805. doi: 10.1007/s00198-013-2468-5
- [20] Konwisser, A., & Korytko, O. (2021). The impact of vitamin D deficiency on maternal outcomes in pregnancy. *International journal of endocrinology (Ukraine)*, 17(1), 63-69. doi: 10.22141/2224-0721.17.1.2021.226433
- [21] Mansur, J. L., Oliveri, B., Giacoia, E., Fusaro, D., & Costanzo, P. R. (2022). Vitamin D: Before, during and after Pregnancy: Effect on Neonates and Children. *Nutrients*, 14(9), 1900. doi: 10.3390/nu14091900
- [22] Monika, Khillan, S., Garg, R., Kaur, P., & Singh, J. (2024). Serum 25 (oh) vitamin D and calcium levels and adverse maternal and perinatal outcomes in pregnancy induced hypertension. Asian Journal of Pharmaceutical and Clinical Research, 17(6), 118-121. doi: 10.22159/ajpcr.2024. v17i6.50510
- [23] Olmos-Ortiz, A., Avila, E., Durand-Carbajal, M., & Díaz, L. (2015). Regulation of calcitriol biosynthesis and activity: focus on gestational vitamin D deficiency and adverse pregnancy outcomes. *Nutrients*, 7(1), 443-80. doi: 10.3390/ nu7010443
- [24] Park, H., Wood, M. R., Malysheva, O. V., Jones, S., Mehta, S., Brannon, P. M., & Caudill, M. A. (2017). Placental vitamin D metabolism and its associations with circulating vitamin D metabolites in pregnant women. Am J Clin Nutr, 106(6), 1439-1448. doi: 10.3945/ajcn.117.153429
- [25] Pilz, S., Zittermann, A., Trummer, C., Theiler-Schwetz, V., Lerchbaum, E., Keppel, M. H., ... & Pandis, M. (2019). Vitamin D testing and treatment: A narrative review of current evidence. *Endocrine Connections*, 8(2), R27-R43. doi: 10.1530/EC-18-0432
- [26] Rosenkrantz, J. L., Gaffney, J. E., Roberts, V. H. J., Carbone, L., & Chavez, S. L. (2021). Transcriptomic analysis of primate placentas and novel rhesus trophoblast cell lines informs investigations of human placentation. *BMC Biol*, 19(1), 127. doi: 10.1186/s12915-021-01056-7
- [27] You, Z., Mei, H., Zhang, Y., Song, D., Zhang, Y., & Liu, C. (2024). The effect of vitamin D deficiency during pregnancy on adverse birth outcomes in neonates: a systematic review and meta-analysis. Front Pediatr, 14(12), 1399615. doi: 10.3389/fped.2024.1399615
- [28] Zhang, H., Wang, S., Tuo, L., Zhai, Q., Cui, J., Chen, D., & Xu, D. (2022). Relationship between Maternal Vitamin D Levels and Adverse Outcomes. *Nutrients*, 14(20), 4230. doi: 10.3390/nu14204230

ЗМІНИ МОРФОГЕНЕЗУ ПЛАЦЕНТИ ЩУРІВ НА ТЛІ ДЕФІЦИТУ ВІТАМІНУ ${\bf D_3}$ Поладич І. В., Савосько С. І., Грабовий О. М., Говсєєв Д. О.

Плацента є ключовим тимчасовим органом, який забезпечує метаболічну, дихальну, ендокринну, імунну та бар'єрну функції між організмом матері та плода. Морфофункціональна цілісність плаценти має вирішальне значення для нормального перебігу вагітності, а її структурні порушення лежать в основі багатьох гестаційних ускладнень. Вітамін D₂, окрім

Vol. 31, №3, Page 13-18

класичних функцій у метаболізмі кальцію та фосфору, виявляє широкий спектр позаскелетних ефектів, включаючи імуномодуляцію, ангіогенез та регуляцію трофобластичної інвазії. Метою дослідження було оцінити морфологічний стан плаценти самиць щурів залежно від вітамін D, статусу шляхом гістологічного та морфометричного аналізу. Дослідження проведено на 36 самицях щурів лінії Wistar, розподілених на три групи: з дефіцитом вітаміну D., з дефіцитом та подальшою корекцією холекальциферолом (1000 МО/кг) і контрольна група. На 16 добу вагітності проведено забори плацент для аналізу. Гістологічні методи та морфометричний аналіз були використані для виявлення змін архітектоніки плаценти. Питомі площі фетальних капілярів (Fv), материнських кров'яних лакун (Mv), цитотрофобластів (Сt) та синцитіотрофобластів (Syn) були обрані для морфометричного аналізу. У групі з дефіцитом вітаміну D, встановлено достовірне зменшення питомої площі синцитіотрофобластів і цитотрофобластів при збільшенні площі материнських лакун, а також зростання індексу Fv/Syn – показника співвідношення фетальних капілярів до площі синцитіотрофобласта. Зміни архітектоніки плаценти, які полягають у збільшенні кровонаповнення материнських лакун та зменшенні кількості клітинних компонентів у плодовій частині плаценти, свідчать про компенсаторну перебудову плацентарної архітектоніки за умов гіпоксії. Після корекції вітаміном D, більшість морфометричних параметрів наблизилися до контрольних значень. Результати дослідження підтверджують важливу роль вітаміну D, у формуванні лабіринтної зони плаценти, порушення якої може бути патогенетично пов'язаним з фето-плацентарною недостатністю. Таким чином, в експериментальному дослідженні доведено, що вітамін D ့ є необхідною складовою для нормального морфогенезу плаценти, розвитку цитотрофобластів та синцитіотрофобластів плодової її частини, що запобігає виникненню дисфункції плаценти. Отримані дані можуть бути використані для розробки підходів до ранньої профілактики гестаційних ускладнень, пов'язаних з дефіцитом вітаміну D₃.

Ключові слова: плацентація, вітамін D_{s} , морфометрія, фетоплацентарна недостатність, експериментальна модель, щури.

Author's contribution

Poladych I. V. – data visualization, project administration, research, formal analysis, methodology and original project writing, review writing and editing.

Savosko S. I. - scientific management, software.

Grabovyi O. M. - scientific management, validation.

Govsieiev D. O.- conceptualization, project administration.

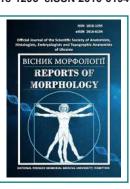
ISSN 1818-1295 eISSN 2616-6194



REPORTS OF MORPHOLOGY

Official Journal of the Scientific Society of Anatomists, Histologists, Embryologists and Topographic Anatomists of Ukraine

journal homepage: https://morphology-journal.com



Dynamics of structural rearrangements in the entorhinal cortex in rats with various neurocognitive disorders after traumatic brain injury

Mizyakina K. V., Dzyak L. A., Tverdokhlib I. V. Dnipro State Medical University, Dnipro, Ukraine

ARTICLE INFO

Received: 24 December 2024 Accepted: 17 June 2025

UDC: 591.481.1-001:57.012.4

CORRESPONDING AUTHOR

e-mail: ivt@dmu.edu.ua Tverdokhlib I. V.

CONFLICT OF INTEREST

The authors have no conflicts of interest to declare.

FUNDING

Not applicable.

DATA SHARING

Data are available upon reasonable request to corresponding author.

Damage to brain tissue and transformation of the microvascular bed after traumatic brain injury determine a wide range of changes in neurons and neuroglial cells, but the dependence of these changes on the localization of damage requires further clarification. The study aims to study the tissue and cellular posttraumatic changes in the structure of the brain entorhinal cortex in rats with various neurocognitive disorders at different times after severe traumatic brain injury. A "shock acceleration model" was used to reproduce severe traumatic brain injury in rats. According to the results of neurological tests, the rats were divided into three groups: the first - animals after trauma with neurocognitive disorders and memory disorders; the second - animals after trauma with neurocognitive disorders without memory disorders; the third comparison group – animals after trauma without neurocognitive disorders. A histological, morphometric and immunohistochemical study of the brain parahippocampal gyrus of the frontal lobe was carried out using the markers β-tubulin, Synaptophysin, GAP43, NCAM1, N-cadherin, GFAP. Statistical processing of the obtained results was carried out in the licensed software package "Statistica v6.1" using parametric and nonparametric methods. The morphological substrate of neurocognitive disorders with memory impairment in the long-term after injury in rats is the irreversible deformation of the cytoarchitectonics of the parahippocampal gyrus and the deepening of the degeneration of neurocytes of the entorhinal cortex due to the blocking of transendothelial transport by astrocytic conglomerates with the destruction of the blood-brain barrier. The progression of neurodegeneration is accompanied by the activation of microglia and leads to the disintegration and migration of macrogliocytes with the formation of an irreversible mosaic astrocytic deficiency, as well as to the formation of glial deposits in the form of couplings around hemocapillaries. The safeguarding of memory function in animals with neurocognitive disorders is carried out by limiting the secondary death of neurocytes and stabilizing the adhesive properties of astroglia of the entorhinal cortex. 10 days after injury, there is an increase in NCAM1 expression with the initiation of cell adhesion, which after 20 days of the experiment leads to axon regeneration and renovation of synaptic activity. This is accompanied by an increase in GAP43 expression by preserved neurocytes with remodeling of presynaptic terminals and restoration of afferentation from the entorhinal cortex to the hippocampal CA1 area 40 days after injury. Thus, compensation for the metabolic and excitotoxic consequences of brain injury is realized through effective neovasculogenesis, limitation of perivascular astrocyte hyperplasia and neuroinflammation, which prevents neurocyte death and leads to activation of synaptic remodeling by GAP43-positive neurons.

Keywords: traumatic brain injury, rats, neurocognitive disorders, entorhinal cortex, morphology.

Introduction

In solving numerous issues related to the treatment and rehabilitation of patients after traumatic brain injury (TBI),

the study of pathomorphological mechanisms that determine the nature of the formation and dynamics of neurocognitive disorders at different times after the injury is of particular interest. After TBI, profound neuronal damage occurs, including activation of apoptotic processes and cell death due to the excitotoxic action of glutamate. Massive secondary neuronal death causes profound neurodegeneration with damage to the blood-brain barrier (BBB), which exacerbates cognitive disorders [4, 9, 27].

Neurocognitive deficiency and memory disorders are primarily caused by damage to nerve cells, but astrocytes, oligodendrocytes, and microglia are also activated in certain affected brain regions [12]. The entorhinal-hippocampal system of neuronal connections plays a crucial role in the formation of long-term memory and in general neurocognitive functions [10]. Located between the neocortex and the hippocampus, the entorhinal cortex serves as the main interface between them and also contains cells involved in spatial navigation and spatial memory. Although the neurons of the hippocampal formation may seem to be only a transit point for the implementation of long-term memory, they actually show great plasticity, manifested mainly through long-term potentiation, which was first discovered in the hippocampus but was later demonstrated in the entorhinal cortex [2, 28].

Current understanding of the structure of the medial and lateral entorhinal cortex suggests that the distribution of neurons and neuropil across II noncellular and III cellular layers is consistent and stable across species, including rodents, primates, and humans [15, 19, 20, 26]. In addition, the pattern of connectivity with the hippocampus also appears to be stable, differing significantly between layers. The outer cellular layers II and III are thought to provide the main input to the hippocampus, while the deep layer V receives input from the hippocampus and subiculum [20, 22, 26].

The use of molecular markers, electrophysiological and anatomical tools has allowed the identification of neurons with layer-specific features and distinct molecular phenotypes. In particular, in rodents, layer II of the medial entorhinal cortex is characterized by a significant presence of pyramidal neurons and large multipolar stellate neurons, while in the lateral cortex, in addition to pyramidal neurons, medium-sized multipolar cells and large fan cells are present [10, 26]. Neurochemically, two distinct types of neurons have been identified in layer II of both subregions of the entorhinal cortex: cells expressing calbindin (which plays a crucial role in preventing neuronal death) and reelin (a glycoprotein involved in synaptic plasticity) [24]. Reelin-positive neurons of the entorhinal cortex project to the dentate gyrus and the CA3 area of the hippocampus; calbindin-positive neurons project to the CA1 region of the hippocampus, the contralateral entorhinal cortex, the olfactory bulb, and the piriform cortex [8, 26].

The morphology of neurons and glial cells of the parahippocampal gyrus is extremely sensitive to various pathological influences, leading to various mnestic disorders even before the appearance of clinically pronounced cognitive disorders [1, 28], but so far the ideas about

the relationship between the sequence of pathogenetic mechanisms of TBI and the nature of cognitive disorders after TBI remain fragmentary. Currently, information about the dynamics of remote post-traumatic changes in intercellular interactions in different parts of the brain is controversial. The information on the sensitivity of various neurons and neuroglial cells to injury and their ability to recover depending on the localization of damage and the nature of hemomicrocirculation rearrangements in the post-traumatic period requires significant clarification.

The aim of the study was to determine tissue and cellular posttraumatic changes in the structure of the brain entorhinal cortex in rats with various neurocognitive disorders at different times after severe traumatic brain injury.

Materials and methods

To TBI modeling in adult nonlinear male rats (aged 4 to 6 months) weighing 300-400 g, the "shock acceleration model" was used [7, 17]. Before the injury, a 2 cm sagittal scalp incision was made along the midline under general anesthesia, exposing the bregma and lambda, and a 1 cm diameter steel coin was fixed using cyanoacrylate glue. Standardized TBI was inflicted by freely falling a 450 g weight from a height of 170 cm. Before TBI modeling, as well as 10, 20, and 40 days after it, rats underwent a comprehensive general and neurological examination, which included: 1) assessment of neurological deficit using the mNSS (Modified Neurological Severity Scores) scale with tests of balance on the tube, asymmetry of paw extension, and placement; 2) open field test; 3) conditioned passive avoidance response test [2].

According to the results of neurological tests, the rats were divided into three groups: the first – animals after TBI with neurocognitive disorders and memory impairments; the second – animals after TBI with neurocognitive disorders without memory impairments; the third comparison group – animals after TBI without neurocognitive disorders. The control group consisted of intact rats aged 4.8±0.6 months and weighing 347±28 g.

All studies with laboratory animals were conducted in compliance with the provisions of the "European Convention for the Protection of Vertebrate Animals Used for Experimental and Other Scientific Purposes" (Strasbourg, 1986), the Vancouver Declaration on Animal Experiments, the Resolution of the First National Congress on Bioethics (Kyiv, 2001), the Regulation on Bioethics of the Ministry of Health of Ukraine dated November 1, 2000. No. 281, Law of Ukraine "On the Protection of Animals from Cruelty" No. 3446-IV of February 21, 2003 in accordance with the EU Council Directive 2010/63/EU on the enforcement of regulations, laws, administrative provisions of the EU Member States on the protection of animals used for scientific purposes [5, 6].

For pathomorphological examination, the rat brain was removed from the cranial cavity after euthanasia, the condition of the soft tissues, relief, presence of hemorrhages

and localization of the slaughter foci were macroscopically assessed. The cerebrum was fixed for 24 hours in a 10 % buffered formalin solution. After fixation, the brain was cut in the frontal plane into slices at the level of the limbic lobe with subsequent manufacture of paraplast blocks. Histological sections 5-7 μ m thick with Nissl staining (thionin with the addition of cresyl violet) or silver impregnation [18, 24] were studied using an AxioSkope A1 light-optical microscope ("Carl Zeiss", Germany).

Immunohistochemical study using primary antibodies (β-tubulin, Synaptophysin, GAP43, NCAM1, N-cadherin, GFAP – "Thermo Scientific", USA) was performed in accordance with the protocol, which included the following steps. Histological sections fixed on slides were unmasked for 20 minutes in a microwave oven at +100 °C in citrate buffer (pH 6.0). To assess the specificity of immunohistochemical staining, control reactions were performed. At the next stage, using the Lab Visison Quanto visualization system ("Thermo Scientific", USA), slides and brain preparations were treated with each reagent for 10 minutes with intermediate washing in Trisbuffered solution. 3,3'-Diaminobenzidine ("DakoCytomation", Denmark) was used as a chromogen. To differentiate cortical structures, the sections were additionally stained with Mayer's hematoxylin according to standards [16, 19].

The studied areas of the brain parahippocampal gyrus were photographed using a digital camera Axiocam ERc 5s ("Carl Zeiss", Germany). The obtained micrographs were processed using the AxioVs40 V 4.6.3.0 software ("Carl Zeiss Imaging Solutions GmbH", Germany). The numerical density of neurocytes, the average diameter of the perikaryon of pyramidal neurons, the numerical density of macrogliocytes, microgliocytes and hemocapillaries of the cortex were calculated using the ImageJ 1.47v software package [21].

The statistical processing of the obtained results was carried out taking into account the Student's t criterion. In the event that the empirical distribution obtained in the study did not correspond to the normal law, the assessment of differences between samples was assessed using the nonparametric Wilcoxon test for related samples and Mann-Whitney for unrelated samples or using the Van der Waerden rank test according to standard procedures [11]. When conducting statistical processing of the obtained quantified results, all necessary calculations were performed in the Excel spreadsheet using the appropriate formulas and using the licensed software package Statistica v6.1 (Statsoft Inc., USA) (serial number AGAR909E415822FA).

Results

The cytomyeloarchitectonics of the parahippocampal gyrus in rats after TBI varied significantly depending on the degree of neurocognitive disorders and the duration of the post-traumatic period. Histological examination of the entorhinal cortex in the anterior part of the gyrus in animals of the first group 10 days after injury showed sharp damage to the cellular composition of the gray matter, as well as critical neurodegenerative and destructive changes, which

led to persistent deformation of the cellular and non-cellular layers of the cortex. The typical five-layer structure of the entorhinal cortex was preserved only on a small part of its length; in most cases, partial or complete dissociation of the II and III layers of neurons with a corresponding thinning of the cortex without the formation of foci of astrocytic gliosis was observed. In the I and IV non-cellular layers of the cortex, numerous deformed dilated microvessels were observed, mainly of the afferent portion of the hemocirculation. Signs of diffuse intercellular and perivascular edema, damage to microvessels, massive cell death of neurocytes, and variable dystrophic changes in neurons were detected after 20 and 40 days of the post-traumatic period, and in some cases the degree of neurodegeneration increased, which indicated the irreversible nature of the pathomorphosis of the changes in the entorhinal cortex (Fig. 1).

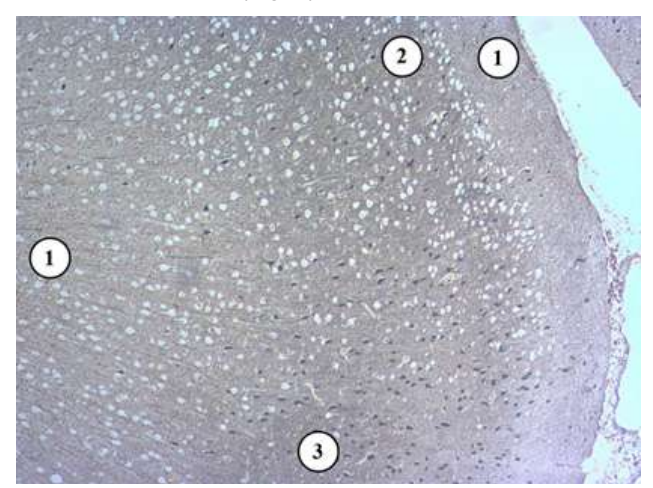


Fig. 1. The rat entorhinal cortex in the first experimental group 40 days after TBI. Inflammatory changes in the neuropil of the I and IV non-cellular layers (1), death of neurocytes of the II layer (2), dystrophic changes in neurocytes and edema in the III cellular layer (3). Silver impregnation. ×40.

In animals of the second experimental group, 10 days after injury, the typical layered structure of the entorhinal cortex was preserved along the entire length of the parahippocampal gyrus. Areas of deformation of the cortical layers and foci of astrocytic gliosis were found in limited numbers and were relatively small in size. The thinning of the cortex occurred due to massive neuronal death in the wide III layer and the variable thickness of the V layer, while in the dense II cellular layer, neurocyte apoptosis was less intense. 10 days after injury, manifestations of moderate edema with damage to hemocapillaries and degenerative changes in various types of neurons were noted. The neuropil of the I and IV non-cellular layers of the cortex contained deformed dilated microvessels, and in some cases, smallfocal hemorrhages were observed. After 20 and 40 days of the post-traumatic period, the cytoarchitectonics of the cortex in this group of animals did not significantly change compared to the previous observation period, but the signs of neuroinflammation were noticeably reduced.

Vol. 31, №3, Page 19-28

In animals of the comparison group, 10 days after TBI, the pathomorphological changes of the entorhinal cortex were significantly inferior in severity to those lesions observed in animals of the first and second experimental groups. A typical five-layered structure of the cortex was observed along the entire length of the parahippocampal gyrus, the thickness was relatively uniform, foci of astrocytic gliosis were rarely detected, and the manifestations of neuroinflammation and neurodegeneration were reduced during the studied period of the post-traumatic period (Fig. 2).

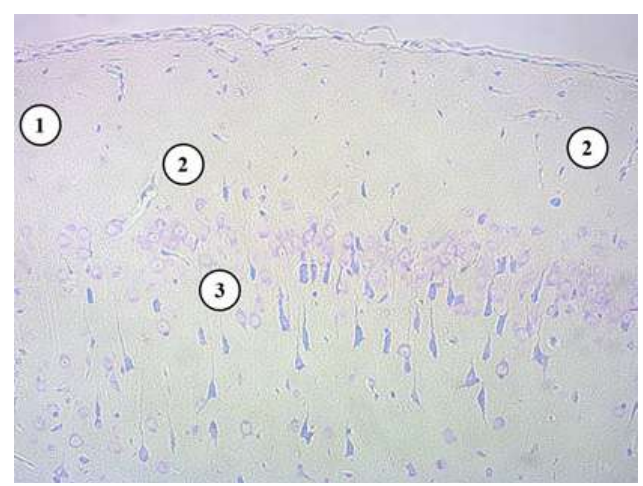


Fig. 2. The rat entorhinal cortex in the comparison group 10 days after TBI. Neuropil of the I non-cellular layer (1), hemocapillaries (2), dense arrangement of neurocytes of the II cellular layer (3). NissI staining. ×200.

The post-traumatic dynamics of the neuronal death of the entorhinal cortex was not the same in different cellular layers of the cortex of the experimental animals and depended on the nature of the neurocognitive disorders. In the animals of the first group, after 10 days of the experiment, massive apoptosis of neurons was observed, which led to the formation of areas of dissociation of the II and III layers of the cortex. After 20 and 40 days after the injury, the apoptotic process continued and spread to neurons of the V layer of the cortex. In animals of the second experimental group, 10 days after injury, apoptotic death was observed mainly in layers III and V of the cortex, while in the second cell layer, apoptosis of neurocytes was limited. It is worth noting that the preservation of layer II neurons, which are the main afferents for the perforant pathway to the dentate gyrus and the CA1 area of the hippocampus, significantly distinguished the nature of neuronal death in these animals from the group of animals with memory impairment. 20 and 40 days after TBI, animals with preserved memory showed a significant decrease in the frequency of apoptosis. In rats of the comparison group, a slight frequency of apoptotic death of neurocytes was observed 10 days after TBI and subsequently became even more limited. Necrotically altered neurons were detected in individual observations in the first experimental group 10 days after injury, mainly in the II layer of the entorhinal cortex near the damaged microvessels. In the second group of animals and in the comparison group, necrotic changes were not observed at any of the studied time points. Manifestations of neurocyte autophagy were observed in individual observations in all groups of rats; their frequency did not change during the post-traumatic period.

Quantitative assessment of the dynamics of the content of neurons in all cell layers of the entorhinal cortex using immunohistochemical identification of neurocytes with β -tubulin showed a sharp decrease in the total numerical density of neurons relative to the normal level in rats of the first and second groups 10 days after injury – by 47.8 % (p<0.05) and 33.9 % (p<0.05), respectively, while in the comparison group the parameter decreased moderately – by 17.8 % (p<0.05). At the same time, in the first and second groups of animals, the numerical density of neurons fluctuated in a limited range at all times of the experiment and was statistically significantly inferior to the indicator of the comparison group (Table 1).

Table 1. Numerical density of neurocytes in the entorhinal cortex, ×10² mm⁻² (M±m).

Time after	Study groups		
injury	First	Second	Comparison
10 days	16.83±1.97 * **	21.31±2.88 * **	26.51±2.44 *
20 days	13.40±1.64 * **	20.13±2.35 * **	28.20±3.65
40 days	9.12±1.59 * **	20.72±1.87 * **	27.52±2.33

Notes: * – p<0.05 when compared with the value in the intact group $(32.21\pm2.63\times10^2\,\text{mm}^2)$; ** – p<0.05 when compared with the value corresponding to the term in the comparison group.

20 and 40 days after TBI in rats without neurocognitive disorders, a gradual densification of neurons and their approximation to normal values was observed due to the limitation of the apoptotic process and the reduction of edema and other tissue signs of neuroinflammation. In animals of the first experimental group, in the long post-traumatic period, there was a decrease in the numerical density of neurons relative to the indicator of intact animals: 20 days after injury - by 58.4 % (p<0.05), 40 days - by 71.7 % (p<0.05). Such negative dynamics of the content of neurons reflected the deepening of the apoptotic process in the entorhinal cortex during the studied period of the experiment. In animals of the second group, the numerical density of neurons in the parahippocampal gyrus 20 days after injury was 37.6 % (p<0.05) lower than the normal level, and 40 days after injury by 35.7 % (p<0.05), not significantly changing compared to the 10th day after injury, which indicated the limitation of apoptosis during the long-term post-traumatic period.

The total density and morphology of neurocytes of different shapes of layers II and III of the entorhinal cortex, located in the anterior part of the parahippocampal gyrus, significantly differed in animals of the studied groups and depended on the duration of the post-traumatic period. In particular, 10 days after TBI in animals with neurocognitive deficit, those neurons that did not undergo apoptosis retained a characteristic conical shape, but often contained signs of

chromatolysis and vacuolization of perikaryons. A significant part of neurons in the V layer of the cortex was represented by hypoxically damaged densified hyperchromic forms with signs of partial chromatolysis and reduced dendrites. During the subsequent post-traumatic period, heteromorphic manifestations of neurodegeneration in animals of the first group intensified, while in animals without memory disorders the degree of neuronal damage noticeably decreased. The most pronounced signs of restoration of neurocyte morphology in animals of this group were observed in the II and III layers of the entorhinal cortex, in which the perforant path of the hippocampus originates. In animals of the comparison group, against the background of moderately pronounced apoptotic and neuroinflammatory processes, 10 days after injury, the appearance of ischemically altered neurons with a densified perikaryon, dark cytoplasm and thinned dendrites was observed. Individual neurocytes of layers III and V had vacuolated cytoplasm with lysis of Nissl substance, however, after 40 days of the post-traumatic period, damaged neurons were found in limited numbers.

Morphometric analysis showed that the size of neurons of the cell layers of the entorhinal cortex 10 days after TBI did not significantly differ between the three experimental groups, but were significantly inferior to the value of the group of intact rats (Table 2).

Table 2. Average diameter of the perikaryon of neurons of the entorhinal cortex, μm (M $\pm m$).

Time after	Study groups		
injury	First	Second	Comparison
10 days	4.063±0.386*	4.082±0.318*	4.184±0.341*
20 days	5.452±0.314	5.356±0.401	5.498±0.415
40 days	5.587±0.353	5.515±0.415	5.458±0.433

Note: * – p<0.05 when compared with the value in the intact group $(9.224\pm1.171 \mu m)$.

At this period, the most significant decrease in the diameter of the perikaryon of neurocytes that did not undergo apoptosis was observed in the first group of animals - by 29.4 % (p<0.05). In animals of the second group, the parameter was 25.8 % lower than the normal level (p<0.05), in animals of the comparison group - 25.2 % (p<0.05). After 20 days, in animals of the first group, the parameter did not change compared to the previous period, being 28.4 % (p<0.05) lower than the indicator of intact animals. In animals of the second group, a noticeable increase in the size of neurocytes was observed, although after 20 days the parameter was 21.6 % (p<0.05) lower than the normal level. In animals of the comparison group, a gradual recovery of the size of neurocytes occurred during this period. After 40 days after injury, in animals of the first group, the average diameter of the perikaryon remained 22.3 % (p<0.05) smaller than the control, in animals of the second group and the comparison group, the corresponding parameters did not differ statistically from the indicator of intact animals.

Immunohistochemical study of the synaptic marker

GAP43, which is associated with the regenerative capacity of axons, showed only background staining of this marker in the entorhinal cortex in intact rats and in groups of animals with neurocognitive disorders 10 days after injury. After 20 and 40 days of the experiment, in animals of the second group and the comparison group, activation of GAP43 expression was observed in the III and V cell layers of the entorhinal cortex, as well as in the neuropil of the wide IV layer (Fig. 3). This nature of the expression of GAP43 molecules indicated remodeling of the presynaptic terminals of the axons of those neurons whose perikaryons are located in the III layer. The greatest increase in GAP43 expression was detected in the white matter of the parahippocampal gyrus and adjacent areas of the hippocampus, which contain components of the perforant pathway.

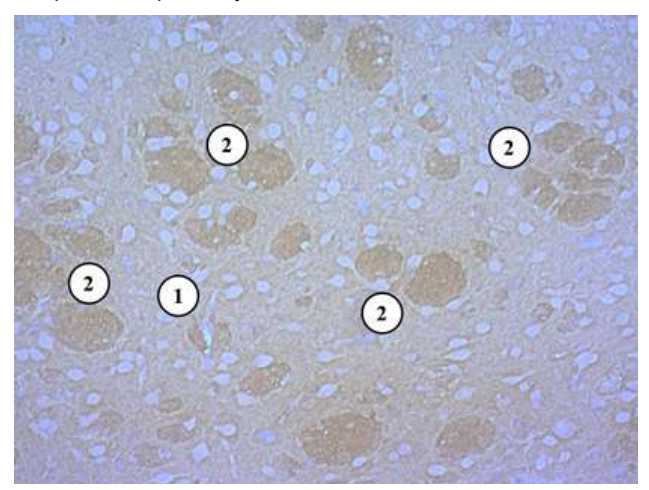


Fig. 3. The rat entorhinal cortex in the second experimental group 20 days after TBI. Damaged hemocapillary (1), group of GAP43-positive processes of neurocytes (2). Immunohistochemistry with antibodies against GAP43. Additional staining with Mayer's hematoxylin. ×200.

The intensity of the immunohistochemical label of the CD56 and N-cadherin markers on the cytolemma of neurocytes of the entorhinal cortex was similar to the nature of the expression of these markers on the surface of intact neurons. The greatest intensity of specific staining was observed in the II laver of neurons in all animals after exposure to TBI, although in the first experimental group it was significantly inferior to the comparison group due to a sharp decrease in the density of neurons due to their apoptotic death after injury. In animals of the second group, the difference with the comparison group was significantly smaller. After 20 days, the expression of markers in the parahippocampal gyrus of rats of the first group became even lower than at the previous period of the experiment, and continued to decrease until the 40th day. In general, the number of CD56- and N-cadherin-positive neurocytes in rats of the second group and the comparison group increased during the 40th day of the post-traumatic period in layers II and III, remaining unchanged in layer V of the entorhinal cortex.

Vol. 31, №3, Page 19-28

The study of the glial component of the cortex of the parahippocampal gyrus revealed significant pathomorphological changes in macrogliocytes both in terms of the nature of their spatial redistribution and proliferative properties. After 10 days after injury, a significant accumulation of astrocytes immunohistochemically labeled with the GFAP marker was observed around microvessels against the background of perivascular edema in groups of animals with neurocognitive disorders. In the spaces between microvessels, on the contrary, the density of fibrous astrocytes was significantly lower than in similar areas of the cortex of intact rats. In these areas, cells with long processes separated from each other were found, which did not contact neighboring astrocytes (Fig. 4, 5).

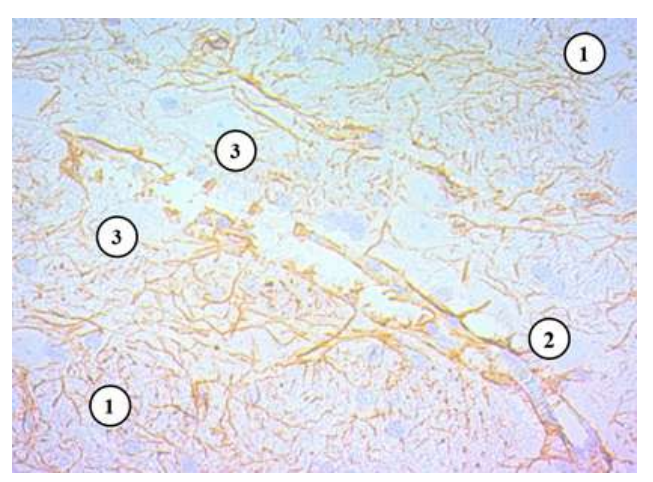


Fig. 4. The rat entorhinal cortex in the first experimental group 10 days after TBI. Fibrous astrocyte processes (1), astrocyte layering on the hemocapillary wall (2), destruction of the hemocapillary wall (3). Immunohistochemistry with antibodies against GFAP. Additional staining with Mayer's hematoxylin. ×400.

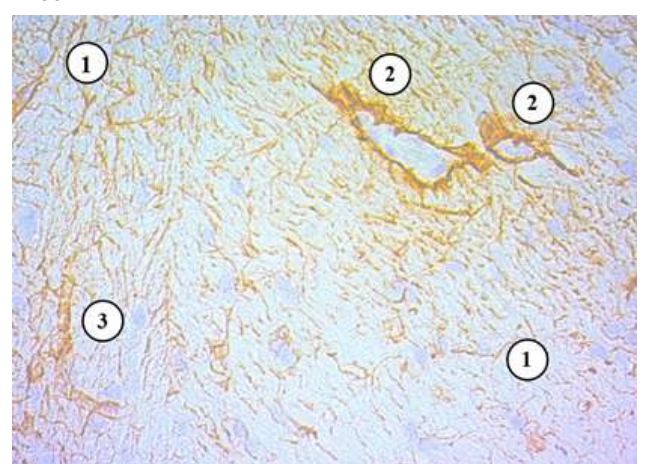


Fig. 5. The rat entorhinal cortex in the second experimental group 10 days after TBI. Fibrous astrocyte processes (1), astrocyte layering on the hemocapillary wall (2), continuous hemocapillary walls (3). Immunohistochemistry with antibodies against GFAP. Additional staining with Mayer's hematoxylin. ×400.

Massive autophagy of gliocytes occurred in areas of

intervascular astrocytic deficiency. In the long-term post-traumatic period, animals of the second group, unlike rats of the first group, had limited perivascular astrocyte hyperplasia. A significant part of microvessels on their surface had normal structures characteristic of typical BBB.

When studying the adhesive properties of astroglia using markers CD56 (NCAM1) and N-cadherin, an uneven distribution of the immunohistochemical label in the entorhinal cortex of animals in all studied groups was revealed. 10 days after injury, protoplasmic astrocytes around hemocapillaries actively expressed both of these markers on their surface, while in the neuropil between microvessels, CD56-negative and N-cadherin-negative fibrous astrocytes were visualized, separated from each other. After 20 and 40 days, the mosaic nature of the expression of CD56 and N-cadherin markers was preserved in the first group of animals. In animals of the second group and the comparison group, astrocytes in the spaces between microvessels demonstrated increased expression of cell adhesion markers.

Quantitative assessment of macrogliocyte density using the glial marker GFAP showed that 10 days after the start of the experiment, the numerical density of cells in the entorhinal cortex was inferior to the normal value in the first group of animals by 28.3 % (p<0.05), in the second - by 24.1 % (p<0.05), in the comparison group – by 17.6 % (p<0.05). 20 days after the injury, the degree of astrocytic deficiency in the animals of the first experimental group increased; in the animals of the second group - it did not change; in the animals of the comparison group - it became less pronounced compared to the previous period of the study (Table 3). 40 days after TBI, in the animals of the first group, the parameter was inferior to the indicator of intact animals by 45.5 % (p<0.05), and to the indicator of the comparison group – by 41.7 % (p<0.05). During this period, the numerical density of macrogliocytes in animals of the second group increased relative to the previous observation period, yielding to the indicator of intact animals by 15.5 % (p<0.05) and not differing to a statistically significant degree from the value in the comparison group.

Table 3. Numerical density of macrogliocytes in the entorhinal cortex, ×10² mm⁻² (M±m).

	, ,		
Time after		Study groups	
injury	First	Second	Comparison
10 days	134.2±14.7 *	142.5±18.0 *	154.3±13.3 *
20 days	113.4±16.4 * **	147.1±15.2 *	168.4±14.9
40 days	102.8±12.2 * **	158.7±19.6	175.1±20.4

Notes: * - p<0.05 when compared with the value in the intact group (187.2±21.7 ×10² mm⁻²); ** - p<0.05 when compared with the value corresponding to the term in the comparison group.

After TBI in animals of all studied groups, morphological changes in microgliocytes in the cellular and non-cellular layers of the entorhinal cortex varied significantly depending on the degree of neurocognitive deficit. The majority of microgliocytes had a flattened shape and developed processes, located mainly in those areas of the neuropil in which astrocyte

thinning and disintegration were observed. In animals with neurocognitive deficit, in contrast to rats of the comparison group, typical transit macrophages and lymphocytes were located perivascularly near neurons, which was associated with the elimination of the remnants of apoptotically altered neurocytes after injury. At the end of the studied post-traumatic period, transit macrophages remained in significant numbers in animals of the first group, while in the second group and the comparison group they were rarely found.

Morphometric analysis of the numerical density of microgliocytes in the entorhinal cortex in all studied groups of animals revealed a significant increase in the parameter 10 days after injury compared to the intact group (Table 4): in the first group – by 72.0 % (p<0.05), in the second – by 65.3 % (p<0.05), in the comparison group – by 51.7 % (p<0.05).

Table 4. Numerical density of microgliocytes of the entorhinal cortex, ×10² mm⁻² (M±m).

Time after	Study groups		
injury	First	Second	Comparison
10 days	2.032±0.255 *	1.951±0.270 *	1.798±0.215 *
20 days	2.126±0.178* **	1.682±0.158 * **	1.374±0.127 *
40 days	1.891±0.233 * **	1.564±0.134 * **	1.227±0.159

Note: * -p < 0.05 when compared with the value in the intact group $(1.182\pm0.167 \times 10^2 \text{ mm}^2)$; ** -p < 0.05 when compared with the value corresponding to the term in the comparison group.

After 20 days, the parameter in the animals of the first group did not change compared to the previous observation period, exceeding the norm by 79.7 % (p<0.05). In the animals of the second group, there was a decrease in the density of microgliocytes, but it exceeded the intact value by 42.4 % (p<0.05). In the animals of the comparison group, the most pronounced reduction of the parameter was observed compared to the previous period: 20 days after the injury, the numerical density of microgliocytes exceeded the normal level by only 16.1 % (p<0.05) and after 40 days it did not differ statistically from it. Unlike the comparison group, 40 days after TBI in animals of the first group the parameter exceeded the normal value by 60.2 % (p<0.05), in animals of the second group - by 32.2 % (p<0.05), and in both groups of animals with neurocognitive deficit the content of microgliocytes statistically significantly exceeded the indicator of the comparison group.

The microvascular component in the parahippocampal gyrus showed various alterative, adaptive and compensatory changes, which significantly depended on the term of the post-traumatic period and differed in the three studied groups of animals. In particular, in animals with neurocognitive disorders 10 days after the injury, massive accumulations of protoplasmic astrocytes were visualized using the GFAP marker on the outer surface of damaged hemocapillaries in the form of dense couplings.

A significant number of damaged arterioles and hemocapillaries with signs of stasis were observed, many vessels had partially or completely obliterated lumens. Microvessels with signs of intravascular microthrombosis surrounded by small foci of secondary hemorrhages, with plasmatic infiltration of the capillary wall and perivascular space were also detected. Single microvessels with necrosis, destruction or fragmentation of the wall were encountered. Some hemocapillaries or endothelial strands did not form connections with astrocytes characteristic of the BBB. In addition to hemocapillaries with damaged structure, a significant increase in the number of newly formed hemocapillaries accompanied by astrocytic glia, with a typical structure of the endothelial wall and normal blood filling was observed.

20 days after injury, a significant number of damaged microvessels remained in the entorhinal cortex of animals with neurocognitive disorders, indicating the presence of a long-term neurodestructive process. Unlike the first group of animals, in the second group, during the long post-traumatic period, numerous newly formed hemocapillaries with fullfledged BBB structures, as well as endothelial groups and outgrowths were observed, indicating the activation of neovasculogenesis. 40 days after injury, a moderate number of pathologically altered microvessels with astrocyte layers on the outer surface remained; single fragmented hemocapillaries and small foci of diapedetic hemorrhages were observed. The greatest intensity of neovasculogenesis in the entorhinal cortex of animals without neurocognitive disorders was observed 10 days after injury; after 20 and 40 days of the experiment, the number of immature newly formed hemocapillaries became noticeably smaller, and the total density of microvessels approached the normal level.

Morphometric study of blood microvessels in the parahippocampal gyrus showed that 10 days after TBI, the total numerical density of intact and pathologically altered microvessels in animals of the first group exceeded the normal value by 58.8 % (p<0.05), in the second group by 48.5 % (p<0.05), and in the comparison group by 42.2 % (p<0.05). After 20 days from the beginning of the experiment, the numerical density of microvessels in animals with neurocognitive deficit did not significantly change compared to the level at the previous period of the experiment, while in animals of the comparison group the parameter significantly decreased and normalized (Table 5). 40 days after TBI, all animals showed relative normalization of the total numerical density of blood microvessels, although the ratio between damaged, normal, and newly formed hemocapillaries differed significantly in the three experimental groups and depended on the degree of neurocognitive deficit.

Table 5. Numerical density of hemocapillaries in the entorhinal cortex, mm⁻² (M±m).

Time after	Study groups		
injury	First	Second	Comparison
10 days	67.82±8.14 *	63.44±10.49 *	60.71±9.87 *
20 days	57.26±5.37 * **	53.32±6.27 * **	45.15±5.32
40 days	47.93±8.30	46.57±7.02	44.67±7.36

Note: * - p<0.05 when compared with the value in the intact group (42.71±3.54 mm 2); ** - p<0.05 when compared with the value corresponding to the term in the comparison group.

Vol. 31, №3, Page 19-28 **25**

Discussion

Focal brain injuries cause persistent cognitive impairments, the types of which are relatively easy to understand based on modern neuroanatomical concepts [10, 18]. It is noteworthy that after TBI, the inflammatory reaction, glutamate toxicity, and activation of apoptotic processes against the background of microcirculatory damage cause massive secondary neuronal death, meanwhile leading to neurodegeneration, which causes aggravation of cognitive impairments [4, 9]. In our study, we analyzed reversible and stable morphological changes in the parahippocampal gyrus of rats for 40 days after the application of standardized symmetric severe TBI in the shock acceleration model. It has been shown that in animals with neurocognitive disorders, a significant increase in the number of newly formed hemocapillaries with a typical endothelial wall structure is observed, however, a large number of densely packed protoplasmic astrocytes are found on the surface of most damaged capillaries. In these cases, astroglia form cell layers on the surface of microvessels in the form of dense couplings, which is accompanied by blocking transendothelial transport. In our opinion, the presence of such pathologically altered hemocapillaries in the entorhinal cortex may be one of the components of persistent neurocognitive deficit.

Our data are confirmed by the results of many researchers who have established the dependence of the combined neurotoxic effect of glutamate and acetylcholine on the degree of destruction of neurons and their processes due to TBI. These neurotransmitters exhibit the greatest neurotoxicity in those brain structures where they are localized together – the entorhinal-hippocampal complex, basal forebrain and limbic cortex [10].

According to our results, the prevention of mnestic damage in animals with neurocognitive disorders is associated with the limitation of neuronal death and the stabilization of the adhesive properties of astroglia in the entorhinal cortex, which makes it impossible to block transendothelial transport by astrocytic layers around hemocapillaries while maintaining the integrity of the bloodbrain barrier. Immunohistochemically, it has been shown that after injury, there is an increase in NCAM1 expression with the initiation of cell adhesion and leads to axon regeneration and restoration of synaptic activity. This is accompanied by an increase in GAP43 expression by preserved neurocytes with remodeling of presynaptic terminals and restoration of afferentation from the entorhinal cortex to the CA1 area of the hippocampus 40 days after injury.

The interpretation of this fact is of particular importance taking into account the literature data on the specific distribution of calbindin- and reelin-positive neurons in the II cell layer of the cortex in rodents: in the medial entorhinal cortex, both types of neurocytes are grouped into spots, while

in the lateral cortex they form two sublayers – reelin (IIa) and calbindin (IIb) [8, 26]. It is calbindin-positive neurons that project to the CA1 region of the hippocampus [10], which, in our opinion, explains the appearance of axon bundles with enhanced GAP43 expression and the restoration of afferentation in the entorhinal-hippocampal system as one of the factors preserving memory function in animals with neurocognitive disorders.

Conclusions

- 1. Irreversible deformation of the cytoarchitectonics of the parahippocampal gyrus and deepening of the degeneration of neurocytes of the entorhinal cortex due to the blocking of transendothelial transport by astrocytic conglomerates with destruction of the blood-brain barrier within 40 days after injury are a morphological substrates of neurocognitive disorders with memory impairments in the long-term period after TBI.
- 2. 20 days after injury in rats with neurocognitive disorders and memory impairments, the numerical density of neurocytes of the entorhinal cortex decreases by 58.4~% (p<0.05), after 40 days by 71.7 % (p<0.05). This is accompanied by the chronicity of neuroinflammation with the activation of neuronal apoptosis and gliocyte autophagy, diffuse axonal damage and inhibition of synaptic transmission.
- 3. The progression of neurodegeneration is accompanied by the activation of microglia and leads to the disintegration and migration of macrogliocytes with the formation of irreversible mosaic astrocytic deficiency, as well as the formation of glial layers in the form of couplings around hemocapillaries.
- 4. The preservation of memory function in animals with neurocognitive disorders is carried out by limiting the secondary death of neurocytes and stabilizing the adhesive properties of astroglia of the entorhinal cortex, which prevents the formation of astrocytic couplings around newly formed hemocapillaries while maintaining the integrity of the bloodbrain barrier. 10 days after injury, there is an increase in NCAM1 expression with the initiation of cell adhesion, which after 20 days of the experiment leads to axon regeneration and restoration of synaptic activity. This is accompanied by an increase in GAP43 expression by preserved neurocytes with remodeling of presynaptic terminals and restoration of afferentation from the entorhinal cortex to the CA1 area of the hippocampus 40 days after injury.
- 5. Compensation for the metabolic and excitotoxic consequences of TBI in animals without neurocognitive disorders is realized through effective neovasculogenesis, limitation of perivascular astrocyte hyperplasia and neuroinflammation 10 days after injury with its subsequent reduction during the 40 days of the experiment, which prevents neurocyte death and leads to activation of synaptic remodeling by GAP43-positive neurons.

References

[1] Ahnaou, A., Moechars, D., Raeymaekers, L., Biermans, R., Manyakov, N. V., & Bottelbergs, A. (2017). Emergence of early alterations in network oscillations and functional connectivity in a tau seeding mouse model of Alzheimer's dis-

- ease pathology. Sci Rep, 7(1), 14189-14194. doi: 10.1038/s41598-017-13839-6
- [2] Amani, M., Lauterborn, J. C., Le, A. A., Cox, B. M., Wang, W., & Quintanilla J. (2021). Rapid aging in the perforant path projections to the rodent dentate gyrus. *J Neurosci*, 41(1), 2301-2312. doi: 10.1523/JNEUROSCI.2376-20.2021
- [3] Bureš, J., Burešová, O., & Huston, J. P. (2016). Techniques and basic experiments for the study of brain and behavior. Second edition. Amsterdam – New York: Elsevier science publishers BV.
- [4] Chary, K., Nissi, M. J., Nykänen, O., Manninen, E., Rey, R. I., Shmueli, K., Sierra, A., & Gröhn, O. (2021). Quantitative susceptibility mapping of the rat brain after traumatic brain injury. NMR Biomed, 34(2), e4438. doi: 10.1002/nbm.4438
- [5] Directive 2010/63/EU of the European Parliament and of the Council of 22 September 2010 on the protection of animals used for scientific purposes. (2010). Official Journal of the European Union, 53(L276), 33-79.
- [6] de l'Europe, C. (1986). European Convention for the protection of vertebrate animals used for experimental and other scientific purposes/Convention européenne sur la protection des animaux vertébrés utilisés à des fins expérimentales ou à d'autres fins scientifiques:[Strasbourg, 18. III. 1986]. Conseil de l'Europe Section des publications.
- [7] Foda, M. A., & Marmarou, A. (1994). A new model of diffuse brain injury in rats. Part II: Morphological characterization. J Neurosurg, 80(2), 301-313. doi: 10.3171/jns.1994.80.2.0301
- [8] Fuchs, E. C., Neitz, A., Pinna, R., Melzer, S., Caputi, A., & Monyer, H. (2016). Local and distant input controlling excitation in layer II of the medial entorhinal cortex. *Neuron*, 89(1), 194-208. doi: 10.1016/j.neuron.2015.11.029
- [9] Griffiths, D. R., Law, L. M., Young, C., Fuentes, A., Truran, S., Karamanova, N., ... & Lifshitz, J. (2022). Chronic Cognitive and Cerebrovascular Function after Mild Traumatic Brain Injury in Rats. *J Neurotrauma*, 39(19-20), 1429-1441. doi: 10.1089/neu.2022.0015
- [10] Hernández-Frausto, M., & Vivar, C. (2024). Entorhinal cortex-hippocampal circuit connectivity in health and disease. Front Hum Neurosci, 18(1), 1448791. doi: 10.3389/ fnhum.2024.1448791
- [11] Hruzieva, T. S., Lekhan, V. M., Ohniev, V. A., Haliienko, L. I., Kriachkova, L. V., & Palamar, B. I. (2020). Біостатистика [Biostatistics]. Вінниця: Нова книга=Vinnytsia: New Book.
- [12] Macks, C., Jeong, D., Bae, S., Webb, K., & Lee, J. S. (2022). Dexamethasone-Loaded Hydrogels Improve Motor and Cognitive Functions in a Rat Mild Traumatic Brain Injury Model. *Int J Mol Sci*, 23(19), 11153. doi: 10.3390/ijms231911153
- [13] Magaki, S., Hojat, S. A., Wei, B., So, A., & Yong, W. H. (2019). An Introduction to the Performance of Immunohistochemistry. *Methods Mol Biol*, 1897, 289-298. doi: 10.1007/978-1-4939-8935-5 25
- [14] Marmarou, A. I., Foda, M. A., & van den Brink, W. (1994). A new model of diffuse brain injury in rats. Part I: Pathophysiology and biomechanics. *J Neurosurg*, 80(2), 291-300. doi: 10.3171/jns.1994.80.2.0291
- [15] Modo, M., Sparling, K., Novotny, J., Perry, N., Foley, L. M., Hitchens, T. K. (2023). Mapping mesoscale connectiv-

- ity within the human hippocampus. *Neuroimage*, 282(1), 120406. doi: 10.1016/j.neuroimage.2023.120406
- [16] Mulish, M., & Welsh, U. (2010). Romeis Mikroscopiche technic. Heidelberg: Spektrum Akademischer Verlag. doi: 10.1007/978-3-8274-2254-5
- [17] Nguyen, T. (2022). Immunohistochemistry: A Technical Guide to Current Practices. Cambridge: Cambridge University Press.
- [18] Nie, L., He, J., Wang, J., Wang, R., Huang, L., Jia, L., ... & Wang, J. (2023). Environmental Enrichment for Stroke and Traumatic Brain Injury: Mechanisms and Translational Implications. Compr Physiol, 14(1), 5291-5323. doi: 10.1002/cphy.c230007
- [19] Ohara, S., Onodera, M., Simonsen, O. W., Yoshino, R., Hioki, H., & Iijima, T. (2018). Intrinsic projections of layer Vb neurons to layers Va, III, and II in the lateral and medial entorhinal cortex of the rat. *Cell Rep*, 24(1), 107-116. doi: 10.1016/j.celrep.2018.06.014
- [20] Ohara, S., Yoshino, R., Kimura, K., Kawamura, T., Tanabe, S., & Zheng, A. (2021). Laminar organization of the entorhinal cortex in macaque monkeys based on cell-type-specific markers and connectivity. Front Neural Circuits, 15(1), 790116. doi: 10.3389/fncir.2021.790116
- [21] Poslavska, О. V. (2016). Визначення лінійних розмірів та площ окремих морфологічних об'єктів на мікрофотографіях за допомогою програми ImageJ. [Determination of linear dimensions and areas of individual morphological objects on photomicrographs using the ImageJ program]. Морфологія=Morphologia, 10(3), 377-381.
- [22] Roy, D. S., Kitamura, T., Okuyama, T., Ogawa, S. K., Sun, C., & Obata, Y. (2017). Distinct neural circuits for the formation and retrieval of episodic memories. *Cell*, 170(1), 1000-1012. doi: 10.1016/j.cell.2017.07.013
- [23] Song, H., Chen, C., Kelley, B., Tomasevich, A., Lee, H., Dolle, J. P., ... & Smith, D. H. (2022). Traumatic brain injury recapitulates developmental changes of axons. *Prog Neu*robiol, 217, 102332. doi: 10.1016/j.pneurobio.2022.102332
- [24] Stranahan, A. M., Haberman, R. P., & Gallagher, M. (2011). Cognitive decline is associated with reduced reelin expression in the entorhinal cortex of aged rats. *Cereb Cortex*, 21(1), 392-400. doi: 10.1093/cercor/bhq106
- [25] Suvarna, S. K., Layton, C., & Bancroft, G. D. (2019). Bancroft's Theory and Practice of Histological Techniques, 8th Edition. Elsevier. doi: 10.1016/B978-0-7020-6864-5.00008-6
- [26] Witter, M. P., Doan, T. P., Jacobsen, B., Nilssen, E. S., & Ohara, S. (2017). Architecture of the entorhinal cortex a review of entorhinal anatomy in rodents with some comparative notes. *Front Syst Neurosci*, 11(46), 1-12. doi: 10.3389/fnsys.2017.00046
- [27] Yang, Z., Zhu, T., Pompilus, M., Fu, Y., Zhu, J., Arjona, K., ... & Febo, M. (2021). Compensatory functional connectome changes in a rat model of traumatic brain injury. *Brain Commun*, 3(4), 244. doi: 10.1093/braincomms/fcab244
- [28] Zhang, K., Chen, L., Li, Y., Paez, A. G., Miao, X., & Cao, D. (2023). Differential laminar activation dissociates encoding and retrieval in the human medial and lateral entorhinal cortex. *J Neurosci*, 43(1), 2874-2884. doi: 10.1523/JNEU-ROSCI.1488-22.2023

ДИНАМІКА СТРУКТУРНИХ ПЕРЕБУДОВ В ЕНТОРИНАЛЬНІЙ КОРІ ЩУРІВ З РІЗНИМИ НЕЙРОКОГНІТИВНИМИ РОЗЛАДАМИ ПІСЛЯ ЧЕРЕПНО-МОЗКОВОЇ ТРАВМИ

Мізякіна К. В., Дзяк Л. А., Твердохліб І. В.

Ушкодження мозкової тканини та перетворення мікросудинного русла після черепно-мозкової травми визначають

Vol. 31, №3, Page 19-28 **27**

широкий спектр змін нейронів і клітин нейроглії, проте залежність цих змін від локалізації ушкоджень потребує подальших уточнень. Метою дослідження було визначення тканинних і клітинних посттравматичних змін структури енторинальної кори головного мозку щурів з різними нейрокогнітивними розладами у різні терміни після тяжкої черепно-мозкової травми. Для відтворення тяжкої черепно-мозкової травми у щурів застосовували «модель ударного прискорення». За результатами неврологічних тестів щури були розподілені на три групи: перша – тварини після травми з нейрокогнітивними розладами і порушеннями пам'яті; друга — тварини після травми з нейрокогнітивними розладами без порушень пам'яті; третя група порівняння — тварини після травми без нейрокогнітивних розладів. Проводили гістологічне, морфометричне та імуногістохімічне дослідження парагіпокампальної звивини з використанням маркерів β-tubulin, Synaptophysin, GAP43, NCAM1, N-cadherin, GFAP. Статистичну обробку отриманих результатів проводили в ліцензійному програмному пакеті «Statistica v6.1» з використанням параметричних і непараметричних методів. Морфологічним субстратом нейрокогнітивних розладів з порушеннями пам'яті у віддаленому періоді після травми у щурів є незворотна деформація цитоархітектоніки парагіпокампальної звивини і поглиблення дегенерації нейроцитів енторинальної кори внаслідок блокування трансендотеліального транспорту астроцитарними конгломератами з деструкцією гематоенцефалічного бар'єру. Прогресування нейродегенерації супроводжується активацією мікроглії і призводить до дезінтеграції та міграції макрогліоцитів з формуванням незворотного мозаїчного астроцитарного дефіциту, а також до утворення гліальних нашарувань у вигляді муфт навколо гемокапілярів. Збереження функції пам'яті у тварин з нейрокогнітивними розладами здійснюється за рахунок обмеження вторинної загибелі нейроцитів і стабілізації адгезивних властивостей астроглії енторинальної кори. Через 10 діб після травми відбувається зростання експресії NCAM1 з ініціацією клітинної адгезії, що через 20 діб експерименту призводить до регенерації аксонів і відновлення синаптичної активності. Це супроводжується зростанням експресії GAP43 збереженими нейроцитами з ремоделюванням пресинаптичних терміналей і відновленням аферентації від енторинальної кори до ділянки СА1 гіпокампа через 40 діб після травми. Таким чином, компенсація метаболічних і ексайтотоксичних наслідків черепно-мозкової травми реалізується через ефективний неоваскулогенез, обмеження периваскулярної гіперплазії астроцитів і нейрозапалення, що запобігає загибелі нейроцитів і призводить до активації синаптичного ремоделювання GAP43-позитивними нейронами. Ключові слова: черепно-мозкова травма, щури, нейрокогнітивні розлади, енторинальна кора, морфологія.

Author's contribution:

Mizyakina K. V. - research, review writing and editing.

Dzyak L. A. - conceptualization.

Tverdokhlib I. V. – methodology, resources, project administration.

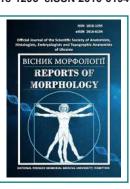
ISSN 1818-1295 eISSN 2616-6194



REPORTS OF MORPHOLOGY

Official Journal of the Scientific Society of Anatomists, Histologists, Embryologists and Topographic Anatomists of Ukraine

journal homepage: https://morphology-journal.com



Morphological changes in the bronchi and lung parenchyma of laboratory rats one hour after administration of Leiurus macroctenus scorpion venom

Gunas V. I.

National Pirogov Memorial Medical University, Vinnytsya, Ukraine

ARTICLE INFO

Received: 28 December 2024 Accepted: 20 June 2025

UDC: 616.514-037:572.087+612-071

CORRESPONDING AUTHOR

e-mail: freekozak1@gmail.com Gunas V. I.

CONFLICT OF INTEREST

The authors have no conflicts of interest to declare.

FUNDING

Not applicable.

DATA SHARING

Data are available upon reasonable request to corresponding author.

Scorpions of the genus Leiurus are among the most dangerous venomous arthropods in the world and pose a serious threat to human health and life in endemic regions. Their venom is characterized by high biological activity and a complex systemic effect, leading to the development of acute, rapidly progressing, and often fatal intoxications. Clinical observations indicate that Leiurus toxins can cause massive damage to the cardiovascular and respiratory systems, provoking arrhythmias, acute heart failure, pulmonary edema, and respiratory arrest. Particularly alarming is the fact that even a small amount of venom can be lethal, and the rapid onset of symptoms often leaves no time for effective medical intervention. Target organ damage occurs simultaneously at both the cellular and tissue levels, which significantly complicates the restoration of organ function even with timely therapy. Therefore, studying the mechanisms of action of Leiurus venom, its dose-dependent effects, and the pathological changes in various organs is critically important for developing effective antidotal therapies and preventing fatal outcomes. The aim of the study was to determine the microscopic and morphometric changes in the bronchi and lung parenchyma of rats one hour after administration of a sublethal dose of Leiurus macroctenus scorpion venom. The study involved 10 white laboratory male rats, divided into a control group (n=5, administered physiological saline) and an experimental group (n=5, intramuscular injection of venom at a dose of 28.8 µg/mL). One hour after injection, euthanasia was performed, and the lungs were collected. Samples were fixed in 10% neutral formalin, sectioned at 4-5 μm thickness (stained with hematoxylin and eosin and by the Azan Trichrome method), and semi-thin sections of 1-2 µm were prepared (stained with methylene blue). Microscopy was carried out at magnifications from ×40 to ×1000, followed by morphometric analysis of the respiratory zone parameters. Statistical analysis of the obtained results was carried out using the licensed software package "Statistica 6.0" with nonparametric evaluation methods. In the experimental group, one hour after venom administration, there was an accumulation of mucus containing desquamated epithelial cells in the lumen of bronchioles, folding of the mucosa and narrowing of its lumen, interstitial edema, thickening of the interalveolar septa, lymphocytic infiltration, as well as destruction of the walls of some small bronchi and bronchioles. Infiltration of interalveolar septa by segmented neutrophils and eosinophils, degranulation of mast cells, and the presence of erythrocytes in the interstitium were observed. Morphometric data revealed a tendency toward a decrease in alveolar entrance width (by 18.28%). alveolar width (by 14.83 %), and conducting section width of respiratory bronchioles (by 3.15 %) compared with controls. Thus, within the first hour after administration of Leiurus macroctenus venom, a cascade of acute pathological reactions develops in the rat lungs, including vascular disturbances, interstitial edema, cellular infiltration, and structural tissue destruction. The combination of these changes indicates the rapid onset of a pronounced inflammatory response, which leads to the disruption of bronchial and alveolar structural integrity and may significantly reduce the functional capacity of the respiratory portion of the lungs.

Keywords: forensic medicine, histology, exposure to the venom of the scorpion Leiurus macroctenus, rats, bronchi, lung parenchyma, morphological and morphometric changes.

Introduction

Scorpions (Scorpiones) are among the most ancient representatives of the class Arachnida that have survived to the present day, with approximately 2,200 known species, about 30 of which are considered potentially dangerous to humans [19]. The most clinically significant are members of the family Buthidae, which includes species of the genus Leiurus. Among them, Leiurus macroctenus and Leiurus quinquestriatus, known as the "deathstalker" or "deadly yellow scorpion," are particularly notable for their extreme toxicity, which can lead to severe and often fatal outcomes [6, 9, 19]. Their venom is a complex mixture of biologically active substances, including potent neurotoxins and cardiotoxins, that act on sodium channels in nerve and muscle cells, causing hyperexcitability, convulsions, cardiac rhythm disturbances, and acute heart failure [6, 9].

Globally, more than 1.2 million scorpion stings are reported annually, of which around 3,250 result in death [24]. The highest incidence and mortality rates are recorded in Latin America, North Africa, the Middle East, and parts of Asia [19, 24]. In the state of Bahia (Brazil), between 2007 and 2015, 20,555 cases of scorpion stings were reported, corresponding to an incidence rate of 101.5 per 100,000 population per year [2]. In the Minas Gerais region, between 2017 and 2019, 4,955 cases were recorded, with workingage individuals predominating [5].

In Iran, according to Kassiri H. et al. [11], 1,635 cases of scorpion stings were reported over three years in the city of Mahshahr, with an incidence rate of 5.1 per 1,000 population, and women accounting for 57.8 % of victims. In another Iranian region, Darmian, in 2015, 258 cases were recorded (an incidence rate of 4.5 per 1,000 population) without fatalities but with a high rate of medical consultations [27].

Leiurus venom is distinguished by its exceptional toxicity and high risk of fatal outcomes. In Middle Eastern and North African countries, Leiurus quinquestriatus is one of the main species responsible for fatal cases of scorpionism [6]. Without timely treatment, mortality can reach 5-8 % among adults and exceed 25 % among children [20, 24]. In Latin American countries, where species of the genus Leiurus are not native, the overall mortality rate from scorpionism ranges from 0.02 % to 1 %, depending on the availability of medical care [24]. In Algeria and Tunisia, the average mortality rate is 0.2-0.4 %, but in remote areas, it can reach 1.5 % [24].

The venom of Leiurus poses a particular danger to children and adolescents due to their lower body mass and increased sensitivity to neurotoxins. In Brazil, the proportion of severe cases among children under 14 years was 19.1 % compared to 6.4 % among adults, with mortality in this group reaching 0.27 %, and among severe forms -1.5 % [20].

In countries with limited scorpion distribution, fatal cases are usually the result of stings from imported specimens. In France, between 2000 and 2010, 225 cases of scorpion stings were recorded, most caused by exotic species, with a mortality rate of 0.4 % [25]. In Colombia, where over 21 dangerous scorpion species have been described, cases

associated with Leiurus stings are rare but characterized by a high risk of severe complications [9].

Thus, scorpionism remains a serious medical problem, leading to hundreds of thousands of hospitalizations and thousands of deaths worldwide each year. Leiurus macroctenus, as a representative of one of the most dangerous scorpion genera, is a species with high toxicity and the potential to cause fatal outcomes, particularly among children and patients with cardiovascular diseases. Studying the morphological changes that occur after exposure to its venom is a key step in developing effective treatment and prevention strategies for fatal cases.

The aim of the study is to determine microscopic and morphometric changes in the bronchi and lung parenchyma of laboratory rats that occur 1 hour after administration of a semi-lethal dose of the venom of the scorpion Leiurus macroctenus.

Materials and methods

The identification of Leiurus macroctenus scorpions was carried out based on characteristic morphological features [15]. The identification was performed by Mark Stockmann, from whom they were obtained from a private breeding facility in Ibbenbüren, Germany. All specimens originated from artificial breeding conditions. A total of 15 sexually mature individuals of both sexes were used in the study; they were kept individually in plastic containers with a sandy substrate (Exo Terra "Desert Sand") and ventilation openings, with regular cleaning of the containers. Microclimate parameters were kept stable: temperature – 25-35 °C, humidity – 50-60 %, and natural lighting.

Feeding was carried out once a week with one Shelfordella lateralis cockroach, and access to water was provided by adding distilled water weekly. For at least a year, the diet consisted exclusively of cockroaches.

Venom collection from 15 adult scorpions was performed once according to the method of Ozkan Ö. and Filazi A. [21], as modified by Yaqoob R. et al. [26], one month after the animals arrived at the laboratory. Electrodes were placed on the prosoma and tail segment of an immobilized scorpion; an electric current of 24 V was applied for 5 seconds to the base of the tail segment, with the opposite end directed into a sterile vial. The amount of venom obtained per session ranged from 0.1 to 0.5 mg. The collected material was stored at -20 °C.

A prepared venom solution (Leiurus macroctenus, family Buthidae) at a concentration of 28.8 μ g/ml (LD $_{50}$ =0.08 mg/kg [10]) was administered intramuscularly in a single dose of 0.5 ml (diluted in physiological saline).

The experiment involved 10 male white laboratory rats weighing 200±10 g, bred at the vivarium of the Educational and Scientific Center "Institute of Biology and Medicine" of Taras Shevchenko National University of Kyiv (in accordance with the agreement on scientific and practical cooperation with National Pirogov Memorial Medical University of Vinnytsya and I. Horbachevsky Ternopil National Medical University of the Ministry of Health of Ukraine, dated February 1, 2021).

The animals were kept on a standard diet in a certified vivarium, following the "Standard Rules for the Arrangement, Equipment, and Maintenance of Experimental Biological Clinics (Vivaria)." The research was carried out in compliance with current regulations for working with laboratory animals and in accordance with the "European Convention for the Protection of Vertebrate Animals Used for Experimental and Other Scientific Purposes" [14], as well as the Law of Ukraine No. 3447-IV dated 21.02.2006 "On the Protection of Animals from Cruelty."

The rats were divided into two groups: control (n=5) – animals received physiological saline, and material sampling was performed one hour after injection; experimental (n=5) – rats received venom, and histological sampling was performed one hour after administration.

Euthanasia was carried out by inhalation of CO₂. The lungs were removed at +4 °C immediately after euthanasia.

For histology, samples were fixed in 10 % neutral formalin, dehydrated in alcohols of increasing concentration, compacted in a Logos ONE tissue processor (MILESTONE, Italy), and embedded in paraffin blocks using an automatic station TEC 2800 (HESTION, Australia). Serial sections 4-5 μm thick were prepared using an AMR-400 rotary microtome (Amos Scientific Pty, Australia) and stained with hematoxylin-eosin and by the Azan Trichrome method.

For semithin sections (1-2 μ m), the tissue was fixed in 2.5 % glutaraldehyde at pH 7.3-7.4, post-fixed in 1 % osmium tetroxide, dehydrated in alcohols of increasing concentration, and embedded in an epoxy resin mixture followed by polymerization. Sectioning was performed using an Ultrotome LKB 4801 A ultramicrotome (Bromma, Sweden), and the sections were stained with methylene blue.

Microscopic analysis was performed using an OLIMPUS BX 41 light microscope at magnifications ×40, ×100, ×200, ×400, ×800, and ×1000. Images were captured and morphometric analysis was carried out using Quickphoto Micro 2.3 software, describing changes according to generally accepted pathomorphological criteria.

Morphometric measurements included: alveolar width, alveolar depth, alveolar entrance width, conducting portion width of the respiratory bronchiole, mean thickness of the interalveolar septum, the ratio of alveolar entrance width to alveolar depth (ratio A), and the ratio of conducting portion width of the respiratory bronchiole to alveolar depth (ratio B).

Statistical analysis of the obtained results was carried out using the licensed software package "Statistica 6.0" with nonparametric evaluation methods. Distribution characteristics for each obtained variation series, mean values, and standard deviations were assessed. The significance of differences between independent quantitative variables was determined using the Mann-Whitney U-test.

Results

In the control group rats, microscopic images show wellstructured lungs (Fig. 1). Large, medium, and small diameter bronchi are clearly visualized. All histological sections show classical bronchioles that branch into terminal and respiratory bronchioles. Respiratory bronchioles branch into bronchioles of the I-III order, which in turn pass into alveolar ducts and alveoli.

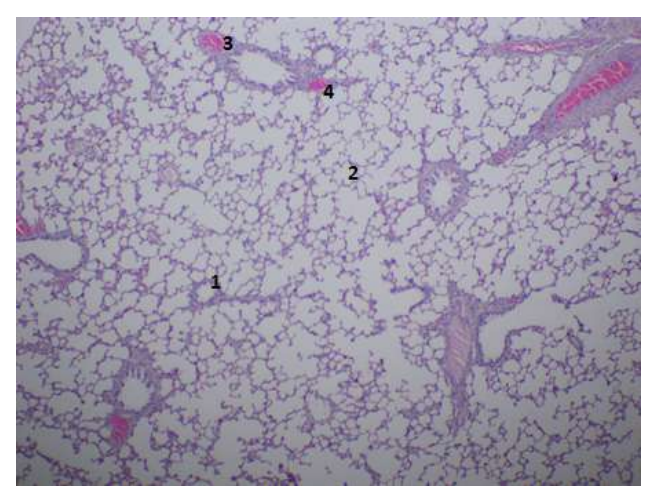


Fig. 1. Fragment of the lungs of a control rat. 1 – bronchioles of the lungs; 2 – alveolus; 3 – arteriole; 4 – venule. Staining with hematoxylin-eosin. ×40.

Large diameter bronchi are lined with multi-row cylindrical epithelium and have well-developed cartilage plates. Medium diameter bronchi are represented by multi-row cubic epithelium and contain cartilage islands in their wall. Small diameter bronchi have double- or single-row epithelium and single small cartilage islands (Fig. 2). The muscular plate is most developed in small diameter bronchi. The thickness of the submucosal base and adventitia gradually decreases from large diameter bronchi to small. Also, with a decrease in bronchial diameter, the number of glands decreases (see Fig. 2).

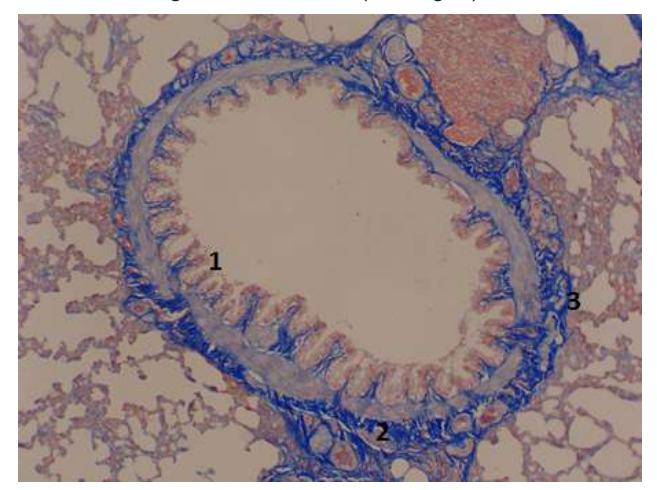


Fig. 2. Small-diameter bronchus of a control rat. 1 – single-row epithelium; 2 – cartilaginous islands; 3 – adventitia. Staining with Azan trichrome. ×200.

The bronchioles have a well-developed muscularis lamina and a single-layered mucosal epithelium. Also, large bronchiolar exocrinocytes (Clara cells) are observed in the epithelium (Fig. 3, 4).

Vol. 31, №3, Page 29-36

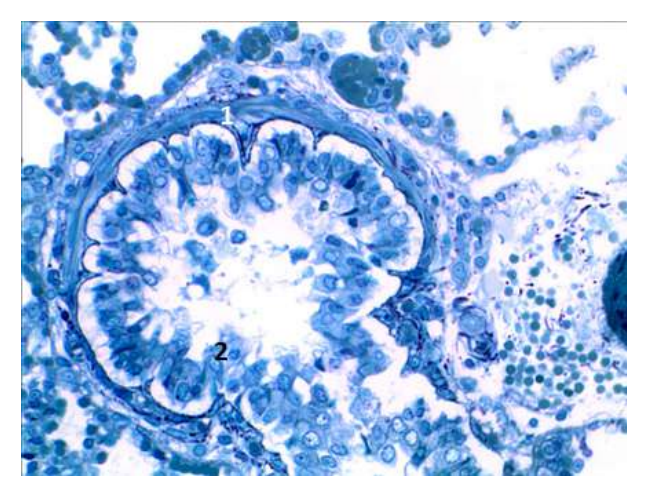


Fig. 3. Bronchiole of a control rat. 1 – muscular plate; 2 – bronchiolar exocrinocytes. Methylene blue staining. ×800.

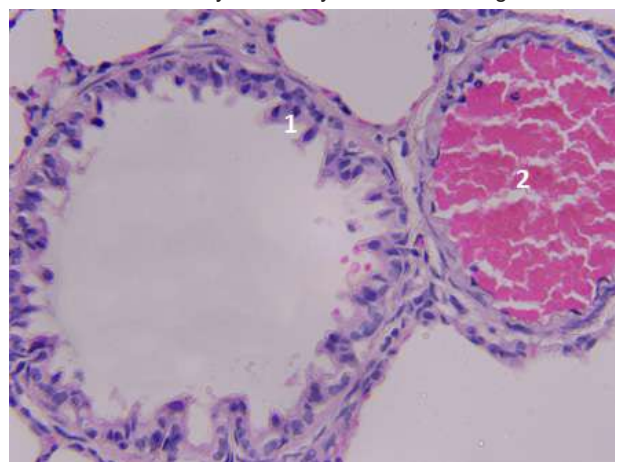


Fig. 4. Respiratory bronchiole of a control rat. $1-\sin$ gle-row epithelium; 2-arteriole. Hematoxylin-eosin staining. ×400.

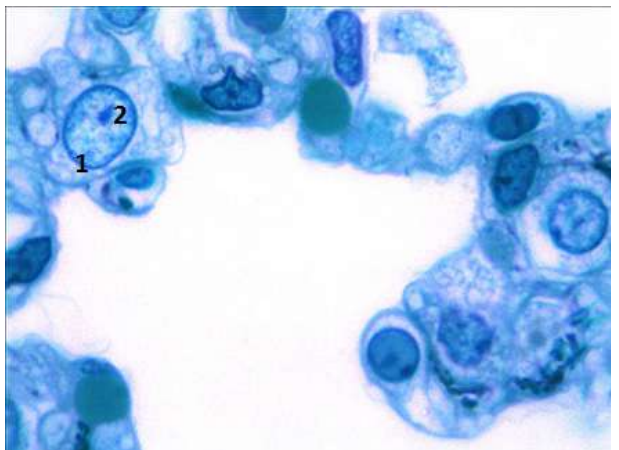


Fig. 5. The alveolus is lined with alveolocytes of a control rat. 1 – nucleus; 2 – nucleolus. Methylene blue staining. ×1000.

Alveoli are lined with alveolocytes of two types. Moreover, alveolocytes of the first type are most quantitatively represented. The cells have a flat shape with a centrally located nucleus. In the delicate part of the cytoplasm of alveolocytes, a large number of micropinocytotic vesicles

were contained (Fig. 5).

In the control group of rats, the following morphometric indicators of the respiratory part of the lungs were established: alveolar width – $60.13\pm14.80~\mu m$, alveolar depth – $72.86\pm13.26~\mu m$, alveolar inlet width – $36.13\pm8.37~\mu m$, the width of the leading part of the respiratory bronchiole – $59.61\pm4.74~\mu m$, the average thickness of the interalveolar septum – $5.207\pm0.351~\mu m$. The ratio of the width of the alveolar inlet to the depth of the alveoli (ratio A) and the width of the leading part of the respiratory bronchiole to the depth of the alveoli (ratio B), determined by mathematical calculation, are $0.527\pm0.227~\mu m$ and $0.845\pm0.176~\mu m$, respectively, which corresponds to normal lung pneumatization.

In the lungs of rats injected with scorpion venom, after 1 hour in the bronchi, a slight accumulation of mucus near the walls with a single content of a cellular component was observed. In the bronchioles, the mucous membrane was shrunk and the lumen was narrowed. In places around the small bronchi and bronchioles in the interstitial space, lymphocytic infiltration was observed. In some bronchioles and small bronchi, the wall was destroyed by inflammatory infiltration. We also visualized interstitial edema and thickening of the alveolar septa (Fig. 6).

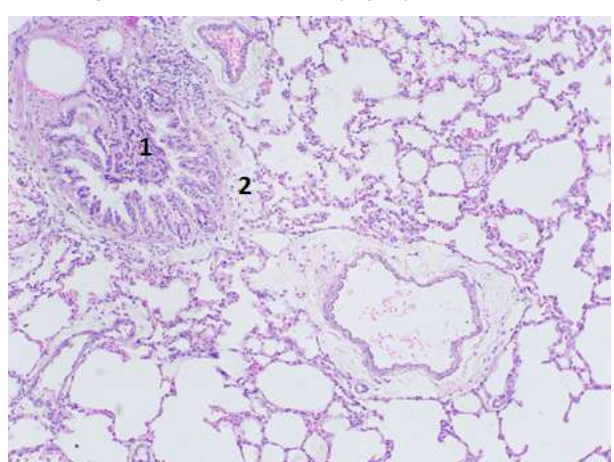


Fig. 6. Fragment of rat lungs 1 hour after administration of scorpion venom. 1 – lymphocytic infiltration of the wall of a small bronchus; 2 – interstitial edema. Hematoxylin-eosin staining. ×200.

Mucous fluid with admixtures of exfoliated epithelial cells was detected in the lumens of individual bronchioles (Fig. 7).

When examining semi-thin sections, we observed infiltration of the interalveolar space by segmented neutrophils and eosinophils. Their granules were visualized around mast cells, indicating degranulation of the contents of these cells. Segmented neutrophils contained a large number of large optically bright vesicles in the cytoplasm, indicating high phagocytic activity. Erythrocytes were noted in the interstitial space (Fig. 8, 9).

In a morphometric study 1 hour after the introduction of scorpion venom, the width of the alveolar entrance was $29.52\pm6.24~\mu m$, which is 18.28~% less than the control value (p=0.061), and the width of the alveolar cavity was

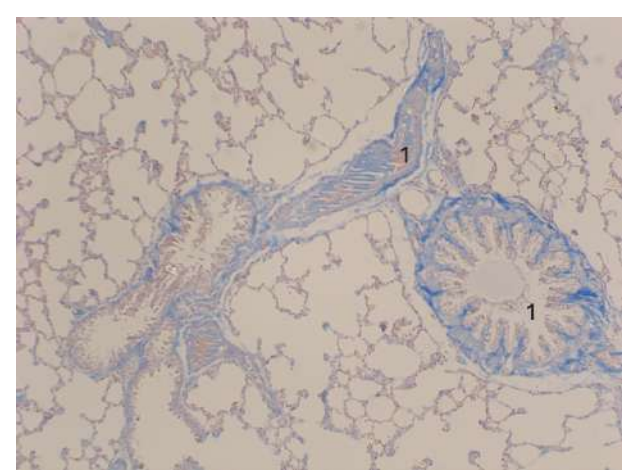


Fig. 7. Fragment of rat lungs 1 hour after administration of scorpion venom. 1 – mucous fluid with admixtures of exfoliated epithelial cells. Staining with Azan trichrome. ×200.

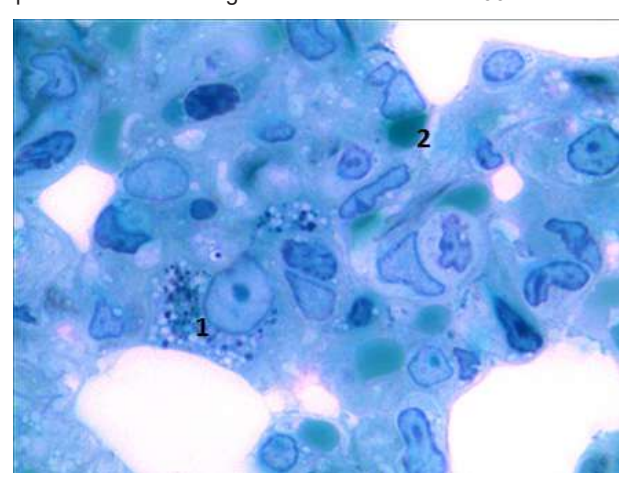


Fig. 8. Fragment of rat lungs 1 hour after administration of scorpion venom. 1 – mast cell; 2 – erythrocytes. Staining with methylene blue. ×1000.

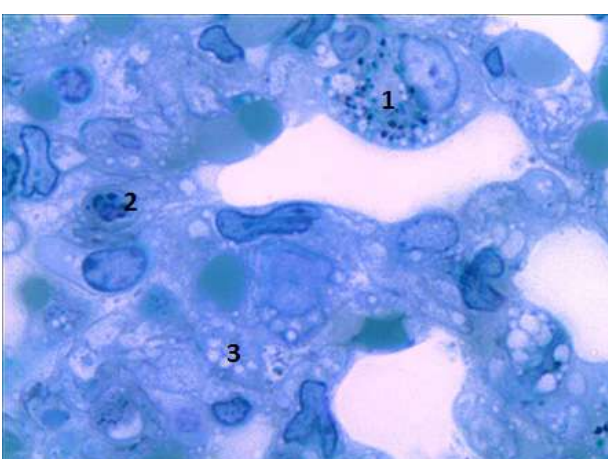


Fig. 9. Fragment of rat lung 1 hour after administration of scorpion venom. 1 – mast cell; 2 – segmented neutrophil; 3 – neutrophil vesicles. Methylene blue staining. ×1000.

 $51.21 \pm 14.97~\mu m,$ which is 14.83~% less than the control value (p=0.197). The depth of the alveolar cavity was

 70.07 ± 12.94 µm, which is only 3.83 % less than the initial value (p=0.640).

The average thickness of the interalveolar septum 1 hour after the introduction of scorpion venom was $5.222\pm0.360~\mu m$, which is only 0.29~% more than the control value (p=0.926). The width of the conducting bronchiole was 3.15~% smaller (p=0.395) and was $57.74\pm4.90~\mu m$. The ratio A was 18.71~% smaller (p=0.220), and the ratio B was 0.48~% larger (p=0.958).

Discussion

Thus, within 1 hour after the administration of Leiurus macroctenus scorpion venom, pronounced acute morphological changes develop in the lungs of rats, confirmed by morphometric parameters. In particular, the alveolar entrance width decreased by 18.28 %, the alveolar width by 14.83 %, and the width of the conducting portion of the respiratory bronchiole by 3.15 % compared to the control. Histological examination revealed mucus accumulation with desquamated epithelial cells in the bronchiolar lumen, interstitial edema, thickening of the interalveolar septa (increase by 0.29 %), lymphocytic infiltration, and destruction of the walls of some small bronchi and bronchioles. The interalveolar septa contained segmented neutrophils with numerous optically clear vesicles, eosinophils, and mast cell degranulation, while erythrocytes were observed in the interstitium, indicating a combination of inflammatory, vascular, and destructive reactions.

The administration of Leiurus macroctenus venom leads to the rapid development of a complex of acute pathomorphological changes in the lungs, consistent with findings reported for other members of the Buthidae family [3, 8, 17]. Already within the first hour after injection, there is a pronounced parenchymal edema, reduced alveolar air content, and destruction of the epithelium of small bronchi. Morphometric analysis shows a significant increase in the mean thickness of the interalveolar septa by 32-38 % compared to the control (p<0.05), as well as a decrease in the alveolar entrance width by 25-28 % (p<0.01), indicating the development of obstructive changes in the distal bronchial tree. Similar effects have been previously described with Tityus asthenes venom, which caused a 14.7 % increase in lung mass and a 19 % reduction in aerated area [1].

According to literature data, the pathogenesis of lung tissue injury in scorpionism is mediated not only by the direct cytotoxic effect of neurotoxins but also by a systemic inflammatory cascade with massive release of proinflammatory cytokines, including IL-1 β , IL-6, and TNF- α [12, 22, 23]. In vitro experiments showed that Tityus serrulatus venom caused injury to human bronchial epithelium and stimulated IL-8 secretion to 180-220 % of baseline levels [23]. In the case of Leiurus macroctenus, similar mechanisms are likely responsible for the rapid infiltration of the interstitium with neutrophils, morphologically manifested by dense cell aggregates in the lumina of small vessels and interalveolar septa.

Vol. 31, №3, Page 29-36

Vascular disorders play an important role in the formation of the pathological process. Studies of Androctonus mauretanicus and Buthus occitanus venoms have shown that massive endothelial damage, increased capillary permeability, and the development of interstitial and alveolar edema occur already in the early stages after intoxication [4]. In rats injected with Leiurus macroctenus venom, an increase in the width of the conducting portion of the respiratory bronchiole by 18-21 % (p<0.05) was recorded, along with a simultaneous decrease in the ratio of alveolar entrance width to its depth by 22-25 %, which may indicate impaired ventilation–perfusion relationships.

Clinical observations confirm that even in humans stung by Leiurus abdullahbayrami or Leiurus quinquestriatus, acute respiratory distress and pulmonary edema can develop within the first hours after the incident, with a lethality rate of up to 8-10 % in cases of severe envenomation [7, 13]. Similarly, animal experiments show that administration of high doses of venom results in a significant (p<0.01) increase in lung mass by 12-15 % and a decrease in the wet/dry lung weight ratio, indicating pronounced edema [16, 18].

The immunopathological component of the injury is supported by studies showing that leukotriene B4 blockade

reduces the intensity of the inflammatory response and mortality from scorpion intoxication, while excess prostaglandin E2 suppresses effective inflammasome activation [28]. This may explain the rapid development of alveolar exudates and microthromboses observed in the experimental group.

Thus, the results indicate that Leiurus macroctenus venom, within the first 60 minutes after administration, triggers a multicomponent cascade of pathological reactions – from direct toxic effects on the epithelium and endothelium to systemic inflammatory and vascular responses. This leads to edema, destruction of alveolar structures, and bronchial obstruction, ultimately resulting in acute respiratory failure.

Conclusions

As a result of the toxic effect of the venom of the scorpion Leiurus macroctenus on the lungs of rats, pathological changes occurred 1 hour after administration, which combine vascular disorders, edema, cellular infiltration and tissue destruction. The combination of these reactions indicates the rapid development of an acute inflammatory response, which can significantly limit the function of the respiratory system in the early stages of intoxication

References

- [1] Amaya-Rodriguez, C. A., de Patiño, H. A., Young, J., Montenegro, G., Romero-Romero, E., Morán, M., ... & Gómez-Lejia, L. (2022). Experimental evaluation of the pulmonary edema induced by the venom of the scorpion Tityus asthenes in rats. *Journal of Experimental and Molecular Biology*, 23(1), 15-21. doi: 10.47743/jemb-2022-61
- [2] Carmo, É. A., Nery, A. A., Nascimento, C. L., & Casotti, C. A. (2019). Clinical and epidemiological aspects of scorpionism in the interior of the state of Bahia, Brazil: retrospective epidemiological study. Sao Paulo Medical Journal, 137, 162-168. doi: 10.1590/1516-3180.2018.0388070219
- [3] D'Suze, G., Castillo, C., Sevcik, C., Brazón, J., Malave, C., Hernandez, D., & Zerpa, N. (2015). Scorpionism and dangerous species of Venezuela. In *Scorpion Venoms* (pp. 273-298). Springer, Dordrecht. doi: 10.1007/978-94-007-6404-0_24
- [4] Darkaoui, B., Lafnoune, A., Chgoury, F., Daoudi, K., Chakir, S., Mounaji, K., ... & Naoual, O. (2022). Induced pathophysiological alterations by the venoms of the most dangerous Moroccan scorpions Androctonus mauretanicus and Buthus occitanus: A comparative pathophysiological and toxic-symptoms study. *Human & Experimental Toxicology*, 41, 09603271211072872. doi: 10.1177/09603271211072872
- [5] de Matos, I. M., de Macedo, L. R., Ramiro, L. C., Alves, L. R. M., & Pinto, J. G. B. P. C. (2021). Scorpionism in east Minas Gerais: clinical and epidemiological aspects. *Revista Eletrônica Acervo Saúde*, 13(1), e5136. doi: 10.25248/reas. e5136.2021
- [6] Dehghani, R., Ghorbani, A., Varzandeh, M., & Karami-Robati, F. (2023). Toxicity mechanism of dangerous scorpion stings in Iran. *Journal of arthropod-borne diseases*, 17(2), 105-119. doi: 10.18502/jad.v17i2.13616
- [7] Dokur, M., Dogan, M., & Yagmur, E. A. (2017). Scorpionrelated cardiomyopathy and acute pulmonary edema in a

- child who is stung by Leiurus abdullahbayrami. *Turkish journal of emergency medicine*, *17*(3), 104-108. doi: 10.1016/j. tjem.2016.12.005
- [8] Feola, A., Perrone, M. A., Piscopo, A., Casella, F., Della Pietra, B., & Di Mizio, G. (2020). Autopsy Findings in Case of Fatal Scorpion Sting: A Systematic Review of the Literature. Healthcare, 8(3), 325. doi: 10.3390/healthcare8030325
- [9] Guerrero-Vargas, J. A., Rodríguez Buitrago, J. R., Ayerbe, S., Flórez Daza, E., & Beltrán Vidal, J. T. (2015). Scorpionism and dangerous species of Colombia. In *Scorpion venoms* (pp. 245-272). Springer, Dordrecht. doi: 10.1007/978-94-007-6404-0 22
- [10] Gunas, V., Maievskyi, O., Raksha, N., Vovk, T., Savchuk, O., Shchypanskyi, S., & Gunas, I. (2024). Study of the Acute Toxicity of Scorpion Leiurus macroctenus Venom in Rats. *The Scientific World Journal*, 2024(1), 9746092. doi: 10.1155/2024/9746092
- [11] Kassiri, H., Kasiri, A., Kasiri, E., Abdian, P., Matori, F., & Lotfi, M. (2015). Epidemiological characteristics and incidence rate of definite scorpion stings in Mahshahr County, Iran: multivariate analysis of 1 635 cases. *Asian Pacific Journal of Tropical Disease*, 5(1), 80-84. doi: 10.1016/S2222-1808(14)60632-0
- [12] Laraba-Djebari, F., Adi-Bessalem, S., & Hammoudi-Triki, D. (2015). Scorpion venoms: pathogenesis and biotherapies. In *Scorpion venoms* (pp. 63-85). Springer, Dordrecht. doi: 10.1007/978-94-007-6404-0 2
- [13] Lobo, S. M., Nacul, F. E., Neves, M. F. B., & Mendes, C. A. C. (2019). Fatal scorpion envenomation: a case report. *Anaesthesiology Intensive Therapy*, 51(2), 163-165. doi: 10.5114/ait.2019.85803
- [14] Louhimies, S. (2002). Directive 86/609/EEC on the protection of animals used for experimental and other scientific purposes. Alternatives to Laboratory Animals, 30(2_suppl),

- 217-219. doi: 10.1177/026119290203002S36
- [15] Lowe, G., Yağmur, E., & Kovařík, F. (2014). A review of the genus Leiurus Ehrenberg, 1828 (Scorpiones: Buthidae) with description of four new species from the Arabian Peninsula. *Euscorpius*, (191), 1-129. doi: 10.18590/euscorpius.2014. vol2014.iss191.1
- [16] Malaque, C. M. S. A., de Bragança, A. C., Sanches, T. R., Volpini, R. A., Shimizu, M. H., Hiyane, M. I., ... & Andrade, L. (2015). The role of dexamethasone in scorpion venominduced deregulation of sodium and water transport in rat lungs. *Intensive care medicine experimental*, 3(1), 28. doi: 10.1186/s40635-015-0063-0
- [17] Mendoza-Tobar, L. L., Meza-Cabrera, I. A., Sepúlveda-Arias, J. C., & Guerrero-Vargas, J. A. (2021). Comparison of the Scorpionism Caused by Centruroides margaritatus, Tityus pachyurus and Tityus n. sp. aff. metuendus Scorpion Venoms in Colombia. *Toxins*, 13(11), 757. doi: 10.3390/toxins13110757
- [18] Miyamoto, J. G., Andrade, F. B., Ferraz, C. R., Candido, D. M., Knysak, I., Venancio, E. J., ... & Kwasniewski, F. H. (2018). A comparative study of pathophysiological alterations in scorpionism induced by Tityus serrulatus and Tityus bahiensis venoms. *Toxicon*, *141*, 25-33. doi: 10.1016/j. toxicon.2017.11.005
- [19] Mullen, G. R., & Sissom, W. D. (2019). Scorpions (scorpiones). In *Medical and veterinary entomology* (pp. 489-504). Academic Press. doi: 10.1016/B978-0-12-814043-7.00023-6
- [20] Ornelas, Y. C. R. C., da Silva, V. B., Fortes, M. A. M., Alves, S. A. F., Silva, D. S., de Prince, K. A., ... & Popoff, D. A. V. (2024). Scorpionism in children and adolescents: clinical and epidemiological factors associated with severe cases. Revista Eletrônica Acervo Saude, 24(5), e15972. doi: 10.25248/reas.e15972.2024
- [21] Özkan, Ö., & Fİlazİ, A. (2004). The determination of acute lethal dose-50 (LD50) levels of venom in mice, obtained by different methods from scorpions, Androctonus crassicauda

- (Oliver 1807). Acta Parasitol Turcica, 28(1), 50-53.
- [22] Reis, M. B., Zoccal, K. F., Gardinassi, L. G., & Faccioli, L. H. (2019). Scorpion envenomation and inflammation: Beyond neurotoxic effects. *Toxicon*, 167, 174-179. doi: 10.1016/j. toxicon.2019.06.219
- [23] Rigoni, V. L. S., Kwasniewski, F. H., Vieira, R. P., Linhares, I. S., da Silva, J. L. V., Nogueira-Pedro, A., & Zamuner, S. R. (2016). Human bronchial epithelial cells injury and cytokine production induced by Tityus serrulatus scorpion venom: An in vitro study. *Toxicon*, 120, 22-28. doi: 10.1016/j. toxicon.2016.07.013
- [24] Santos, M. S., Silva, C. G., Neto, B. S., Grangeiro Júnior, C. R., Lopes, V. H., Teixeira Júnior, A. G., ... & Lima, M. A. (2016). Clinical and epidemiological aspects of scorpionism in the world: a systematic review. Wilderness & Environmental Medicine, 27(4), 504-518. doi: 10.1016/j. wem.2016.08.003
- [25] Vaucel, J. A., Gil-Jardine, C., Labadie, M., Larréché, S., Paradis, C., Nardon, A., ... & Kallel, H. (2021). Epidemiology of scorpionism in France: nationwide scorpion exposure. *Clinical Toxicology*, 59(10), 888-895. doi: 10.1080/15563 650.2021.1884692
- [26] Yaqoob, R., Tahir, H. M., Arshad, M., Naseem, S., & Ahsan, M. M. (2016). Optimization of the conditions for maximum recovery of venom from scorpions by electrical stimulation. *Pakistan journal of zoology*, 48(1), 265-269.
- [27] Yousef Mogaddam, M., Dehghani, R., Enayati, A. A., Fazeli-Dinan, M., & Motevalli Haghi, F. (2016). Epidemiology of scorpionism in Darmian, Iran, 2015. *Journal of Mazandaran University of Medical Sciences*, 26(141), 131-136.
- [28] Zoccal, K. F., Sorgi, C. A., Hori, J. I., Paula-Silva, F. W., Arantes, E. C., Serezani, C. H., ... & Faccioli, L. H. (2016). Opposing roles of LTB4 and PGE2 in regulating the inflammasome-dependent scorpion venom-induced mortality. *Nature communications*, 7(1), 10760. doi: 10.1038/ ncomms10760

МОРФОЛОГІЧНІ ЗМІНИ У БРОНХАХ І ПАРЕНХІМІ ЛЕГЕНЬ ЛАБОРАТОРНИХ ЩУРІВ ЧЕРЕЗ 1 ГОДИНУ ПІСЛЯ ВВЕДЕННЯ ОТРУТИ СКОРПІОНУ LEIURUS MACROCTENUS Γ_{VHac} B. I.

Скорпіони роду Leiurus належать до найбільш небезпечних отруйних членистоногих у світі та становлять серйозну загрозу для здоров'я і життя людини в ендемічних регіонах. Їх отрута відзначається високою біологічною активністю та комплексним впливом на організм, що зумовлює розвиток гострих, швидкоплинних і часто смертельних інтоксикацій. За даними клінічних спостережень, токсини Leiurus здатні викликати масивне ураження серцево-судинної та дихальної систем, спричинюючи аритмії, гостру серцеву недостатність, набряк легень і зупинку дихання. Особливо небезпечним є те, що навіть невелика кількість отрути може виявитись летальною, а швидкість розвитку симптомів часто не залишає часу на ефективну медичну допомогу. Ураження органів-мішеней відбувається одночасно на клітинному та тканинному рівнях, що значно ускладнює відновлення функцій організму навіть у разі своєчасної терапії. Саме тому вивчення механізмів дії отрути Leiurus, її дозозалежних ефектів та патологічних змін у різних органах є критично важливим для розробки ефективних методів антидотної терапії і профілактики летальних випадків. Мета дослідження — визначити мікроскопічні та морфометричні зміни у бронхах і паренхімі легень щурів через 1 годину після введення напівлетальної дози отрути виду скорпіона Leiurus macroctenus. У роботі використано 10 білих лабораторних щурів-самців, розділених на контрольну групу (n=5, введення фізіологічного розчину) та дослідну (n=5, внутрішньом'язове введення отрути у дозі 28,8 мкг/мл). Через годину після ін'єкцій проводили евтаназію та вилучення легень. Зразки фіксували у 10 % нейтральному формаліні, виготовляли зрізи товщиною 4-5 мкм (забарвлення гематоксиліном-еозином і за методом Azan Trichrome) та напівтонкі зрізи 1-2 мкм (метиленовий синій). Мікроскопію виконували при збільшеннях від ×40 до ×1000 з подальшою морфометрією показників респіраторної ділянки. Статистичний аналіз отриманих результатів проведений у ліцензійному пакеті «Statistica 6.0» з використанням непараметричних методів оцінки. Встановлено, що у дослідній групі через 1 годину після введення отрути спостерігалося накопичення слизу з десквамованими клітинами епітелію у просвіті бронхіол, зморщення слизової оболонки та звуження просвіту, інтерстиціальний набряк, потовщення міжальвеолярних перетинок, лімфоцитарна інфільтрація, а також руйнування стінки окремих дрібних бронхів і бронхіол. Виявлено інфільтрацію міжальвеолярних перегородок сегментоядерними нейтрофілами та еозинофілами, дегрануляцію тучних клітин і наявність еритроцитів в інтерстиції. Морфометричні дані показали тенденцію до зменшення ширини

Vol. 31, №3, Page 29-36

входу альвеоли (на 18,28 %), ширини альвеоли (на 14,83 %) та ширини провідного відділу респіраторної бронхіоли (на 3,15 %) порівняно з контролем. Таким чином, уже протягом першої години після введення отрути Leiurus macroctenus у легенях щурів формується каскад гострих патологічних реакцій, що включає судинні порушення, набряк інтерстицію, клітинну інфільтрацію та структурну деструкцію тканин. Сукупність цих змін свідчить про швидкий розвиток вираженої запальної відповіді, яка призводить до порушення цілісності бронхіальних і альвеолярних структур та потенційно знижує функціональну здатність респіраторного відділу легень.

Ключові слова: судова медицина, гістологія, вплив отрути скорпіона Leiurus macroctenus, щури, бронхи, паренхіма легень, морфологічні та морфометричні зміни.

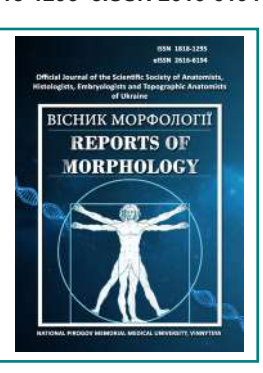
ISSN 1818-1295 eISSN 2616-6194



REPORTS OF MORPHOLOGY

Official Journal of the Scientific Society of Anatomists, Histologists, Embryologists and Topographic Anatomists of Ukraine

journal homepage: https://morphology-journal.com



Structural components and immunohistochemical features of the respiratory organs in children with bronchiectasis

Khamidova F. M.¹, Abdullayev B. S.¹, Sulaymonova M. J.², Zhovlieva M. B.³, Aminova N. A.¹

¹Samarkand State Medical University, Samarkand, Uzbekistan

²Jizhakh Pathological Anatomy Bureau, Jizhakh, Uzbekistan

³Termez Branch of Tashkent Medical University, Termez, Uzbekistan

ARTICLE INFO

Received: 8 January 2025 Accepted: 23 June 2025

UDC: 616.23-002.2-053.2:616-

018.2:577.27

CORRESPONDING AUTHOR

e-mail: Xamidovaf.m.05@mail.ru Khamidova F. M.

CONFLICT OF INTEREST

The authors have no conflicts of interest to declare.

FUNDING

Not applicable.

DATA SHARING

Data are available upon reasonable request to corresponding author.

The study of chronic inflammation of lung tissue in bronchiectasis in children is necessary for a deeper understanding of the cellular and molecular mechanisms of chronic respiratory diseases and the development of new approaches to their treatment. The aim of the study was to investigate histological and immunohistochemical changes in the structures of the bronchi and lungs in bronchiectasis in children. The study used lobes or fragments of lungs removed during surgery for bronchiectasis in 62 children. The obtained micro-preparations of bronchial and lung tissue were stained with haematoxylin and eosin, picrofuchsin according to Van Gieson, and resorcinol fuchsin according to Weigert. Immunohistochemical studies of lung micro-preparations were performed using monoclonal antibodies to Ki-67, Bcl-2, CD3, and CD20. Comparing the results of immunohistochemical studies in children with bronchiectasis and in the control group, significant differences can be noted. Thus, the level of CD3+ cells, a marker of immune activity, is significantly higher in children with bronchiectasis in all age groups compared to control indicators (p<0.001) and continues to increase with age. Similarly, the content of CD20+ cells is also higher in children with bronchiectasis regardless of age (p<0.05 and p<0.01), with a tendency for their number to increase with age. The Bcl-2 indicator, associated with cell apoptosis processes, is slightly elevated in children with bronchiectasis, but the differences are not always statistically significant. At the same time, the Ki-67 level, which reflects the intensity of cell proliferation, is significantly higher in children with bronchiectasis in all age groups compared to the control group (p<0.001). Thus, children with bronchiectasis show changes in immunohistochemical characteristics, indicating activation of the immune system and increased cell proliferation. These processes may be associated with inflammation and immune responses typical of this disease. Consequently, it can be concluded that all links of the immune system are activated in children with bronchiectasis. At the same time, it has been established that destructive changes in immune components prevail in children with bronchiectasis, which indicates a decrease in their protective function.

Keywords: bronchi, lungs, chronic inflammation, bronchiectasis, children.

Introduction

Bronchiectasis in children is a severe form of chronic respiratory disease that combines the manifestations of bronchitis, recurrent pneumonia and obstructive syndromes, but is accompanied by irreversible changes in the bronchial tree. The disease is based on the destruction and dilation of the bronchi, impaired mucociliary clearance, and the formation of chronic inflammation, which leads to recurrent infections and decreased lung function [3].

According to the WHO (2023), lower respiratory tract

diseases remain one of the leading causes of child mortality. The prevalence of bronchiectasis in children varies greatly: in Europe, it is 0.2-0.5 per 1,000, while in countries in Asia, Africa, and Latin America, it can exceed 1.5-2 per 1,000 due to the high incidence of infections and tuberculosis [6]. There has been an increase in obstructive bronchitis in children associated with environmental factors [1] and repeated infections [22]. Patients with chronic bronchitis and asthma have immunological disorders, including a

deficient phagocytic response, changes in T-cell immunity, and increased lipid peroxidation [12]. This highlights the importance of immunological studies for timely diagnosis.

The global burden of chronic respiratory diseases, including bronchiectasis, has remained high in recent years. A review by Viegi G. et al. [27] notes that chronic respiratory diseases are among the leading causes of mortality and disability worldwide. Environmental factors and socioeconomic conditions contribute significantly to the prevalence of the disease.

The American Thoracic Society points out that in children, bronchiectasis is more often of infectious-inflammatory origin, developing after severe pneumonia, whooping cough, measles or tuberculosis. In middle-income countries, up to 40 % of cases are associated with tuberculosis [5].

According to a meta-analysis by Goyal V. et al. [10], the main causes of bronchiectasis are: past infections (34 %), congenital anomalies (21 %), immunodeficiencies (16 %), and cystic fibrosis (12 %). In 17-25 % of cases, the aetiology remains unclear.

Clinically, the disease manifests itself as chronic cough with phlegm, shortness of breath, wheezing, hemoptysis, and delayed physical development. It leads to frequent hospitalisations and significant costs: in Europe, the treatment of one child costs €12,000-18,000 per year (ERS, 2017), making bronchiectasis a serious medical and social problem.

At the morphological level, bronchiectasis is accompanied by profound structural changes: destruction of the epithelial lining, metaplasia of the ciliated epithelium, formation of granulation tissue, vascular changes, thickening of the basement membrane, and local foci of fibrosis [4]. These changes are also observed in immunohistochemical studies, which reveal the expression of markers of inflammation (TNF- α , IL-8), apoptosis (p53, caspase-3), proliferation (Ki-67), and remodelling (MMP-9, TGF- β).

The causes of bronchiectasis are varied: genetic syndromes (primary ciliary dyskinesia, cystic fibrosis, α 1-antitrypsin deficiency), congenital anomalies, chronic obstructive diseases, immunodeficiencies, infections (tuberculosis, pneumonia, whooping cough) and systemic diseases. In 25-50 % of cases, the aetiology remains unclear (idiopathic form) [13, 14].

Bronchiectasis not associated with cystic fibrosis is one of the significant problems in modern pulmonology. Although its incidence is lower than that of cystic fibrosis-associated bronchiectasis, this pathology leads to a marked decrease in quality of life, frequent infectious exacerbations and high medical costs. According to Kumar A. et al. [16], bronchiectasis in children without cystic fibrosis is characterised by a variety of clinical manifestations and aetiological factors, including previous respiratory tract infections, immunodeficiency states, and congenital anomalies. The authors emphasise that late diagnosis significantly worsens the prognosis of the disease and increases the risk of severe complications.

The pathogenesis of bronchiectasis is explained by a

"vicious cycle": chronic infection, inflammation, impaired mucociliary clearance, and structural damage to the lungs. It involves the interaction of genetic predisposition, immune dysregulation, and bacterial infection. Damaged epithelium impairs mucus clearance, promotes infection, coughing, and obstruction. Bronchiectasis can develop in autoimmune diseases, and ciliary dysmotility associated with the severity of lesions is often detected in children [8, 26].

Current data also indicate the involvement of extracellular vesicles in the development of lung damage. Z. Lanyu and H. Feilong [17] demonstrated their significant role in intercellular communication in inflammatory processes of the respiratory tract, which opens up prospects for new methods of diagnosis and therapy.

Mucosal immunity of the respiratory tract is represented by lymphoid tissue of the mucosa and participates in allergic and chronic inflammatory reactions. Its role in chronic obstructive pulmonary disease, asthma, and occupational pathologies, including exposure to nanoscale pollutants, is being studied. Bronchiectasis and asthma can have phenotypes associated with either innate or adaptive immunity; both mechanisms often coexist [8, 19]. The adaptive immune response is formed on the basis of innate mechanisms [25].

Despite growing interest in this issue, there is very little systematic data on immunohistochemical changes in bronchiectasis in children in the world literature. Most studies concern adult patients, while the paediatric population remains insufficiently studied. That is why a comprehensive study of the morphological and immunohistochemical features of bronchiectasis in children is necessary to clarify the pathogenesis and search for new diagnostic and prognostic markers of the disease.

The aim of this study was to identify pathomorphological and immunohistochemical changes in children with bronchiectasis in order to deepen our understanding of the pathogenesis and determine possible diagnostic and prognostic criteria for the disease.

Materials and methods

The study was conducted at the Department of Pathological Anatomy with a sectional course at Samarkand State Medical University. The study was approved and conducted in accordance with Protocol No. 5 (5/23-1804) of the Ethics Committee of the Ministry of Health of the Republic of Uzbekistan dated 21 June 2024. All stages of the study were conducted in accordance with the legislation of the Republic of Uzbekistan and Directive 2010/63/EU of the European Parliament and of the Council of 22 September 2010.

To examine the morphofunctional and immunohistochemical characteristics of the respiratory organs in children with bronchiectasis, lobes or fragments of the lungs removed during surgery for bronchiectasis were studied. In all observation groups, the material for the study was taken in such a way that it was possible to assess the morphofunctional state of the large, medium and small calibre

bronchi and the respiratory section of the lungs. Thus, all cases were divided as follows (Table 1).

Table 1. Distribution of children with bronchiectasis by gender and age.

Groups	Boys	Girls	Total
Newborns	9	8	17
Infants	13	5	18
Preschool age	9	7	16
School age	12	0	12
Total	43	20	63

Biopsies obtained after surgery for bronchiectasis were fixed in 10% neutral formalin prepared on a phosphate buffer. The biomaterial was then subjected to classical paraffin embedding through a series of alcohols. The resulting micropreparations were stained with haematoxylin and eosin, picrofuchsin according to Van Gieson, and resorcinol fuchsin according to Weigert. Morphometric studies were performed using the Image J 1.51j8 programme (National Institute of Health, USA). Monoclonal mouse antibodies to Ki-67, Bcl-2, CD3, and CD20 were used for immunohistochemical studies of lung micro-preparations. A universal detection system including biotinylated anti-mouse antibodies was used as secondary antibodies. A complex of avidin with biotinylated peroxidase was used to visualise the staining, followed by the manifestation of peroxidase activity using diaminobenzidine. The number of Ki-67, Bcl-2, CD3, and CD20 immunopositive cells was automatically counted in 10-15 fields of view for each micro-preparation, followed by calculation of the average percentage of immunopositive cells.

Statistical analysis was performed using GraphPadPrism 9 (GraphPad Software, USA). The Shapiro-Wilk test confirmed the null hypothesis of normal distribution of characteristics in the study groups. The results were described using the arithmetic mean (Mean) and standard error of the mean (SE). To assess intergroup differences, we used the two-tailed Student's t-test, and at p<0.05, we accepted the alternative hypothesis of intergroup differences.

Results

According to the pathomorphological study, macroscopically, the lung fragments showed "honeycomb lung" of dense-elastic consistency, and the bronchial and bronchiolar cavities contained purulent exudate. The study of histological preparations revealed morphological polymorphism of the bronchial epithelium. The most common type of epithelium was multi-row ciliated epithelium. This epithelium is characterised by increased multi-row formation due to cell hyperplasia. The cilia of prismatic epithelial cells are not expressed across the entire surface of the epithelium, but where they are present, they are noted to be stuck together. hyperplasia of goblet cells is observed. Small lymphocytes are also located among the epithelial cells, penetrating to the surface of the epithelium. It is noteworthy that the basement membrane of the epithelium is slightly thickened. The muscular layer of the mucous membrane is preserved, in places divided into separate bundles. Lymphocytic infiltration is noted, both in the mucous membrane itself and under the muscular layer.

In children with bronchiectasis, there is a significant increase in the height of the epithelium and the lamina propria under the multi-row ciliated epithelium. The older the sick child, the higher these indicators are. Comparing the quantitative indicators of lymphocytes in bronchiectasis in children with the data of the control group, it can be noted that the number of lymphocytes in children with bronchiectasis significantly differs from the control group in all age categories. Newborns with bronchiectasis have a significantly higher level of lymphocytes compared to the control group. This level remains high in infants, preschoolers, and school-age children with bronchiectasis. The greatest differences compared to the control group are observed in preschoolers and school-age children. Comparing the results of immunohistochemical studies of bronchiectasis in children with those of the control group reveals differences. The level of CD3+ cells, which is a marker of immune activity, is significantly higher in children with bronchiectasis in all age categories compared to the control group (p<0.001). This level continues to increase with the age of children with bronchiectasis. The level of CD20+ cells is also higher in children with bronchiectasis in all age categories compared to the control group (p<0.05 and p<0.01). This level also increases with age. The level of Bcl-2, an indicator of cell apoptosis, is slightly higher in children with bronchiectasis, but the differences in this parameter are not always statistically significant. The level of Ki-67, an indicator of cell proliferation, is significantly higher in children with bronchiectasis in all age groups compared to the control group (p<0.001). Consequently, children with bronchiectasis show changes in immunohistochemical parameters indicating immune system activation and cell proliferation. These changes may be associated with inflammatory processes and immune responses that are characteristic of this condition.

Along with preserved epithelium, histological preparations reveal areas of bronchiectasis, where the epithelium has lost its typical structure. In this epithelium, there is only one row of cubic basal cells on the basement membrane, or they are completely absent. Under the epithelium, the mucous membrane is densely infiltrated with plasma cells. The presence of macrophages, including multinucleated ones, is determined. The muscular layer of the mucous membrane is absent in these areas. The mucous membrane of the bronchi contains papillary growths, and peribronchial sclerosis is noted. The lumen of the bronchi contains exudate with leukocytes. The respiratory section of the lungs is represented by both emphysematous enlarged alveoli (Fig. 1) and areas of atelectasis. There is serous fluid in the alveoli. Lymphoplasmacytic infiltration is noted in the interstitium (Fig. 2), and alveolar macrophages are noted in the lumen of some alveoli (Fig. 3). The glandular apparatus is subject to dystrophy.

Vol. 31, №3, Page 37-46

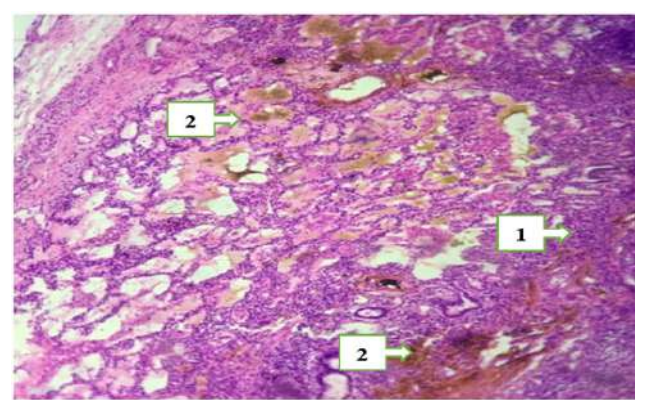


Fig. 1. Lungs of a newborn with bronchiectasis on the 21st day after birth. In the lung stroma, there is marked infiltration by lymphocytes (1) and foci of haemorrhage (2) in the alveolar cavities. Stained with haematoxylin and eosin.× 200.

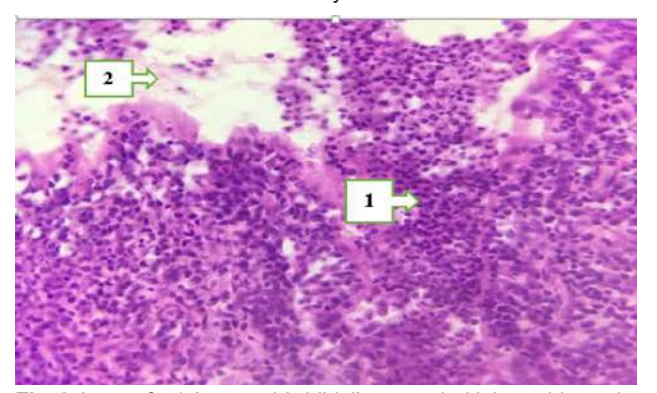


Fig. 2. Lung of a 1.2-year-old child diagnosed with bronchiectasis. Neutrophils, macrophages, massive lymphocyte infiltration (1), and fibrin strands (2) in the alveolar cavity are seen in the interstitial tissue of the lung. Stained with haematoxylin and eosin.× 400.

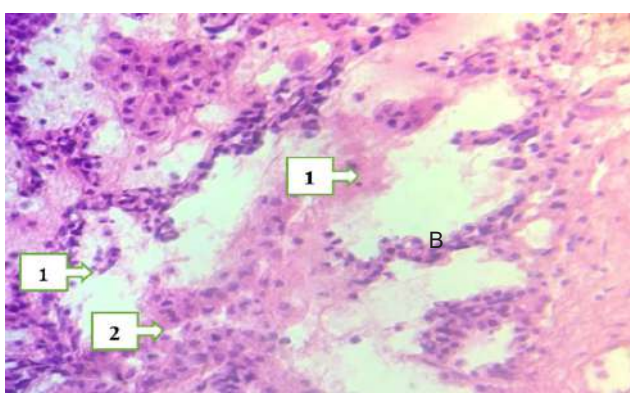


Fig. 3. Emphysematous enlargement of the alveoli (1) and infiltration of lymphocytes and macrophages (2) in the interstitial tissue of the lung. Stained with haematoxylin and eosin. ×400.

In some cases, chronic inflammation leads to dystrophic changes in the cartilage. The changes described above indicate the presence of a purulent inflammatory process accompanying bronchiectasis.

In moderate and severe forms of the disease, the mucous membrane is infiltrated by lymphocytes and mast cells. In the severe stage of the disease, the epithelium is single-layered and undifferentiated. Weakening of the protective mechanisms leads to epithelial restructuring, hyperplasia of goblet cells and bronchial glands, discoordination of secretion, and disruption of mucociliary transport. Secretion of viscous sputum increases, and bronchial wall oedema occurs. Granulation tissue gradually increases, muscle bundles hypertrophy, perivascular sclerosis develops, and subsequently fibrosis of the bronchial muscle layer occurs (Fig. 4).

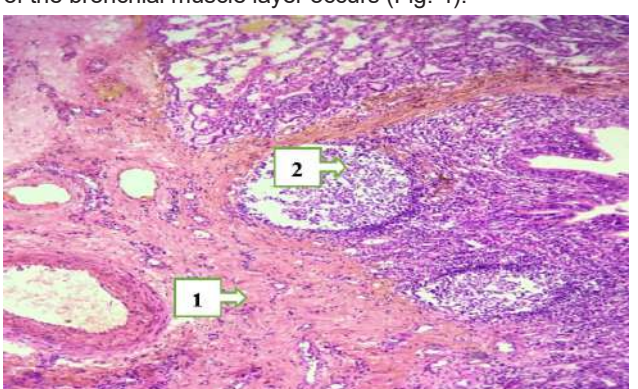


Fig. 4. Lungs of a 7-year-old child. Large foci of sclerosis (1) and purulent exudate (2). Stained with haematoxylin and eosin. ×400.

The formation of mucociliary insufficiency is caused by an active inflammatory process in the bronchi, a disruption in the structure of the bronchial mucosa, an increase in the viscosity of bronchial secretions, and a decrease in the frequency of cilia beating in the ciliated epithelium. In chronic obstruction, epithelial desquamation, squamous metaplasia, and loss of cilia by ciliated cells are observed (Fig. 5). Foci of sclerosis and fuchsinophilia of collagen fibres are noted under areas of epithelial metaplasia (Fig. 6).

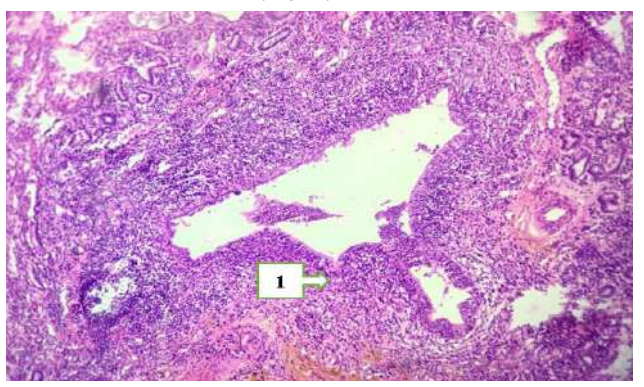


Fig. 5. Small-calibre bronchus of a 1.5-month-old child. Metaplasia of multi-row ciliated epithelium into multi-layered squamous non-keratinising epithelium (1) and pronounced lymphocytic infiltration in the submucosa of a small-calibre bronchus. Stained with haematoxylin and eosin. ×400.

The chronic course of the process is characterized by the migration of polymorphonuclear leukocytes of the neutrophil series, macrophages, and lymphocytes, mainly into the submucosal layer of the terminal bronchioles, with the formation of lymphoid infiltrates surrounding the glands.

During exacerbation of obstruction, the migration of polymorphonuclear leukocytes into the thickness of the

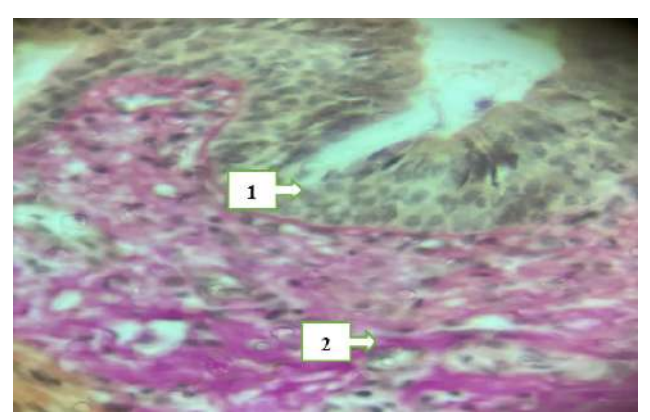


Fig. 6. Medium-calibre bronchus of a 2.3-year-old child. Metaplasia of multi-row ciliated epithelium into multi-layered non-keratinising squamous epithelium (1) and sclerosis of the submucosa of the bronchus (2). Stained using the Van Gieson method. ×400.

epithelium and into the lamina propria of the bronchial mucosa predominates, and in bronchioles with a diameter of less than 4 mm, infiltration of the entire wall is observed. Due to the absence of an adventitial membrane in the bronchioles, inflammation can freely spread to the lung tissue, usually with the development of X-ray-negative micropneumonia. In addition, as the pathology progresses, there is a significant increase in the percentage of airways containing these same cellular elements, as well as lymphocytes and plasma cells.

The accumulation of inflammatory cells contributes to an increase in the thickness of the walls of the small airways in patients with pathology and structural changes such as epithelial metaplasia and an increase in smooth muscle cells, goblet cells, hyperplasia and hypertrophy of the glands of the submucosal layer of the bronchial wall.

In addition to structures reflecting manifestations of a chronic non-specific inflammatory process, signs of congenital and acquired pathology were noted in the lungs of patients. In addition, peribronchial proliferation of adipose tissue around the large bronchi was detected. In some of the subjects, the presence of irregularly shaped cartilage and foci of sclerosis was noted, which is also considered a congenital malformation (Fig. 7).

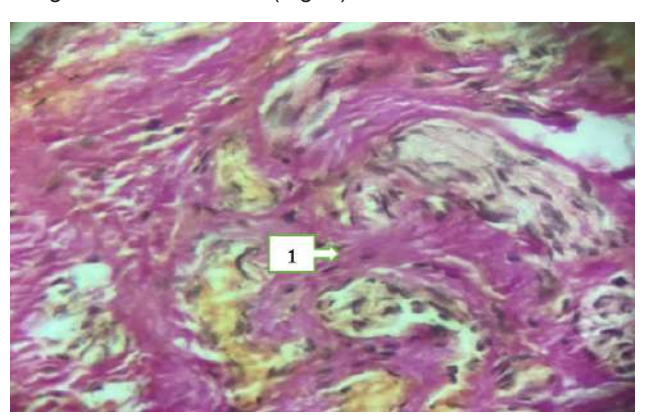


Fig. 7. Lungs of a child 1 month after birth. Foci of fibrosis and sclerosis (1). Stained with haematoxylin and eosin. ×400.

Underdevelopment of the bronchial tree is manifested by the presence of a large number of small bronchial tubes in the large bronchi. Similar clusters of small-diameter bronchial tubes are also found in the respiratory section. Extensive areas of atelectasis, degenerative changes in alveolar cells and bronchial epithelium are found in the lung parenchyma.

There is also hyperplasia and metaplasia of the bronchiolar epithelium into a multilayered squamous epithelium combined with small areas of emphysema. The interalveolar septa are thickened and edematous; there is proliferation of fibroblastic elements in the interstitium and fibrous structures.

When measuring the thickness of the mucous membrane of the large bronchi of newborns with bronchiectasis, it was 18.5 µm, medium-calibre bronchi 9.6 µm, and small-calibre bronchi 6.0 µm. When comparing the height of the epithelial covering to the lamina propria, it exceeded it in the main and lobar bronchi by 2.88 times, in medium-calibre bronchi by 2.90 times, and in small-calibre bronchi by 1.64 times. Compared to the control group, the thickness of large bronchi exceeded 0.64 times, medium bronchi 0.91 times, and small bronchi 0.90 times. The size of the bronchi in bronchiectasis increases with age. For example, in newborns in the control group, large bronchi have an average diameter of about 18.32 mm, while in preschool children with bronchiectasis, it is about 76.70 mm. The height of the lamina propria also increases with age and bronchial size. While in newborns in the control group the lamina propria in the large bronchi is about 9.44 mm, in newborns with bronchiectasis of the large bronchi the lamina propria under the multi-row ciliated epithelium is about 9.83 mm, in preschool children - about 23.60 mm, and in school-age children – about 36.24 mm.

According to our data, the percentage of lymphocytes in the bronchial mucosa of newborns born with bronchiectasis is 16.10 %, while in the respiratory tract it is 11.15 % and in the lamina propria it is 43.15 %. When comparing the epithelium to the lamina propria, it is 4.25 times greater, as large clusters of lymphocytes are found in the lamina propria. In the respiratory department, there are 0.75 times more lymphocytes compared to the control group. In infants with bronchiectasis, the percentage of lymphocytes is approximately the same as in newborns with bronchiectasis. In preschool and school-age children with bronchiectasis, there is a further increase in the percentage of lymphocytes, especially in the lamina propria and respiratory section of the lung, 18.80 % and 46.78 %, respectively (Fig. 8).

When studying the immunohistochemical reaction to Ki-67-positive cells in the lungs of newborns, they were detected both in the lung parenchyma and in the interstitial tissue. In the interstitial tissue, Ki-67-positive cells were evenly distributed throughout the section in the acini in each field of view. In the walls of the large bronchi, we observed single Ki-67-positive cells distributed throughout the entire area of the epithelium in quantities ranging from 1 to 5 cells, which accounted for an average of 46.51 % of the total number of cells in the bronchial mucosa. In the small bronchi, the

Vol. 31, №3, Page 37-46

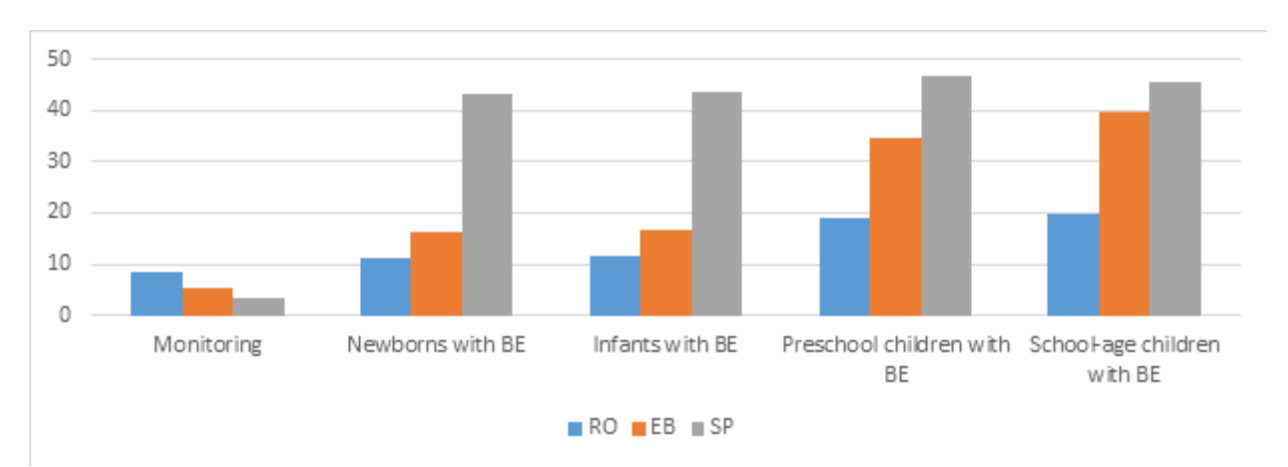


Fig. 8. Percentage of lymphocytes in the bronchi and lungs in children with bronchiectasis; BE – bronchiectasia, RO – respiratory department, EB – bronchial epithelium, SP – own plate.

number of Ki-67-positive cells reached 9 per alveolus. Single Ki-67-positive cells were also found in the ductal epithelium of the bronchial glands (Fig. 9). Based on the localization and intensity of the immunohistochemical reaction in the cells of the studied material, it was found that large clusters of Ki-67-positive cells were located in the small bronchi rather than in the large ones. These differences, indicating the state of proliferation processes in the lungs, were obtained by counting the number of labeled cells. Table 2 presents data on the expression of certain protein markers in the cells of children with bronchiectasis. The measurement results are given as a percentage of the total number of cells and are presented for the following markers: CD3, CD20, Bcl-2, and Ki-67. Based on the data presented in Table 2, in newborns with bronchiectasis, the percentage of cells expressing CD3 (Fig. 10) and CD20 is approximately 32.62 % and 34.61 %, respectively. Bcl-2 expression is approximately 4.32 % of cells, and Ki-67 expression is approximately 46.31 %. In infants with bronchiectasis, there is increased expression of CD3 and CD20, approximately 35.62 % and 36.24 %, respectively.

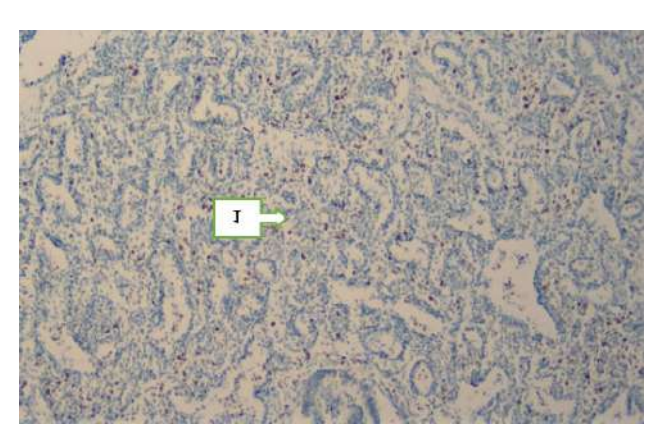


Fig. 9. Lungs of a newborn 21 days after birth. Ki-67 staining (brown cell nuclei). In the centre of the photo, alveolar cells with Ki-67-positive cells are visible (1). DAB chromagen staining.× 100.

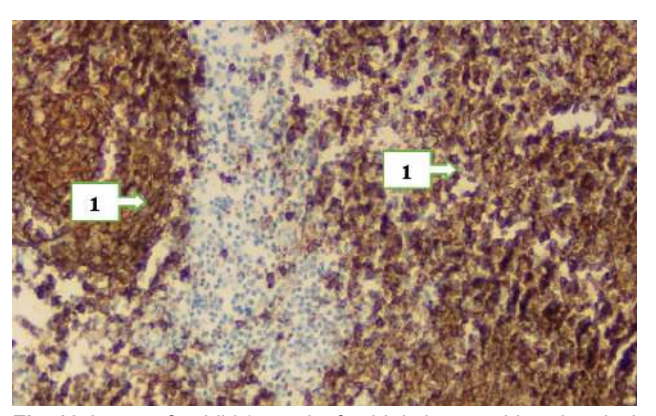


Fig. 10. Lungs of a child 1 month after birth. Immunohistochemical reaction to CD3-positive cells. CD3-positive cells are detected near the focus of fibrosis and sclerosis (1). Pronounced CD20-positive cells. DAB chromagen staining.× 200.

Table 2. Immunohistochemical study indicators for bronchiectasis in children (%).

•	•			
Groups	CD3	CD20	Bcl-2	Ki-67
Newborns with BE	32.62±2.80*	34.61±4.22*	4.33±2.81	46.30±3.62***
Infancy with BE	35.62±4.11	36.22±2.93**	4.81±3.43	49.22±4.64***
Preschool age	48.44±3.63***	53.81±3.71***	5.60±2.90	56.90±3.81***
School age	56.13±4.32	56.34±3.90	5.82±3.81	64.70±4.70***

Note: * – data reliability compared to control group indicators (*-p<0.05; **-p<0.01; ***-p<0.001).

The expression of Bcl-2 is about 4.81 %, and Ki-67 is about 49.22 %. In preschool and school-age children with bronchiectasis, the expression of CD3 and CD20 continues to increase, reaching approximately 48.44 % and 53.81 % in preschool age and 56.13 % and 56.34 % in school age, respectively (see Table 2). The expression of Bcl-2 (Fig. 11) and Ki-67 also increases with age, reaching values of approximately 5.60 % and 56.90 % in preschool age and 5.82% and 64.70% in school age, respectively (see Table 2).

It should be noted that these data indicate changes in the expression of protein markers in the cells of children with bronchiectasis depending on age. The expression of CD3 and CD20 indicates activation of the immune system, while the expression of Bcl-2 and Ki-67 may indicate changes in cell survival and proliferation.



Fig. 11. Lung of an 8-month-old child with bronchiectasis. Immunohistochemical reaction to Bcl-2-positive cells (1) in areas of emphysematous enlarged alveoli. DAB chromagen staining. ×100.

In our studies (Table 3), we observed moderate expression of CD3, CD20, and Ki-67 (++) markers in the bronchial epithelium, with a slightly elevated level of Bcl-2 (+). In the area of the bronchial basement membrane, there is increased expression of CD3 and CD20 (++), Ki-67 was weakly expressed (+), while Bcl-2 was absent (-). In the smooth muscle tissue of the bronchial wall, CD3 expression was low (+), CD20 expression was moderate (++), and Ki-67 expression was maximal (+++); no Bcl-2 expression was detected (-).

Table 3. Results of immunohistochemical examination of the lungs of children with bronchiectasis.

•				
Structural elements of the bronchial wall and lung	CD3	CD20	Ki-67	Bcl-2
Bronchial epithelium	++	++	++	+
Basement membrane	++	++	+	-
Smooth muscle tissue of the bronchial wall	+	++	+++	-
Interalveolar septa	+++	+++	+++	++
Endothelium of blood vessels	+++	+++	++	-
Smooth muscle tissue of blood vessels	+	++	++	+
Pericyte elements of vessels	+	+	+	-
Areas of fibrosis	+	+	+++	-

Note: "-" no expression; "+" minimal expression; "++" moderate expression; "+++" high expression of the marker under study.

Interalveolar septa show high activity of all major markers (see Table 3): CD3, CD20 and Ki-67 (+++), Bcl-2 is also noticeable (++). The vascular endothelium is characterised by strong expression of CD3 and CD20 (+++), Ki-67 is moderately expressed (++), and Bcl-2 is absent (-). In vascular smooth muscle tissue, CD3 expression is low (+), CD20 expression is moderate (++), Ki-67 expression is also moderate (++), and Bcl-2 expression is weak (+). Pericytic

elements of the vessels show low activity of all markers CD3, CD20 and Ki-67 (+), while Bcl-2 is absent (-). In areas of fibrosis, weak expression of CD3 and CD20 (+) is detected, while Ki-67 is maximally expressed (+++), and Bcl-2 is not detected (-).

At the same time, high Ki-67 staining is noted in the interalveolar septa, smooth muscle tissue, and areas of bronchial wall fibrosis, and moderate staining is noted in the bronchial epithelium and pulmonary tissue vessels (see Table 3).

Discussion

The complex mechanisms of pathogenesis in bronchiectasis are emphasised by many researchers. An interaction between immunogenetic susceptibility, immune dysregulation, bacterial infection, and lung damage is suggested. Damaged epithelium impedes mucus clearance and facilitates bacterial infection with increased coughing, sputum production, and airflow obstruction. Bronchiectasis may be present in autoimmune disease as well as in conditions of immune dysregulation [3]. Many children have ciliary dysmotility, which correlates with the presence and severity of bronchiectasis [25].

Thus, immunohistochemical analysis of lung tissue in children with bronchiectasis shows pronounced activity of both T-lymphocytes (CD3+) and B-lymphocytes (CD20+) in virtually all structural elements of the lung, especially in the interalveolar septa and vascular endothelium, as in previous studies. High levels of Ki-67 marker expression in the interalveolar septa, bronchial smooth muscle tissue, and areas of fibrosis indicate active cell proliferation processes. Bcl-2 expression was detected only in individual structures, which indicates uneven apoptotic activity and may indicate the predominance of proliferative processes over programmed cell death mechanisms. Taken together, these data confirm the presence of active inflammatory and reparative processes in the lung tissue of children with bronchiectasis, reflecting the chronic nature of the disease and the intensity of immune defence [3]. Children with bronchiectasis show noticeable changes in the morphometric parameters of the bronchial mucosa of various calibres. These changes are characterised by a significant increase in the height of the epithelium and the lamina propria under the multi-row ciliated epithelium (). The older the sick child, the higher these parameters are [15].

Chronic inflammation accompanied by activation of neutrophils, macrophages and T lymphocytes, hyperproduction of proinflammatory cytokines (IL-1 β , IL-6, TNF- α), as well as impaired regulation of apoptosis and tissue repair processes, plays a particularly important role in the pathogenesis of bronchiectasis. Immunological studies indicate that children with bronchiectasis often show signs of secondary immunodeficiency – a decrease in the number of CD3+, CD4+ and CD8+ cells, an imbalance in the Th1/Th2 ratio, a decrease in IFN- γ and IgA synthesis, and IgE hyperproduction [23]. This creates a tendency for bacterial

Vol. 31, №3, Page 37-46

infections to persist and inflammation to become chronic [9].

Medical science is actively studying the protective mechanisms of the lungs, which, thanks to innate and adaptive immunity, resist the constant exposure to pathogens, allergens, and toxins. Epithelial cells, leukocytes, and resident immune cells secrete factors that regulate inflammation and have a bactericidal effect, which explains the low incidence of pulmonary infections in healthy people [13]. The respiratory tract epithelium protects the lungs from inhaled pathogens and metabolites. Mucus produced by goblet cells and glands is continuously moved from the distal sections to the larynx by the movement of cilia, ensuring the cleansing of the respiratory tract [14]. Epithelial defects caused by infection lead to impaired drainage, mucus obstruction, and loss of respiratory function; significant damage to the respiratory tract may be irreversible, making early intervention a key goal of therapy [11]. The innate immune system is capable of forming a "memory" of past exposures [2]; its epithelial components are laid down in prenatal ontogenesis and later supplemented by lymphoid structures. Pulmonary neuroendocrine cells are considered part of the innate immune system [7, 17].

Comparing the quantitative indicators of lymphocytes in bronchiectasis in children with the data of the control group, it can be noted that the number of lymphocytes in children with bronchiectasis differs significantly from the control group in all age categories. Newborns with bronchiectasis have significantly higher lymphocyte levels compared to the control group. This level remains high in infants, preschoolers, and school-age children with bronchiectasis. The greatest differences compared to the control group are observed in preschoolers and school-age children [28].

The immunological mechanisms of bronchiectasis pathogenesis are discussed in detail in a number of studies. For example, Murray P. J. and Wynn T. A. [18] described both the protective and pathogenic functions of macrophages in inflammatory lung diseases. Macrophage subpopulations play a key role in maintaining the balance between reparative and damaging processes. Supplementing these data, Pollard J. W. [20] showed that trophic macrophages can participate in both tissue repair and chronic inflammation.

Comparing the results of immunohistochemical studies of bronchiectasis in children with those of the control group reveals some differences. The level of CD3+ cells, which is

a marker of immune activity, is significantly higher in children with bronchiectasis in all age groups compared to the control group (p<0.001). This level continues to increase with the age of children with bronchiectasis. The level of CD20+ cells is also higher in children with bronchiectasis in all age categories compared to the control group (p<0.05 and p<0.01). This level also increases with age. The level of Bcl-2, an indicator of cell apoptosis, is slightly higher in children with bronchiectasis, but the differences in this parameter are not always statistically significant. The level of Ki-67, an indicator of cell proliferation, is significantly higher in children with bronchiectasis in all age groups compared to the control group (p<0.001), which is similar to pneumonia to some extent.

A clinical example described by Satvaldieva E. and colleagues [21] demonstrates the difficulties of late diagnosis of bronchiectasis in children. The article presents the case of a two-year-old child in whom the disease was detected at an advanced stage, requiring intensive care. The authors emphasise the need for early recognition of the pathology and timely application of comprehensive treatment measures.

An important aspect is the study of the epithelial barrier of the respiratory tract. A study by Strengert M. and Knaus U. G. [24] showed that disruption of the integrity of the lung epithelium contributes to the progression of inflammation and infection, which is especially relevant for patients with bronchiectasis.

A ten-year review by Zaid A. A. et al. [29] on the clinical aspects of non-cystic fibrosis bronchiectasis showed that early detection and the use of comprehensive patient management strategies can significantly reduce the frequency of exacerbations and improve the prognosis of the disease.

Conclusion

- 1. Children with bronchiectasis show changes in immunohistochemical parameters indicating immune system activation and cell proliferation. These changes may be associated with the inflammatory processes and immune responses characteristic of this condition.
- 2. Children with bronchiectasis show activation of all components of the immune system. It has been found that in children with bronchiectasis, destructive changes predominate in the components of immunity, indicating their insufficient protective function.

References

- [1] Albano, G. D., Montalbano, A. M., Gagliardo, R., Anzalone, G., & Profita, M. (2022). Impact of air pollution in airway diseases: role of the epithelial cells (cell models and biomarkers). *International journal of molecular sciences*, 23(5), 2799. doi: 10.3390/ijms23052799
- [2] Berical, A., Lee, R. E., Randell, S. H., & Hawkins, F. (2019). Challenges facing airway epithelial cell-based therapy for cystic fibrosis. *Frontiers in pharmacology*, 10, 74. doi: 10.3389/fphar.2019.00074
- [3] Boyton, R. J., & Altmann, D. M. (2016). Bronchiectasis: current concepts in pathogenesis, immunology, and microbiology.
- Annual Review of Pathology: Mechanisms of Disease, 11(1), 523-554. doi: 10.1146/annurev-pathol-012615-044344
- [4] Bush, A., Deterding, R. R., Li, A., Ratjen, F., Sly, P., Zar, H., & Wilmott, R. W. (Eds.). (2023). Kendig and Wilmott's Disorders of the Respiratory Tract in Children-E-Book. Elsevier Health Sciences.
- [5] Chang, A. B., Bell, S. C., Torzillo, P. J., King, P. T., Maguire, G. P., Byrnes, C. A., ... & Grimwood, K. (2015). Chronic suppurative lung disease and bronchiectasis in children and adults in Australia and New Zealand Thoracic Society of Australia and New Zealand guidelines. *Medical Journal*

- of Australia, 202(1), 21-23. doi: 10.5694/mja14.00287
- [6] Chotirmall, S. H., & Chalmers, J. D. (2018). RESPIRE: breathing new life into bronchiectasis. Eur Respir J, 51(1), 1702444. doi: 10.1183/13993003.02444-2017
- [7] Crane, M. J., Lee, K. M., FitzGerald, E. S., & Jamieson, A. M. (2018). Surviving deadly lung infections: innate host tolerance mechanisms in the pulmonary system. *Frontiers* in *Immunology*, 9, 1421. doi: 10.3389/fimmu.2018.01421
- [8] Crystal, R. G., Randell, S. H., Engelhardt, J. F., Voynow, J., & Sunday, M. E. (2008). Airway epithelial cells: current concepts and challenges. *Proceedings of the American Thoracic Society*, 5(7), 772-777. doi: 10.1513/pats.200805-041HR
- [9] Fraser, C. S., & José, R. J. (2023). Insights into personalised medicine in bronchiectasis. *Journal of Personalized Medicine*, 13(1), 133. doi: 10.3390/jpm13010133
- [10] Goyal, V., McPhail, S. M., Hurley, F., Grimwood, K., Marchant, J. M., Masters, I. B., & Chang, A. B. (2020). Cost of hospitalization for bronchiectasis exacerbation in children. *Respirology*, 25(12), 1250-1256. doi: 10.1111/resp.13828
- [11] José, R. J., & Brown, J. S. (2014). Bronchiectasis. *British Journal of Hospital Medicine*, 75(Sup10), C146-C151. doi: 10.12968/hmed.2014.75.Sup10.C146
- [12] Кагітоva, N. (2022). Иммунный статус и клиникодиагностические особенности течения хронического бронхита у детей [Immune status and clinical-diagnostic features of chronic bronchitis in children]. Международный журнал научной педиатрии=International Journal of Scientific Pediatrics, 1(7), 25-30. doi: 10.56121/2181-2926-2022-7-25-30
- [13] Khaitov, M. R., Ilina, N. I., Luss, L. V., & Babakhin, A. A. (2017). Мукозальный иммунитет респираторного тракта и его роль при профессиональных патологиях [Mucosal immunity of the respiratory tract and its role in occupational pathologies]. Медицина экстремальных ситуаций=Medicine of Extreme Situations, 3(61), 8-24.
- [14] Kharchenko, V. V., Mantulina, L. A., Nikishina, E. I., Bakhmet, A. A., & Klochkova, S. V. (2016). Состояние слизистой оболочки трахеобронхиального дерева в норме у людей зрелого возраста [Condition of the tracheobronchial mucosa in healthy adults of mature age]. *Человек и его здоровье=Мап and His Health*, (3), 89-99. doi: 10.21626/vestnik/2016-3/14
- [15] King, P. T. (2018). The role of the immune response in the pathogenesis of bronchiectasis. *BioMed research international*, 2018(1), 6802637. doi: 10.1155/2018/6802637
- [16] Kumar, A., Lodha, R., Kumar, P., & Kabra, S. K. (2015). Non-cystic fibrosis bronchiectasis in children: clinical profile, etiology and outcome. *Indian pediatrics*, 52(1), 35-37. doi: 10.1007/s13312-015-0563-8
- [17] Lanyu, Z., & Feilong, H. (2019). Emerging role of extracellular vesicles in lung injury and inflammation. *Biomedicine* & *Pharmacotherapy*, 113, 108748. doi: 10.1016/j.biopha.2019.108748

- [18] Murray, P. J., & Wynn, T. A. (2011). Protective and pathogenic functions of macrophage subsets. *Nature reviews* immunology, 11(11), 723-737. doi: 10.1038/nri3073
- [19] Pifferi, M., Caramella, D., Ragazzo, V., Cangiotti, A. M., Macchia, P., & Boner, A. L. (2008). Bronchiectasis in children with recurrent pneumonia: an immunopathological damage associated with secondary ciliary dysmotility. *International Journal of Immunopathology and Pharmacology*, 21(1), 215-219. doi: 10.1177/039463200802100124
- [20] Pollard, J. W. (2009). Trophic macrophages in development and disease. *Nature reviews immunology*, 9(4), 259-270. doi: 10.1038/nri2528
- [21] Satvaldieva, E., Yusupov, A. S., Urumbaev, R. M., Murodova, M. S., & Kollas, E. V. (2021). Клинический случай интенсивной терапии ребенка 2-х лет с бронхоэктатической болезнью (поздняя диагностика) [A clinical case of intensive care for a 2-year-old child with bronchiectasis (late diagnosis)]. Eurasian Bulletin of Pediatrics=Eurasian Bulletin of Pediatrics, 2(9), 34-40.
- [22] Shamsiev, F., & Turakulova, H. (2023). Клинические и иммунологические особенности бронхообструктивного синдрома у детей [Clinical and immunological features of bronchial obstructive syndrome in children]. Международный журнал научной педиатрии=International Journal of Scientific Pediatrics, 2(5), 22-26. doi: 10.56121/2181-2926-2023-5-22-26
- [23] Stakan, T. A., Shevtchenko, N. I., & Salivontchik, A. P. (2008). Clinical value of studying of immune mechanisms protection features and inflammatory reaction at chronic bronchopulmonary pathologies at children. *Health and Ecology Issues*, 105. doi: 10.51523/2708-6011.2008-5-2-23
- [24] Strengert, M., & Knaus, U. G. (2011). Analysis of epithelial barrier integrity in polarized lung epithelial cells. In *Perme-ability barrier: methods and protocols* (pp. 195-206). Totowa, NJ: Humana Press. doi: 10.1007/978-1-61779-191-8_13
- [25] Suzuki, T., Chow, C. W., & Downey, G. P. (2008). Role of innate immune cells and their products in lung immunopathology. The international journal of biochemistry & cell biology, 40(6-7), 1348-1361. doi: 10.1016/j.biocel.2008.01.003
- [26] Vendrell, M., de Gracia, J., Olveira, C., Martínez, M. Á., Girón, R., Máiz, L., ... & Solé, A. (2008). Diagnóstico y tratamiento de las bronquiectasias. *Archivos de bronconeu-mologia*, 44(11), 629-640. doi: 10.1157/13128330
- [27] Viegi, G., Maio, S., Fasola, S., & Baldacci, S. (2020). Global burden of chronic respiratory diseases. *Journal of aerosol* medicine and pulmonary drug delivery, 33(4), 171-177. doi: 10.1089/jamp.2019.1576
- [28] Yuan, R., Yu, J., Jiao, Z., Li, J., Wu, F., Yan, R., ... & Chen, C. (2021). The roles of tissue-resident memory T cells in lung diseases. Frontiers in Immunology, 12, 710375. doi: 10.3389/fimmu.2021.710375
- [29] Zaid, A. A., Elnazir, B., & Greally, P. (2010). A decade of non-cystic fibrosis bronchiectasis 1996-2006. *Ir Med J*, 103(3), 77-79. PMID: 20666070

СТРУКТУРНІ КОМПОНЕНТИ ТА ІММУННОГІСТОХІМІЧНІ ОСОБЛИВОСТІ ОРГАНІВ ДИХАННЯ У ДІТЕЙ ПРИ БРОНХОЕКТАЗІЯХ

Хамідова Ф. М., Абдуллаєв Б. С., Сулаймонова М. Ж., Жовлієва М. Б., Амінова Н. А.

Вивчення хронічного запалення легеневої тканини при бронхоектазіях у дітей є необхідним для глибшого розуміння клітинних і молекулярних механізмів хронічних респіраторних захворювань та розробки нових підходів до їх терапії. Мета дослідження— вивчити гістологічні та імуногістохімічні зміни структур бронхів і легень при бронхоектазіях у дітей. У роботі використано частки або фрагменти легень, видалені під час операцій з приводу бронхоектазій у 62 дітей. Отримані мікропрепарати тканин бронхів і легень забарвлювали гематоксиліном та еозином, пікрофуксином

Vol. 31, №3, Page 37-46

за Ван Гізоном, резорцин-фуксином за Вейгертом. Імуногістохімічні дослідження мікропрепаратів легень виконані з використанням моноклональних антитіл до Кі-67, ВсІ-2, СD3, СD20. Порівнюючи результати імуногістохімічних досліджень у дітей із бронхоектазіями та в контрольній групі, виявлено виражені відмінності. Так, рівень CD3+ клітин — маркера імунної активності — був значно вищим у дітей із бронхоектазіями в усіх вікових групах порівняно з контролем (р<0,001) і продовжував зростати зі збільшенням віку. Аналогічно, вміст CD20+ клітин також був вищим у дітей із бронхоектазіями незалежно від віку (р<0,05 і р<0,01), із тенденцією до його збільшення у старших дітей. Показник ВсІ-2, пов'язаний із процесами апоптозу клітин, у дітей із бронхоектазіями був дещо підвищеним, проте різниця не завжди досягала статистичної значущості. Водночає рівень Кі-67, що відображає інтенсивність клітинної проліферації, був достовірно вищим у дітей із бронхоектазіями у всіх вікових групах порівняно з контролем (р<0,001). Таким чином, у дітей із бронхоектазіями виявляються зміни імуногістохімічних характеристик, які свідчать про активізацію імунної системи та посилену клітинну проліферацію. Ці процеси можуть бути пов'язані із запаленням та імунними реакціями, типовими для даного захворювання. Відповідно, можна зробити висновок, що у дітей із бронхоектазіями активізуються всі ланки імунної системи. При цьому встановлено, що в них переважають деструктивні зміни імунних компонентів, що вказує на зниження їх захисної функції.

Author's contribution

Khamidova F. M. – ideological concept of the work, writing the text; editing articles.

Abdullayev B. S. - concept and design, acquisition, analysis, or interpretation of data, manuscript drafting, manuscript revision.

Sulaymonova M. J. - collection and analysis of literature sources, compilation of text.

Zhovlieva M. B. – concept and design, acquisition, analysis, or interpretation of data, manuscript drafting, manuscript revision.

Aminova N.A. – concept and design, acquisition, analysis, or interpretation of data, manuscript drafting, manuscript revision.

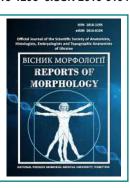
ISSN 1818-1295 eISSN 2616-6194



REPORTS OF MORPHOLOGY

Official Journal of the Scientific Society of Anatomists, Histologists, Embryologists and Topographic Anatomists of Ukraine

journal homepage: https://morphology-journal.com



Histological changes in the dentate gyrus of the hippocampus in rats with induced colon adenocarcinoma and after correction with nanomaterials

Chebernina I. O.^{1,2}, Nebesna Z. M.¹, Ohinska N. V.¹, Hetmaniuk I. B.¹, Kulbitska V. V.¹

¹I. Horbachevsky Ternopil National Medical University, Ternopil, Ukraine ²State Establishment Lugansk State Medical University, Rivne, Ukraine

ARTICLE INFO

Received: 23 January 2025 Accepted: 25 June 2025

UDC: 612.822.3:616-006.6-092:615.9

CORRESPONDING AUTHOR

e-mail: chebernina_io@tdmu.edu.ua Chebernina I. O.

CONFLICT OF INTEREST

The authors have no conflicts of interest to declare.

FUNDING

Not applicable.

DATA SHARING

Data are available upon reasonable request to corresponding author.

The hippocampus plays a significant role in the formation of multiple central nervous system functions and is highly sensitive to pathological influences, as demonstrated in numerous experimental studies. However, the impact of induced colorectal adenocarcinoma on the structural organization of the hippocampus remains unclear. Therefore, the aim of our study was to investigate histological changes in the dentate gyrus under conditions of N,N-dimethylhydrazine (DMH)-induced colon cancer in rats, as well as to evaluate the corrective effects of Au/Ag/Fe nanomaterials. A total of 45 white rats were used and divided into three groups: Group I - intact rats, Group II - rats with DMH-induced oncogenesis, Group III – rats with DMH-induced adenocarcinoma receiving a composition of Au/Ag/Fe nanomaterials. Carcinogenesis was induced by subcutaneous administration of N,N-dimethylhydrazine (DMH, batch D161608, Sigma-Aldrich Sp. z o.o., Japan) once weekly for 30 weeks in the interscapular region. The composition of Au/Ag/Fe nanomaterials was administered intragastrically once daily for 21 days to rats of Group III. Brain samples were processed according to standard histological protocols, and sections were stained with toluidine blue and hematoxylineosin. Morphological changes were visualized using a MICROmed SEO SCAN microscope equipped with a Vision CCD camera. Histological examination revealed that rats of Group II demonstrated the most pronounced alterations in the granular layer of the dentate gyrus, including decreased cell density, presence of activated glial cells and shadow cells, nuclear pyknosis, and disrupted ratios of normochromic to hyperand hypochromic neurons. Hemodynamic disturbances with the development of stasis, sludge, and perivascular edema were also observed. Administration of the Au/Ag/Fe nanocomposite contributed to restoration of the structural organization of the granular layer, with increased cell density, reduction of glial elements, and normalization of hippocampal stratification. Correction with nanomaterials substantially improved the morphological state of the hippocampus, reduced the severity of pathological alterations, promoted restoration of the cellular architecture of the dentate gyrus, and normalized the condition of the microvascular network.

Keywords: brain, hippocampus, carcinogenesis, dentate gyrus, nanoparticles, neurons, histological changes.

Introduction

The hippocampus, together with the dentate gyrus, subicular complex, and entorhinal cortex, constitutes the hippocampal formation, which is located at the floor of the temporal horn of the lateral ventricle and is part of the medial temporal lobe in all mammals. This structure, closely interconnected with the adjacent cortex through which most of its connections are mediated, plays a pivotal role in the

central nervous system, underpinning processes of memory, learning, and emotional regulation, while also exhibiting high sensitivity to pathological influences [5, 14, 25, 26].

A reduction in its volume and associated cognitive impairments have been documented in patients with chronic obstructive pulmonary disease, liver cirrhosis, pancreatitis, and in individuals undergoing hemodialysis [4, 24, 28, 29].

Experimental models of disease have similarly revealed structural alterations: in induced colitis, metabolite clearance is impaired, amyloid plaques accumulate, microglia and astrocytes are activated, leading to neuronal death and cognitive deficits [30, 32]. In bone inflammation, osteoblasts overproduce lipocalin-2, which damages neurons in the CA1 field of the hippocampus [31]. Comparable changes have also been described under conditions such as streptozotocin-induced diabetes mellitus, gut dysbiosis, high-fructose diets, and viral infections [8, 16, 19, 23]. Arterial hypertension leads to hippocampal volume reduction due to layer atrophy, decreased neurogenesis in the CA1 field, and lowered levels of brain-derived neurotrophic factor [11].

Conversely, hippocampal function improves in both animals and humans in response to physical exercise. This phenomenon is attributed to enhanced hippocampal neurogenesis, increased cell proliferation, improved synaptic plasticity, and higher dendritic density. It is believed that neurogenesis and cell proliferation are major determinants of hippocampal function, learning, and memory [3, 11]. Current evidence suggests that impaired adult hippocampal neurogenesis may contribute to cognitive decline in neurological disorders and to the emergence of psychological symptoms in psychiatric conditions [9, 12].

The vulnerability of the hippocampus has made it a focal point in studies of epilepsy, Alzheimer's disease, and neuroinflammation. Concurrently, contemporary research increasingly explores nanoparticles as promising agents for modulating pathological changes in brain tissue. Due to their small size, these particles are able to cross the bloodbrain barrier and influence cellular metabolism and immune mechanisms [7, 21]. For instance, silica nanoparticles exhibit cytostatic properties under phototherapy, while calcium hydroxyapatite, silver, and gold nanoparticles selectively inhibit cancer cell proliferation [22, 27]. Silver nanoparticles are considered a "two-in-one" therapeutic system, as they not only exert cytotoxic activity through the release of reactive silver ions but also transport cytotoxic agents to target tissues [11]. Iron nanoparticles are used for drug delivery across the blood-brain barrier owing to their magnetic properties and lower toxicity. Zinc nanoparticles reduce cell viability and induce apoptosis, including in neuroblastoma cell models; in Parkinson's disease models, they alter dopamine levels and may have neuroprotective potential [17].

Of particular importance for modeling systemic brain effects is N,N-dimethylhydrazine (DMH), a carcinogen that induces colorectal adenocarcinoma. Its metabolites damage DNA, provoke oxidative stress and chronic inflammation, thereby recapitulating multistage carcinogenesis akin to the human condition. This makes the DMH model a valuable tool not only for studying tumor growth but also for investigating the distant consequences of colorectal cancer, including effects on the brain.

The aim of our study was to investigate histological changes in the dentate gyrus in a rat model of N,N-dimethylhydrazine-induced colorectal cancer, and under

conditions of correction with Au/Ag/Fe-based nanomaterials.

Materials and methods

The study involved 45 white laboratory rats of the Wistar strain, maintained under standard vivarium conditions at I. Horbachevsky Ternopil National Medical University, Ministry of Health of Ukraine. The animals had free access to drinking water and were fed a standard diet *ad libitum*. All procedures involving animals were conducted in accordance with the European Convention for the Protection of Vertebrate Animals Used for Experimental and Other Scientific Purposes (Strasbourg, 1986), the Law of Ukraine "On the Protection of Animals from Cruelty," the ethical principles of experiments (Kyiv, 2001), and were approved by the Bioethics Committee of I. Horbachevsky Ternopil National Medical University (Protocol No. 75, dated 01.11.2023).

Colorectal adenocarcinoma was induced by subscapular administration of N,N-dimethylhydrazine (DMH, batch D161608, Sigma-Aldrich Sp. z o.o., Japan) once every seven days over a period of 30 weeks. The animals were divided into four groups: Group I – intact white rats; Group II – white rats with DMH-induced carcinogenesis; Group III – rats with DMH-induced adenocarcinoma that received a nanomaterial composition of Au/Ag/Fe. The animals in Group III were administered an aqueous dispersion of Au/Ag/Fe nanoparticles intragastrically once daily for three weeks.

Animals in Group II were sacrificed after 30 weeks, and those in Group III after 21 days, for further analysis of changes in the dentate gyrus of the hippocampus. For euthanasia, the animals were anesthetized via intraperitoneal injection of 10 % thiopental sodium solution at a dose of 50 mg/kg (Arterium, Ukraine), followed by decapitation.

Subsequent sample processing was performed using standard histological techniques, including embedding in paraffin blocks. Sections 4-5 µm thick were prepared using the AMR400 microtome (Amos, Australia) and stained by two methods: hematoxylin and eosin, and Nissl staining with toluidine blue. Histological preparations were examined using a MICROmed SEO SCAN microscope equipped with a Vision CCD video camera.

Results

The histological structure of the hippocampus in animals of Group I (control) corresponded to the typical morphological pattern. Microscopic examination revealed the characteristic three-layered organization of this structure. The molecular layer (*stratum moleculare*) was sparsely populated with cells and contained dendrites of granule neurons. Occasional small glial cell nuclei were observed, and the staining was faint.

Neurons of the granule cell layer (*stratum granulosum*) were small, round to oval in shape, and closely packed, typically arranged in 4-8 rows. The cell nuclei were normochromatic, well-defined, round, with a prominent nucleolus and predominantly euchromatic content. The cytoplasm appeared faintly visible, forming a thin rim around the nucleus, and was weakly stained.

The polymorphic layer (*stratum polymorphe*) contained large polygonal cells, including mossy neurons, which were distributed more loosely and irregularly, often among fibrous structures. Nuclei in this layer exhibited greater morphological variability compared to granule neurons (Fig. 1).

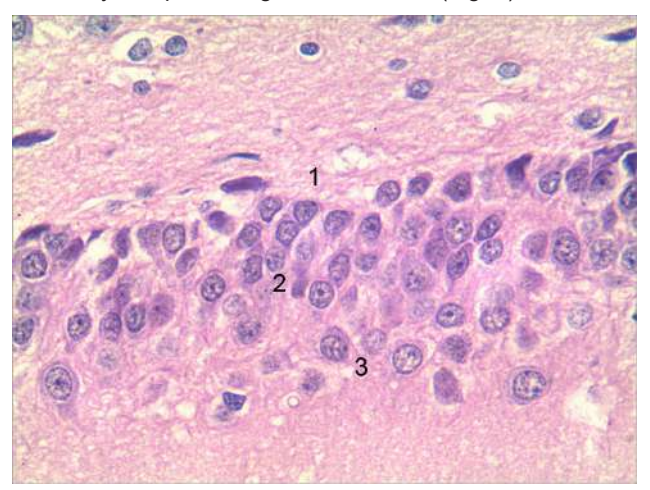


Fig. 1. Histological organization of the dentate gyrus of the hippocampus in control group rats. 1 – molecular layer, 2 – granule cell layer, 3 – polymorphic layer. Hematoxylin and eosin staining. ×200.

After seven months of modeling colorectal adenocarcinoma, pronounced dystrophic changes characteristic of chronic toxic damage and neurodegeneration were observed in the dentate gyrus of the hippocampus. Loss of stratification of the dentate gyrus layers was noted, with indistinct boundaries between the molecular, granule cell, and polymorphic layers. Neurons in the granule cell layer were deformed, exhibiting pyknotic nuclei and cytoplasmic destruction, with the appearance of intercellular vacuoles.

Cells with marked hypochromia were identified, characterized by faintly stained nuclei and cytoplasm, lacking signs of basophilic substance. Some neurocytes exhibited shrunken, hyperchromatic nuclei typical of pyknosis, with loss of nuclear contour clarity. In certain areas, shadow cells – residual bodies of neurocytes that had undergone degenerative and necrotic changes – were observed. Enlarged perivascular spaces and pericellular edema were also noted.

Within the granule cell layer, polygonal hyperchromatic cells identified as activated glia were present. In the polymorphic layer, some neurocytes were deformed, with nuclei displaced from the central position and a predominance of heterochromatin within the nuclei (Fig. 2).

In hippocampal micropreparations of rats with DMH-induced colorectal cancer treated with the nanoparticle composition, regenerative changes were observed in comparison to Group II. These included restoration of the structural organization of the granule cell layer and increased cell density. A reduction in the number of polygonal atypical cells was noted, indicating a diminished impact of the pathological process. The boundaries between the layers

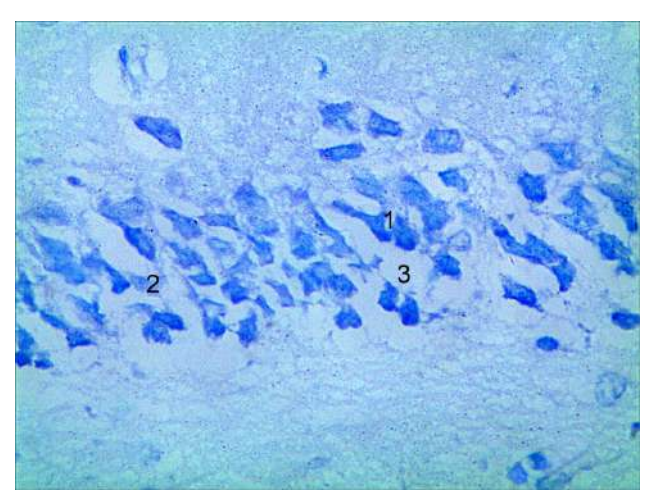


Fig. 2. Histological changes in the granule cell layer of the dentate gyrus of the hippocampus after 7 months of carcinogenesis modeling. 1 – hyperchromatic neurocytes, 2 – shadow cells, 3 – pericellular edema. Nissl staining. ×200.

were more distinct, and hypo- and hyperchromatic neurocytes were less frequently encountered. Hemocapillaries were moderately engorged, with clearly defined walls and no pronounced perivascular edema. These findings suggest a neuroprotective or restorative effect of the administered nanomaterials (Fig. 3).

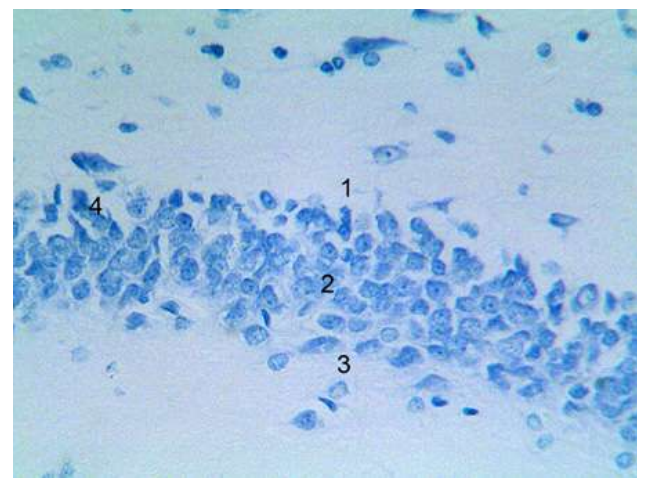


Fig. 3. Histological changes in the granule cell layer of the dentate gyrus of the hippocampus in rats with induced carcinogenesis and nanoparticle-based correction. 1 – molecular layer, 2 – granule cell layer, 3 – polymorphic layer, 4 – isolated hyperchromatic neurocytes. Nissl staining. ×200.

Discussion

The obtained histological studies demonstrate that *in situ* induction of colorectal adenocarcinoma using N,N-dimethylhydrazine leads to significant histological alterations in the hippocampus, particularly in the dentate gyrus. A reduction in neuronal density, appearance of pyknotic nuclei, dystrophic changes in the cytoplasm, and microglial activation were observed. Vascular alterations were noted, especially in the hemomicrocirculatory compartment, with the

Vol. 31, №3, Page 47-52

development of stasis, sludge formation, and perivascular edema.

These hippocampal layer changes can be attributed to oxidative stress in the context of carcinogenesis, the development of neuroinflammation with microglial activation, and suppression of neurogenesis. A key role in the structural changes of the hippocampus is played by the inhibition of neurogenesis in the granule cell layer of the dentate gyrus – one of the few regions in the adult brain where neurogenesis occurs. Additionally, dysfunction of the glutamatergic system significantly contributes to the histological alterations, ultimately resulting in the loss of synaptic connections. These observations are consistent with previous studies that have shown chronic systemic stress can induce neurodegenerative changes in the hippocampus, particularly through disruptions in antioxidant defense systems and inflammatory responses [2, 31, 32].

For instance, streptozotocin-induced gestational diabetes in pregnant rats leads to morphohistological alterations in the hippocampus of offspring, including a reduction in CA3 area size, decreased neuronal density, and disorganization of pyramidal cell architecture. In a model of acute gastrointestinal inflammation in rats, reduced neuroactivity and decreased density of dendritic spines in hippocampal neurons were reported, indicating structural remodeling at the synaptic level. Ovariectomy resulted in reduced synaptic transmission between the CA3 and CA1 regions and microglial activation [20].

Administration of the Au/Ag/Fe nanoparticle composition exhibited a positive effect on hippocampal morphology. There was restoration of cell density in the granule cell layer, a decrease in the number of glial cells, and clearer demarcation of the dentate gyrus layers. These findings suggest a potential neuroprotective effect of the nanomaterials, likely mediated by their antioxidant and anti-inflammatory properties [6].

Similar effects of nanoparticles have been reported in other studies. For example, selenium administration in a chronic stress model in rats led to behavioral improvement and a reduction in oxidative stress levels in the hippocampus [8, 9, 21]. Another study demonstrated that gold nanoparticles combined with alpha-lipoic acid exerted neuroprotective effects against radiation-induced brain injury in rats [1]. Nanoparticles that are inherently toxic (e.g., silicon dioxide) may reduce neurotoxicity and preserve hippocampal structure in the offspring of experimental animals when properly combined with antioxidants. This underscores the importance not only of nanoparticle type but also the context of their application.

Another critical aspect is neurovascular interaction. Vascular risk factors, including hypertension, are closely linked to hippocampal volume reduction. The use of nanoparticles that enhance endothelial function or possess vasoprotective properties may represent a promising strategy for preventing cognitive decline in vascular-related conditions [9, 10, 21].

Thus, the results of our study confirm the potential of Au/Ag/Fe nanomaterials as a means for correcting neurodegenerative changes in the hippocampus caused by systemic pathological processes such as carcinogenesis. Based on the cited studies, it can be hypothesized that such nanocomposites may target multiple key pathogenic mechanisms – oxidative stress, microglial activation, vascular dysfunction, and impaired neuroplasticity.

Further research is required to elucidate the detailed mechanisms of action of these nanomaterials and assess their potential application in clinical practice.

Conclusions

- 1. It was established that significant degenerative changes occur in the "neurocyte-hemocapillary-gliocyte" triad of the hippocampus in animals with *in situ* DMH-induced colorectal adenocarcinoma after seven months.
- 2. The use of Au/Ag/Fe nanoparticles as a corrective intervention markedly improves the morphological state of the hippocampus, reduces pathological alterations, and promotes the restoration of the cellular architecture of the dentate gyrus and the vascular network.

References

- [1] Abdelkader, N. F., El-Batal, A. I., Amin, Y. M., Hawas, A. M., Hassan, S. H. M., & Eid, N. I. (2022). Neuroprotective Effect of Gold Nanoparticles and Alpha-Lipoic Acid Mixture against Radiation-Induced Brain Damage in Rats. *International journal of molecular sciences*, 23(17), 9640. doi: 10.3390/ ijms23179640
- [2] Barbosa, D. A. N., Gattas, S., Salgado, J. S., Kuijper, F. M., Wang, A. R., Huang, Y., ... & Halpern, C. H. (2023). An orexigenic subnetwork within the human hippocampus. *Nature*, 621(7978), 381-388. doi: 10.1038/s41586-023-06459-w
- [3] Blume, G. R., & Royes, L. F. F. (2024). Peripheral to brain and hippocampus crosstalk induced by exercise mediates cognitive and structural hippocampal adaptations. *Life sciences*, 352, 122799. doi: 10.1016/j.lfs.2024.122799
- [4] Chen, H. J., Qiu, J., Qi, Y., Fu, L., Fu, Q., Wu, W., ... & Chen, F. (2023). Hippocampal subfield morphology in regular hemodialysis patients. *Nephrology, dialysis, transplantation:* official publication of the European Dialysis and Transplant

- Association European Renal Association, 38(4), 992-1001. doi: 10.1093/ndt/gfac263
- [5] Chettih, S. N., Mackevicius, E. L., Hale, S., & Aronov, D. (2024). Barcoding of episodic memories in the hippocampus of a food-caching bird. *Cell*, 187(8), 1922-1935.e20. doi: 10.1016/j.cell.2024.02.032
- [6] Dadkhah, M., Afshari, S., Samizadegan, T., Shirmard, L. R., & Barin, S. (2024). Pegylated chitosan nanoparticles of fluoxetine enhance cognitive performance and hippocampal brain derived neurotrophic factor levels in a rat model of local demyelination. *Experimental gerontology*, 195, 112533. doi: 10.1016/j.exger.2024.112533
- [7] Dheyab, M. A., Aziz, A. A., Khaniabadi, P. M., Jameel, M. S., Oladzadabbasabadi, N., Rahman, A. A., ... & Mehrdel, B. (2023). Gold nanoparticles-based photothermal therapy for breast cancer. *Photodiagnosis and photodynamic therapy*, 42, 103312. doi: 10.1016/j.pdpdt.2023.103312
- [8] Dumetz, F., Ginieis, R., Bure, C., Marie, A., Alfos, S., Pallet,

- V., & Bosch-Bouju, C. (2022). Neuronal morphology and synaptic plasticity in the hippocampus of vitamin A deficient rats. *Nutritional neuroscience*, *25*(4), 779-790. doi: 10.108 0/1028415X.2020.1809877
- [9] Elcombe, E. L., Lagopoulos, J., Duffy, S. L., Lewis, S. J., Norrie, L., Hickie, I. B., & Naismith, S. L. (2015). Hippocampal volume in older adults at risk of cognitive decline: the role of sleep, vascular risk, and depression. *J Alzheimers Dis*, 44(4), 1279-1290. doi: 10.3233/JAD-142016
- [10] Elfakharany, S. A., Eskaros, S. S., Azhary, N. M. E., Abdelmonsif, D. A., Zeitoun, T. M., Ammar, G. A. G., & Hatem, Y. A. (2024). Neuroprotective Role of Selenium Nanoparticles Against Behavioral, Neurobiochemical and Histological Alterations in Rats Subjected to Chronic Restraint Stress. *Molecular neurobiology*, 61(12), 10159-10181. doi: 10.1007/s12035-024-04196-3
- [11] Feng, R., Rolls, E. T., Cheng, W., & Feng, J. (2020). Hypertension is associated with reduced hippocampal connectivity and impaired memory. *EBioMedicine*, 61, 103082. doi: 10.1016/j.ebiom.2020.103082
- [12] Fotuhi, M., Do, D., & Jack, C. (2012). Modifiable factors that alter the size of the hippocampus with ageing. *Nat Rev Neurol*, 8(4), 189-202. doi: 10.1038/nrneurol.2012.27
- [13] Gao, J., Wang, X., & Wan, Q. (2025). One nanoparticle delivers two different neuroprotective amino acids into ischemic brain and protects against neuronal death in rat cerebral ischemia injury. *Molecular and cellular neurosciences*, 133, 104009. doi: 10.1016/j.mcn.2025.104009
- [14] Insausti, R., Muñoz-López, M., & Insausti, A. M. (2023). The CA2 hippocampal subfield in humans: A review. *Hippocam-pus*, 33(6), 712-729. doi: 10.1002/hipo.23547
- [15] Jiang, X., Tang, L., Zhang, Y., Bai, Y., Luo, H., Wang, R., ... & Wang, X. (2024). Does sedentary time and physical activity predict chronic back pain and morphological brain changes? A UK biobank cohort study in 33,402 participants. BMC public health, 24(1), 2685. doi: 10.1186/s12889-024-20188-3
- [16] Kakizaki, M., & Watanabe, R. (2017). IL-10 expression in pyramidal neurons after neuropathogenic coronaviral infection. Neuropathology: official journal of the Japanese Society of Neuropathology, 37(5), 398-406. doi: 10.1111/neup.12386
- [17] Khafajah, Y., Shaheen, M., Natour, D. E., Merheb, M., Matar, R., & Borjac, J. (2024). Neuroprotective Effects of Zinc Oxide Nanoparticles in a Rotenone-Induced Mouse Model of Parkinson's Disease. *Nanotheranostics*, 8(4), 497-505. doi: 10.7150/ntno.95863
- [18] Kovács, D., Igaz, N., Gopisetty, M. K., & Kiricsi, M. (2022). Cancer Therapy by Silver Nanoparticles: Fiction or Reality?. *International journal of molecular sciences*, 23(2), 839. doi: 10.3390/ijms23020839
- [19] Li, J. M., Yu, R., Zhang, L. P., Wen, S. Y., Wang, S. J., Zhang, X. Y., ... & Kong, L. D. (2019). Dietary fructose-induced gut dysbiosis promotes mouse hippocampal neuroinflammation: a benefit of short-chain fatty acids. *Microbiome*, 7(1), 98. doi: 10.1186/s40168-019-0713-7
- [20] Matisz, C. E., Semenoff, N., Ahmed, A. F., Griffin, L., Wallace, L. E., McNabb, P., ... & Gruber, A. J. (2022). Acute gut inflammation reduces neural activity and spine maturity in hippocampus but not basolateral amygdala. *Scientific reports*, 12(1), 20169. doi: 10.1038/s41598-022-24245-y

- [21] Mahdipour, R., Ebrahimi, V., Hosseini, M., Soukhtanloo, M., Rastegar-Moghaddam, S. H., Malvandi, A. M., & Mohammadipour, A. (2024). Grape seed extract protects rat offspring hippocampus from the silicon dioxide nanoparticles' neurotoxicity. *Metabolic brain disease*, 39(6), 1027-1038. doi: 10.1007/s11011-024-01373-0
- [22] Min, S. H., Lei, W., Jun, C. J., Yan, Z. S., Guang, Y. X., Tong, Z., ... & Xing, H. (2023). Design strategy and research progress of multifunctional nanoparticles in lung cancer therapy. Expert opinion on investigational drugs, 32(8), 723-739. doi: 10.1080/13543784.2023.2254683
- [23] Nader, S., Karlovich, E., Cortes, E. P., Insausti, R., Meloni, G., Jacobs, M., ... & Morgello, S. (2023). Predictors of hippocampal tauopathy in people with and at risk for human immunodeficiency virus infection. *Journal of neurovirology*, 29(6), 647-657. doi: 10.1007/s13365-023-01181-9
- [24] Sachdev, P. S., Anstey, K. J., Parslow, R. A., Wen, W., Maller, J., Kumar, R., ... & Jorm, A. F. (2006). Pulmonary function, cognitive impairment and brain atrophy in a middle-aged community sample. *Dementia and geriatric cognitive disorders*, 21(5-6), 300-308. doi: 10.1159/000091438
- [25] Shi, H. J., Wang, S., Wang, X. P., Zhang, R. X., & Zhu, L. J. (2023). Hippocampus: Molecular, Cellular, and Circuit Features in Anxiety. *Neuroscience bulletin*, 39(6), 1009-1026. doi: 10.1007/s12264-023-01020-1
- [26] Schultz, C., & Engelhardt, M. (2014). Anatomy of the hippocampal formation. Front Neurol Neurosci, 34, 6-17. doi: 10.1159/000360925
- [27] Torfeh, A., Abdolmaleki, Z., Nazarian, S., & Shirazi Beheshtiha, S. H. (2021). Modafinil-coated nanoparticle increases expressions of brain-derived neurotrophic factor, glial cell line-derived neurotrophic factor and neuronal nuclear protein, and protects against middle cerebral artery occlusion-induced neuron apoptosis in the rat hippocampus. *Anatomical record (Hoboken, N.J.: 2007)*, 304(9), 2032-2043. doi: 10.1002/ar.24581
- [28] Wang, M., Cui, J., Liu, Y., Zhou, Y., Wang, H., Wang, Y., ... & Yu, Y. (2019). Structural and functional abnormalities of vision-related brain regions in cirrhotic patients: a MRI study. *Neuroradiology*, 61(6), 695-702. doi: 10.1007/ s00234-019-02199-9
- [29] Wang, M., Wang, Y., Wang, Z., & Ren, Q. (2023). The Abnormal Alternations of Brain Imaging in Patients with Chronic Obstructive Pulmonary Disease: A Systematic Review. *Journal of Alzheimer's disease reports*, 7(1), 901-919. doi: 10.3233/ADR-220083
- [30] Wang, X., Wang, Z., Cao, J., Dong, Y., & Chen, Y. (2023). Gut microbiota-derived metabolites mediate the neuroprotective effect of melatonin in cognitive impairment induced by sleep deprivation. *Microbiome*, 11(1), 17. doi: 10.1186/s40168-022-01452-3
- [31] Yu, Z., Ling, Z., Lu, L., Zhao, J., Chen, X., Xu, P., & Zou, X. (2020). Regulatory Roles of Bone in Neurodegenerative Diseases. Frontiers in aging neuroscience, 12, 610581. doi: 10.3389/fnagi.2020.610581
- [32] Yuan, F., Hong, X. P., Duan, Y. J., Chen, J. R., & Han, Y. M. (2021). Electroacupuncture at "Zusanli" (ST36) ameliorates tau hyperphosphorylation in pancreas and hippocampus of diabetic rats. *Zhen ci yan jiu=Acupuncture research*, 46(11), 901-906. doi: 10.13702/j.1000-0607.200921

Vol. 31, №3, Page 47-52

ГІСТОЛОГІЧНІ ЗМІНИ ЗУБЧАСТОЇ ЗВИВИНИ ГІПОКАМПА ЩУРІВ З ІНДУКОВАНОЮ АДЕНОКАЦИНОМОЮ ТОВСТОЇ КИШКИ ТА ЗА УМОВ КОРЕКЦІЇ НАНОМАТЕРІАЛАМИ

Чеберніна І. О., Небесна З. М., Огінська Н. В., Гетманюк І. Б., Кульбіцька В. В.

Гіпокамп займає значне місце у формуванні різноманітних функцій центральної нервової системи, і є дуже чутливим до патологічних впливів, що відтворено у численних експериментах. Досі залишається неясним вплив індукованої аденокарциноми товстої кишки на структурну організацію гіпокампа, тому метою нашого дослідження було вивчення гістологічних змін зубчастої звивини на фоні N,N-диметилгідразин-індукованого раку товстої кишки щурів та за умов корекції наноматеріалами Аи/Аg/Fe. Для постановки досліду було використано 45 білих щурів та поділено їх на 3 групи: I – інтактні білі щури, II – білі щури, яким моделювали ДМГ-індукований онкогенез, III – щури з ДМГ-індукованою аденокарциномою, які отримували композицію наноматеріалів Au/Ag/Fe. Для індукції канцерогенезу використовували N,N-диметилгідразин (ДМГ, серія D161608, Sigma-Aldrich Sp. z о.о., Японія) 1 раз на 7 днів протягом 30 тижнів підшкірно у міжлопаткову ділянку. Композицію наноматеріалів Au/Ag/Fe у вигляді розчину уводили внутрішньошлунково 1 раз на добу протягом 21 дня щурам III групи. Зразки головного мозку обробляли згідно стандартних гістологічних методик, зрізи забарвлювали толуідиновим синім та гемотиксилін-еозином, візуалізацію змін здійснювали за допомогою мікроскопа MICROmed SEO SCAN та відеокамери Vision CCD. При дослідженні встановлено, що у ІІ групи щурів виявлено найбільш виражені зміни у зернистому шарі зубчастої звивини гіпокампа: зменшення щільності клітин, появу активованої глії, клітин-тіней, пікноз ядер, порушення співвідношення нормохромних клітин до гіпер- та гіпохромних нейроцитів, порушення гемодинаміки органу з розвитком стазів, сладжів, периваскулярних набряків. Застосування композиції наночастинок призвело до відновлення структурної організації зернистого шару, встановлено збільшення щільності клітин, зменшення гліальних клітин, нормалізація стартифікації шарів гіпокапма. Корекція наноматеріалами суттєво покращує морфологічний стан гіпокампа, зменшує ступінь патологічних змін, сприяє відновленню клітинної архітектоніки зубчастої звивини та нормалізації стану судин гемомікроциркуляторного русла.

Ключові слова: головний мозок, гіпокамп, канцерогенез, зубчаста звивина, наночастинки, нейроцити, гістологічні зміни.

Author's contribution

Chebernina I. O. – data curation, formal analysis, investigation, methodology, visualization, conceptualization, writing – original draft. Nebesna Z. M. – conceptualization, investigation, visualization, writing – review&editing.

Hetmaniuk I. B. – conceptualization, formal analysis, validation, investigation, project administration, methodology, writing – original draft, supervision

Ohinska N. V. – conceptualization, formal analysis, validation, investigation, methodology, writing – original draft, funding acquisition, software, supervision.

Kulbitska V. V. - formal analysis, validation, investigation, project administration, funding acquisition, software, supervision.

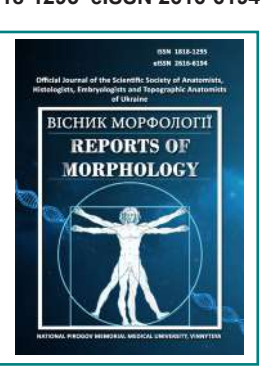
ISSN 1818-1295 eISSN 2616-6194



REPORTS OF MORPHOLOGY

Official Journal of the Scientific Society of Anatomists, Histologists, Embryologists and Topographic Anatomists of Ukraine

journal homepage: https://morphology-journal.com



Modeling of the linear dimensions required for constructing the correct dental arch form in young males and females with physiological occlusion, regardless of facial type, based on the characteristics of cephalometric parameters according to the Burstone method and computed tomographic tooth measurements

Orlovskyi I. V.¹, Beliaiev E. V.¹, Isakova N. M.¹, Kasianenko D. M.¹, Cherkasova L. A.², Dyakova O. V.¹, Gunas I. V.¹

¹National Pirogov Memorial Medical University, Vinnytsya, Ukraine ²Bogomolets National Medical University, Kyiv, Ukraine

ARTICLE INFO

Received: 10 January 2025 Accepted: 2 July 2025

UDC: 616.314-073.75:616.314.2-007.2:519.876.5

CORRESPONDING AUTHOR

e-mail: antilitsoooo@gmail.com Orlovskyi I. V.

CONFLICT OF INTEREST

The authors have no conflicts of interest to declare.

FUNDING

Not applicable.

DATA SHARING

Data are available upon reasonable request to corresponding author.

Proper modeling of dental arch form is one of the key objectives of modern orthodontics, as it determines the stability of both functional and aesthetic treatment outcomes. Most existing approaches are based only on odontometric parameters or take into account facial type, which limits the accuracy of prediction. The use of cephalometric parameters according to the Burstone method combined with computed tomographic measurements of teeth makes it possible to integrate data from different levels, thereby providing a more reliable basis for dental arch modeling. This approach opens opportunities for individualized orthodontic treatment of young males and females with physiological occlusion and for improving its effectiveness. The aim of the study was to develop and analyze regression models of linear dimensions required for constructing the correct dental arch form in Ukrainian young males and females with physiological occlusion, regardless of facial type, depending on the characteristics of cephalometric parameters according to the Burstone method and computed tomographic tooth measurements. Based on the data bank of the Research Center and the Department of Pediatric Dentistry of the National Pirogov Memorial Medical University, Vinnytsya cephalograms (41 young males and 68 young females with physiological occlusion) were analyzed to obtain linear and angular measurements according to the Burstone method, while computed tomograms were used for morphometric assessment of teeth and dental arches. Regression models of the linear dimensions required for constructing the correct dental arch form, depending on cephalometric parameters and computed tomographic measurements, were built using the licensed software package "Statistica 6.0". It was established that in males, all 18 possible significant models were constructed with a determination coefficient greater than 0.6 (R2 ranging from 0.694 to 0.894, p<0.001), whereas in females only 10 significant models were obtained (R² ranging from 0.605 to 0.775, p<0.001). Analysis of the frequency of inclusion of computed tomographic tooth dimensions and cephalometric parameters into the regression models showed that in males the most frequent predictors were crown width in the mesiodistal plane (26.09 %) and in the vestibulo-oral plane (14.49 %), cephalometric parameters (18.84 %), and tooth length (13.04 %); while in females, cephalometric parameters (28.57 %), crown width and length in the mesiodistal plane (21.42 % and 9.52 % respectively), and tooth length (10.71 %) predominated. When analyzing the frequency of inclusion of individual teeth into the regression models, it was found that in males the most frequent were the maxillary and mandibular incisors (24.11 % and 20.53 % respectively), maxillary and mandibular premolars (16.07 % and 14.28 % respectively), and maxillary canines (10.71 %). In females, the most frequent were maxillary and mandibular incisors (43.33 % and 20.00 % respectively), mandibular canines, and mandibular premolars (11.66 % each).

Keywords: dentistry, teleradiometry using the Burstone method, computed tomography dimensions of teeth and dental arches, regression analysis, Ukrainian young males and females, physiological occlusion.

Introduction

Modern dentistry and orthodontics face a high prevalence of dentoalveolar system pathologies. The problem is further complicated by the fact that the clinical manifestations of these conditions vary significantly depending on age, sex, sociocultural, and ethnic factors, which necessitates an indepth investigation of the morphological patterns of growth and dental arch formation in healthy individuals.

According to numerous studies, maxillofacial injuries are among the most common types of bodily trauma. In a retrospective analysis conducted in Qatar, the prevalence of maxillofacial trauma reached 10.6 % among all hospitalized patients, with mandibular fractures (41.4 %) and dental injuries (32.8 %) predominating [1]. Similar results were reported in South Africa, where the share of maxillofacial injuries was 8.4 %, with interpersonal conflicts and traffic accidents being the leading causes [23]. In India, mandibular fractures accounted for more than 55 % of all cases, whereas other fracture sites were significantly less prevalent [27]. Epidemiological studies have shown that 20-25 % of maxillofacial fractures are accompanied by dental injuries, further complicating the clinical course and treatment [25].

The problem of traumatic dental injuries is particularly relevant in children and adolescents. A systematic review and meta-analysis revealed that the prevalence of dental trauma in this age group was 17.5 %, with falls (50-60 %) and sports injuries (20-25 %) being the main etiological factors [5]. A study in the United States among preschool-aged children showed that up to 22.7 % had experienced at least one episode of dental trauma, which was linked to a range of socioeconomic factors and the level of physical activity [9].

Another important orthodontic issue is impacted teeth, which often lead to secondary pathologies and require surgical or orthodontic correction. In a study from Saudi Arabia, the prevalence of impacted teeth was 13.4 %, with third molars (8.6 %) and canines (2.5 %) being the most affected [2]. Another study on an Arab population reported a 2.1 % prevalence of impacted canines [3]. Iranian researchers found that the prevalence of impacted teeth among young adults reached 17.6 %, with mandibular third molars being the most frequently affected [4].

Malocclusions remain the most widespread orthodontic pathology in children and adolescents, regardless of ethnic background. According to a review covering different geographical regions, the overall prevalence of malocclusion ranges from 39 % to 93 %, depending on age and population characteristics [11]. In Turkey, the prevalence among children and adolescents reached 64.4 %, with Angle Class I accounting for 55.7 %, Class II for 32.5 %, and Class III for 11.8 % [18]. Similar data were reported in China, where 45.5 % of children aged 3-5 years were affected, most commonly with sagittal and vertical deviations in

tooth relationships [32]. In Central Anatolia, malocclusion prevalence in adolescents was 56.7 %, with 38 % requiring orthodontic treatment [8]. In Saudi Arabia, prevalence rates ranged from 62 % to 73 %, confirming the global trend of high malocclusion frequency [28].

An important aspect in the study of orthodontic pathology is not only the clinical but also the anthropological perspective. For example, Kenessey D. E. et al. [13] demonstrated that the prevalence of dental crowding is significantly influenced by sociocultural and economic factors. The authors found that in countries with a high level of urbanization, crowding prevalence reached 37-40 %, whereas in traditional societies it was considerably lower – around 20 %. This once again confirms the multifactorial nature of dentoalveolar anomalies.

Thus, the analysis of the literature indicates a high prevalence of both traumatic injuries and orthodontic pathologies across different age groups and populations. Taking these factors into account is crucial in developing scientifically based models of a harmonious dental arch. The use of cephalometric parameters according to Burstone, combined with CT-based measurements of tooth dimensions, opens up new prospects for predictive algorithms that consider not only individual anatomical characteristics but also general patterns of occlusal development.

The aim of the study was to develop and analyze regression models of the linear dimensions required for constructing the correct dental arch form in Ukrainian young males and females with physiological occlusion, regardless of facial type, based on the characteristics of cephalometric parameters according to the Burstone method and computed tomographic tooth measurements.

Materials and methods

From the data bank of the Research Center and the Department of Pediatric Dentistry at the National Pirogov Memorial Medical University, Vinnytsya, primary computed tomograms and cephalograms were obtained for 41 Ukrainian young males (aged 17-21 years) and 68 Ukrainian young females (aged 16-20 years) with physiological occlusion. Computed tomography (using the dental conebeam CT scanner Planmeca ProMax 3D Mid, Finland) and cephalometric examinations (using the dental cone-beam CT scanner Veraviewepocs 3D Morita, Japan) were performed on the basis of voluntary informed consent at the private dental clinic Vininermed and at the Planmeca 3D Center for Maxillofacial Diagnostics. The Bioethics Committee of the National Pirogov Memorial Medical University, Vinnytsya (Protocol No. 6 dated 07.05.2025) confirmed that the studies conducted did not contradict the main bioethical principles of the Declaration of Helsinki, the Council of Europe Convention

on Human Rights and Biomedicine (1977), the relevant WHO regulations, or the laws of Ukraine.

Measurements according to the Burstone C. J. method [10] were performed in the OnyxCeph³™ application, version 3DPro (Image Instruments GmbH, Germany) on standardly obtained teleradiograms created in the 3D Slicer v5.4.0 software with points marked on 3D objects.

According to this method, the following indicators were determined.

Skull base and horizontal skeletal indices (Fig. 1):

distance Ar-Pt – back of the skull base, distance between points \underline{Ar} and \underline{Pt} , determines the length of the posterior part of the base of the skull, parallel to the horizontal line according to Burstone (HR Line, line drawn through point \underline{N} and seven degrees above $\underline{S-N}$ line) (mm);

distance Pt-N – front part of the skull base, distance from the point Pt to N, determines the length of the front part of the base of the skull, parallel to the horizontal line by Burstone (mm);

angle NAPog – the angle of the skeletal profile, determines the convexity of the face, is formed by lines <u>N-A</u> and <u>A-Pog</u> (°);

distance N-A – distance characterizing the position of the upper jaw, distance from the perpendicular (N-Vert) to the horizontal line according to Burstone dropped from the point N, and point N (mm);

distance N-B — distance characterizing the position of the lower jaw, the distance from the perpendicular to the horizontal line according to Burstone dropped from the point \underline{N} , and point \underline{B} (mm);

distance N-Pog – distance characterizing the position of the chin, distance from the perpendicular (N-Vert) to the horizontal line according to Burstone dropped from the point N, and point N.

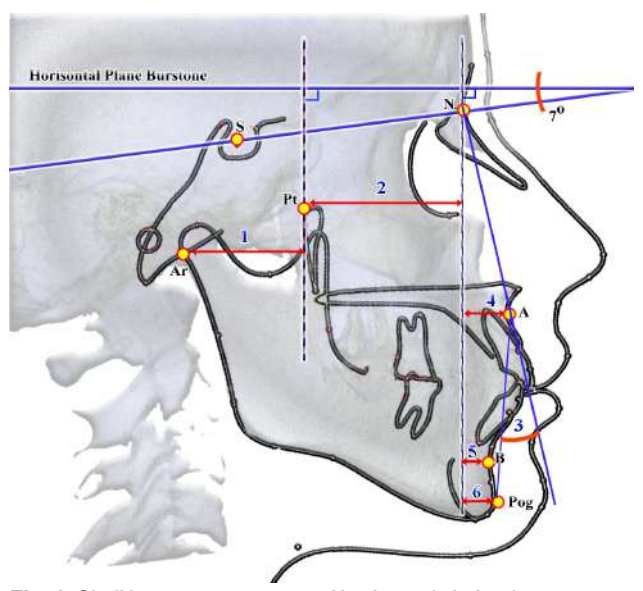


Fig. 1. Skull base parameters and horizontal skeletal parameters determined by cephalometric methods C. J. Burstone. 1 – distance Ar-Pt; 2 – distance Pt-N; 3 – angle NAPog; 4 – distance N-A; 5 – distance N-B; 6 – distance N-Pog.

Vertical skeletal and dental indicators (Fig. 2):

distance **N-ANS** – front upper face height, determines the length of the upper part of the front face height, the distance from the point \underline{N} to \underline{ANS} (mm);

distance **ANS-Gn** – front lower face height, determines the length of the lower part of the front face height from the point <u>ANS</u> to <u>Gn</u> (mm);

distance **PNS-N** – back top face height, defines the length of the top of the back face height from the point <u>PNS</u> to the horizontal line by Burstone (mm);

angle **MP-HP** – angle of the lower jaw to the horizontal line according to Burstone, formed by the mandibular plane <u>tGo-Me</u> and a line by Burstone (°);

distance **1u-NF** – distance from the cutting edge of the most anterior upper central incisor to the palatal plane, length of the perpendicular to the line <u>ANS-PNS</u>, drawn from the point <u>Is1u</u> (mm);

distance **1I-MP** – distance from the cutting edge of the most anterior lower central incisor to the mandibular plane, length of the perpendicular to the line <u>tGo-Me</u>, dropped from a point <u>Is1L</u> (mm);

distance **6u-NF** – distance from the mesial buccal tip of the upper first large canine to the palatal plane, length of the perpendicular to the line <u>ANS-PNS</u>, drawn from the point <u>6u</u> (mm);

distance **6I-MP** – distance from the mesial buccal tip of the lower first large canine to the mandibular plane, length of the perpendicular to the line $\underline{\text{tGo-Me}}$, dropped from a point $\underline{\text{6L}}$ (mm).

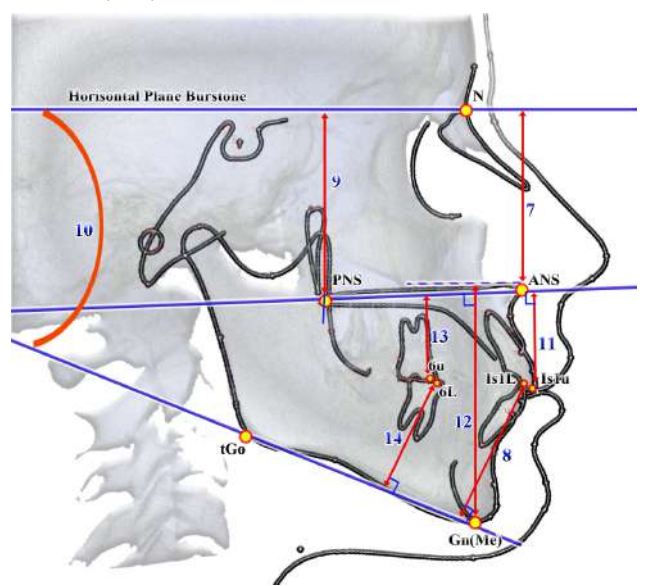


Fig. 2. Vertical skeletal and dental parameters determined by cephalometric methods C. J. Burstone. 7 – distance N-ANS; 8 – distance ANS-Gn; 9 – distance PNS-N; 10 – angle MP-HP; 11 – distance 1u-NF; 12 – distance 1l-MP; 13 – distance 6u-NF; 14 – distance 6l-MP.

Inter-jaw indices (Fig. 3):

distance **ANS-PNS** – length of the upper jaw, distance from the point <u>ANS</u> to <u>PNS</u> parallel to the horizontal line by

Vol. 31, №3, Page 53-61 **55**

Burstone (mm);

distance Ar-Go - length of the mandibular branch, distance from the point \underline{Ar} to \underline{tGo} (mm);

distance **Go-Pog** – length of the base of the lower jaw, distance from the point <u>Pog</u> to <u>tGo</u> (mm);

distance B-Pog – distance from point \underline{Pog} to point \underline{B} , parallel to the mandibular plane (line $\underline{tGo-Me}$) (mm);

angle **arGoMe/ArGoGn** – gonial angle, angle formed by lines <u>Ar-tGo</u> and <u>tGo-Gn</u> (°).

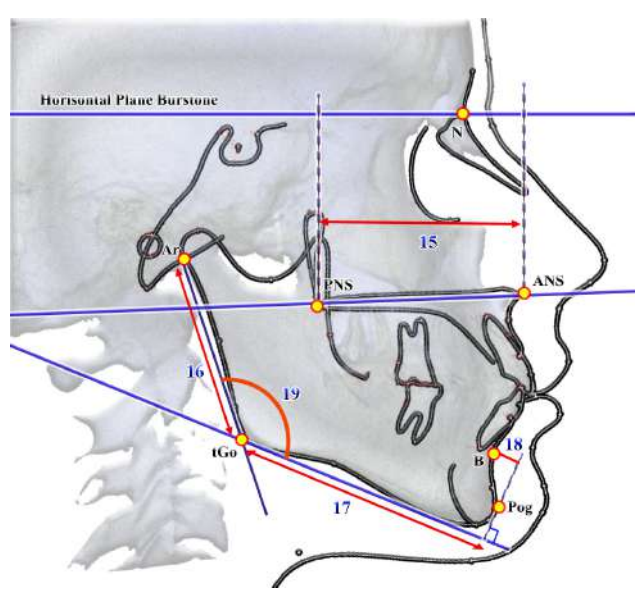


Fig. 3. Inter-jaw indicators determined by the cephalometric method C. J. Burstone. 15 – distance ANS-PNS; 16 – distance Ar-Go; 17 – distance Go-Pog; 18 – distance B-Pog; 19 – angle arGoMe/ArGoGn.

Maxillofacial indicators (Fig. 4):

angle **OP-HP** – angle of inclination of the closing plane, the angle formed by the lines <u>apOcP-ppOcP</u> and <u>HR-Line</u> (°); distance **A-B** – distance from point <u>A</u> to the point <u>B</u>, on the closing plane (<u>apOcP-ppOcP</u>) (mm);

angle **Max1-SpP/Max1-NF** – the angle of inclination of the upper central incisors to the palatal plane, the angle formed by the lines <u>Ap1u-Is1u</u> and <u>ANS-PNS</u> (°);

angle **Mand1-MeGo/Mand1-Mp** – the angle of inclination of the lower central incisors to the mandibular plane, the angle formed by the lines $\underline{Is1L-Ap1L}$ and $\underline{tGo-Gn}$ (°).

Morphometric study of teeth and dental arches was carried out using the software applications i-Dixel One Volume Viewer (Ver.1.5.0) J Morita Mfg. Cor and Planmeca Romexis Viewer (ver. 3.8.3.R 15.12.14) Planmeca OY.

In previous studies, no significant differences or tendencies were found when comparing the computed tomographic dimensions of the corresponding teeth on the right and left sides. Therefore, we used the mean values of the corresponding teeth in the maxilla and mandible: 11 or 41 – maxillary or mandibular central incisors, 12 or 42 – maxillary or mandibular lateral incisors, 13 or 43 – maxillary or mandibular canines, 14 or 44 – maxillary or mandibular first premolars,

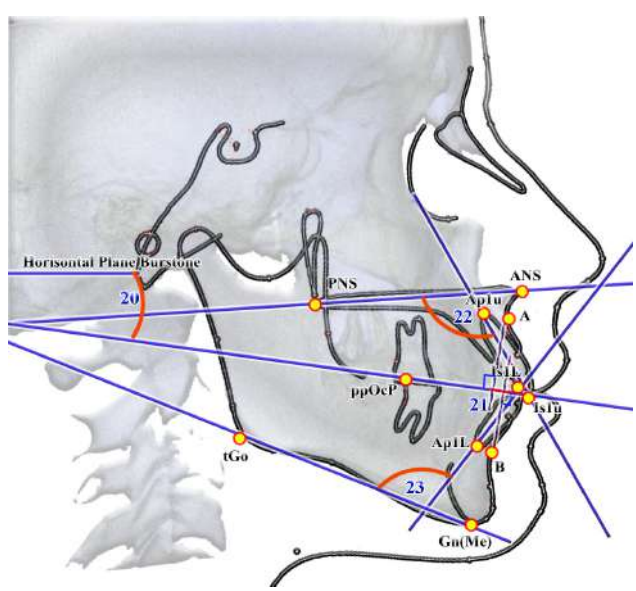


Fig. 4. Dental and maxillofacial parameters determined by cephalometric method C. J. Burstone. 20 – angle OP-HP; 21 – distance A-B; 22 – angle Max1-SpP/Max1-NF; 23 – angle Mand1-MeGo/Mand1-Mp.

15 or 45 – maxillary or mandibular second premolars, 16 or 46 – maxillary or mandibular first molars.

Tooth morphometry included the determination of the following distances (mm) [26]: crown width of the corresponding teeth in the mesiodistal (MdK) and vestibulo-oral (VoK) planes; cervical width of the corresponding teeth in the mesiodistal (MdC) and vestibulo-oral (VoC) planes; tooth length (identical) in the mesiodistal and vestibulo-oral planes (MdLD); crown length of the corresponding teeth in the mesiodistal (MdLK) and vestibulo-oral (VoLK) planes; root length of the corresponding teeth in the mesiodistal (MdLR) and vestibulo-oral (VoLR) planes.

Dental arch morphometry included the determination of the following distances (mm) [26]: between the cusp tips (distance 13 23Bugr) and root apices (distance 13 23Apx) of the canines in the maxilla and between the cusp tips (distance 33 43Bugr) and root apices (distance 33 43Apx) of the canines in the mandible; between the palatal root apices (distance mapex 6), mesial vestibular root apices (distance napx_6), distal vestibular root apices (distance dapx_6), and mesial vestibular cusps (distance VestBM) of the maxillary first molars and the distal (distance dapx 46) and mesial (distance mapx 46) root apices of the mandibular first molars; between premolar (distance PonPr) and molar (distance PonM) Pont's points; between the crowns of the central incisors and the lines connecting the canines (distance DL_C), first premolars (distance DL F), and molars (distance DL S) of the maxilla; as well as the distances characterizing the position of the canine (distance GL_1), premolar (distance GL_2), and molar (distance GL_3) lines relative to the hard palate.

By means of the stepwise regression analysis method, using the licensed statistical package "Statistica 6.0," modeling of the linear dimensions required for constructing the

correct dental arch form depending on the characteristics of cephalometric parameters according to the Burstone method and computed tomographic tooth dimensions was carried out.

Results

It was established that in Ukrainian *young males* with physiological occlusion, regardless of facial type, the significant regression models (with a determination coefficient R²>0.60) of the linear dimensions required for constructing the correct dental arch form, depending on the characteristics of cephalometric parameters according to the Burstone method and computed tomographic tooth measurements, are represented by the following equations:

distance PonPr (young males)= $10.43 + 1.066 \times MdK12 + 1.425 \times MdK15 - 0.525 \times MdLR12 + 2.571 \times MdK45 + 3.213 \times MdK41 - 0.345 \times MdLD14 + 0.293 \times MdLD11 - 0.315 \times MdLD13 - 0.760 \times MdK46 + 0.153 \times Ar-Pt - 0.075 \times Pt-N (R^2=0.894, F_{(11.29)}=22.17, p<0.001, Std.Error of estimate=0.793);$

 $\begin{array}{l} \textit{distance PonM (young males)} = 31.31 + 2.184 \times \text{VoK}15 \\ + 1.024 \times \text{MdLD44} - 0.463 \times \text{MdLD14} - 0.127 \times \text{Ar-Go_Gn} + \\ 1.914 \times \text{MdK}15 - 1.637 \times \text{VoK}42 - 0.100 \times \text{Ar-Pt (R}^2 = 0.722, \\ F_{(7.33)} = 15.95, \ p < 0.001, \ \text{Std.Error of estimate} = 1.351); \end{array}$

distance 13_23Bugr (young males)= $8.242 + 2.802 \times MdK12 + 2.025 \times MdK13 - 0.760 \times VoLR12 - 0.660 \times VoK14 + 1.416 \times MdK41 + 2.207 \times MdC41 - 1.485 \times VoC41 + 0.315 \times VoLR42 - 0.044 \times PNS-N (R^2=0.855, F_(9.31)=20.37, p<0.001, Std.Error of estimate=0.867);$

distance 13_23Apx (young males)= $46.02 + 1.758 \times MdC12 - 0.111 \times Ar-Go + 1.534 \times MdK11 - 1.612 \times VoK16 + 1.587 \times VoK45 - 1.833 \times MdK13 - 1.572 \times VoC43 + 0.453 \times MdLD14 - 0.522 \times MdLR43 (R²=0.712, F_(9.30)=8.23, p<0.001, Std.Error of estimate=1.399);$

distance VestBM (young males)= $31.25 + 1.390 \times VoK15 + 0.820 \times MdLD44 - 0.160 \times Ar-Go_Gn - 0.571 \times MdLD14 + 1.868 \times MdK44 + 1.622 \times MdK15 (R^2=0.805, F_(6.34)=23.33, p<0.001, Std.Error of estimate=1.269);$

 $\begin{array}{l} \textit{distance napx_6 (young males)} = 37.57 + 2.906 \times \text{MdC42} \\ - 2.669 \times \text{VoK16} + 4.525 \times \text{MdK12} - 0.685 \times \text{VoLR13} + \\ 0.810 \times \text{MdLD45} - 0.914 \times \text{VoLR11} - 0.082 \times \text{N-ANS (R}^2 = 0.716, \\ F_{(7.33)} = 11.90, \ p < 0.001, \ \text{Std.Error of estimate} = 1.873); \end{array}$

distance dapx_6 (young males)= -23.49 + 2.973 × VoK15 + $3.030 \times MdK46 - 5.057 \times MdC13 + 1.121 \times VoLK13 + 2.296 \times MdK12 + 3.425 \times MdK15 + 2.377 \times VoC13 - 1.996 \times MdC16 (R^2=0.764, F_(8.32)=12.95, p<0.001, Std.Error of estimate=2.374);$

 $\begin{array}{l} \textit{distance mapex_6 (young males)} = 2.105 + 2.549 \times \text{MdK45} \\ + \ 3.769 \times \text{MdK15} + \ 1.767 \times \text{MdK12} + \ 1.943 \times \text{MdC41} - \\ 0.658 \times \text{MdLR42} + \ 0.481 \times \text{MdLD44} - \ 0.752 \times \text{MdLK13} + \\ 1.797 \times \text{MdK41} - 0.116 \times \text{Ar-Go_Gn} + 0.114 \times \text{OP-HP (R}^2 = 0.875, \\ F_{(10.30)} = 20.99, \ p < 0.001, \ \text{Std.Error of estimate} = 1.354); \end{array}$

distance 33_43Bugr (young males)= -3.152 + 1.207×MdK12 + 2.501×MdK42 - 0.461×MdLR11 + 0.356×MdLD43 - 0.254×VoLR13 - 0.040×N-ANS + 0.224×MdLR42 + 0.638×MdK46 (R²=0.776, $F_{(8.32)}$ =13.83, p<0.001, Std.Error of estimate=0.781);

 $\begin{array}{l} \textit{distance} \quad 33_43 \textit{Apx} \; \; (\textit{young males}) = \; 21.96 \; + \\ 0.894 \times \textit{MdLD43} - 0.104 \times \textit{Pt-N} + 4.782 \times \textit{VoK43} - 2.128 \times \textit{VoK42} \\ -2.628 \times \textit{VoC43} - 0.449 \times \textit{MdLD45} - 2.010 \times \textit{MdK15} \; (R^2 = 0.747, \\ F_{(7.33)} = 13.94, \; p < 0.001, \; Std. Error \; of \; estimate = 1.283); \end{array}$

distance mapx_46 (young males)= $1.572 + 1.588 \times MdLK12 + 2.105 \times MdK45 + 2.971 \times VoK16 - 0.633 \times MdLD45 - 1.890 \times VoK46 - 0.096 \times Ar-Go + 3.025 \times MdK42 + 1.515 \times MdK15 (R^2=0.806, F_(8.31)=16.11, p<0.001, Std.Error of estimate=1.343);$

distance dapx_46 (young males)= $40.58 - 0.164 \times Mand1-MP - 0.172 \times Pt-N + 2.143 \times VoK16 + 1.953 \times MdK45 + 2.070 \times MdC12 - 0.533 \times MdLR12 (R²=0.736, F_(6.33)=15.36, p<0.001, Std.Error of estimate=1.584);$

distance DL_C (young males)= -10.80 + 0.831×MdK11 + 0.825×VoK41 - 0.359×VoLK41 + 0.307×VoLK13 + 0.107×A-B + 0.081×Ar-Pt + 0.853×MdK44 (R^2 =0.825, $F_{(7.33)}$ =22.25, p<0.001, Std.Error of estimate=0.618);

distance DL_F (young males)= $4.159 + 1.585 \times MdK11 + 0.820 \times VoK15 - 0.357 \times VoLK42 - 0.715 \times VoK45 + 1.117 \times VoC42 - 0.054 \times Ar-Go_Gn + 0.429 \times VoK14 - 0.195 \times MdLR42 (R^2=0.849, F_{(8.32)}=22.42, p<0.001, Std.Error of estimate=0.670);$

distance DL_S (young males)= -1.341 + 1.912×MdK11 + $0.766 \times VoK15 + 0.253 \times A - B + 0.595 \times MdLK12 - 0.163 \times MdLK41 + 0.704 \times VoK11$ (R²=0.860, F_(6.34)=34.93, p<0.001, Std.Error of estimate=0.759);

distance GL_1 (young males)= $7.522 + 0.355 \times N$ -A-Pog + $0.415 \times 6u$ -NF - $0.651 \times VoLR12 + 0.839 \times MdLK13 - 0.126 \times PNS-N + 1.729 \times VoC41 - 0.526 \times MdLR12$ (R²=0.707, $F_{(7.33)}$ =11.36, p<0.001, Std.Error of estimate=1.445);

distance GL_2 (young males)= $10.23 + 3.060 \times VoK12 - 1.148 \times MdLR12 + 0.161 \times N-A-Pog + 1.000 \times MdLD13 - 0.982 \times MdLD45 + 0.715 \times MdLK11 - 1.904 \times MdK41 (R^2=0.694, F_(7.33)=10.68, p<0.001, Std.Error of estimate=1.604);$

distance GL_3 (young males)= $30.96 + 0.198 \times 6u-NF - 0.085 \times Ar-Go_Gn - 0.821 \times MdLD45 + 0.827 \times MdLD11 - 0.075 \times Mand1-MP - 1.337 \times MdK16 + 2.868 \times MdK42 (R^2=0.704, F_(7.33)=11.20, p<0.001, Std.Error of estimate=1.250);$

where, here and in the following equations, R^2 – coefficient of determination; $F_{(!)}$ =! – critical $_{(!)}$ and obtained (!) Fisher's test value; p – confidence level; Std.Error of estimate – standard error of estimate.

It was established that in Ukrainian *young females* with physiological occlusion, regardless of facial type, the significant regression models (with a determination coefficient R²>0.60) of the linear dimensions required for constructing the correct dental arch form, depending on the characteristics of cephalometric parameters according to the Burstone method and computed tomographic tooth measurements, are represented by the following equations:

distance 13_23Bugr (young females)= 18.61 + 1.254×MdK11+1.666×VoC12-0.153×MP-HP-0.052×MdC43 + 0.447×B-Pog - 0.641×VoC11 + 0.271×MdLK42 + 0.584×VoLK11 - 0.568×VoLK43 - 0.084×Go-Pog + 0.108×Ar-Pt (R²=0.611, $F_{(11.56)}$ =7.88, p<0.001, Std.Error of estimate=1.160);

Vol. 31, №3, Page 53-61

distance 13_23Apx (young females)= 9.787 + $3.071 \times MdK11 + 0.910 \times MdLD45 - 0.537 \times MdLD43 - 2.704 \times VoC11 + 1.526 \times MdC41 + 0.112 \times 1I-MP + 1.645 \times VoK11 - 1.730 \times MdK43 - 0.386 \times MdLD15 (R^2=0.608, F_{(9.58)}=9.98, p<0.001, Std.Error of estimate=1.652);$

distance mapex_6 (young females)= -0.898 + $4.351 \times MdK11 + 0.540 \times 1u-NF + 0.715 \times MdLK42 + 3.153 \times VoK12 - 2.567 \times MdC12 - 0.341 \times 1l-MP + 0.454 \times MdLD44 - 2.461 \times VoC11 + 1.670 \times VoK16 - 1.878 \times MdK43 (R^2=0.606, F_{(10.57)}=8.78, p<0.001, Std.Error of estimate=2.164);$

 $\begin{array}{l} \textit{distance mapx_46 (young females)} = 36.41 + \\ 0.697\times\text{N-Pog} + 0.975\times\text{MdLK12} - 0.070\times\text{MdC43} - 0.576\times\text{N-B} \\ + 1.458\times\text{MdK41} - 1.342\times\text{VoK44} + 1.364\times\text{MdK13 (R}^2 = 0.701, \\ F_{(7.54)} = 18.12, \ p<0.001, \ \text{Std.Error of estimate} = 1.595); \end{array}$

 $\begin{array}{l} \textit{distance dapx_46 (young females)} = 47.90 + 0.562 \times \text{N-Pog} \\ + 0.563 \times \text{VoLR42-0.487} \times \text{N-A} + 2.936 \times \text{MdC12-1.875} \times \text{MdK44} \\ + 0.718 \times \text{MdLK12-1.475} \times \text{MdC41 (R}^2 = 0.714, F_{(7.54)} = 19.29, p < 0.001, Std.Error of estimate = 1.834); \end{array}$

 $\begin{array}{l} \textit{distance DL_C (young females)} = -7.488 + 0.451 \times \text{MdK11} \\ + \ 0.594 \times \text{MdLD11} - \ 0.263 \times \text{MdLD14} - \ 0.188 \times \text{B-Pog} + \\ 0.617 \times \text{MdK46} - \ 0.612 \times \text{VoLK11} + \ 0.438 \times \text{VoLK12} + \\ 0.674 \times \text{VoK42} - \ 0.200 \times \text{VoLR42} \ (\text{R}^2 = 0.653, \ \text{F}_{(9.58)} = 12.11, \\ \text{p<0.001, Std.Error of estimate=0.685)}; \end{array}$

distance DL_F (young females)= -11.27 + 1.014×MdK11 + 0.045×Mand1-MP + 0.869×VoC11 + 0.803×MdK13 - 0.175×B-Pog + 0.512×MdK16 (R^2 =0.656, $F_{(6.61)}$ =19.41, p<0.001, Std.Error of estimate=0.847):

distance DL_S (young women)= $-5.658 + 1.232 \times MdK11 + 0.841 \times MdK45 + 0.293 \times MdLD41 + 0.066 \times Mand1-MP$ - $0.437 \times MdLD44 + 0.759 \times MdK16 + 0.239 \times MdLD11 + 0.618 \times MdK44 (R^2=0.775, F_(8.59)=25.42, p<0.001, Std.Error of estimate=0.830);$

distance GL_2 (young women)= $14.73 - 0.199 \times Max1-NF + 0.654 \times MdLK11 + 0.547 \times 6u-NF + 1.236 \times MdK41 + 0.478 \times MdLK42 - 0.373 \times 1u-NF + 0.331 \times 6l-MP - 0.189 \times ANS-PNS + 0.733 \times VoK43 (R²=0.613, F_(9.58)=10.21, p<0.001, Std. Error of estimate=1.603);$

distance GL_3 (young women)= $16.40 + 0.605 \times MdLK12 - 0.334 \times ANS-PNS + 0.242 \times ANS-Gn_M - 0.150 \times Op-HP - 1.251 \times VoC11 + 0.075 \times Ar-Go_Gn + 0.573 \times MdC11 - 0.166 \times MdLK41 (R²=0.605, F_(8.59)=11.31, p<0.001, Std.Error of estimate=1.393).$

Coefficients of determination of reliable regression equations of the quantity distance PonPr (R²=0.369, p<0.001), distance PonM (R²=0.483, p<0.001), distance VestBM (R²=0.466, p<0.001), distance napx_6 (R²=0.442, p<0.001), distance dapx_6 (R²=0.477, p<0.001), distance 33_43Bugr (R²=0.280, p<0.001), distance 33_43Apx (R²=0.334, p<0.001) \pm a distance GL_1 (R²=0.468, p<0.001) in Ukrainian young women, without taking into account the type of face, the values were less than 0.60 and therefore have no significant significance for practical dentistry.

Discussion

Thus, in Ukrainian young males with physiological occlusion, all 18 possible significant regression models of

the linear parameters of dental arches depending on the characteristics of cephalometric parameters according to the Burstone method and computed tomographic tooth dimensions were constructed, with a determination coefficient greater than 0.6 (R²=0.694 to 0.894, p<0.001 in all cases).

Analysis of the frequency of inclusion of cephalometric parameters according to the Burstone method and computed tomographic tooth dimensions into the regression equations in Ukrainian *young males* with physiological occlusion showed the following percentage of inclusion into the models: crown width of the tooth in the mesiodistal plane (26.09 %), cephalometric parameters according to the Burstone method (18.84 %), crown width of the tooth in the vestibulo-oral plane (14.49 %), tooth length (13.04 %), root length of the tooth in the mesiodistal plane (6.52 %), cervical width of the tooth in the mesiodistal plane (5.07 %), cervical width of the tooth in the vestibulo-oral plane, crown length of the tooth in the mesiodistal plane, and root length of the tooth in the vestibulo-oral plane (4.35 % each), crown length of the tooth in the vestibulo-oral plane (2.90 %).

Analysis of the frequency of inclusion of the corresponding teeth into the regression equations in Ukrainian *young males* with physiological occlusion showed the following percentage of inclusion into the models: maxillary incisors (24.11 % of all variables, including 8.93 % central incisors and 15.18 % lateral incisors), mandibular incisors (20.53 % of all variables, including 9.82 % central incisors and 10.71 % lateral incisors), maxillary premolars (16.07 % of all variables, including 5.36 % first premolars and 10.71 % second premolars), mandibular premolars (14.28 % of all variables, including 4.46 % first premolars and 9.82 % second premolars), maxillary canines (10.71 %), mandibular canines (5.36 %), maxillary first molars (5.36 %), mandibular first molars (3.57 %).

In Ukrainian *young females* with physiological occlusion, only 10 of the 18 possible significant regression models of the linear parameters of dental arches depending on the characteristics of cephalometric parameters according to the Burstone method and computed tomographic tooth dimensions were constructed, with a determination coefficient greater than 0.6 (R²=0.605 to 0.775, p<0.001 in all cases).

Analysis of the frequency of inclusion of cephalometric parameters according to the Burstone method and computed tomographic tooth dimensions into the regression equations in Ukrainian *young females* with physiological occlusion showed the following percentage of inclusion into the models: cephalometric parameters according to the Burstone method (28.57 %), crown width of the tooth in the mesiodistal plane (21.42 %), tooth length (10.71 %), crown length of the tooth in the mesiodistal plane (9.52 %), cervical width of the tooth in the mesiodistal plane (8.33 %), crown width and cervical width of the tooth in the vestibulo-oral plane (7.14 % each), crown length of the tooth in the vestibulo-oral plane (4.76 %), root length of the tooth in the vestibulo-oral plane (2.38 %).

Analysis of the frequency of inclusion of the corresponding teeth into the regression equations in Ukrainian *young* females with physiological occlusion showed the following

percentage of inclusion into the models: maxillary incisors (43.33 % of all variables, including 30.00 % central incisors and 13.33 % lateral incisors), mandibular incisors (20.00 % of all variables, including 10.00 % central incisors and 10.00 % lateral incisors), mandibular canines (11.67 %), mandibular premolars (11.66 % of all variables, including 8.33 % first premolars and 3.33% second premolars), maxillary first molars (5.00 %), maxillary canines (3.33 %), maxillary premolars (3.33 % of all variables, including 1.67 % first premolars and 1.67% second premolars), mandibular first molars (1.67 %).

The results obtained in our study confirm the existence of close correlations between the linear parameters of the dental arches and the anthropometric features of the craniofacial region. This is consistent with previous scientific findings demonstrating that cranial and facial morphology plays a key role in the formation of proper occlusion and tooth position.

In patients with hypodontia, the severity of the defect is directly related to changes in craniofacial morphology: with an increasing number of missing teeth, reductions in dental arch length and palatal depth were observed, which influenced occlusal harmony [6]. Similar results were obtained in a Japanese sample, where in patients with congenital tooth absence, facial length and the relationship between basal bones differed significantly from the control group (p<0.05) [29]. Genetic factors have also been highlighted, with evidence that specific gene variations associated with tooth agenesis correlate with distinctive changes in facial morphology [24]. This confirms the multifactorial nature of the issue and emphasizes the need to combine odontometric and cephalometric parameters in modeling dental arches.

Variations in craniofacial structure directly affect the timing and patterns of permanent tooth eruption. In children with a mesofacial type, eruption timing was closer to population averages, whereas dolichofacial patients showed delays [7]. This is particularly important in evaluating arch length during adolescence, since eruption time and tooth position directly determine oral cavity morphology.

Craniofacial morphology also significantly impacts the risk of third molar retention. An analysis of over 1,000 patients showed that a narrow ratio between the mandibular body and ramus increased the likelihood of impaction by 15-20 % [14]. Similar patterns were reported, demonstrating that the number of preserved teeth in the jaw correlates with the length and width of craniofacial structures, further supporting the relationship between overall morphology and the condition of dental arches [21].

Other studies focused on the relationship between vertical and transverse facial parameters and jaw morphology. In dolichofacial individuals, mandibular width was 2-3 mm smaller compared to brachyfacial patients, which is clinically relevant for arch modeling [19]. In males with a vertical facial type, hard palate thickness was reduced by 0.5-0.7 mm, and maxillary width by 2 mm compared to mesofacial counterparts (p<0.01) [20]. Comparable findings were reported among Nigerian adolescents, where vertical facial height correlated

with the overall skeletal pattern (r=0.62), enabling prediction of dental arch morphology from cephalometric data [31].

Cone-beam CT studies revealed correlations between facial growth patterns and cortical bone thickness. In patients with vertical facial types, bone thickness in the molar region was reduced by 20-25 % compared to brachyfacial patients (p<0.01), which is critical for orthodontic tooth movement and treatment stability [12]. A morphometric relationship was also established between the palate and craniofacial morphology in Class III patients: in 68 % of cases, combined palatal narrowing and decreased maxillary width were observed (p<0.05) [22].

Special attention has been given to studies exploring the relationship between aesthetic facial parameters and periodontal tissue characteristics. The facial index and lip profile significantly affect gingival morphology. In males with a broad face, gingival thickness was 0.2-0.3 mm greater than in females (p<0.05) [16]. Likewise, dolichofacial patients were more prone to gingival recession in the mandibular incisor region, while brachyfacial individuals demonstrated more favorable periodontal stability (p<0.05) [17]. Three-dimensional scanning confirmed associations between gingival biotype and cephalometric parameters: a thin biotype was more common among individuals with narrow and elongated faces (57 % vs. 28 %, p<0.01) [30].

Facial height also directly correlates with transverse jaw parameters. It was shown that with increasing facial height, maxillary width decreased by an average of 1.5 mm and mandibular width by 1.2 mm, influencing tooth alignment and occlusal development [15]. These findings align with the results of our study, where we also identified strong correlations between cephalometric indicators and dental arch form.

Conclusion

- 1. In Ukrainian young males and females with physiological occlusion, significant (p<0.001) regression models with a determination coefficient greater than 0.6 were constructed for the linear parameters of dental arches depending on the characteristics of computed tomographic tooth dimensions and cephalometric parameters according to the Burstone method (in males all 18 possible models R^2 =0.694 to 0.894; in females only 10 models R^2 =0.605 to 0.775).
- 2. When analyzing the frequency of inclusion of computed tomographic tooth dimensions and cephalometric parameters according to the Burstone method into the models, in males the most frequent predictors were crown width of the tooth in the mesiodistal plane (26.09 %), cephalometric parameters (18.84 %), crown width of the tooth in the vestibulo-oral plane (14.49 %), and tooth length (13.04 %); whereas in females cephalometric parameters (28.57 %), crown width of the tooth in the mesiodistal plane (21.42 %), tooth length (10.71 %), and crown length of the tooth in the mesiodistal plane (9.52 %).
- 3. When analyzing the frequency of inclusion of the corresponding teeth into the regression models that considered cephalometric parameters according to the Burstone method, in males the most frequently included were

Vol. 31, №3, Page 53-61 **59**

maxillary incisors (24.11 %), mandibular incisors (20.53 %), maxillary premolars (16.07 %), mandibular premolars (14.28 %), and maxillary canines (10.71 %); whereas in

females – maxillary incisors (43.33 %), mandibular incisors (20.00 %), mandibular canines, and mandibular premolars (11.67 % each).

References

- [1] Al-Hassani, A., Ahmad, K., El-Menyar, A., Abutaka, A., Mekkodathil, A., Peralta, R., ... & Al-Thani, H. (2022). Prevalence and patterns of maxillofacial trauma: a retrospective descriptive study. European journal of trauma and emergency surgery, 48(4), 2513-2519. doi: 10.1007/s00068-019-01174-6
- [2] Al-wusaybie, M. M., Al-Ramil, A. M., Al-Wosaibi, A. M., & Bukhary, M. T. (2018). Prevalence of impacted teeth and associated pathologies—A radiographic study, Al Ahsa, Saudi Arabia Population. *The Egyptian Journal of Hospital Medicine*, 70(12), 2130-2136. doi: 10.12816/0045040
- [3] Al-Zoubi, H., Alharbi, A. A., Ferguson, D. J., & Zafar, M. S. (2017). Frequency of impacted teeth and categorization of impacted canines: A retrospective radiographic study using orthopantomograms. *European journal of dentistry*, 11(01), 117-121. doi: 10.4103/ejd.ejd 308 16
- [4] Arabion, H., Gholami, M., Dehghan, H., & Khalife, H. (2017). Prevalence of impacted teeth among young adults: A retrospective radiographic study. *Journal of Dental Materials and Techniques*, 6(3), 131-137.
- [5] Azami-Aghdash, S., Azar, F. E., Azar, F. P., Rezapour, A., Moradi-Joo, M., Moosavi, A., & Oskouei, S. G. (2015). Prevalence, etiology, and types of dental trauma in children and adolescents: systematic review and meta-analysis. *Medical journal of the Islamic Republic of Iran*, 29(4), 234. PMID: 26793672
- [6] Bajraktarova Miševska, C., Kanurkova, L., Bajraktarova Valjakova, E., Georgieva, S., Bajraktarova, B., Georgiev, Z., & Sotirovska Ivkovska, A. (2016). Craniofacial morphology in individuals with increasing severity of hypodontia. South European Journal of Orthodontics and Dentofacial Research, 3(1), 12-17. doi: 10.5937/sejodr3-15218
- [7] Banu, A. M., Şerban, D. M., Pricop, M. O., Urechescu, H. C., Roi, C. I., & Şerban, C. L. (2018). Craniofacial morphology and its relation to the eruption pattern of permanent teeth in the supporting zone of the dentition in a group of Romanian children in Timişoara. Rom J Morphol Embryol, 59(2), 491-497. PMID: 30173253
- [8] Bilgic, F., Gelgor, I. E., & Celebi, A. A. (2015). Malocclusion prevalence and orthodontic treatment need in central Anatolian adolescents compared to European and other nations' adolescents. *Dental press journal of orthodontics*, 20(6), 75-81. doi: 10.1590/2177-6709.20.6.075-081.oar
- [9] Born, C. D., Jackson, T. H., Koroluk, L. D., & Divaris, K. (2019). Traumatic dental injuries in preschool-age children: Prevalence and risk factors. *Clinical and experimental dental research*, 5(2), 151-159. doi: 10.1002/cre2.165
- [10] Burstone, C. J., James, R. B., Legan, H., Murphy, G. A., & Norton, L. A. (1979). Cephalometrics for orthognathic surgery. J Oral Surg, (36), 269-277. PMID: 273073
- [11] Cenzato, N., Nobili, A., & Maspero, C. (2021). Prevalence of dental malocclusions in different geographical areas: scoping review. *Dentistry Journal*, 9(10), 117. doi: 10.3390/ dj9100117
- [12] Gaffuri, F., Cossellu, G., Maspero, C., Lanteri, V., Ugolini, A., Rasperini, G., ... & Farronato, M. (2021). Correlation between facial growth patterns and cortical bone thickness assessed with cone-beam computed tomography in young adult untreated patients. *The Saudi dental journal*, 33(3),

- 161-167. doi: 10.1016/j.sdentj.2020.01.009
- [13] Kenessey, D. E., Vlemincq-Mendieta, T., Scott, G. R., & Pilloud, M. A. (2023). An anthropological investigation of the sociocultural and economic forces shaping dental crowding prevalence. *Archives of Oral Biology*, 147, 105614. doi: 10.1016/j.archoralbio.2023.105614
- [14] Kindler, S., Ittermann, T., Bülow, R., Holtfreter, B., Klausenitz, C., Metelmann, P., ... & Daboul, A. (2019). Does craniofacial morphology affect third molars impaction? Results from a population-based study in northeastern Germany. *PloS one*, 14(11), e0225444. doi: 10.1371/journal.pone.0225444
- [15] Klinge, A., Becktor, K., Lindh, C., & Becktor, J. P. (2017). Craniofacial height in relation to cross-sectional maxillary and mandibular morphology. *Progress in orthodontics*, 18(1), 32. doi: 10.1186/s40510-017-0187-8
- [16] Kolte, R. A., Kolte, A. P., Kharkar, V. V., & Bawankar, P. (2020). Influence of facial index, facial profile, lip size, and angulations of teeth on gingival characteristics of anterior teeth: A gender-based evaluation. *Journal of Esthetic and Restorative Dentistry*, 32(5), 496-504. doi: 10.1111/jerd.12600
- [17] Kong, J., Hartsfield Jr, J. K., Aps, J., Naoum, S., Lee, R., Miranda, L. A., & Goonewardene, M. S. (2023). Effect of craniofacial morphology on gingival parameters of mandibular incisors. *The Angle Orthodontist*, 93(5), 545-551. doi: 10.2319/101122-700.1
- [18] Londono, J., Ghasemi, S., Moghaddasi, N., Baninajarian, H., Fahimipour, A., Hashemi, S., ... & Dashti, M. (2023). Prevalence of malocclusion in Turkish children and adolescents: A systematic review and meta-analysis. *Clinical and experimental dental research*, 9(4), 689-700. doi: 10.1002/cre2.771
- [19] Mastroianni, D., & Woods, M. G. (2019). 3D-CT assessment of mandibular widths in young subjects with different underlying vertical facial patterns. *Journal of the World Federation of Orthodontists*, 8(2), 78-86. doi: 10.1016/j.ejwf.2019.02.005
- [20] Ning, R., Guo, J., Li, Q., & Martin, D. (2021). Maxillary width and hard palate thickness in men and women with different vertical and sagittal skeletal patterns. *American Journal of Orthodontics and Dentofacial Orthopedics*, 159(5), 564-573. doi: 10.1016/j.ajodo.2019.12.023
- [21] Oeschger, E. S., Kanavakis, G., Cocos, A., Halazonetis, D. J., & Gkantidis, N. (2022). Number of teeth is related to craniofacial morphology in humans. *Biology*, 11(4), 544. doi: 10.3390/biology11040544
- [22] Paoloni, V., Gastaldi, G., Franchi, L., De Razza, F. C., & Cozza, P. (2020). Evaluation of the morphometric covariation between palatal and craniofacial skeletal morphology in class III malocclusion growing subjects. *BMC Oral Health*, 20(1), 152. doi: 10.1186/s12903-020-01140-4
- [23] Pillay, L., Mabongo, M., & Buch, B. (2018). Prevalence and aetiological factors of maxillofacial trauma in a rural district hospital in the Eastern Cape. South African Dental Journal, 73(5), 348-353. doi: 10.17159/2519-0105/2018/v73no5a4
- [24] Rodrigues, A. S., Teixeira, E. C., Antunes, L. S., Nelson-Filho, P., Cunha, A. S., Levy, S. C., ... & Antunes, L. A. A.

- (2020). Association between craniofacial morphological patterns and tooth agenesis-related genes. *Progress in orthodontics*, *21*(1), 9. doi: 10.1186/s40510-020-00309-5
- [25] Ruslin, M., Wolff, J., Boffano, P., Brand, H. S., & Forouzanfar, T. (2015). Dental trauma in association with maxillofacial fractures: an epidemiological study. *Dental traumatology*, 31(4), 318-323. doi: 10.1111/edt.12176
- [26] Ryabov, T. V. (2025). Correlations between teleradiometric indicators according to the Steiner method and the sizes of teeth and dental arches in Ukrainian young men and young women with physiological occlusion and a wide facial type. Вісник Вінницького національного медичного університету=Reports of Vinnytsia National Medical University, 29(2), 229-236. doi: 10.31393/reports-vnmedical-2025-29(2)-09
- [27] Saravanan, T., Balaguhan, B., Venkatesh, A., Geethapriya, N., & Karthick, A. (2020). Prevalence of mandibular fractures. *Indian Journal of Dental Research*, 31(6), 971-974. doi: 10.4103/ijdr.IJDR 286 18
- [28] Slaghour, M. A., Bakhsh, A. K., Hadi, I. H., Jably, R. M., Alqahtani, M. S., Alqahtani, A. A., ... & Al-Jalooud, A. H.

- (2019). Dental occlusion and malocclusion: Prevalence, types and treatment. *EC Dental Science*, 18(8), 1776-1783.
- [29] Takahashi, Y., Higashihori, N., Yasuda, Y., Takada, J. I., & Moriyama, K. (2018). Examination of craniofacial morphology in Japanese patients with congenitally missing teeth: a cross-sectional study. *Progress in Orthodontics*, 19(1), 38. doi: 10.1186/s40510-018-0238-9
- [30] Valletta, R., Pango, A., Tortora, G., Rongo, R., Simeon, V., Spagnuolo, G., & D'Antò, V. (2019). Association between gingival biotype and facial typology through cephalometric evaluation and three-dimensional facial scanning. *Applied Sciences*, 9(23), 5057. doi: 10.3390/app9235057
- [31] Yemitan, T. A., Oludare, Y. S., & Ogunbanjo, B. O. (2018). Vertical facial height and its correlation with skeletal pattern among young nigerian orthodontic patients. *Int J Dentistry Oral Sci*, 5(8), 661-666. doi: 10.19070/2377-8075-18000130
- [32] Zhou, X., Zhang, Y., Wang, Y., Zhang, H., Chen, L., & Liu, Y. (2017). Prevalence of malocclusion in 3-to 5-year-old children in Shanghai, China. *International journal of environmental research and public health*, 14(3), 328. doi: 10.3390/ijerph14030328

МОДЕЛЮВАННЯ ЛІНІЙНИХ РОЗМІРІВ НЕОБХІДНИХ ДЛЯ ПОБУДОВИ КОРЕКТНОЇ ФОРМИ ЗУБНОЇ ДУГИ В ЮНАКІВ І ДІВЧАТ ІЗ ФІЗІОЛОГІЧНИМ ПРИКУСОМ БЕЗ УРАХУВАННЯ ТИПУ ОБЛИЧЧЯ В ЗАЛЕЖНОСТІ ВІД ОСОБЛИВОСТЕЙ ЦЕФАЛОМЕТРИЧНИХ ПОКАЗНИКІВ ЗА МЕТОДОМ BURSTONE ТА КОМП'ЮТЕРНО-ТОМОГРАФІЧНИХ РОЗМІРІВ ЗУБІВ Орловський І. В., Беляєв Е. В., Ісакова Н. М., Касьяненко Д. М., Черкасова Л. А., Дякова О. В., Гунас І. В.

Правильне моделювання форми зубних дуг є одним із ключових завдань сучасної ортодонтії, оскільки воно визначає стабільність функціональних і естетичних результатів лікування. Більшість існуючих підходів ґрунтуються лише на одонтометричних показниках, або враховують тип обличчя, що обмежує точність прогнозування. Використання телерентгенографічних параметрів за методом Burstone у поєднанні з комп'ютерно-томографічними вимірами зубів дозволяє інтегрувати дані різних рівнів, забезпечуючи більш обґрунтоване формування зубних дуг. Такий підхід відкриває можливості для індивідуалізації ортодонтичного лікування юнаків і дівчат із фізіологічним прикусом та підвищення його ефективності. Мета дослідження – розробка та аналіз регресійних моделей лінійних розмірів необхідних для побудови коректної форми зубної дуги в українських юнаків і дівчат із фізіологічним прикусом без урахування типу обличчя в залежності від особливостей телерентгенографічних показників за методом Burstone та комп'ютерно-томографічних розмірів зубів. На отриманих з банку даних науково-дослідного центру та кафедри стоматології дитячого віку Вінницького національного медичного університету ім. М. І. Пирогова телерентгенограмах (41 юнак і 68 дівчат із фізіологічним прикусом) проведено вимірювання лінійних і кутових показників за методом Burstone, а на комп'ютерних томограмах морфометричне дослідження зубів та зубних дуг. Регресійні моделі лінійних розмірів необхідних для побудови коректної форми зубної дуги в залежності від телерентгенометричних показників і комп'ютерно-томографічних розмірів зубів побудовані за допомогою ліцензійного пакету «Statistica 6.0». Встановлено, що в юнаків побудовані усі 18 можливих достовірних моделей із коефіцієнтом детермінації більшим 0,6 (R²= від 0,694 до 0,894, p<0,001); а у дівчат – лише 10 достовірних моделей (R²= від 0,605 до 0,775, p<0,001). При аналізі частоти входження до регресійних моделей комп'ютернотомографічних розмірів зубів і телерентгенометричних показників за методом Burstone встановлено: в юнаків найбільш часто входять ширина коронкової частини зуба у мезіо-дистальній площині (26,09 %) та вестибуло-оральній площині (14,49 %), телерентгенометричні показники (18,84 %) та довжина зуба (13,04 %); у дівчат – телерентгенометричні показники (28,57 %), ширина та довжина коронкової частини зуба у мезіо-дистальній площині (відповідно 21,42 % і 9,52 %) та довжина зуба (10,71 %). При аналізі частоти входження до регресійних моделей відповідних зубів встановлено, що в юнаків найбільш часто входять верхні та нижні різці (відповідно 24,11 % і 20,53 %), верхні та нижні малі кутні зуби (відповідно 16,07 % і 14,28 %) та верхні ікла (10,71 %), а у дівчат – верхні та нижні різці (відповідно 43,33 % і 20,00 %), нижні ікла та нижні малі кутні зуби (по 11,66 %).

Ключові слова: стоматологія, телерентгенометрія за методом Burstone, комп'ютерно-томографічні розміри зубів і зубних дуг, регресійний аналіз, українськи юнаки та дівчата, фізіологічний прикус.

Author's contribution

Orlovskyi I. V. – research, methodology and writing of the original draft, formal analysis.

Beliaiev E. V. – conceptualization.

Isakova N. M. - review writing and editing.

Kasianenko D. M. - software.

Cherkasova L. A. – data visualization.

Dyakova O. V. – validation.

Gunas I. V. - supervision.

Vol. 31, №3, Page 53-61

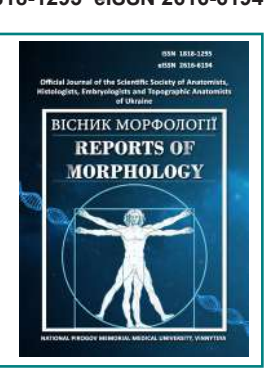
ISSN 1818-1295 eISSN 2616-6194



REPORTS OF MORPHOLOGY

Official Journal of the Scientific Society of Anatomists, Histologists, Embryologists and Topographic Anatomists of Ukraine

journal homepage: https://morphology-journal.com



Differences in the structural organisation of liver tissue in experimental rats 1 and 3 hours after administration of Leiurus macroctenus scorpion venom

Haidai O. S.1, Dzevulska I. V.1, Samborska I. A.2, Shvager O. V.3

¹Bogomolets National Medical University, Kyiv, Ukraine ²ML Dila Laboratory of Pathomorphology, Kyiv, Ukraine

³Educational and Scientific Centre "Institute of Biology and Medicine", Taras Shevchenko National University of Kyiv, Kyiv, Ukraine

ARTICLE INFO

Received: 5 February 2025 Accepted: 11 Juli 2025

UDC: 615.9: 616-00/616-008. 616-

099.616.3

CORRESPONDING AUTHOR

e-mail: lenaustimenko23@gmail.com Haidai O. S.

CONFLICT OF INTEREST

The authors have no conflicts of interest to declare.

FUNDING

Not applicable.

DATA SHARING

Data are available upon reasonable request to corresponding author.

Scorpion bites are a serious threat to human health and life in almost all countries of the world. The amount and toxicity of the poison that enters the body of the victims depend on the interspecific variability of these animals. Scorpion venom usually causes the development of local, cardiotoxic, neurotoxic and vegetative effects. The study aimed to determine the differences in the structural organisation of the liver tissue of experimental rats 1 and 3 hours after the administration of the venom of the scorpion Leiurus macroctenus. The study was conducted on 10 male rats (200±10 g), which were injected intramuscularly with 0.5 ml of a solution of venom (28.8 µg/ml; LD_{E0}=0.08 mg/ kg) of the scorpion Leiurus macroctenus, dissolved in saline (0.9 %). The control group (10 rats) was injected with only 0.5 ml of saline (0.9 %). For microscopic examination, samples of liver tissue from animals of all groups were taken. The pieces were fixed in 10 % formalin solution for 1 day. Then, the pieces were dehydrated in alcohols of increasing concentration and embedded in paraffin blocks. Histological preparations of rat livers were stained with hematoxylin and eosin. Histological preparations were studied using a SEO SCAN light microscope and photodocumented using a Vision CCD Camera video camera with an image output system from histological preparations. One hour after the rats were administered the venom of the scorpion Leiurus macroctenus, no pronounced changes in the structural organisation of the liver of experimental rats were observed. Infiltration of the portal tracts and sometimes the surrounding parenchyma of the organ with lymphocytes, histiocytes and neutrophilic leukocytes was noted. Hepatocytes near the foci of infiltration underwent vacuolar dystrophy, which are reactive changes in response to the action of the venom. In rats that were withdrawn from the experiment three hours after the administration of the venom of the scorpion Leiurus macroctenus, more pronounced changes in the structural organisation of the liver were observed. Areas of disruption of the order of the hepatic lamellae were noted, and the number of binucleated hepatocytes increased, as well as their nuclear-cytoplasmic index. An increase in the number of Kupffer cells was detected; the presence of vacuolar or fatty dystrophy characterised the vast majority of hepatocytes. Pronounced infiltration of the portal tracts and the surrounding liver parenchyma was observed with a predominance of lymphocytes and macrophages. Keywords: scorpions, liver, inflammation, macrophages, lymphocytes.

Introduction

Scorpion stings are a serious threat to human health and life in almost all countries of the world. The amount and toxicity of the venom that enters the body of the victims depend on the interspecific variability of these animals. Scorpion venom usually causes the development of local, cardiotoxic, neurotoxic and vegetative effects. Depending

on the predominance of one or another component in the venom, a wide range of clinical signs and symptoms can be observed from local reactions (hyperemia, pain, oedema) to serious consequences, including respiratory, gastrointestinal, cardiovascular or neurological complications [7, 12, 15]. The severity of poisoning depends on the size and type of

scorpion, the amount of venom injected, the body weight of the victim, and the victim's sensitivity to the venom. Studies in recent decades have reported damage to the kidneys, liver, pancreas, heart, and hemolytic disorders as a result of poisoning with toxins from some scorpion species [8, 11].

The evolution of scorpions is approximately 400 million years, during which they have spread throughout the world. To date, more than 2,700 extant species of these animals, numbering about 20 families, have been registered. The extraordinary resistance, adaptability to changing climate conditions, and high survival rate of scorpions have contributed to their colonisation in tropical, subtropical, and temperate regions of almost all continents, except Antarctica and several Pacific islands [1, 14, 30]. However, in recent years, the expansion of human civilisation and the growth of the human population have led to a sharp reduction in the usual habitats of scorpions, but have significantly increased the frequency of poisonings due to their bites.

The liver is one of the essential organs that provide the body's immune defence with a high density of myeloid (such as Kupffer cells, neutrophils or macrophages) and lymphoid (such as natural killer cells, T cells or B cells) immune cells. The human liver contains about 1010 resident lymphocytes, including B cells, T cells and natural killer (NK) cells. Lymphocyte migration increases in response to the activation of inflammatory processes, and intrahepatic compartmentalisation of lymphocytes determines the morphological variant of organ damage [9, 23, 27]. Toxic liver damage due to exposure to poisons, including those of animal origin, is often associated with lymphocytic infiltration, and the nature and degree of inflammation determine the rate of progression and severity of damage. The mechanisms by which toxic compounds activate immune-mediated pathways of liver damage are still being actively studied; however, liver infiltration by effector lymphocytes is a common phenomenon, leading to the destruction of hepatocytes and cholangiocytes and a persistent shift in the structural and functional characteristics of the organ [2, 19, 27].

The study aims to determine the differences in the structural organisation of the liver tissue of experimental rats 1 and 3 hours after the administration of Leiurus macroctenus scorpion venom.

Materials and methods

The study used ten white male laboratory rats weighing approximately 200±10 g (10 – control group was injected with only 0.5 ml of 0.9 % saline; 10 – experimental group), which were housed in the vivarium of the Educational and Scientific Centre "Institute of Biology and Medicine" of Taras Shevchenko National University of Kyiv. The rats were maintained on a standard diet in an accredited vivarium, following the "Standard Rules for the Arrangement, Equipment and Maintenance of Experimental Biological Clinics (Vivaria)". The experiments were conducted in accordance with the current regulatory standards governing research with laboratory animals and in accordance with the principles of the "European Convention for the Protection of Vertebrate Animals Used for Experimental and Other Scientific Purposes" [16]. In addition, all procedures with animals complied with

the legislation of Ukraine, in particular the Law No. 3447-IV of February 21, 2006 "On the Protection of Animals from Cruelty and Ethical Norms and Rules for Working with Laboratory Animals", which was approved by the Bioethics Committee of the O. O. Bogomolets National Medical University (protocol No. 191 of 01/27/2025).

The rats used in the experiment were divided into two groups: experimental group 1 (5 rats) – histological material was collected 1 hour after the introduction of the poison; and experimental group 2 (5 rats), in which the liver tissues were collected three hours after exposure to the poison. The venom of a scorpion from the Buthidae family, genus Leiurus, species Leiurus macroctenus, was administered to rats once intramuscularly (0.5 ml of venom solution previously dissolved in saline; 28.8 μ g/ml; LD₅₀=0.08 mg/kg) [16, 17]. Rats were euthanised by carbon dioxide inhalation, and the liver was immediately removed at 4 °C.

Liver tissue samples from animals of all groups were taken for microscopic examination. The pieces were fixed in 10 % formalin solution for 1 day. Then the pieces were dehydrated in alcohols of increasing concentration and embedded in paraffin blocks. Histological preparations of rat livers were stained with hematoxylin and eosin. Histological preparations were studied using a SEO SCAN light microscope and photographed using a Vision CCD Camera with an image output system from histological preparations [18].

Results

Microscopic studies one hour after administration of Leiurus macroctenus scorpion venom to rats demonstrated the appearance of minor shifts in the normal histoarchitectonics of the animal liver. Hepatocytes were predominantly hexagonal in shape and contained one nucleus, but the presence of binucleate cells was noted. The cytoplasm of hepatocytes was oxyphilic and contained numerous inclusions. Their nuclei had 1-2 nucleoli, and the chromatin occupied a marginal position under the nuclear envelope. Hepatocytes formed hepatic plates that were ordered and located radially from the central vein (Fig. 1).

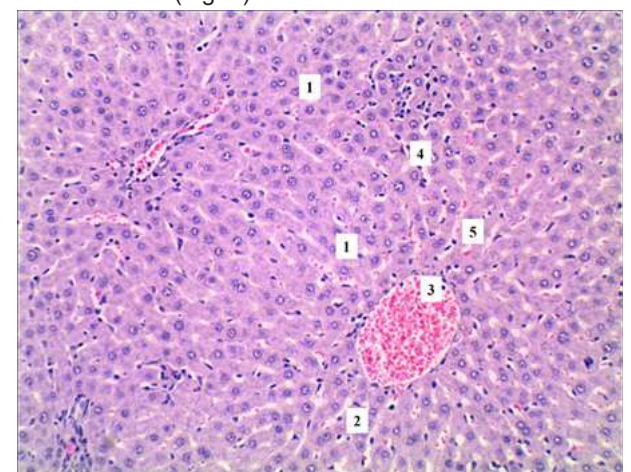


Fig. 1. Microscopic organisation of the liver of an experimental rat 1 hour after administration of the venom of the scorpion Leiurus macroctenus. Hepatocytes (1), hepatic laminae (2), lumen of the central vein (3), space of Disse (4), lumen of the sinusoidal capillary (5). Staining with hematoxylin and eosin. ×100.

Vol. 31, №3, Page 62-68 **63**

Sinusoidal capillaries between hepatic beams were somewhat dilated, and their lumen was mainly filled with erythrocytes. Endothelial lining of capillaries – without signs of desquamation from the basement membrane. Their endothelial cells are somewhat flattened and contain fenestrae in the cytoplasm. The presence of perisinusoidal Kupffer cells in the space of Disse was observed, which had an irregular shape and were distinguished by the presence of processes. They were characterised by elongated hyperchromic nuclei and weakly oxyphilic cytoplasm with numerous inclusions and a well-developed Golgi complex (see Fig. 1, Fig. 2).

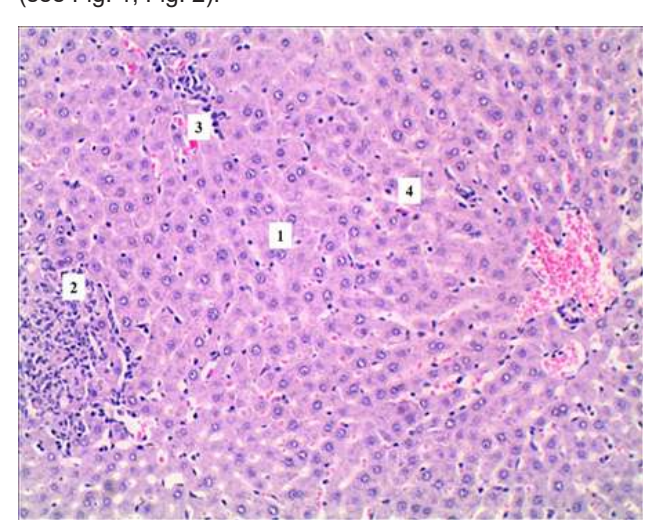


Fig. 2. Histological structure of the liver of an experimental rat 1 hour after administration of the venom of the scorpion Leiurus macroctenus. Hepatocytes (1), lymphohistiocytic infiltration (2), lumen of the sinusoidal capillary (3), space of Disse (4). Staining with hematoxylin and eosin. ×100.

The lumen of the central vein in most histological specimens is dilated. The endothelial cells of the inner lining of the vascular wall are elongated, and their nuclei are hyperchromic. Stasis of formed blood elements, mainly erythrocytes, was noted in the lumen of the central vein (see Fig. 1).

A characteristic feature of the structural organisation of the liver one hour after the start of the experimental study was pronounced histiocytic and lymphocytic infiltration of the portal tracts, sometimes with the presence of neutrophilic leukocytes. Accumulations of lymphocytes were detected around the portal vein and bile ducts. However, partial infiltration of the surrounding parenchyma was also observed in some fields of view. It should be noted that in these areas, individual hepatocytes had signs of vacuolar dystrophy. These structural changes can be regarded as initial reactive changes in response to the action of scorpion venom toxins. The walls of the bile ducts under these conditions did not undergo pronounced changes. They were lined with one row of cubic cells. Their nuclei occupied a central position and contained one nucleolus. Chromatin had a marginal location, formed clumps or was diffusely scattered. The hepatic artery was distinguished by the presence of elongated endothelial cells of the inner membrane with round or oval hyperchromic nuclei. Some endothelial cells protruded into the lumen of the vessel in the form of palisades. The lumen of the hepatic vein was dilated, sometimes with erythrocyte stasis (Fig. 3).

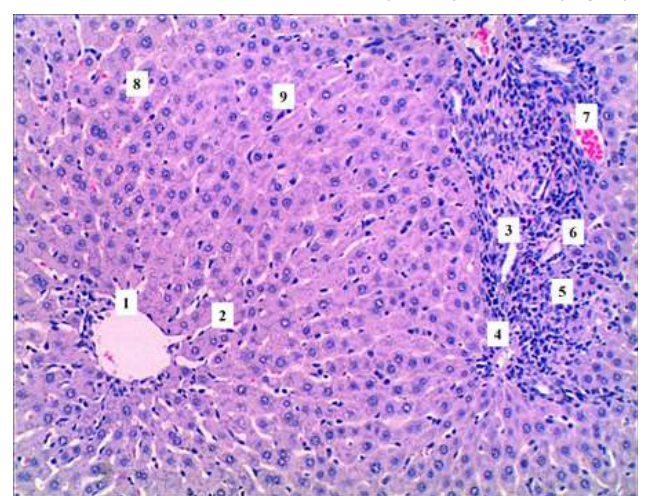


Fig. 3. Morphological organisation of the liver of an experimental rat 1 hour after administration of the venom of the scorpion Leiurus macroctenus. Central vein lumen (1), hepatic lamellae (2), bile duct lumen (3), hepatic artery (4), lymphohistiocytic infiltration (5), portal vein (6), hepatic vein (7), sinusoidal capillary lumen (8), Disse's space (9). Hematoxylin and eosin staining. ×100.

Histological studies of the liver tissue of experimental rats three hours after the start of the experiment and the administration of the scorpion venom Leiurus macroctenus demonstrated the presence of more pronounced changes in the morphological structure of the organ. Hepatocytes formed hepatic plates, which were located mainly radially from the central vein; however, in some fields of view, disturbances in the order of liver cells were noted. The latter had a polygonal shape; their cytoplasm was eosinophilic with numerous signs of vacuolar and fatty dystrophy. The nuclei of hepatocytes were rounded, hyperchromic, and contained 1-2 nucleoli. In the vast majority of hepatocyte nuclei, heterochromatin prevailed, which accumulated under the karyolemma. The karyoplasm was clear and oedematous. Compared with the previous study group, the number of binucleated cells increased, and the nuclear-cytoplasmic index of hepatocytes also increased (Fig. 4).

The lumens of the sinusoidal capillaries of the liver were significantly dilated. Endotheliocytes were characterised by an elongated shape, weakly eosinophilic cytoplasm, and hyperchromic nuclei. In the lumens of the sinusoidal capillaries, accumulations of formed blood elements were observed, in particular erythrocytes and occasionally lymphocytes. In the spaces of Disse between the walls of the sinusoidal hemocapillaries of the liver and hepatocytes, accumulations of Kupffer cells were detected. Their number also increased compared to the study group one hour after the administration of the poison. They had an elongated or close to oval shape, clear cytoplasm, and hyperchromic

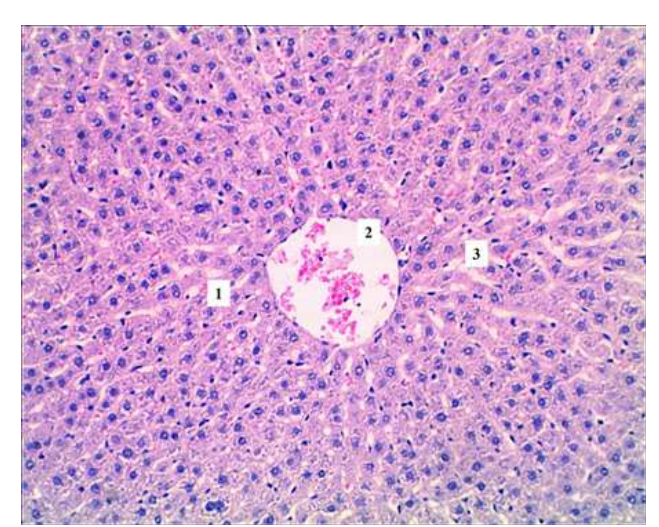


Fig. 4. Histological structure of the liver of an experimental rat 3 hours after administration of the venom of the scorpion Leiurus macroctenus. Liver lamellae (1), lumen of the central vein (2), lumen of the sinusoidal capillary (3). Staining with hematoxylin and eosin. ×100.

nuclei. The presence of an insignificant number of fibroblasts in the intercellular connective tissue, which was somewhat edematous, was also noted (Fig. 5).

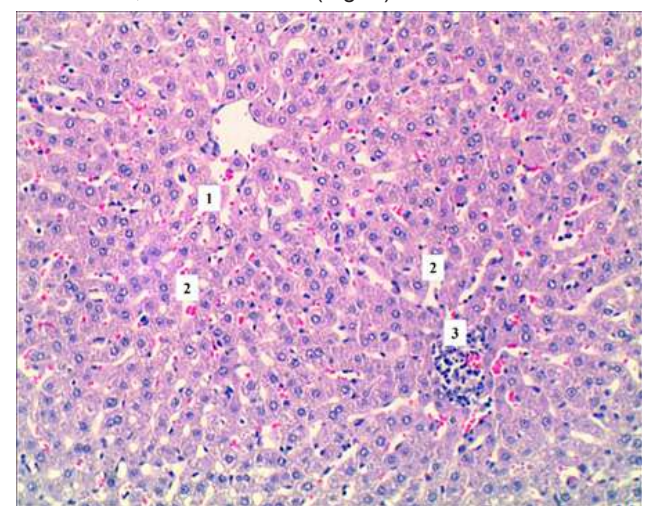


Fig. 5. Microscopic changes in the liver of an experimental rat 3 hours after administration of the venom of the scorpion Leiurus macroctenus. Hepatocytes (1), lumens of sinusoidal capillaries (2), inflammatory infiltrate (3). Staining with hematoxylin and eosin. ×100.

The lumens of the central veins were significantly dilated and markedly full of blood, contained clusters of erythrocytes, and their adhesion to the vein wall was also noted. The endothelial cells of the inner membrane of the central vein had a flattened shape, oxyphilic cytoplasm, and markedly hyperchromic nuclei. Individual endothelial cells in the form of palisades were directed into the lumen of the vein. Moderately pronounced lymphocytic infiltration was observed around the central vein (Fig. 6).

The portal tracts were characterised by significant lymphocytic infiltration. The lumens of the bile ducts were



Fig. 6. Microscopic organisation of the liver of an experimental rat 3 hours after administration of the venom of the scorpion Leiurus macroctenus. Hepatic lamellae (1), hepatocytes (2), lumen of the central vein (3), portal tract (4), interlobular bile duct (5), interlobular artery (6), lumen of the sinusoidal capillary (7). Staining with hematoxylin and eosin. ×100.

dilated, and their wall was represented by one row of cubic cells with an increased nuclear-cytoplasmic index. The cytoplasm of these cells was weakly oxyphilic, the nuclei contained one nucleolus, had a clear karyoplasm, and the chromatin occupied a marginal position. The walls of the interlobular bile ducts were slightly thickened. Thickened, edematous walls also distinguished the interlobular arteries. Their epithelial lining was sometimes incomplete, and areas of desquamation of the endothelium from the basement membrane were detected. The muscular coat of the arteries had signs of oedema and was represented mainly by smooth muscle cells with homogeneous eosinophilic cytoplasm and elongated hyperchromic nuclei. The lumens of the interlobular veins were often narrowed due to infiltration and contained formed blood elements (Fig. 7).

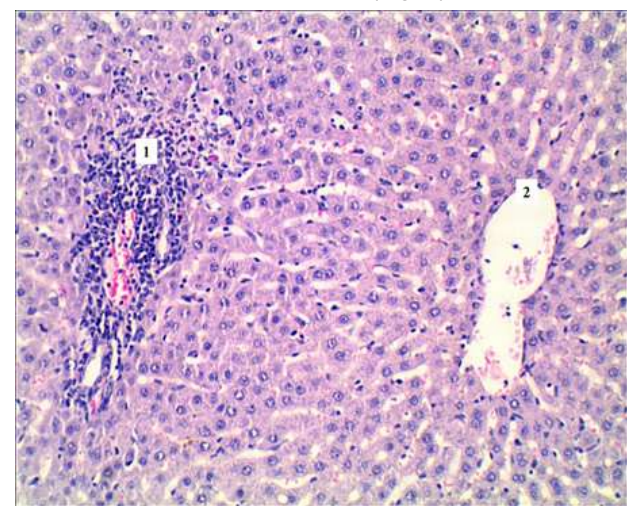


Fig. 7. Histological changes in the liver of an experimental rat 3 hours after administration of the venom of the scorpion Leiurus macroctenus. Inflammatory infiltrate (1), lumen of the central vein (2). Staining with hematoxylin and eosin. ×100.

Vol. 31, №3, Page 62-68 **65**

A distinctive feature of this study group was the formation of foci of pronounced lymphocytic infiltration, but not only in the areas of the portal tracts. These infiltrates were represented by lymphocytes, macrophages and to a lesser extent, plasma cells and segmented neutrophils. In the areas of infiltration, narrowing of the lumens of the sinusoidal hemocapillaries of the liver, a significant degree of vacuolar dystrophy of hepatocytes, and their apoptosis were detected. The appearance of karyolysis and karyopyknosis of the nuclei distinguished individual hepatocytes. A denser arrangement of hepatocytes was observed around the inflammatory infiltrates.

Discussion

Thus, one hour after the administration of the venom of the scorpion Leiurus macroctenus to rats, infiltration of the portal tracts and the organ parenchyma with various types of leukocytes was noted. Hepatocytes near the foci of infiltration underwent vacuolar dystrophy. In rats that were withdrawn from the experiment three hours after the administration of the venom, areas of disruption of the order of the hepatic lamellae were noted, an increase in the number of Kupffer cells was detected, and the presence of vacuolar or fatty dystrophy characterised the majority of hepatocytes. H. A. Fetaih et al. [13] studied histopathological changes in the structure of the liver under the influence of the venom of the scorpion Androctonus amoreuxi in experiments on mice. 6 hours after the administration of $\frac{1}{4}$ LD₅₀, significant blood stasis was detected in the vessels of the organ. On the 4th day, hydropic degeneration of hepatocytes, karyolysis and karyorrhexis of nuclei were noted. An increase in the concentration of the poison, namely ½ LD₅₀, after 9 hours of observation showed the appearance of extramedullary hematopoiesis islands in the liver and dilation of sinusoidal capillaries. Already on the 4th day of the study, at the indicated dose of poison, dilation of blood vessels, fibrinoid degeneration, and deposition of weakly basophilic homogeneous material in the portal zones of the organ were detected.

The bites of scorpions, Leurus quinquestriatus, have been proven to cause changes in the morphological organisation of the rat liver. Histological examination of the organ after injection of the poison to animals at a dose of 0.03 mg/kg revealed pronounced oedema of hepatocytes, which led to a change in the shape of the cells and the "disappearance" of most sinusoidal capillaries. The cytoplasm of hepatocytes underwent vacuolization and the appearance of areas that were not stained with hematoxylin and eosin. Hypochromia of the nuclei and their pyknotic changes were noted. Degenerative changes of individual nuclei and chromatin margination were also observed. In some fields of view, hepatocyte necrosis and congestion in the portal vein branch were present [5, 26].

Studies by Khemili D. [20] showed that the venom of scorpions Androctonus australis hector at a dose of 0.5 mg/kg caused the development of pronounced pathological changes in the liver parenchyma, including necrosis of hepatocytes, destruction of hepatic architectonics and

massive immigration of inflammatory cells into the sinusoids.

Clinical observations of patients after scorpion bites and experimental studies demonstrate cases of toxic hepatitis and coagulopathy. In biochemical studies under these conditions, an increase in ALT, AST, LDH, and, rarely, hyperbilirubinemia is recorded. The mechanisms of involvement of liver damage caused by scorpion bites remain unclear, although the hypothesis of direct hemolytic and cytotoxic effects of the venom prevails. In addition, stimulation of neurotransmitters, catecholamines and the release of cytokines and inflammatory mediators are usually associated with hepatotoxicity and haematological disorders. In addition, intravascular hemolysis, coagulopathy, and thrombocytopenia are characteristic, which may act as indirect factors of liver damage [3, 6, 22]. The development of oxidative stress almost always characterises liver damage due to factors of various origins. Recent studies have demonstrated that there are specific patterns of protein expression in the liver that are induced in mammalian cells in response to hydroperoxide stress. This modulation occurs due to the activation of redox transcription factors, such as Egr-1, NF-kappaB, and AP-1, as well as G proteins [21]. Cellular kinases, especially the mitogen-activated protein kinase family, also play an essential role. Protein expression disorders emphasise the importance of signalling pathways dependent on the balance of redox processes. Excessive production of ROS exposes the liver to oxidative stress and leads to hepatocyte apoptosis [4, 10]. Currently, the study of cellular mechanisms that protect against oxidative stress is highly relevant. Despite the minimal amount of data, only a few specific genes are known that are crucial for the control of cellular function in cases of oxidative liver damage. Apurinic/ apyrimidinic endonuclease (APE)/redox factor (Ref)-1 is a prime example of this mechanism. The APE/Ref1 enzyme is a key driver of excision repair, which exhibits properties of repair and redox control.

Activation of inflammatory processes and oxidative stress underlie the pathogenesis of organ damage caused by scorpion venom. However, the relationship between them is not fully understood. Toll-like receptors play a crucial role in stimulating the inflammatory response, and evidence is accumulating that TLRs, in particular TLR4, may be involved in both redox imbalance and inflammation induction. Recent studies have demonstrated that blocking TLR4 attenuates the inflammatory response mediated by neutrophils, as evidenced by a decrease in the number of these cells in the blood, as well as inhibition of their degranulation and sequestration in lung, liver, and kidney tissues [29]. In addition, TAK-242 (a small-molecule inhibitor of Toll-like receptors) caused a significant decrease in the content of nitrites, malondialdehyde and carbonyl groups of proteins, associated with an improvement in the functioning of the antioxidant defence system in all organs studied, except the heart [20]. It has been proven that the TLR family of receptors is involved in warning the immune system about the possible negative impact of factors of various origins, and

the receptors themselves can be activated by DAMPs, which are released under the influence of stress factors, including scorpion stings, as previously noted [24, 30].

Conclusions

1. One hour after the administration of Leiurus macroctenus scorpion venom to rats, no pronounced changes in the structural organisation of the liver of experimental rats were observed. Infiltration of the portal tracts and sometimes the surrounding parenchyma of the organ with lymphocytes, histiocytes and neutrophil leukocytes was noted. Hepatocytes near the foci of infiltration underwent vacuolar dystrophy, which are reactive changes in response

to the action of the venom.

2. In rats that were removed from the experiment three hours after the administration of Leiurus macroctenus scorpion venom, more pronounced changes in the structural organisation of the liver were observed. Areas of disruption of the order of the hepatic lamellae were noted, and the number of binucleated hepatocytes increased, as well as their nuclear-cytoplasmic index. An increase in the number of Kupffer cells was detected; the presence of vacuolar or fatty dystrophy characterised the vast majority of hepatocytes. Pronounced infiltration of the portal tracts and surrounding liver parenchyma with a predominance of lymphocytes and macrophages was observed.

References

- [1] Abroug, F., Ouanes-Besbes, L., Tilouche, N., & Elatrous, S. (2020). Scorpion envenomation: state of the art. *Intensive Care Med*, 46(3), 401-410. doi: 10.1007/s00134-020-05924-8
- [2] Adams, D. H., Ju, C., Ramaiah, S. K., Uetrecht, J., & Jaeschke, H. (2010). Mechanisms of immune-mediated liver injury. *Toxicol Sci*, 115(2), 307-321. doi: 10.1093/toxsci/kfq009
- [3] Al-Asmari, A., Khan, H. A., & Manthiri, R. A. (2015). Effect of Androctonus bicolor scorpion venom on the activities of serum enzymes in rats. *Int J Clin Exp Med*, 8(7), 11734-11737. PMID: 26380012
- [4] Al-Asmari, A. K., Riyasdeen, A., & Islam, M. (2018). Scorpion Venom Causes Apoptosis by Increasing Reactive Oxygen Species and Cell Cycle Arrest in MDA-MB-231 and HCT-8 Cancer Cell Lines. J Evid Based Integr Med, 23, 2156587217751796. doi: 10.1177/2156587217751796
- [5] Al-Harbi, H. A., Al-Hasavi, Z. M. (2014). Effects of Leurus quinquestriatus scorpion venom on histological structure of the liver and kidney. Glo Adv Res J Environ Sci Toxicol, 3(4), 49-56.
- [6] Almeida, J. S., Ravetti, C. G., Nobre, V. A., Vassallo, P. F., & Melo de Andrade, M. V. (2025). New biomarkers in scorpion stings. *Toxicon*, 255, 108258. doi: 10.1016/j. toxicon.2025.108258
- [7] Bahloul, M., Bouchaala, K., Chtara, K., Kharrat, S., & Bouaziz, M. (2024). Myocardial Ischemia after Severe Scorpion Envenomation: A Narrative Review. Am J Trop Med Hyg, 111(6), 1178-1183. doi: 10.4269/ajtmh.24-0163
- [8] Bahloul, M., Regaieg, K., Chabchoub, I., Kammoun, M., Chtara, K., & Bouaziz, M. (2017). Severe scorpion envenomation: pathophysiology and the role of inflammation in multiple organ failure. *Med Sante Trop*, 27(2), 214-221. doi: 10.1684/mst.2017.0688
- [9] Crispe, I. N. (2016). Hepatocytes as Immunological Agents. J Immunol, 196(1), 17-21. doi: 10.4049/jimmunol.1501668
- [10] Daachi, F., Adi-Bessalem, S., Megdad-Lamraoui, A., & Laraba-Djebari, F. (2025). Influence of envenomation timing on peripheral immune and oxidative responses in experimental scorpion envenomation. J Venom Anim Toxins Incl Trop Dis, 31, e20240059. doi: 10.1590/1678-9199-JVATI TD-2024-0059
- [11] Darkaoui, B., Lafnoune, A., Chgoury, F., Daoudi, K., Chakir, S., Mounaji, K., ... & Naoual, O. (2022). Induced pathophysiological alterations by the venoms of the most dangerous Moroccan scorpions Androctonus mauretanicus and Buthus occitanus: A comparative pathophysiological and toxic-

- symptoms study. *Hum Exp Toxicol*, *41*, 9603271211072872. doi: 10.1177/09603271211072872
- [12] Das, B., Patra, A., & Mukherjee, A. K. (2020). Correlation of Venom Toxinome Composition of Indian Red Scorpion (*Mesobuthus tamulus*) with Clinical Manifestations of Scorpion Stings: Failure of Commercial Antivenom to Immune-Recognize the Abundance of Low Molecular Mass Toxins of This Venom. *J Proteome Res*, 19(4), 1847-1856. doi: 10.1021/acs.jproteome.0c00120
- [13] Fetaih, H. A., Shoukry, N. M., Soliman, B. A., Mohallal, M. E., & Khaled, H. S. (2013). Histopathological changes in liver of mice after experimental envenomation with Androctonus amoreuxi scorpion venom. *J Egypt Soc Parasitol*, 43(2), 447-456. doi: 10.12816/0006401
- [14] Furtado, A. A., Daniele-Silva, A., Silva-Júnior, A. A. D., & Fernandes-Pedrosa, M. F. (2020). Biology, venom composition, and scorpionism induced by brazilian scorpion Tityus stigmurus (Thorell, 1876) (Scorpiones: Buthidae): A mini-review. *Toxicon*, 185, 36-45. doi: 10.1016/j.toxicon.2020.06.015
- [15] Godoy, D. A., Badenes, R., Seifi, S., Salehi, S., & Seifi, A. (2021). Neurological and Systemic Manifestations of Severe Scorpion Envenomation. *Cureus*, 13(4), e14715. doi: 10.7759/cureus.14715
- [16] Gunas, V., Maievskyi, O., Raksha, N., Vovk, T., Savchuk, O., Shchypanskyi, S., ... & Gunas, I. (2023). Protein and peptide profiles of rats' organs in scorpion envenomation. *Toxicol Rep*, 10, 615-620. doi: 10.1016/j.toxrep.2023.05.008
- [17] Gunas, V., Maievskyi, O., Raksha, N., Vovk, T., Savchuk, O., Shchypanskyi, S., ... & Gunas, I. (2024). Study of the Acute Toxicity of Scorpion *Leiurus macroctenus* Venom in Rats. *ScientificWorldJournal*, 2024, 9746092. doi: 10.1155/2024/9746092
- [18] Horalskyi, L. P., Khomych, V. T., & Kononskyi, O. I. (2015). Основи гістологічної техніки і морфофункціональні методи дослідження у нормі та при патології: навч. посіб. [Fundamentals of histological technique and morphofunctional research methods in normal and pathology: study guide]. Житомир: Полісся=Zhytomyr: Polissya.
- [19] Kawashima, K., Andreata, F., Beccaria, C. G., & Iannacone, M. (2024). Priming and Maintenance of Adaptive Immunity in the Liver. Annu Rev Immunol, 42(1), 375-399. doi: 10.1146/ annurev-immunol-090122-041354
- [20] Khemili, D., Laraba-Djebari, F., & Hammoudi-Triki, D. (2020). Involvement of Toll-like Receptor 4 in Neutrophil-Mediated Inflammation, Oxidative Stress and Tissue Damage In-

Vol. 31, №3, Page 62-68

- duced by Scorpion Venom. *Inflammation*, *43*(1), 155-167. doi: 10.1007/s10753-019-01105-y
- [21] Kleniewska, P., Piechota-Polanczyk, A., Michalski, L., Michalska, M., Balcerczak, E., Zebrowska, M., ... & Goraca, A. (2013). Influence of block of NF-kappa B signaling pathway on oxidative stress in the liver homogenates. Oxid Med Cell Longev, 2013, 308358. doi: 10.1155/2013/308358
- [22] Köse, A., Biricik, S., Bozkurt, S., Cavuşoğlu, C., & Ayrık, C. (2016). Toxic Hepatitis and Coagulopathy due to Scorpion Sting. *Annals of Clinical Case Reports*, 1, 1212. doi: 10.25107/2474-1655.1212
- [23] Kubes, P., & Jenne, C. (2018). Immune Responses in the Liver. Annu Rev Immunol, 36, 247-277. doi: 10.1146/ annurev-immunol-051116-052415
- [24] Mihm, S. (2018). Danger-Associated Molecular Patterns (DAMPs): Molecular Triggers for Sterile Inflammation in the Liver. *Int J Mol Sci*, 19(10), 3104. doi: 10.3390/ ijms19103104
- [25] Ronca, V., Gerussi, A., Collins, P., Parente, A., Oo, Y. H., & Invernizzi, P. (2025). The liver as a central "hub" of the immune system: pathophysiological implications. *Physiol Rev*, 105(2), 493-539. doi: 10.1152/physrev.00004.2023
- [26] Salman, M. M. A., Kotb, A. M., Haridy, M. A. M., Golka, K., & Hammad, S. (2017). Effect of a bradykinin-potentiating

- factor isolated from scorpion venom (Leiurus quinquestriatus) on some blood indices and lipid profile in irradiated rats. *Mol Cell Biochem*, *434*(1-2), 1-6. doi: 10.1007/s11010-017-3029-6
- [27] Shuai, Z., Leung, M. W., He, X., Zhang, W., Yang, G., Leung, P. S., ... & Eric Gershwin, M. (2016). Adaptive immunity in the liver. *Cell Mol Immunol*, 13(3), 354-368. doi: 10.1038/ cmi.2016.4
- [28] Siqueira, T. S., Dos Santos, A. J., Santos, J. L. C., da Silva, R. R. N., Silva, J. R. S., & Santos, V. S. (2024). Scorpion envenomation in Brazil and its relationship with the social determinants of health: A population-based ecological study. *Acta Trop*, 253, 107165. doi: 10.1016/j.actatropica.2024.107165
- [29] Veloso Júnior, P. H. H., Simon, K. S., de Castro, R. J. A., Coelho, L. C., Erazo, F. A. H., de Souza, A. C. B., ... & Bocca, A. L. (2019). Peptides ToAP3 and ToAP4 decrease release of inflammatory cytokines through TLR-4 blocking. *Biomed Pharmacother*, 118, 109152. doi: 10.1016/j. biopha.2019.109152
- [30] Zhu, R., Wang, Y., Zhang, L., & Guo, Q. (2012). Oxidative stress and liver disease. *Hepatol Res*, 42, 741-749. doi: 10.1111/j.1872-034X.2012.00996.x

ВІДМІННОСТІ СТРУКТУРНОЇ ОРГАНІЗАЦІЇ ТКАНИНИ ПЕЧІНКИ У ЕКСПЕРИМЕНТАЛЬНИХ ЩУРІВ ЧЕРЕЗ 1 ТА 3 ГОДИНИ ПІСЛЯ ВВЕДЕННЯ ОТРУТИ СКОРПІОНА LEIURUS MACROCTENUS Гайдай О. С., Дзевульська І. В., Самборська І. А., Швагер О. В.

Укуси скорпіонів є серйозною загрозою для здоров'я та життя людей майже в усіх країнах світу. Кількість і токсичність отрути, яка потрапляє до організму постраждалих залежить від міжвидової мінливості цих тварин. Отрута скорпіона зазвичай спричиняє розвиток місцевих, кардіотоксичних, нейротоксичних і вегетативних ефектів. Мета дослідження – визначити відмінності структурної організації тканини печінки експериментальних щурів через 1 та 3 години після введення отрути скорпіонів Leiurus macroctenus. Дослідження проводили на 10 щурах-самцях щурів (200±10 г), яким внутрішньом'язово вводили 0,5 мл розчину отрути (28,8 мкг/мл; LD50=0,08 мг/кг) скорпіона Leiurus macroctenus, розчиненого у фізіологічному розчині (0,9 %). Контрольній групі (10 щурів) вводили лише 0,5 мл фізіологічного розчину (0,9 %). Для мікроскопічного дослідження вилучали зразки тканини печінки тварин всіх груп. Шматочки фіксували в 10 % розчині формаліну протягом 1 доби. Далі проводили дегідратацію шматочків в спиртах зростаючої концентрації та заливали в парафінові блоки. Забарвлення гістологічних препаратів печінки щурів здійснювали гематоксиліном та еозином. Гістологічні препарати вивчали за допомогою світлового мікроскопа SEO SCAN та фотодокументували за допомогою відеокамери Vision CCD Camera з системою виводу зображення з гістологічних препаратів. Через одну годину після введення щурам отрути скорпіонів Leiurus macroctenus не спостерігали виражених зрушень структурної організації печінки експериментальних щурів. Відмічали інфільтрацію портальних трактів та подекуди оточуючої паренхіми органу лімфоцитами, гістіоцитами та нейтрофільними лейкоцитами. Гепатоцити поблизу вогнищ інфільтрації зазнавали вакуольної дистрофії, що є реактивними змінами у відповідь на дію отрути. У щурів, яких виводили з експерименту через три години після введення отрути скорпіонів Leiurus macroctenus спостерігали більш виражені зміни структурної організації печінки. Відмічали ділянки порушення впорядкованості печінкових пластинок, збільшувались чисельність двоядерних гепатоцитів, а також їх ядерно-цитоплазматичний індекс. Виявляли зростання кількості клітин Купфера, переважна більшість гепатоцитів характеризувалась наявністю вакуольної чи жирової дистрофії. Спостерігали виражену інфільтрацію портальних трактів та оточуючої паренхіми печінки з переважанням лімфоцитів і макрофагів. Ключові слова: скорпіони, печінка, запалення, макрофаги, лімфоцити.

Author's contribution

Haidai O. S. - conceptualization, research, writing of the original draft.

Dzevulska I. V. – methodology, formal analysis.

Samborska I. A. – project administration, resources.

Shvager O. V. - validation, software.

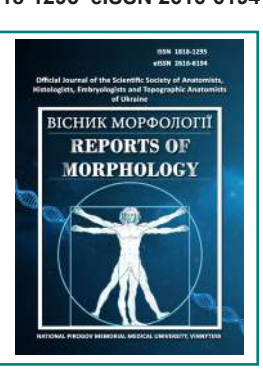
ISSN 1818-1295 eISSN 2616-6194



REPORTS OF MORPHOLOGY

Official Journal of the Scientific Society of Anatomists, Histologists, Embryologists and Topographic Anatomists of Ukraine

journal homepage: https://morphology-journal.com



Long-term effects of heavy metal salts on morphometric parameters and functional state of the sexually mature rats' pineal gland

Hryntsova N. B., Romaniuk A. M.

Medical Institute, Sumy State University, Sumy, Ukraine

ARTICLE INFO

Received: 16 January 2025 Accepted: 18 Juli 2025

UDC: 611.42+611.018.83]:616-

092.9:613.63

CORRESPONDING AUTHOR

e-mail: natalia.gryntsova@gmail.com Hryntsova N. B.

CONFLICT OF INTEREST

The authors have no conflicts of interest to declare.

FUNDING

The work was carried out with the support of the EU grant "Next Generation EU" through the Recovery and Resilience Plan of Slovakia within the framework of project No. 09103-03-V01-00147 (2023-2026), the research project "Morphological aspects of experimental pathology of internal organs and musculoskeletal system", state registration No. 0123U101135 and the research project "Modern views on the morphogenesis of general pathological processes", state registration No. 0119U100887.

DATA SHARING

Data are available upon reasonable request to corresponding author.

Environmental pollution with heavy metals poses a great threat to living organisms and constitutes one of the major problems of modern society. The pineal gland controls the endocrine, nervous, and immune systems, integrates the systemic response to adverse factors affecting the body's resistance. The aim of the study is to investigate the correlation relationships between the dimensions of the pineal gland in sexually mature rats and its other morphometric parameters under conditions of prolonged exposure to a complex of heavy metal salts. Animals from 3 experimental groups were subjected for 30, 60, and 90 days to simulated microelementosis by adding to their drinking water a mixture of heavy metal salts: zinc (ZnSO,×7H,O) -5 mg/L, copper (CuSO $_4$ ×5H $_2$ O) - 1 mg/L, iron (FeSO $_4$) - 10 mg/L, manganese $(MnSO_4 \times 5H_2O) - 0.1 \text{ mg/L}, \text{ lead } (Pb(NO_3)_2) - 0.1 \text{ mg/L}, \text{ and chromium } (K_2Cr_2O_7) - 0.1 \text{ mg/L}$ 0.1 mg/L. Morphological, morphometric, and statistical research methods were used. In the pineal gland of experimental animals, as a result of exposure to heavy metal salts, adaptive-compensatory processes developed and rearrangements occurred in the correlation relationships between the parameters of pineal dimensions and other morphometric indicators of the gland. A decrease in organometric parameters of the gland was observed on the 30th and 90th days of the experiment, with their increase on the 60th day of the study. The strongest correlation between the length of the pineal gland and the glial cell-neuronal index was observed on the 30th day of the experiment; between the length and width of the pineal gland, the length and the average diameter of the karyon/optical density of nuclei on the 60th day; and between the width of the gland and the average diameter of the karyon on the 90th day of the experiment. Adaptive rearrangements in the pineal gland at different stages of pollutant exposure had a wave-like pattern and were determined by the tension of adaptive-compensatory processes at the early stages of the study (30th day), which were replaced by compensatory hypertrophy of the organ on the 60th day of the experiment and by the gradual exhaustion of the functional adaptive capacities of the pineal gland in response to long-term exposure to heavy metal salts (90th day). **Keywords:** pineal gland sizes, heavy metals, correlations.

Introduction

In recent years, interest in the pineal gland has been increasing, which is explained not only by its ability to produce melatonin, considered one of the factors regulating

biorhythms, but also by its neuroendocrine mediation with hormonal and neurotransmitter activity [5]. The pineal gland is a small neuroendocrine organ, its main function being the regulation of sleep through the synthesis and secretion of melatonin [23, 26]. In humans, approximately 80 % of the pineal gland consists of pinealocytes that produce melatonin [26], and the volume of the pineal gland is proportional to the endogenous melatonin level [15, 20]. The volume of the pineal gland may vary under different physiological or pathological conditions, which may alter melatonin production [21, 22]. Some authors indicate that melatonin secretion is associated with the volume of the pineal gland, particularly with the volume of the pineal parenchyma [15, 20, 31]. To date, the influence of pineal gland size changes on the development of several diseases and pathological conditions of the body has been established.

In patients with Alzheimer's disease, reduced endogenous melatonin levels [23, 32] and smaller pineal gland size compared with healthy individuals of the control group were observed [17, 23]. T. Matsuoka et al. [18] believe that a reduction in pineal parenchymal volume is one of the factors contributing to the development of Alzheimer's disease. Therefore, pineal parenchymal volume can be used as a predictor of Alzheimer's disease development in clinical practice. A number of other authors state that pineal gland volume, particularly its parenchymal (i.e., non-cystic) volume, likely reflects melatonin levels or melatonin secretion both in healthy subjects [15, 20] and in patients with affective disorders [9]. A large number of studies have been devoted to investigating the impact of pineal gland size changes on mental disorders. A significant decrease in pineal gland volume was observed in certain subtypes of depression, and these changes correlated with specific depressive symptoms, indicating a relationship between pineal disorders and the clinical subtype and/or symptomatology of major depression [28, 31].

Melatonin secretion disturbances in patients with schizophrenia [4] confirm its involvement in the pathophysiology of this mental disorder. Magnetic resonance imaging (MRI) studies have shown smaller pineal gland volumes in patients with schizophrenia regardless of the disease stage, attention deficit hyperactivity disorder [6, 7, 12, 29]. In addition, MRI studies indicate the role of pineal gland atrophy as a stable marker of vulnerability in psychosis [27]. In healthy individuals, smaller pineal gland volume correlates with greater sleep rhythm disturbances [15, 31]. Pineal gland volume changes may be associated with various clinical conditions, including primary insomnia [8, 31]. Apart from pineal atrophy, hypertrophy of the pineal gland also deserves attention, as it leads to insulin resistance, early tooth eruption and malformation, dry skin, thick nails, hirsutism, and enlargement of the external genitalia in children [16].

Environmental pollution with heavy metals poses a great threat to living organisms and constitutes one of the major problems of modern society [1, 2]. The rate of heavy metal spread in the environment and their generation has significantly increased compared to the past century [19].

Currently, the impact of xenobiotics on central nervous system dysfunction has been proven, including effects on

the development of dementia, amyotrophic lateral sclerosis, delayed neural development, Parkinson's disease, and Alzheimer's disease [3, 11, 14]. The pineal gland, through melatonin, controls the endocrine, nervous, and immune systems, integrates the systemic response to adverse factors [10], optimizes brain activity, and at the same time counteracts pathological processes that cause its disruption. It has now been established that disturbances in the melatonin-producing function of the pineal gland may be both congenital and acquired during life, as a result of various negative external and internal environmental factors [13].

The aim of the study is to investigate the correlation relationships between the dimensions of the pineal gland in sexually mature rats and its other morphometric parameters under conditions of prolonged exposure to a complex of heavy metal salts.

Materials and methods

Animals

The experiment was conducted on 36 white sexually mature male rats weighing 200-250 g, aged 7-8 months, which were divided into 6 groups (3 control groups and 3 experimental groups). Animals of all groups were kept under standard vivarium conditions, where identical conditions of housing, feeding, proper care, and natural lighting (day/night) were maintained, with a constant ambient temperature (20-22 °C). Animals had free access to drinking water. The study was carried out during the autumn-winter period.

Model of experimental microelementosis

The experimental groups included rats that for 30, 60, and 90 days received, together with drinking water, a mixture of heavy metal salts: zinc (ZnSO4×7H2O) – 5 mg/L, copper (CuSO4×5H2O) – 1 mg/L, iron (FeSO4) – 10 mg/L, manganese (MnSO4×5H2O) – 0.1 mg/L, lead (Pb(NO3)2) – 0.1 mg/L, and chromium (K2Cr2O7) – 0.1 mg/L. The chosen concentration of salts in the mixture was determined by the presence of such concentrations of these salts in the soil and drinking water of some regions of Ukraine according to literature sources (Report on the state of the environment in Sumy region in 2000).

Withdrawal of animals from the experiment

Groups of experimental and control animals were withdrawn from the experiment after prior thiopental anesthesia (at a dose of 30-40 mg/10 g of body weight) on the 30th, 60th, and 90th days from the beginning of the experiment, in accordance with national and international bioethics standards. All animal studies were conducted in compliance with the provisions of the European Convention for the Protection of Vertebrate Animals used for Experimental and Other Scientific Purposes (Strasbourg, 1986) and the "General Ethical Principles of Animal Experiments," approved by the First National Congress on Bioethics (Kyiv, 2001, Ukraine), Protocol No. 4 of 06.03.2020 of the Bioethics Commission of Sumy State University. The subject of the study was the pineal gland of experimental and control animals.

Extraction technique and histological studies

To assess the morphological and morphometric parameters of the pineal gland, generally accepted procedures of the microanatomical (histological) research method were used with hematoxylin-eosin staining. The morphofunctional state of the pineal gland was assessed according to a number of microscopic indicators: length and width of the pineal gland (mm), vascular area (µm²), cross-sectional area of pinealocyte nuclei (µm²), mean diameter of the karyon (a.u.), optical density of nuclei (a.u.), glial cell-neuronal index (a.u.). General morphological and morphometric analysis was performed using a light optical microscope "Leica DM 500" with objectives ×4, ×10, ×40, eyepieces - 7 and 10. Photodocumentation of the obtained results was carried out using a digital video camera "Leica DM IC C50 HD Camera". The software "Leica Application Suite LAS EZ version 20.0 [Build: 292] Copyright @ 2010" was used.

Statistics

Statistical processing of the obtained data was performed using methods of variation statistics with the STATISTIKA software package, version 10 ("StatSoft Inc.," USA). Data were presented as mean value (X) ± standard deviation (SD). Normality of data distribution was verified using the Kruskal-Wallis test and Wilcoxon test. For comparison of two independent samples, in the case of normal distribution of data, Student's t-test was used; in the case of data distribution differing from normal, the Mann-Whitney U-test was used. Differences in indicators were considered significant at p<0.05. Correlation analysis was performed using Spearman's correlation coefficient (rs). Interpretation of the correlation analysis results was carried out according to Sheddock's scale. At r≤0.3 the correlation was considered weak, at 0.4<r<0.7 – moderate. At r≥0.7 the relationship was considered strong. A positive value of the coefficient indicated a direct relationship between the values (direct, positive correlation), when an increase in one characteristic led to an increase in another. A negative value of the coefficient indicated an inverse (inverse, negative) relationship between the studied parameters, when an increase in one characteristic led to a decrease in another.

Results

After a 30-day period of exposure to the complex of heavy metal salts, the pineal gland of rats in the experimental group macroscopically preserved its anatomical structure and remained in close connection with the extra-organ vascular plexus located beneath the roof and on the walls of the third ventricle of the brain. The pineal gland had an oval shape, but its linear parameters underwent changes. The length of the gland decreased by 4.3 % (p>0.05, t=1.99), and the width significantly decreased by 21.8 % (p<0.001, t=5.26) compared with the indicators of the control animals (Fig. 1, Table 1).

The vascular lumen area increased 1.5 times (p<0.0001) relative to the indicators of the control animals. A vivid confirmation of the morphological rearrangements in the pineal gland is provided by the general morphometric indicators of

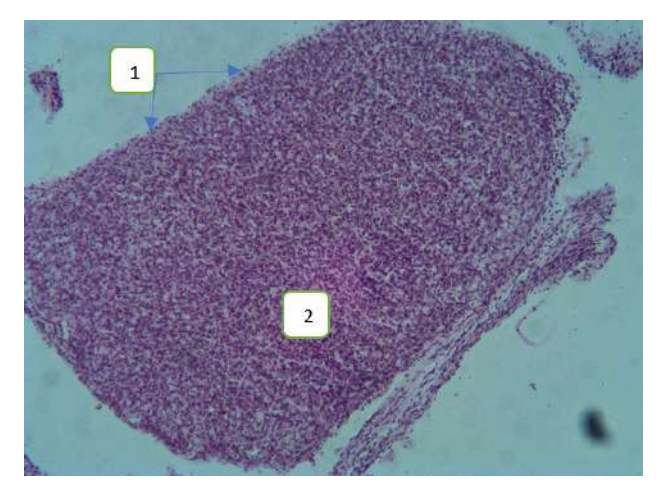


Fig. 1. Rat pineal gland after 30 days of exposure to heavy metal salts. 1 – connective tissue capsule of the pineal gland, 2 – parenchyma. Hematoxylin-eosin, ×40.

Table 1. Results of a morphometric study of the structural components of the pineal gland of sexually mature rats exposed to heavy metal salts (X±CD).

Indicator	Groups of laboratory animals					
	Control rats		Experime	Experimental rats		
	30	60	90	30	60	90
Epiphysis length, mm	1.186±	1.123±	1.192±	1.135±	1.186±	1.021±
	0.024	0.071	0.033	0.009*	0.061	0.942
Epiphysis width, mm	0.912±	0.816±	0.911±	0.713±	0.838±	0.871±
	0.031	0.096	0.032	0.021***	0.072	0.061
Vascular area,	58.58±	61.27±	62.85±	90.27±	137.8±	108.7±
µm²	0.42	0.67	6.89	39.65***	1.6***	26.4
Cross-sectional area of pinealocyte nuclei, µm²	4.451± 0.133	7.272± 1.242	50.24± 4.53	27.02± 8.10***	25.22± 3.09***	45.61± 4.42
Average diameter of carion, a.u.	1.841±	3.231±	2.141±	5.383±	4.333±	1.841±
	0.112	0.372	0.893	0.212***	0.711	0.521
Optical density of nuclei, a.u.	114.1±	110.1±	101.6±	149.4±	83.21±	96.12±
	1.2	1.1	4.2	14.8*	5.41***	1.44
Gliocyte- neuronal index, a.u.	0.443	0.371± 0.122	0.441	0.585± 0.839	1.231± 0.583	0.997± 1.822

Notes: * $- p \le 0.05$, ** - p < 0.01; *** $- p \le 0.001$.

pinealocyte nuclei. The nuclear cross-sectional area of pinealocytes and their optical density increased 6.0 times (p<0.0001) and by 31 % (p<0.05), respectively. The mean diameter of the karyon increased 2.9 times relative to the control animals (p<0.001, t=15.83). In the peripheral regions of the gland, especially subcapsularly, slightly increased activity of the glial response was observed. The glial cell-neuronal index increased and exceeded the indicators of the

Vol. 31, №3, Page 69-76

control animals by 74 % (p>0.05) (see Table 1).

On the 60th day of the experiment, the pineal gland retained its oval shape, and its size slightly increased compared with the control animals: length by 5.6 % (p>0.05) and width by 2.7 % (p>0.05). The vascular lumen area increased 2.25 times (p<0.001, t=43.65) relative to the indicators of the control animals. The nuclear area and the mean diameter of the pinealocyte karyon showed dynamic increases compared with the control animals, 3.5 times (p<0.001, t=5.38) and by 34 %, respectively. At the same time, the optical density of pinealocyte nuclei decreased by 24.4 % (p<0.001, t=4.90). A further increase in the glial cell-neuronal index was revealed, which exceeded the indicators of the control animals by 3.3 times (p>0.05) (Fig. 2, see Table 1).

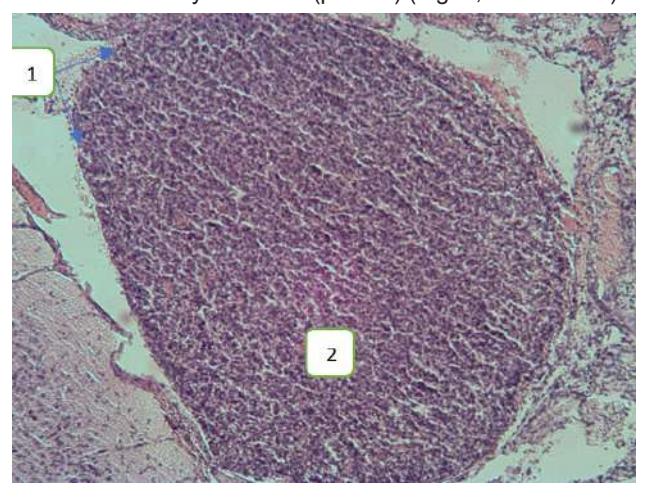


Fig. 2. Rat pineal gland after 60 days of exposure to heavy metal salts. 1 – connective tissue capsule of the pineal gland, 2 – parenchyma. Hematoxylin-eosin, ×40.

An increase in the experimental period to 90 days led to further organometric rearrangements in the pineal gland. The length of the gland decreased by 13.7 % (p>0.05) and the width by 4.7 % (p>0.05) compared with the indicators of the control animals. The length of the pineal gland in rats at the 30-day term of the study exceeded that of rats at the 90-day term of the experiment by 9.8 % (p>0.05). The width of the pineal gland in rats at the 30-day term, on the contrary, significantly decreased by 21.9 % relative to the width of the pineal gland in rats at the 90-day term of the experiment (p<0.05, t=2.38). The vascular lumen area increased by 73 % (p>0.05) relative to the control animals and decreased by 21 % (p>0.05) relative to the 60-day experimental animals. The nuclear cross-sectional area of pinealocytes and the mean diameter of the karyon decreased by 9.2 % (p>0.05) and 14 % (p>0.05), respectively, compared with the control animals. The optical density of pinealocyte nuclei also continued to decrease, by 5.4 % (p>0.05) relative to the control animals, but increased by 15.5 % (p<0.05, t=2.31) compared with the 60-day experimental animals. The glial cell-neuronal index in the pineal gland of experimental animals increased 2.96 times (p>0.05) compared with the indicators of the control animals (Fig. 3, see Table 1).

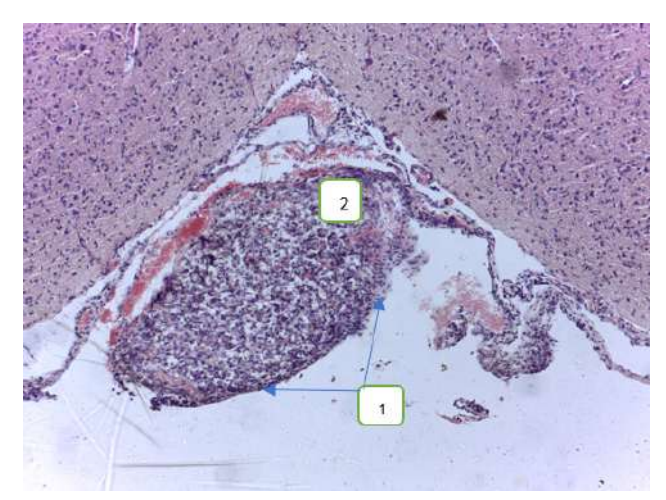


Fig. 3. Rat pineal gland after 90-day exposure to heavy metal salts. 1 – connective tissue capsule of the pineal gland, 2 – parenchyma. Hematoxylin-eosin, ×40.

After conducting morphometric studies, correlations were established between the size of the gland and other morphometric indicators of the structural components of the pineal gland of sexually mature rats under the influence of heavy metal salts (Table 2).

Table 2. Correlations between morphometric indicators of structural components of the pineal gland of sexually mature rats under conditions of exposure to heavy metal salts.

Indicators	Groups of laboratory animals					
	30		60		90	
	Control	Experi- ment	Control	Experi- ment	Control	Experi- ment
Length and width of the epiphysis	-0.208	0.051	0.255	0.064	0.874**	-0.203
Epiphyseal length and nuclear opti- cal density	0.593	0.350	0.274	0.452	0.697	-0.163
Epiphysis length and average carion diameter	0.361	0.036	0.333	0.722	0.552	-0.203
Epiphysis length and gliocyte- neuronal index	0.045	0.746*	0.852***	0	0.693	0.042
Epiphysis length and cross-sec- tional area of the nuclei	0	-0.343	0.250	-0.080	-0.080	-0.020
Epiphyseal width and average carion diameter	0.361	-0.059	0.936***	-0.074	0.227	1.000***
Epiphyseal width and cross- sectional area of nuclei	0.662	0.291	-0.341	-0.336	0.0821	-0.076
Epiphyseal width and gliocyte-neuronal index	0.637	0	0.495	0.462	0.691	0.032
Epiphyseal width and nuclear optical density	0.495	0.453	0.652	-0.080	0.338	0.305

Notes: * $- p \le 0.05$, ** - p < 0.01; *** $- p \le 0.001$.

Discussion

The presented study aimed to fill the gap in the investigation of the morphofunctional state of the pineal gland through the use of the morphometric method with the application of correlation analysis. According to modern literature sources, it is known that to date there are still no clearly defined criteria for assessing the morphofunctional state of the pineal gland. Some authors indicate that this criterion may be the size of pinealocyte nuclei, others-the total number and ratio of pools of light and dark pineal cells, as well as the growth pattern of the connective tissue stroma. Morphometry, applied at different structural levels of the morphological organization of the body, allows objectification of the obtained results and meets the requirements of modern evidence-based medicine [30].

Analyzing the set of morphological and morphometric rearrangements in the pineal gland of experimental animals that received heavy metal salts, and taking into account the data of the same indicators in control animals, the results of Pearson's correlation analysis make it possible to note the following:

In the pineal gland of experimental animals, as a result of long-term (90-day) exposure to heavy metal salts, adaptive-compensatory processes developed, and rearrangements occurred in the correlation relationships between the parameters of pineal dimensions and its other morphometric indicators.

Thus, on the 30th day of the experiment, a significant decrease in pineal size parameters was revealed: by 4.3 % for length and by 21.8 % for width compared with the indicators of control animals. Correlation between length and width changed from a negative weak non-significant correlation in controls to a weak positive non-significant correlation in the pineal glands of experimental animals. The vascular lumen area significantly increased 1.5 times, the nuclear cross-sectional area of pinealocytes and their optical density increased 6.0 times and by 31 %, respectively. The mean diameter of the pinealocyte karyon increased 2.9 times relative to the indicators of control animals. These morphometric rearrangements led to a weakening of the correlations between pineal size and nuclear area, optical density, and mean karyon diameter compared with control indicators. According to the literature [25], the identified correlations allowed determination of the degree of process interrelation. The fewer and weaker the connections. the more flexible the system became in responding to pathological environmental changes. The obtained results indicated significant tension of adaptive-compensatory processes in the organ in response to the action of heavy

At the same time, new correlations arose. Adaptive processes in the pineal gland to the influence of heavy metal salts were vividly manifested in the increased activity of astrocytic glia.

As is known, astrocytes perform a variety of functions in the central nervous system and are the main regulators of homeostasis. In response to the effect of heavy metal salts on the pineal gland, a protective astroglial reaction developed, which correlates with the findings of other authors [24]. The glial cell-neuronal index increased and exceeded the indicators of control animals by 74 %; the correlation between pineal length and the glial cell-neuronal index significantly increased and acquired a strong positive significant value.

An extension of the experimental period to 60 days led to a non-significant increase in the linear dimensions of the pineal gland compared with control indicators by 5.6 % (for length) and by 2.7 % (for width). Unlike the 30day term of the experiment, a weakening of the correlation between length and width of the pineal gland was observed compared with controls, to a weak positive non-significant correlation. There was a significant increase in vascular lumen area (2.25 times), nuclear cross-sectional area of pinealocytes (3.5 times), and mean karyon diameter (34 %). At the same time, the optical density of pinealocyte nuclei, on the contrary, decreased by 24.4 %. Unlike the previous term, there was a strengthening of the correlation between pineal length and mean karyon diameter to a strong positive significant correlation compared with controls. At the same time, the correlation between pineal width and mean karyon diameter, on the contrary, underwent a significant weakening from a strong positive significant correlation in controls to a weak negative non-significant correlation in the object. The correlation between pineal size and nuclear area in both controls and objects had a weak negative non-significant correlation. Strengthening of the correlation between pineal length and the optical density of pinealocyte nuclei was observed, reaching a moderate positive non-significant correlation, while at the same time weakening of the correlation to a weak negative non-significant correlation (for gland width) was noted compared with control indicators.

The correlation between the linear parameters of the organ and the vascular lumen area can be considered a stable value both for controls and for objects at the level of a weak positive non-significant correlation (for length) and a moderate positive non-significant correlation (for width).

Further increase in the glial cell-neuronal index, which exceeded the indicators of control animals by 3.3 times, indicated further protective action of astrocytic glia in response to the action of heavy metal salts on the pineal gland and the development of reactive astrogliosis in the organ. At the same time, with relative stability of correlations for this index and pineal width (moderate positive non-significant), there was a complete absence of correlation for pineal length and the glial cell-neuronal index in the object compared with controls.

Thus, hypertrophy of the organ, significant hypertrophy of pinealocyte nuclei, an increase in mean karyon diameter, and at the same time a decrease in nuclear optical density indicated significant enhanced functional activity of the pineal gland in response to the action of heavy metal salts at the 60-day term of the experiment.

On the 90th day of heavy metal exposure to the organism

Vol. 31, №3, Page 69-76

of experimental animals, a decrease in linear parameters of the pineal gland was noted: by 13.7 % (for length) and by 4.7 % (for width) compared with control animals. Analyzing the changes in correlations in the pineal gland at this term of the study, it should be noted that there was a significant weakening of the correlation between length and width (from a strong positive significant correlation in controls to a weak negative non-significant correlation in the object), as well as between size and other morphometric indicators. The organ showed somewhat reduced vascular congestion compared with the previous experimental term, but it was still present. This was evidenced by an increase in vascular lumen area by 73 % relative to control animals, but a decrease of 21 % compared with 60-day animals. At the same time, there was significant strengthening of correlations between pineal size and vascular area, from a moderate negative non-significant correlation to a moderate positive non-significant correlation (for width) and a weak positive non-significant correlation (for length). Morphometric indicators of pinealocyte nuclear area and mean karyon diameter decreased relative to control animals by 9.2 % and 14 %, respectively. Although pinealocyte nuclear optical density decreased by 5.4 % compared with controls, it still increased by 15.5 % relative to 60-day animals. The correlation between pineal length (width) and pinealocyte nuclear area weakened to a weak negative non-significant correlation. At the same time, if the relationship between pineal length and nuclear optical density/mean karyon diameter in the object acquired a weak negative non-significant correlation, the correlation between pineal width and nuclear optical density was more stable and had the indicators of a moderate positive non-significant correlation both in controls and in the object. The correlation between pineal width and mean karyon diameter in the group of experimental animals was significantly strengthened compared with controls and acquired the value r=1, which indicated a perfect positive linear relationship between variables. That is, at the 90-day term of the experiment, the functional activity of pinealocyte nuclei depended more on organ width than on its length.

The glial cell-neuronal index continued to increase, being 2.96 times higher than in control animals. Astrocytic glial cells continued to perform their protective role in the gland in neutralizing the negative effects of heavy metal salts on the organ. At the same time, the correlation between pineal size significantly weakened from a moderate positive non-significant correlation in controls to a weak positive non-

References

- [1] Alengebawy, A., Abdelkhalek, S. T., Qureshi, S. R., & Wang, M. Q. (2021). Heavy metals and pesticides toxicity in agricultural soil and plants: ecological risks and human health implications. *Toxics*, 9(3), 42. doi: 10.3390/toxics9030042
- [2] Ali, H., Khan, E., & Ilahi, I. (2019). Environmental chemistry and ecotoxicology of hazardous heavy metals: environmental persistence, toxicity, and bioaccumulation. *Journal of chemistry*, 2019(1), 6730305. doi: 10.1155/2019/6730305
- [3] Bakulski, K. M., Seo, Y. A., Hickman, R. C., Brandt, D., Vadari,

significant correlation in the group of experimental animals.

Thus, the set of such morphometric rearrangements in the pineal gland on the 90th day of the study indicated organ hypotrophy and significant tension of compensatory-adaptive processes in the gland, as well as gradual exhaustion of the functional adaptive capacities of the pineal gland in response to long-term exposure to heavy metal salts in the organisms of experimental animals.

Analyzing the correlations between size parameters and other morphometric indicators of the pineal gland in animals of different experimental groups, it can be noted that on the 30th day of the experiment the strongest correlation was observed between pineal length and the glial cell-neuronal index. On the 60th day of the experiment the strongest correlations were observed between pineal length and width, length and mean karyon diameter/nuclear optical density. On the 90th day of the experiment the strongest correlation was observed between pineal width and mean karyon diameter.

Thus, in the pineal gland of experimental animals, as a result of long-term (90-day) exposure to heavy metal salts, adaptive-compensatory processes developed, characterized by a phased course, which correlates with the opinion of other authors [33].

Conclusions

- 1. A decrease in organometric parameters of the pineal gland (length and width) was established on the 30th and 90th days of the study, and their increase was observed on the 60th day of the experiment.
- 2. The influence of changes in pineal gland size parameters on the morphometric state of certain functionally significant indicators of the gland was established: the area of pinealocyte nuclei, the glial cell-neuronal index, the mean diameter of the karyon, and the optical density of nuclei.
- 3. Prolonged (90-day) intake of a complex of heavy metal salts by experimental animals led to the emergence of new correlations in the organ and the development of a general adaptation syndrome, with a wave-like pattern of adaptive rearrangements at different stages of pollutant exposure.
- 4. The state of significant tension of adaptive-compensatory processes in the pineal gland at the early stages of the study was replaced by compensatory hypertrophy of the organ on the 60th day of the experiment, and by hypotrophy and gradual exhaustion of the functional adaptive capacities of the pineal gland in response to long-term exposure to heavy metal salts.
 - H. S., Hu, H., & Park, S. K. (2020). Heavy Metals Exposure and Alzheimer's Disease and Related Dementias. *J Alzheimers Dis*, 76(4), 1215-1242. doi: 10.3233/JAD-200282
- [4] Bastos, M. A. V., Bastos, P., Portella, R. B., Soares, L. F. G., Conde, R. B., Rodrigues, P. M. F., & Lucchetti, G. (2019). Pineal gland and schizophrenia: a systematic review and meta-analysis. *Psychoneuroendocrinology*, 104, 100-114. doi: 10.1016/j.psyneuen.2019.02.024
- [5] Berhouma, M., Ni, H., Delabar, V., Tahhan, N., Memou, S. S,

- Mottolese, C., & Vallee, B. (2015). Update on the management of pineal cysts: Case series and a review of the literature. *Neurochirurqie*, *61*(2-3), 201-217. doi: 10.1016/j. neuchi.2013.08.010
- [6] Bersani, G., Garavini, A., Iannitelli, A., Quartini, A., Nordio, M., Di Biasi, C., & Pancheri, P. (2002). Reduced pineal volume in male patients with schizophrenia: no relationship to clinical features of the illness. *Neurosci Lett*, 329(2), 246-248. doi: 10.1016/S0304-3940(02)00617-1
- [7] Bumb, J. M., Mier, D., Noelte, I., Schredl, M., Kirsch, P., Hennig, O., & Sobanski, E. (2016). Associations of pineal volume, chronotype and symptom severity in adults with attention deficit hyperactivity disorder and healthy controls. *Eur. Neuropsychopharmacol*, 26(7), 1119-1126. doi: 10.1016/j.euroneuro.2016.03.016
- [8] Bumb, J. M., Schilling, C., Enning, F., Haddad, L., Paul, F., Lederbogen, F., ... & Nolte, I. (2014). Pineal gland volume in primary insomnia and healthy controls: a magnetic resonance imaging study. J Sleep Res, 23(3), 274-280. doi: 10.1111/jsr.12125
- [9] Carpenter, J. S., Abelmann, A. C., Hatton, S. N., Robillard, R., Hermens, D. F., Bennett, M. R., ... & Hickie, I. B. (2017). Pineal volume and evening melatonin in young people with affective disorders. *Brain imaging and behavior*, 11(6), 1741-1750. doi: 10.1007/s11682-016-9650-2
- [10] Chuang, J. I., Chen, S. S., & Lin, M. T. (1993). Melatonin decreases brain serotonin release, arterial pressure and heart rate in rats. *Pharmacology*, 47(2), 91-97. doi: 10.1159/000139083
- [11] Engwa, G. A., Ferdinand, P. U., Nwalo, N. F., & Unachukwu, M. N. (2019). Mechanism and Health Effects of Heavy Metal Toxicity in Humans. In: Karcioglu O, Arslan B, editors. Poisoning in the modern world: new tricks for an old dog? BoD–Books on Demand. doi: 10.5772/intechopen.82511
- [12] Fındıklı, E., Inci, M. F., Gökçe, M., Fındıklı, H. A., Altun, H., & Karaaslan, M. F. (2015). Pineal gland volume in schizophrenia and mood disorders. *Psychiatr. Danub*, 27(2), 153-158. PMID: 26057310
- [13] Korshniak, V. O. (2016). Роль мелатоніну в нейроендокринній регуляції нервової системи у хворих з наслідками закритих черепно-мозкових травм [The role of melatonin in neuroendocrine regulation of the nervous system in patients with consequences of closed craniocerebral injuries (literature review)]. Міжнародний журнал неврології=International Neurological Journal, 4, 108-113.
- [14] Li, B., Xia, M., Zorec, R., Parpura, V., & Verkhratsky, A. (2021). Astrocytes in heavy metal neurotoxicity and neurodegeneration. *Brain Res*, 1, 1752, 147234. doi: 10.1016/j. brainres.2020.147234
- [15] Liebrich, L. S., Schredl, M., Findeisen, P., Groden, C., Bumb, J. M., & Nölte, I. S. (2014). Morphology and function: MR pineal volume and melatonin level in human saliva are correlated. *J Magn Reson Imaging*, 40(4), 966-971. doi: 10.1002/imri.24449
- [16] Lombardi, D., Scheithaeur, B. W., Villani, R. M., Giovanelli, M., & de Tribolet, N. (1996), Cavernous haemangioma of the pineal region. *Acta Neurochir* (Wien), 138(6), 678-683. doi: 10.1007/BF01411472
- [17] Matsuoka, T., Imai, A., Fujimoto, H., Kato, Y., Shibata, K., Nakamura, K., ... & Narumoto, J. (2018). Reduced pineal volume in Alzheimer disease: a retrospective crosssectional MR imaging study. *Radiology*, 286(1), 239-248. doi: 10.1148/radiol.2017170188

- [18] Matsuoka, T., Oya, N., Yokota, H., Akazawa, K., Yamada, K., & Narumoto, J. (2020). Alzheimer's Disease Neuroimaging Initiative. Pineal volume reduction in patients with mild cognitive impairment who converted to Alzheimer's disease. *Psychiatry and Clinical Neurosciences*, 74(11), 587-593. doi: 10.1111/pcn.13103/full
- [19] Merian, E. (1984). Introduction on environmental chemistry and global cycles of chromium, nickel, cobalt beryllium, arsenic, cadmium and selenium, and their derivatives. *Toxicological and Environmental Chemistry*, 8(1), 9-38. doi: 10.1080/02772248409357038
- [20] Nölte, I., Lütkhoff, A. T., Stuck, B. A., Lemmer, B., Schredl, M., Findeisen, P., & Groden, C. (2009). Pineal volume and circadian melatonin profile in healthy volunteers: an interdisciplinary approach. *Journal of Magnetic Resonance Imaging: An Official Journal of the International Society for Magnetic Resonance in Medicine*, 30(3), 499-505. doi: 10.1002/jmri.21872
- [21] Park, J., Han, J. W., Lee, J. R., Byun, S., Suh, S. W., Kim, T., ... & Kim, K. W. (2018). Lifetime coffee consumption, pineal gland volume, and sleep quality in late life. *Sleep*, 41(10), zsy127. doi: 10.1093/sleep/zsy127
- [22] Park, J., Han, J. W., Suh, S. W., Byun, S., Han, J. H., Bae, J. B., ... & Kim, K. W. (2020). Pineal gland volume is associated with prevalent and incident isolated rapid eye movement sleep behavior disorder. *Aging (Albany NY)*, 12(1), 884-893. doi: 10.18632/aging.102661
- [23] Park, J., Suh, S. W., Kim, G. E., Lee, S., Kim, J. S., Kim, H. S., ... & Kim, K. W. (2020). Smaller pineal gland is associated with rapid eye movement sleep behavior disorder in Alzheimer's disease. *Alzheimer's Research & Therapy*, 12(1), 157. doi: 10.1186/s13195-020-00725-z
- [24] Pekny, M., & Pekna, M. (2016). Reactive gliosis in the pathogenesis of CNS diseases. *Biochimica et Biophysica* Acta, 1862(3), 483-491. doi: 10.1016/j.bbadis.2015.11.014
- [25] Pesotskaya, L. A., Kuchuk, N. G., Lakyza, T. V., Evstigneev, I. V., Usenko, A. V., & Yarchuk E. A. (2016). Особенности корреляционных взаимосвязей при железодефицитных анемиях различной этиологии [Peculiarities of correlation relationships in iron deficiency anemia of various etiologies]. Системи управління, навігації та зв'язку=Control, Navigation and Communication Systems, (1), 52-57.
- [26] Reiter, R. J. (1981). The mammalian pineal gland: structure and function. Am J Anat, 162(4), 287-313. doi: 10.1002/ aja.1001620402
- [27] Takahashi, T., Sasabayashi, D., Takayanagi, Y., Higuchi, Y., Mizukami, Y., Akasaki, Y., ... & Suzuki, M. (2021). Potential contribution of pineal atrophy and pineal cysts toward vulnerability and clinical characteristics of psychosis. *NeuroIm*age: Clinical, 32, 102805. doi: 10.1016/j.nicl.2021.102805
- [28] Takahashi, T., Sasabayashi, D., Yücel, M., Whittle, S., Lorenzetti, V., Walterfang, M., ... & Allen, N. B. (2020). Pineal gland volume in major depressive and bipolar disorders. Frontiers in Psychiatry, 11, 450. doi: 10.3389/fpsyt.2020.00450
- [29] Takahashi, T., Nakamura, M., Sasabayashi, D., Nishikawa, Y., Takayanagi, Y., Nishiyama, S., ... & Suzuki, M. (2019). Reduced pineal gland volume across the stages of schizophrenia. Schizophrenia Research, 206, 163-170. doi: 10.1016/j.schres.2018.11.032
- [30] Williams, M. A. (1977). Quantitative Methods in Biology (Practical methods in electron microscopy, vol 6, part 2). Amsterdam: Oxford: North-Holland Publishing Co.
- [31] Zhao, W., Zhu, D. M., Zhang, Y., Zhang, C., Wang, Y., Yang,

Vol. 31, №3, Page 69-76

- Y., ... & Yu, Y. (2019). Pineal gland abnormality in major depressive disorder. *Psychiatry Research: Neuroimaging*, 289, 13-17. doi: 10.1016/j.pscychresns.2019.05.004
- [32] Wu, Y. H., & Swaab, D. F. (2005). The human pineal gland and melatonin in aging and Alzheimer's disease. *Journal of pineal research*, 38(3), 145-152. doi: 10.1111/j.1600-
- 079X.2004.00196.x
- [33] Zetner, D., Andersen, L. P. H., & Rosenberg, J. (2016). Melatonin as protection against radiation injury: a systematic review. *Drug research*, 66(06), 281-296. doi: 10.1055/s-0035-1569358

ДОВГОТРИВАЛИЙ ВПЛИВ СОЛЕЙ ВАЖКИХ МЕТАЛІВ НА МОРФОМЕТРИЧНІ ПОКАЗНИКИ ТА ФУНКЦІОНАЛЬНИЙ СТАН ЕПІФІЗА СТАТЕВОЗРІЛИХ ЩУРІВ

Гринцова Н. Б., Романюк А. М.

Забруднення навколишнього середовища важкими металами несе велику загрозу для живих організмів та формує одну з головних проблем сучасного суспільства. Епіфіз контролює ендокринну, нервову та імунну системи, інтегрує системну реакцію на несприятливі фактори, що впливають на опірність організму. Метою роботи є дослідження кореляційних взаємозв'язків між розмірами епіфіза статевозрілих щурів та його іншими морфометричними показниками за умови тривалого впливу на організм комплексу солей важких металів. Тваринам 3-х дослідних груп продовж 30-ти, 60-ти та 90-та діб моделювали мікроелементоз шляхом додавання до питної води суміші солей важких металів: цинку (ZnSO4×7H2O) – 5 мг/л, міді (CuSO4×5H2O) – 1 мг/л, заліза (FeSO4) – 10 мг/л, марганцю (MnSO4×5H2O) – 0,1 мг/л, свинцю (Pb(NO3)2) – 0,1 мг/л і хрому (K2Cr2O7) – 0,1 мг/л. Використовували морфологічні, морфометричні та статистичні методи дослідження. У епіфізі піддослідних тварин у результаті впливу солей важких металів розвивалися адаптивнокомпенсаторні процеси та відбувалися перебудови в кореляційних зв'язках між показниками розмірів епіфіза та іншими морфометричними показниками залози. Спостерігалося зменшення органометричних показників залози на 30-ту та 90-ту добу експеримента та їх збільшення на 60-ту добу досліду. Найбільша сила кореляційного зв'язку між довжиною епіфіза та гліоцито-нейрональним індексом спостерігалася на 30-ту добу експеримента; між довжиною та шириною епіфіза, довжиною та середнім діаметром каріона/оптичною щільністю ядер на 60-ту добу та між шириною залози та середнім діаметром каріона на 90-ту добу експеримента. Адаптаційні перебудови у епіфізі на різних строках впливу полютантів мали хвилеподібний характер та визначалися напруженням адаптивно-компенсаторних процесів на ранніх термінах досліду (30-та доба), що змінювалися компенсаторною гіпертрофією органу на 60-ту добу експерименту та поступовим вичерпанням функціональних адаптивних можливостей епіфіза у відповідь на довготривалий вплив солей важких металів (90-та доба).

Ключові слова: розміри епіфіза, важкі метали, кореляційні зв'язки.

Author's contribution

Hryntsova N. B. – data visualization, research, methodology and original project writing, resources, software. *Romaniuk A. M.* – conceptualization, formal analysis and verification, project administration, editing, supervision.

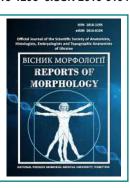
ISSN 1818-1295 eISSN 2616-6194



REPORTS OF MORPHOLOGY

Official Journal of the Scientific Society of Anatomists, Histologists, Embryologists and Topographic Anatomists of Ukraine

journal homepage: https://morphology-journal.com



Morphology and morphometry of the rat lacrimal gland duct system: a comparative analysis of the extraorbital, intraorbital, and Harderian glands

Katsenko A. L., Sherstiuk O. O., Hryn V. H, Svintsytska N. L., Bilash V. P., Ustenko R. L., Piliuhin A. V. Poltava State Medical University, Poltava, Ukraine

ARTICLE INFO

Received: 29 January 2025 Accepted: 24 Juli 2025

UDC: 617.764.1:612.08:599.323.4

CORRESPONDING AUTHOR

e-mail: akatsenko@gmail.com Katsenko A. L.

CONFLICT OF INTEREST

The authors have no conflicts of interest to declare.

FUNDING

Not applicable.

DATA SHARING

Data are available upon reasonable request to corresponding author.

In our studies, we assumed that the lacrimal gland of the laboratory rat, like its human counterparts, is a polymeric organ that has its own specifics. This primarily concerns the syntopic relationships in the three-dimensional space of the glands themselves and their microstructures. Therefore, when studying the lacrimal glands of the rat (extraorbital, infraorbital and Garder's), as well as when studying human glands, we needed to identify the level of structural organization of diverse tissues that would correspond to the concept of a structural-functional unit. The purpose of the study: to characterize morphometrically and histologically the terminal departments and the system of excretory ducts of the extraorbital, intraorbital and Garder's lacrimal glands of the rat and to determine their general biological and species-specific features. A morphometric and histological analysis of the extraorbital, intraorbital and Garder's lacrimal glands of the laboratory rat was carried out. The results obtained were processed in Microsoft Excel. It was found that the terminal sections have a larger outer diameter and wall thickness compared to the interstitial ducts. The intralobular ducts are characterized by larger luminal lumens, which contributes to the effective accumulation and evacuation of secretion. In the Garder gland, the terminal sections often have an irregular shape and narrow lumens, and the interstitial ducts are almost identical in diameter to the terminal ones. Myoepithelial cells participate in the reduction and modulation of secretion, creating a "milking" effect that ensures secretion. Comparison of the obtained data with the morphometry of the human lacrimal gland allows us to identify general biological patterns of the organization of the excretory system and species-specific adaptations to the type of secretion and functional needs. The results of the study are important for a deeper understanding of the morphofunctional organization of the lacrimal glands and can serve as a basis for further physiological and pathological studies of exocrine glands.

Keywods: rat lacrimal glands, extraorbital gland, intraorbital gland, Harderian gland, terminal portions, morphometry.

Introduction

The lacrimal glands are important components of the exocrine system, responsible for synthesizing and secreting a substance that provides lubrication, protection, and homeostasis for the eye's surface. A detailed study of the morphology of the terminal parts and efferent ducts of these glands is of great importance for understanding the functional organization of the excretory system, as well as for evaluating adaptive mechanisms in different animal species and humans [3, 7, 13, 17].

Despite numerous studies of the lacrimal glands anatomy and histology in humans and laboratory animals, there is still

a lack of information about the morphometric parameters of the duct system, the relationship between their structural components, and the functional significance of different types of ducts. It's particularly important to study the epithelial and myoepithelial components, the nature of duct branching, and the interrelations of diameters between the terminal and intercalated parts, as well as the intralobular and lobular ducts [8, 14, 19].

The importance of the study is also due to the need for a comparative analysis of the morphology of rat lacrimal glands with analogous human structures. This allows for the identification of general biological patterns in the structure of the excretory system, as well as specific adaptations that reflect species-specific characteristics of the glands, the type of secretion and the functional needs of the organism. Special attention should be paid to the Harderian gland, which has structural features compared to the intra- and extraorbital lacrimal glands of rats, requiring detailed morphometric and histological analysis [15, 16, 18, 22].

Thus, a systematic study of the morphology of the terminal parts and efferent ducts of rat lacrimal glands is highly relevant. It provides a basis for further functional-comparative studies, the creation of models of the morphofunctional organization of exocrine glands and the development of methods for the diagnosis and treatment of lacrimal gland pathologies in humans [9, 12, 20, 29].

Aim of the study: to morphometrically and histologically characterize the terminal parts and duct system of the extraorbital, intraorbital, and Harderian lacrimal glands of the rat and to determine their general biological and species-specific features.

Materials and Methods

This scientific article is a part of the research work of the Department of Human Anatomy: "Morpho-functional study of internal organs of humans and laboratory animals in various aspects of experimental medicine", state registration number 0121U108258, years of execution 2021-2025.

For the study, we used 30 lacrimal glands (intraorbital, extraorbital, and Harderian) from 10 male laboratory rats. The glands were obtained by dissection using our own method, after euthanasia with thiopental sodium anesthesia at a dose of 75 mg/kg of the animal's body weight intramuscularly in the upper third of the hind leg's thigh.

After removal, the glands were fixed in a 10 % neutral formalin solution and then processed using a standard paraffin method. Series of thin histological sections, 4-5 μ m thick, were obtained from the paraffin blocks and stained with hematoxylin and eosin for subsequent morphological analysis.

A preliminary sequential analysis of histological sections allowed us to evaluate the morphological features of the glands and prepare the material for morphometric measurements. Morphometric studies were conducted using a Levenhuk D740T digital microscope with the corresponding software for photography and analysis, and the obtained data were systematized in Microsoft Excel tables [1, 23, 27].

All laboratory animals were kept in standard conditions at the experimental-biological clinic (vivarium) of Poltava State Medical University, in accordance with the rules for keeping experimental animals established by the Directive of the European Parliament and of the Council (2010/63/EU), the order of the Ministry of Education and Science, Youth and Sports of Ukraine dated 01.03.2012 № 249 "On the approval of the procedure for conducting experiments and experiments on animals by scientific institutions," and the "General Ethical Principles for Experiments on Animals,"

adopted by the Fifth National Congress on Bioethics (Kyiv, 2013), (Protocol № 240 from 20.06.2025 of the meeting of the Commission on Biomedical Ethics of Poltava State Medical University).

Results

Sequential analysis of histological sections from the extraorbital, intraorbital, and Harderian lacrimal glands of rats allowed us to trace the course and branching of the efferent ducts, the cellular composition of their walls, and changes in their diameters at different levels using the morphometric method. Based on the data obtained, we identified several gradations of duct diameters.

A morphometric study of the epithelial components of the rat glands was performed, specifically the terminal parts and efferent ducts that are part of the structural and functional unit – the lobule. Within the lobule, the intercalated ducts (intercalated segments or terminal ducts) constitute the initial segment of the branched efferent duct system and end with a widening that forms the terminal part of the gland. According to our data, the intercalated duct of the extraorbital gland has an outer diameter of $23.79 \pm 0.23~\mu m$, a luminal opening (inner diameter) of $9.700 \pm 0.160~\mu m$, and a wall thickness of $7.040 \pm 0.290~\mu m$.

The intercalated duct in the extraorbital gland typically integrates with a single spherical terminal part, which has an outer diameter of 40.16±0.23 μ m, an inner diameter of 6.560±0.090 μ m, and a wall thickness of 16.80±0.21 μ m (Table 1).

Table 1. Basic metric indicators of the epithelial components of the rat lacrimal gland lobules (M±m, μm).

ine rat iac	ililiai giariu i	obules (M±III,	μπ).	
Extraorbital lacrimal gland of a laboratory rat				
Cross-	T	Ducts		
sectional profile diameter	Terminal portion	Intercalated	Intralobular	Lobular
Outer	40.16±0.23	23.79±0.23	31.92±0.19	55.40±0.36
Inner	6.560±0.090	9.700±0.160	14.14±0.18	27.54±0.22
Wall thickness	16.80±0.91	7.040±0.290	8.890±0.160	13.93±0.24
Intraorbital lacrimal gland of a laboratory rat				
Cross-		Ducts		
sectional profile diameter	Terminal portion	Intercalated	Intralobular	Lobular
Outer	53.36±0.45	24.54±0.44	65.89±0.80	95.76±0.45
Inner	8.150±0.140	6.160±0.090	35.49±0.31	78.46±0.27
Wall thickness	22.60±0.29	9.190±0.250	15.20±0.32	8.650±0.120
Harderian gland of a laboratory rat				
Cross-		Ducts		
sectional profile diameter	ile portion	Intercalated	Intralobular	Lobular
Outer	48.99±0.32	25.88±0.20	55.09±0.21	72.91±0.38
Inner	9.920±0.170	9.490±0.120	32.28±0.18	48.48±0.79
Wall thickness	19.53±0.18	8.200±0.200	11.40±0.28	12.22±0.17

The terminal parts have a thick wall, with their inner lumen accounting for almost one-third of their volume. The wall of the terminal part consists of two layers of highly specialized epithelial cells: one type has transformed into secretory epitheliocytes, while the other has gained contractile abilities during morphological differentiation. The myoepithelial cells, in this case, have taken a basal location relative to the secretory cells. The nuclei of the myoepithelial cells, in comparison to their cytoplasm, stain well and are therefore quite well-visualized, thus indicating their presence (Fig. 1).

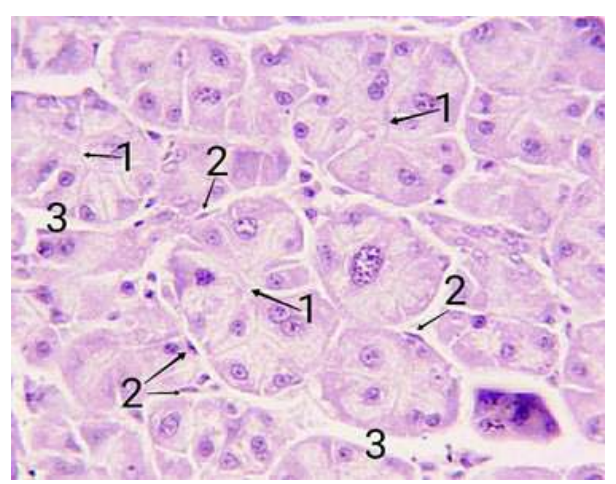


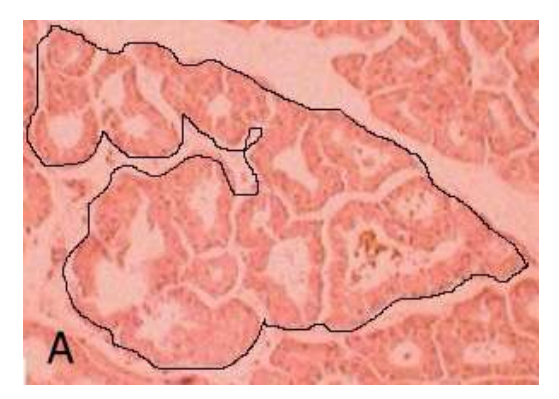
Fig. 1. Extraorbital lacrimal gland of a laboratory rat. 1 – terminal parts; 2 – myoepithelial cell nuclei; 3 – interlobular connective tissue layer. Paraffin section. Hematoxylin-eosin. ×400.

A noticeable finding is that the outer diameter of the terminal part is almost two times larger compared to the terminal (intercalated) part. The wall thickness of these parts also differs by a factor of two, which is related to the different size of the secretory epithelial cells, the number of cell layers, and their shape within the wall.

Numerous intralobular ducts of the rat's extraorbital lacrimal gland have an outer diameter of 31.92±0.19 $\mu m,$ a lumen of 14.14±0.18 $\mu m,$ and a wall thickness of 8.890±0.160 $\mu m.$ This indicates a gradual increase in the diameter of the excretory ducts along the direction of the laminar flow of the secret.

Based on the morphometric data of the extraorbital gland ducts and the study of 2D and 3D reconstructions, it can be argued that the most capacious chain for the accumulation and storage of the secret in the excretory system of the studied glands is the large number of intralobular ducts within the lobule. The terminal (intercalated) ducts, with their narrow luminal openings, act as chains for the retention of the secret.

The intercalated duct of the intraorbital lacrimal gland has an outer diameter of $24.54\pm0.44~\mu m$, a luminal opening (inner diameter) of $6.160\pm0.090~\mu m$, and a wall thickness of $9.190\pm0.254~\mu m$ (Fig. 2, 3). This duct typically also integrates a single terminal part, which has an outer diameter of $53.36\pm0.45~\mu m$, an inner diameter of $8.150\pm0.140~\mu m$, and a wall thickness of $22.60\pm0.29~\mu m$ (see Table 1).



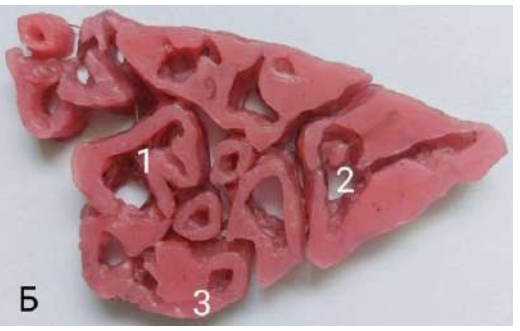


Fig. 2. Intraorbital lacrimal gland of a laboratory rat. **A** – Serial histological section, on which a wax plastic reconstruction was based. Paraffin section. Hematoxylin-eosin. $\times 400$. **B** – Plastic reconstruction of the microanatomical structures of the gland lobule. 1 – intercalated duct; 2 – intralobular duct; 3 – terminal part. $\times 400$.

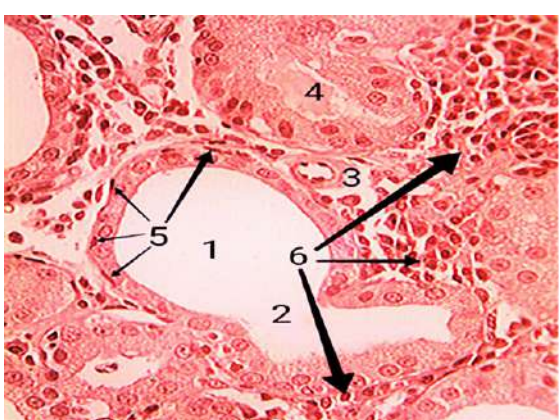


Fig. 3. Lobular duct of the intraorbital lacrimal gland of a laboratory rat. 1 – lumen of the lobular duct; 2 – point where the intralobular duct drains into the lobular duct; 3 – precapillary arteriole; 4 – secret in the duct lumen; 5 – myoepithelial cell nuclei (indicated by arrows); 6 – lymphoplasmacytic infiltration of connective tissue. Paraffin section. Hematoxylin-eosin. ×400.

Just like in the rat's extraorbital gland, the outer diameter of the terminal part in the intraorbital gland is also more than twice as large as that of the terminal (intercalated) part. The wall thickness of these parts also differs by almost two times, which may be related to the different size of the secretory epithelial cells, the number of cell layers, and their shape within the wall. Numerous intralobular ducts have an outer diameter of $65.89\pm0.80~\mu m$, a lumen of $35.49\pm0.31~\mu m$, and a wall thickness of $15.20\pm0.32~\mu m$. This similarly indicates

Vol. 31, №3, Page 77-83

a gradual increase in the diameter of the excretory ducts in the direction of the laminar flow of the secret. This trend continues for the lobular duct, which has the largest outer and inner diameters.

It is important to note that sections of the *Harderian gland* sometimes show a slightly different picture within the lobule compared to the other lacrimal glands of the laboratory rat. Specifically, there are terminal parts with poorly defined lumens, as they do not have a spherical shape. Additionally, the lumens of some ducts within the lobule are narrow or not visible at all in the sections. This is especially true for the lumens of the ducts that are directly adjacent to the terminal parts. In cases where the lumens of the terminal parts are well-visualized, they may have an irregular shape, which complicates their identification and the acquisition of morphometric data (Fig. 4, 5). In our opinion, this is also related to the plane of the section that captured the epithelial components of this particular histological series.



Fig. 4. Garder's gland of a laboratory rat. 1 – lumen of the intralobular duct; 2 – finger-like terminal part; 3 – intercalated (excretory) duct. Paraffin section. Hematoxylin-eosin. ×400.



Fig. 5. Fragment of a Harderian gland lobule with partially removed secretory elements. 1 – dense connective tissue layers between the ducts and terminal parts; 2 – terminal parts; 3 – intercalated duct; 4 – intralobular duct. Wax reconstruction. ×100.

As a rule, a lobule of the Harderian gland consists of aggregates that contain lacrimal ducts of the smallest inner diameter and their corresponding saccular and regular spherical terminal parts, which form clusters. The intercalated

ducts have an outer diameter of 25.88±0.20 µm, a lumen of 9.490 ± 0.120 µm, and a wall thickness of 8.200 ± 0.210 µm. The lumen of the terminal part of the Harderian gland measures 9.920±0.170 µm and is connected to the lumen of only one lacrimal tubule, the dimensions of which are practically the same at 9.490±0.120 µm. The smallest lacrimal ducts merge to form larger-diameter ducts located within the volume occupied by the lobule. As a rule, there are no more than three orders of branching for the intralobular ducts, which corresponds to the division of analogous efferent ducts in the studied rat lacrimal glands. They are also located collaterally relative to the axial intralobular duct and can integrate a certain number of alveolar-tubular aggregates. Their morphometric parameters are presented in Table 1. The longest and largest ducts of the Harderian gland are located outside the lobules.

In the Harderian gland, the morphometric values for the lumens (inner diameters) of the terminal and intercalated parts are almost identical, averaging 9.920±0.170 μm and 9.490±0.120 μm , respectively. The inner diameter of the lobular duct is only 1.3 times larger than that of the intralobular ducts, which represents an insignificant change in this parameter. The wall thickness of the ducts in all the studied glands does not differ significantly.

Discussion

A sequential morphological and morphometric analysis of histological sections from the extraorbital, intraorbital, and Harderian lacrimal glands of rats allowed for a detailed characterization of the structure and functional features of the efferent ducts and terminal parts within the lobule as a structural-functional unit. Within the studied glands, a gradual increase in duct diameters was found in the direction of the laminar flow of the secret. This is consistent with the principle of optimizing flow and accumulating secret in the axial parts of the excretory system [24, 26]. The intralobular ducts were found to be the most capacious for the accumulation and storage of the secret, while the narrow terminal (intercalated) ducts serve a function of secret retention.

Morphometric data on the terminal parts and intercalated ducts showed that the outer diameter of the terminal part in all studied glands exceeds the corresponding diameter of the intercalated duct by almost a factor of two. This indicates the morphological differentiation of the epithelial components, which ensures the effectiveness of secretion. The wall thickness of the terminal part was also significantly greater than that of the intercalated ducts, which is due to a larger number of layers of secretory cells and the presence of myoepithelial cells with basal nucleus location. The presence of myoepithelium is crucial for the active release of secretion, especially thick protein-based secretions. It provides a so-called "milking" effect, which is mechanical assistance in evacuating the secret from the acini into the duct system [6, 11]. This is consistent with known data on the role of myoepithelial cells in modulating secretory function and maintaining the mechanical integrity of the gland [25].

Unlike human lacrimal glands, the walls of the efferent ducts at all levels in rats did not show cells of the diffuse endocrine system (APUD-system), which are typical companions of glandulocytes in the efferent ducts of many human exocrine glands [5]. This points to species-specific features in the morphofunctional organization of rat glands. At the same time, a characteristic feature of all studied rat glands is the pronounced lymphocytic infiltration of the interstitium, which is especially noticeable along the course of the efferent ducts and in their immediate vicinity. This phenomenon likely reflects constant immunological control within the gland tissues and may be related to maintaining the homeostasis of the secret. This aligns with the understanding of the important role of local inflammatory-oxidative mechanisms in maintaining tissue balance [4, 10, 28].

The rat's Harderian gland demonstrates some morphological differences compared to the extra- and intraorbital lacrimal glands. In particular, the terminal parts often have poorly defined lumens or an irregular shape, which complicates their identification and precise morphometry. These features may be explained by the section plane of the histological series and the specific organization of the lobules, where the terminal parts and minimal efferent ducts form compact clusters.

A comparison of the morphometric indicators of the efferent ducts and terminal parts of rat glands with literature data on the lacrimal gland of mature humans reveals both general biological patterns and significant structural differences [2, 21]. For example, the principle of a gradual increase in duct diameters is maintained in both species. However, differences in the presence of cells of the diffuse endocrine system and the distribution of myoepithelial cells reflect species-specific adaptations to the nature of the secret and the functional needs of the glands. This data allows us to conclude that the morphological organization of the rat lacrimal gland lobule ensures the effective evacuation of the secret while maintaining a local immune defense function. It also optimizes the ratio between the volume of the luminal opening and the wall thickness of the ducts for different segments of the excretory system.

Thus, our own research confirms that the efferent ducts of rat lacrimal glands form a complex, branched system of

epithelial tubules of varying lengths, whose diameters change gradually within the lobule. The significant number of terminal parts and the specific organization of myoepithelial cells ensure effective secretion, while the absence of APUD cells and the peculiarities of lymphocytic infiltration reflect species-specific aspects of the morphofunctional organization of rat glands. A comparative analysis with humans allows us to outline the general principles of excretory system organization and species-specific adaptations that can be used for further experimental and comparative studies.

Moving forward, it is relevant to study the changes in the morphometric parameters of the duct system under pathological conditions and the dependence of gland structure on the type of secretion. This would allow for the creation of models for the optimal functioning of the excretory system.

Conclusions

1. Based on the morphometric and histological analysis of the extraorbital, intraorbital, and Harderian lacrimal glands of rats, it was established that the terminal parts have a significantly larger outer diameter and thicker wall compared to the terminal intercalated ducts. This is due to the morphological specialization of the secretory and myoepithelial cells. The intralobular ducts have larger luminal openings and outer diameters, which ensures the effective accumulation and evacuation of secretion.

2. In the Harderian gland, some morphological differences are observed: the terminal parts often have an irregular shape and narrow lumens, while the intercalated ducts are almost identical to the terminal parts in inner diameter. Myoepithelial cells, located near the basal part of the secretory cells, participate in the contraction and modulation of secretion, creating a "milking" effect.

3. The wall thickness of the ducts in all the studied glands remains relatively stable, and the absence of diffuse endocrine system cells underscores the species-specific characteristics of rat glands. A comparison with the morphology of the human lacrimal gland demonstrates general biological patterns in the organization of the excretory system while also revealing species-specific adaptations to the type of secretion and the functional needs of the organism.

References

- [1] Boniao, E. L., Torres, M. A., Bothra, N., Saini, P., Gungab, A., Lim, B. X. H., ... & Ali, M. J. (2024). Geometric morphometric anatomy of the lacrimal punctum in normal population: Punctum update (PUP) study Paper 5. Annals of anatomy=Anatomischer Anzeiger: official organ of the Anatomische Gesellschaft, 255, 152274. doi: 10.1016/j. aanat 2024 152274
- [2] Butovich, I. A., Yuksel, S., Leonard, B., Gadek, T., Polans, A. S., & Albert, D. M. (2021). Novel Lipids of the Rabbit Harderian Gland Improve Tear Stability in an Animal Model of Dry Eye Disease. Journal of Ocular Pharmacology and Therapeutics: the Official Journal of the Association for Ocular Pharmacology and Therapeutics, 37(10), 545-555. doi: 10.1089/jop.2021.0015
- [3] Dankis, M., Carlsson, T., Aronsson, P., Tobin, G., & Winder, M. (2021). Novel insights into muscarinic and purinergic responses in primary cultures of rat lacrimal gland myoepithelial cells. *Invest Ophthalmol Vis Sci*, 62(12), 19. doi: 10.1167/iovs.62.12.19
- [4] Delcroix, V., Mauduit, O., Yang, M., Srivastava, A., Umazume, T., de Paiva, C. S., ... & Makarenkova, H. P. (2023). Lacrimal Gland Epithelial Cells Shape Immune Responses through the Modulation of Inflammasomes and Lipid Metabolism. *International Journal of Molecular Sciences*, 24(5), 4309. doi: 10.3390/ijms24054309
- [5] Di Zazzo, A. (2022). Pathogenesis of the Homeostatic Failure of Ocular Surface as Morpho-Functional Unit. *Journal of Clinical Medicine*, 11(16), 4685. doi: 10.3390/jcm11164685

Vol. 31, №3, Page 77-83

- [6] García-Posadas, L., Hodges, R. R., Utheim, T. P., Delcroix, V., Makarenkova, H. P., & Dartt, D. A. (2020). Lacrimal gland myoepithelial cells are altered in a mouse model of dry eye disease. *The American Journal of Pathology*, 190(10), 2067-2079. doi: 10.1016/j.ajpath.2020.06.013
- [7] Jaffet, J., Mohanty, A., Veernala, I., Singh, S., Ali, M. J., Basu, S., ... & Singh, V. (2023). Human Lacrimal Gland Derived Mesenchymal Stem Cells Isolation, *Propagation, and Characterization. Investigative Ophthalmology & Visual Science*, 64(10), 12. doi: 10.1167/iovs.64.10.12
- [8] Khan, S., Fitch, S., Knox, S., & Arora, R. (2022). Exocrine gland structure-function relationships. *Development*, 149(1), dev197657. doi: 10.1242/dev.197657
- [9] Kim, S. H., Min, H. K., Lee, S. H., Lee, K. A., & Kim, H. R. (2022). Ultrasonographic evaluation of lacrimal glands in patients with primary Sjögren's syndrome. *Clinical and Experimental Rheumatology*, 40(12), 2283-2289. doi: 10.55563/ clinexprheumatol/em2xlu
- [10] Li, N., Li, Y., Hu, J., Wu, Y., Yang, J., Fan, H., ... & Jiang, L. (2022). A Link Between Mitochondrial Dysfunction and the Immune Microenvironment of Salivary Glands in Primary Sjogren's Syndrome. Frontiers in Immunology, 13, 845209. doi: 10.3389/fimmu.2022.845209
- [11] Mauduit, O., Delcroix, V., Wong, A., Ivanova, A., Miles, L., Lee, H. S., & Makarenkova, H. (2024). A closer look into the cellular and molecular biology of myoepithelial cells across various exocrine glands. *The Ocular Surface*, 31, 63-80. doi: 10.1016/j.jtos.2023.12.003
- [12] Mittal, R., Patel, S., & Galor, A. (2021). Alternative therapies for dry eye disease. *Current opinion in ophthalmology*, 32(4), 348-361. doi: 10.1097/ICU.000000000000768
- [13] Murashima, A. A. B., Sant'Ana, A. M. S., Faustino-Barros, J. F., Machado Filho, E. B., da Silva, L. C. M., Fantucci, M. Z., ... & Rocha, E. M. (2024). Exorbital Lacrimal Gland Ablation and Regrafting Induce Inflammation but Not Regeneration or Dry Eye. *International Journal of Molecular Sciences*, 25(15), 8318. doi: 10.3390/ijms25158318
- [14] Nakashima, K., Kato, H., Kurata, R., Qianwen, L., Hayakawa, T., Okada, F., ... & Sekiguchi, K. (2023). Gap junction-mediated contraction of myoepithelial cells induces the peristaltic transport of sweat in human eccrine glands. *Communications Biology*, 6(1), 1175. doi: 1038/s42003-023-05557-9
- [15] Rahman, M. M., Kim, D. H., Park, C. K., & Kim, Y. H. (2021). Experimental Models, Induction Protocols, and Measured Parameters in Dry Eye Disease: Focusing on Practical Implications for Experimental Research. *International Journal of Molecular Sciences*, 22(22), 12102. doi: 10.3390/ ijms222212102
- [16] Santillo, A., Chieffi Baccari, G., Minucci, S., Falvo, S., Venditti, M., & Di Matteo, L. (2020). The Harderian gland: Endocrine function and hormonal control. *General and Comparative Endocrinology*, 297, 113548. doi: 10.1016/j. yqcen.2020.113548
- [17] Shashidhar, D., Thangarajan, R., Theruveethi, N., & Bonkuri, S. (2021). Morphological Changes in the Lacrimal Gland of Anophthalmic Socket in Relation to the Contralateral Normal Eye in Male Wistar Albino Rats: A Histopathology

- Study. Current Eye Research, 46(12), 1816-1821. doi: 10. 1080/02713683.2021.1945107
- [18] Singh, S., & Basu, S. (2022). Ultrastructural study of the lacrimal glands in severe dry eye disease following Stevens-Johnson syndrome. *The Ocular Surface*, 23, 204-206. doi: 10.1016/j.jtos.2021.10.005
- [19] Singh, S., Brabletz, S., Arnold, P., Schicht, M., & Paulsen, F. (2023). Epithelial-mesenchymal transition in the lacrimal gland morphogenesis, damage and repair. *The Ocular Surface*, 29, 401-405. doi: 10.1016/j.jtos.2023.06.008
- [20] Singh, S., Jasani, G., Basu, S., & Varma, D. R. (2024). Radiological Imaging of the Lacrimal Gland in Sjogren's Syndrome: A Systematic Review and Meta-Analysis. *Current Eye Research*, 49(11), 1115-1122. doi: 10.1080/0271 3683.2024.2349637
- [21] Singh, S., Pal, P., & Murthy, S. (2021). Palpebral lobe of the human lacrimal gland: Morphometric analysis in normal versus dry eyes. *British Journal of Ophthalmology*, 105(10), 1387-1392. doi: 10.1136/bjophthalmol-2020-316929
- [22] Starčević, A., Radojičić, Z., Djurić Stefanović, A., Trivić, A., Milić, I., Milić, M., ... & Djoric, I. (2023). Morphometric and volumetric analysis of lacrimal glands in patients with thyroid eye disease. *Scientific Reports*, 13(1), 16345. doi: 10.1038/s41598-023-43083-0
- [23] Tirado-Ornelas, H. A., Cazadero-Márquez, J. R., Cruz-Argüelles, C. A., Kleemann-Jaramillo, J. E., Meza-Bautista, M. Á., & Santos-Franco, J. A. (2024). Morphometric analysis of the foramen ovale in the Mexican population using computed tomography scan. Surgical Neurology International, 15, 148. doi: 10.25259/SNI_227_2024
- [24] Tóth-Molnár, E., & Ding, C. (2020). New insight into lacrimal gland function: Role of the duct epithelium in tear secretion. *The Ocular Surface*, 18(4), 595-603. doi: 10.1016/j. jtos.2020.07.002
- [25] Wood, J. P. M., Chidlow, G., Halliday, L. A., Casson, R. J., Selva, D., & Sun, M. (2022). Histochemical Comparison of Human and Rat Lacrimal Glands: Implications for Bio-Engineering Studies. *Translational Vision Science & Tech*nology, 11(11), 10. doi: 10.1167/tvst.11.11.10
- [26] Yasui, T., Miyata, K., Nakatsuka, C., Tsukise, A., & Gomi, H. (2021). Morphological and histochemical characterization of the secretory epithelium in the canine lacrimal gland. *European Journal of Histochemistry: EJH*, 65(4), 3320. doi: 10.4081/ejh.2021.3320
- [27] Yavas, O. (2025). Histochemical and Immunohistochemical Identification of Mast Cells in the Rat Lacrimal Glands. *Veterinary Ophthalmology*. doi: 10.1111/vop.70005
- [28] Yelins'ka, A. M., Akimov, O. Y., & Kostenko, V. O. (2019). Role of AP-1 transcriptional factor in development of oxidative and nitrosative stress in periodontal tissues during systemic inflammatory response. *Ukrainian Biochemical Journal*, 91(1), 80-85. doi: 10.15407/ubj91.01.080
- [29] Zhai, Y., Li, M., Gui, Z., Wang, Y., Hu, T., Liu, Y., & Xu, F. (2021). Whole Brain Mapping of Neurons Innervating Extraorbital Lacrimal Glands in Mice and Rats of Both Genders. Frontiers in Neural Circuits, 15, 768125. doi: 10.3389/fncir.2021.768125

МОРФОЛОГІЯ ТА МОРФОМЕТРІЯ СИСТЕМИ ВИВІДНИХ ПРОТОК СЛЬОЗОВИХ ЗАЛОЗ ЩУРА: ПОРІВНЯЛЬНИЙ АНАЛІЗ ЕКСТРАОРБІТАЛЬНОЇ, ІНТРАОРБІТАЛЬНОЇ ТА ГАРДЕРОВОЇ ЗАЛОЗ

Каценко А. Л., Шерстюк О. О., Гринь В. Г., Свінцицька Н. Л., Білаш В. П., Устенко Р. Л., Пілюгін А. В.

У своїх дослідженнях ми виходили з того, що сльозова залоза лабораторного щура, як і її аналоги у людини, є полімерним

органом, який має свою специфіку. Це в першу чергу стосується синтопічних взаємин в тривимірному просторі самих залоз та їх мікроструктур. Тому при дослідженні сльозових залоз щура (екстраорбітальної, інфраорбітальної та Гардерової), як і при вивченні залоз людини, нам було необхідно виявити той рівень структурної організації різнохарактерних тканин, який би відповідав поняттю структурно-функціональної одиниці. Мета дослідження: охарактеризувати морфометрично та гістологічно кінцеві відділи та систему вивідних проток екстраорбітальної, інтраорбітальної та Гардерової сльозових залоз щура та визначити їх загально-біологічні та видоспецифічні особливості. Проведений морфометричний та гістологічний аналіз екстраорбітальної, інтраорбітальної та Гардерової сльозових залоз лабораторного щура. Отримані результати оброблені в програмі Microsoft Excel. Встановлено, що кінцеві відділи мають більший зовнішній діаметр і товщину стінки порівняно зі вставними протоками. Внутрішньочасточкові протоки характеризуються більшими люмінальними просвітами, що сприяє ефективному накопиченню та евакуації секрету. У Гардеровій залозі кінцеві відділи часто мають неправильну форму та вузькі просвіти, а вставні протоки майже ідентичні кінцевим за діаметром. Міоепітеліальні клітини беруть участь у скороченні та модулюванні секреції, створюючи «milking» – ефект, що забезпечує виділення секрету. Порівняння отриманих даних з морфометрією сльозової залози людини дозволяє виділити загально-біологічні закономірності організації екскреторної системи та видоспецифічні адаптації до типу секрету й функціональних потреб. Результати дослідження мають значення для глибшого розуміння морфофункціональної організації сльозових залоз та можуть слугувати базою для подальших фізіологічних і патологічних досліджень екзокринних залоз.

Ключові слова: сльозові залози щура, екстраорбітальна залоза, інтраорбітальна залоза, Гардерова залоза, кінцеві відділи, морфометрія.

Author's contribution

Katsenko A. L. - conceptualization, research, methodology and writing of the original draft.

Sherstiuk O. O. - conceptualization, methodology and writing of the original draft, supervision.

Hryn V. H. - supervision, project administration, review writing and editing.

Svintsytska N. L. – formal analysis and validation, data visualization, software.

Bilash V. P. - data visualization, formal analysis and validation.

Ustenko R. L. - review writing and editing, software, data visualization.

Piliuhin A. V. - resources, software.

Vol. 31, №3, Page 77-83

Signed for print 16.09.2025
Format 60x84/8. Printing offset. Order № 6878. Circulation 100. Vinnytsia. Printing house "TVORY", Nemyrivske shose St., 62a, Vinnytsya, 21034
Phone: 0 (800) 33-00-90, (096) 97-30-934, (093) 89-13-852, (098) 46-98-043

e-mail: tvory2009@gmail.com http://www.tvoru.com.ua